Preclinical Development of Antisense Conjugates for the Treatment of Myotonic Dystrophy 1

Jessica Stoodley

St Cross College

Reading for DPhil in Paediatrics

Department of Paediatrics

University of Oxford

Supervisors:

Dr Miguel Varela

Professor Matthew Wood

Michaelmas Term 2024

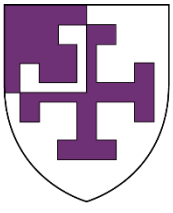

Acknowledgements

I would especially like to thank:

Simeon Stoodley for your unswerving love and support, for enabling me to stay late when needed and making sure I still got dinner, for being willing to let me offload when experiments didn't go to plan and for always believing that I could do this.

Frank and Alison Wood for making it possible for me to do my DPhil in the first place and for your constant encouragement, love and support.

Sophia Stoodley for being a super sleeper and allowing me to go into the lab well-rested, for making it impossible for me not to have a work-life balance and for bringing me joy every single day.

Samuel Wood for your support and belief.

Miguel Varela for all the hours of time you have spent providing guidance, support and advice and for always being positive and encouraging.

Matthew Wood for your support, feedback and guidance.

Suzan Hammond for giving me a positive first experience of academia and for helping me with the DPhil application process.

Chantelle Alderson for helping me obtain my initial DPhil funding and maternity pay.

Carlo Rinaldi for sitting at a lab bench with me one evening almost seven years ago and convincing me to take a job in the Wood group, with reassurance that it would be fine. I'm not sure I would still be in science, let alone have done a DPhil, without that conversation.

David Seoane-Miraz for all your help and advice and especially your help with ELISAs while I was on maternity leave.

Mathieu Fischer for showing me the ropes in the DM1 team, for running ethidium gels when I was pregnant and for letting me attempt to speak French during the hours long harvest sessions.

Rebecca Chalcroft for all of your help and expertise with the *in vivo* work and making it seem like nothing was ever too much trouble.

Yahya Jad and François Halloy for making this whole project possible by giving up time to synthesise the ASO conjugates.

Jesús Reiné for your help with cell sorting and flow experiments, creating great figures and your overarching positivity.

Natalia Galindo Riera for your help with splicing analysis and general advice and tips.
Ruth Ellerington for your help setting up animal experiments before my maternity leave and the amazing cakes that were a part of lab-life with you.
Dhanu Gupta for your help with flow cytometry experiments and asking questions that make me think more deeply about my work.
Nina Ahlskog for all of the tips, tricks, secrets and advice you have passed on over the last six to seven years.
Ania Kordala for inspiring me and showing me that a DPhil is possible as a Mum and for your constant friendship before and during this journey.
Ambra Speciale for your friendship, moral support and always being there to solve science problems and life dilemmas.
Ioulia Vorobieva for your friendship and moral support.
Amarjit Bhomra for being the best lab/operations manager in the universe, being available to solve problems and for your advice and friendship.
Jasminka Arezina for keeping the lab functioning and always helping me find everything I needed.
The Furling group at INSERM for their collaboration with data in DMSXL mice and FISH experiments in immortalised myoblasts.
Carl Webster at AstraZeneca for providing $8D3_{130}$ and NIP228 antibodies.
IDRM and BSB Animal facility staff for looking after the mice.
Muscular Dystrophy UK, Medical Research Council and Department of Paediatrics for the funding of my project, salary and maternity pay.
And lastly to my cats, **Snowy and especially Smokey**, for being constant companions during the DPhil writing, making it a less lonely process. I have hopefully managed to remove the extra words you tried to add…

Thank you all so much!

Table of Contents

Acknowledgements **1**
Table of Contents **3**
Abstract **6**
List of figures **8**
List of Tables **9**
List of Abbreviations **10**
Introduction **14**
Introduction to Myotonic Dystrophy 1 14
Animal models of DM1 17
MBNL proteins 21
CUGBP Elav-like family protein 1 (CELF1) 26
DM1 as multisystemic disorder 27
Disease modifying therapeutics for neuromuscular disease 35
Introduction to antisense oligonucleotides (ASOs) 35
Chemical modification of ASOs 37
ASO conjugation 40
Therapeutic strategies for DM1 47
Aims of Study **51**
Results Chapter 1 – *In vitro* evaluation of cell-penetrating peptide conjugated PMOs (CPP-PMOs) for the treatment of DM1 ..... **53**
Results **53**
In vitro toxicity testing of DEL01-$(CAG)_7$ in human renal epithelial cells reveals reduced compound-induced toxicity 54
Pip6a-$(CAG)_7$ and P1.9-$(CAG)_7$ induce elevations in KIM-1 release from human renal epithelial cells 58
In vitro screening of CPP-$(CAG)_7$ PMOs in DM1 myoblasts corrects the DM1-specific mis-splicing phenotype 61
DEL01-$(CAG)_7$ reduces the number of RNA *foci* and facilitates MBNL release in DM1 myoblasts 65
Discussion **67**

In vitro screening of DEL01-$(CAG)_7$ demonstrates favourable toxicity relative to pip6a-$(CAG)_7$ 67

In vitro screening of DEL01-$(CAG)_7$ demonstrates favourable efficacy on ameliorating DM1 mis-splicing 70

DEL01-$(CAG)_7$ reduces the number of nuclear *foci* in patient derived DM1 myoblasts 72

Results Chapter 2 – *In vivo* evaluation of DEL01-$(CAG)_7$ as an improved a therapy for DM1 75

Results 75

Novel CPP, DEL01, enhances the therapeutic window and reach of $(CAG)_7$ in HSA-LR mice, relative to previously developed CPPs 75

Administration of DEL01-$(CAG)_7$ in HSA-LR mice reverses the functional and molecular DM1 phenotype 76

Administration of DEL01-$(CAG)_7$ enhances PMO distribution to critically affected DM1 tissues, beyond the skeletal muscles 83

DEL01-$(CAG)_7$ reduces nephrotoxicity in HSA-LR mice 87

Treatment of DMSXL mice with DEL01-$(CAG)_7$ shows enhanced delivery to key tissues targets but no phenotypic correction 92

Discussion 98

Single 30 mg/kg dose of DEL01-$(CAG)_7$ is sufficient for reversal of DM1 phenotype in HSA-LR mice 98

DEL01-$(CAG)_7$ administration in HSA-LR mice exhibits an enhanced therapeutic window relative to previous CPP-$(CAG)_7$ conjugates 100

DEL01-$(CAG)_7$ demonstrates an improved therapeutic reach with enhanced penetration into critically affected tissues *in vivo* 103

DEL01-$(CAG)_7$ fails to display correction of the DM1 phenotype in DMSXL Mice 107

Results Chapter 3 – Preclinical development of Ab-PMOs for the treatment of DM1 111

Results 111

Evaluation of BBT-8D3$_{130}$-$(CAG)_7$ in HSA-LR mice 112

Understanding the failings of BBT-8D3$_{130}$-$(CAG)_7$ to penetrate and treat skeletal muscles in HSA-LR mice 126

Discussion 143

Anti-TfR1 targeting Ab-PMO, BBT-8D3$_{130}$-$(CAG)_7$, penetrates the CNS 143

Anti-TfR1 targeting Ab-PMO, BBT-8D3$_{130}$-$(CAG)_7$, penetrates the heart 148

Anti-TfR1 targeting Ab-PMO, BBT-8D3$_{130}$-(CAG)$_7$, fails to treat skeletal muscles in HSA-LR mice 149
Ab-PMOs present a safe toxicological profile 153
TfR1 is differentially expressed in DM1 cellular and animal models 154
General discussion: 158
The therapeutic landscape of DM1 158
Antisense therapy 158
Small molecules 160
Gene Therapy 162
Impact of this study 163
Conclusion 167
Materials and Methods 169
2.1 Materials 169
2.1.1 Antisense oligonucleotide (ASO) conjugates 169
2.2 Methods 170
2.2.1 Cell culture 170
2.2.2 Animal work 173
2.2.3 Nucleic acid analysis methods 178
2.2.4 Immunohistochemistry methods for microscopy 182
2.2.5 Fluorescent activated cell sorting and flow cytometry methods 185
2.2.6 Western blot and ELISA methods 190
2.2.7 Data analysis and visualisation 193
Bibliography 194

Abstract

Myotonic dystrophy type 1 (DM1) is a complex autosomal dominant neuromuscular disorder that affects approximately 1 in 8,000 individuals. DM1 impacts multiple organ systems, including skeletal muscle, heart and central nervous system (CNS), leading to a diverse range of symptoms. Despite ongoing research efforts, no curative treatments are currently approved and readily available to patients. Antisense oligonucleotide (ASO) based therapies are some of the most advanced treatments being tested in DM1 patient clinical trials. These approaches utilise ASOs conjugated to moieties, such as cell-penetrating peptides or antibodies, designed to enhance their delivery into skeletal muscles and the heart. However, no therapy has yet been specifically developed that aims to additionally penetrate the CNS and treat the neurological symptoms experienced by patients. Furthermore, cell-penetrating peptide ASO conjugates (CPP-ASOs) can be associated with nephrotoxicity at higher doses, resulting in a trade-off between efficacy and toxicity, highlighting the need for further optimization to broaden their therapeutic window.

In this study I have tested CPP-ASO and antibody-ASO strategies for treatment of critically affected DM1 tissues: skeletal muscle, heart and CNS. *In vitro* assessment of the novel CPP-ASO, DEL01-$(CAG)_7$, identified DEL01-$(CAG)_7$ as a leading CPP-ASO candidate, with a more favorable therapeutic window and lower toxicity compared to earlier CPP-ASO iterations. Subsequent *in vivo* testing confirmed these findings, demonstrating enhanced delivery to skeletal muscle, heart and significantly reduced nephrotoxicity, relative to its previous CPP-PMOs. Although, DEL01-$(CAG)_7$, was unsuccessful in treating the milder DMSXL mouse model for DM1, it successfully reversed the DM1 phenotype in the more

severe HSA-LR mouse model. Coupled with its promising safety profile these results overall support the continued development of DEL01-$(CAG)_7$ towards clinical trials.

To address the challenge of CNS delivery in DM1, I also tested the potential of ASO conjugation to a CNS optimized, anti-transferrin receptor 1 (anti-TfR1)- targeting antibody. The antibody-ASO conjugate, BBT-$8D3_{130}$-$(CAG)_{7,}$ was evaluated *in vivo* and successfully increased ASO distribution to the CNS. However, although systemically delivered, it failed to also achieve sufficient concentrations for the effective of the DM1 phenotype correction in skeletal muscles. It was concluded that this was likely due to the specific chemical properties of the compound rather than inherent limitations of anti-TfR1 antibodies, suggesting that further optimization of the conjugate's chemical characteristics is necessary to improve therapeutic efficacy. Nevertheless, the study serves as a proof-of-concept for being able to treat the CNS in DM1 using anti-TFR1 targeting delivery strategies.

Overall, this study highlights promising advancements in ASO-based therapies for DM1, with DEL01-$(CAG)_7$ showing potential for further preclinical development as a safer alternative to current CPP-PMOs and anti-TfR1 targeting offering a promising strategy for addressing CNS involvement. Furthermore, the study findings underscore the need for continued optimization of ASO conjugates to balance safety and efficacy while addressing the challenges of multi-organ targeting.

List of Figures

Figure *1*: A schematic showing the genetic cause of DM1 and its generation of pathological RNA transcripts. 15
Figure *2*: Effect of CPP-PMO conjugates on human proximal tubule epithelial kidney cell viability. 56
Figure *3*: Levels of KIM-1 released from CPP-PMO treated human proximal tubule epithelial kidney cells. 60
Figure *4*: CPP-$(CAG)_7$ PMOs demonstrate partial correction of DM1-specific molecular phenotype in DM1 muscle cells. 64
Figure *5*: Treatment with DEL01-$(CAG)_7$ reduces the number of RNA foci and MBNL1 sequestration in DM1 muscle cells. 66
Figure *6*: Functional assessment CPP-PMO treatment activity in DM1, HSA-LR mice. 79
Figure *7*: Functional assessment of the activity of CPP-PMO treatment upon skeletal muscle mis-splicing in DM1, HSA-LR mice. 82
Figure *8*: Tissue biodistribution of CPP-PMO conjugates in DM1, HSA-LR mice. 85
Figure *9*: Toxicological assessment of CPP-PMOs in DM1, HSA-LR mice. 91
Figure *10*: Functional and observational assessment of DEL01-$(CAG)_7$ treated DMSXL mice. 94
Figure *11*: Treatment of DMSXL mice with DEL01-$(CAG)_7$ achieves skeletal muscle delivery but fails to correct DM1 phenotype. 97
Figure *12*: Toxicological assessment of Ab-PMOs in DM1, HSA-LR mice. 115
Figure *13*: BBT-$8D3_{130}$-CAG_7 penetrates CNS tissues and colocalises with neurons. 118
Figure *14*: Peripheral tissue biodistribution and efficacy of anti-TfR1-PMO conjugates in ameliorating DM1 skeletal muscle phenotype in DM1 mice. 122
Figure *15*: Treatment of HSA-LR mice with 100 mg/kg BBT-$8D3_{130}$-$(CAG)_7$ fails to improve the DM1 phenotype. 125
Figure *16*: DM1 patient-derived myotubes exhibit reduced TfR1 expression. 129
Figure *17*: Analysis of Tfrc transcript expression across tissues in HSA-LR, WT and SMA mice. 131
Figure *18*: Analysis of TfR1 protein expression across tissues in HSA-LR, WT and SMA mice. 133
Figure *19*: Elevated TfR1 expression in DM1 HSA-LR skeletal muscles is reversed upon treatment. 135
Figure *20*: Analysis of CD71 (TfR1) cell surface expression in single skeletal muscle cells of HSA-LR, WT and SMA mice. 138
Figure *21*: Comparison of Ab-PMOs for SMA and DM1 in HSA-LR mice. 141
Figure *22*: Schematic of myotonia testing in HSA-LR mice. 176

List of Tables

Table *1*: Histopathological assessment of HSA-LR mouse liver and kidney tissues 14 d post-administration with 30 mg/kg or 40 mg/kg of DEL01-$(CAG)_7$. 89
Table *2*: CPP amino acid sequences. 170
Table *3*: Oligonucleotide primer sequences for the splicing analysis of alternative exons. 180
Table *4*: Oligonucleotide primer sequences for qRT-PCR analysis. 181
Table *5*: Antibodies used for Immunostainings, FISH and western blot. 185
Table *6*: List of antibodies used for flow cytometry and cell sorting analysis. 187
Table *7*: List of ELISA probes for the detection of PMOs in tissues. 193

List of Abbreviations

2’F – 2’ fluoro

2’MOE – 2’-O-(2-Methoxyethyl)

2’OMe – 2’-O-methyl

3’UTR – 3’ untranslated region

Ab-ASO – antibody-antisense oligonucleotide

Ab-PMO – antibody-phosphorodiamidate morpholino oligonucleotide

ADC – antibody drug conjugate

ALP – alkaline phosphatase

ALT – alanine transaminase

AMPAR – α-amino-3-hydroxy-5-methyl-4-isoxazolepropionic acid receptor

ASO – antisense oligonucleotide

AST – aspartate transaminase

BBB – blood-brain-barrier

BIN1 – bridging integrator 1

CD – cluster of differentiation

CDM1 – congenital muscular dystrophy 1

CELF1 – CUGBP elav-like family member 1

CEt – constrained ethyl

CLCN1 – chloride voltage-gated channel 1

CMV – cytomegalovirus

CNS – central nervous system

CPP – cell-penetrating peptide

CPP-PMO – cell-penetrating peptide-phosophorodiamidate morpholino oligonucleotide

CSE – cell surface expression

DAPI – 4′,6-diamidino-2-phenylindole

DM1 – myotonic dystrophy 1

DMD – Duchenne muscular dystrophy

DMPK – dystrophia myotonica protein kinase

DMT1 – divalent metal transporter 1

EDTA – ethylenediaminetetraacetic acid

ELISA – enzyme-linked immunosorbent assay

EMA – European medicines agency

FACS – fluorescent activated cell sorting

FCS – familial chylomicronemia syndrome

FDA – federal drugs agency

FISH – fluorescent *in situ* hybridisation

FVB/N – friend leukaemia virus B strain

FSHD – facioscapulohumeral muscular dystrophy

GABA – gamma-aminobutyric acid

GalNAc – N-acetylgalactosamine

GFAP – glial fibrillary acidic protein

GLT1 – glutamate transporter 1

GSK3B – glycogen synthase kinase-3 beta

HATTR – hereditary transthyretin amyloidosis

hDMPK – human dystrophia myotonica protein kinase gene

HIF – hypoxia inducible factor

hnRNP – heterogeneous nuclear ribonucleoprotein

HRE – hypoxia response element

HRPTEpC – human renal proximal tubule epithelial cell

HSA-LR – human skeletal actin – long repeat

IgG – immunoglobulin G

INSERM – institut national de la santé et de la recherche médicale

INSR-A – insulin receptor A

INSR-B – insulin receptor B

iPS – induced pluripotent stem cell

IRE – iron response element

IRP – iron response protein

ISSN1 – intron splice silencer N1

KDa – kilo Daltons

KIM-1 – kidney injury marker 1

LC50 – lethal concentration 50

LNA – locked nucleic acid

LTP – long term potentiation

mAb – monoclonal antibody

MFI – mean fluorescent intensity

MBNL1 – muscleblind like protein 1

MBNL2 – muscleblind like protein 2

mDmpk – murine dystrophia myotonica protein kinase gene

miRNAs – micro ribonucleic acid

MPSII – mucopolysaccharidosis type II

mRNA – messenger ribonucleic acid

NFT – neurofibrillary tangle

NMDA – N-methyl-D-aspartate

NLS – nuclear localization signal

PBS – phosphate buffered saline

PBS-T – phosphate buffered saline-0.1% tween 20

PFA – paraformaldehyde

PMO – phosphorodiamidate morpholino oligonucleotide

PNA – peptide nucleic acid

PS – phosphorothioate

PVDF - polyvinylidene fluoride

RBFOX2 – RNA binding fox-1 homolog 2

RNA – ribonucleic acid

RT-PCR – real time polymerase chain reaction

RT-qPCR – real time quantitative polymerase chain reaction

SEM – standard error mean

SERCA – sarcoendoplasmic reticulum calcium ATPase

siRNA – small interfering ribonucleic acid

SMA – spinal muscular atrophy

SOS1 – son of sevenless homolog 1

SSC – saline sodium citrate

TA – tibialis anterior muscle

TAE – tris-acetate edta

TE – tris-edta

TfR1 – transferrin receptor 1

TfR2 – transferrin receptor 2

UV – ultraviolet

vHot – video hand opening time

WT – wild-type

ZnF – zinc finger

Introduction

Introduction to Myotonic Dystrophy 1

Myotonic Dystrophy 1 (DM1) is a rare autosomal dominant genetic disorder and the most common form of muscular dystrophy in adults. The disease was first described by Hans Steinert in 1909 and is primarily characterised by muscle weakness, myotonia (prolonged muscle contraction) and atrophy, although the disease is multi-systemic, affecting multiple organs within the body (Harper P, 2001). The prevalence of DM1 is 0.5-18.1 per 100,000 people world-wide (Theadom et al., 2014), however, more recent reports indicate that milder cases are under-diagnosed and that the prevalence of the genetic cause could be 2-3 times higher (Johnson et al., 2021).

The genetic cause of DM1 is a tandem CTG trinucleotide repeat expansion in the 3 prime untranslated region (3' UTR) of the myotonic dystrophy protein kinase (*DMPK*) gene (Brook et al., 1992; Y. H. Fu et al., 1992; Mahadevan M et al., 1992). Transcription of the expanded CTG repeats, gives rise to the production of CUG repeat expanded ribonucleic acid (RNA) (as shown in Figure 1). These RNA repeat expansions form hairpin-like structures called RNA *foci* that act via a toxic gain of function mechanism, sequestering and interfering with key transcription and splicing regulators, in particular muscleblind-like protein 1 and 2 (MBNL1 and MBNL2) (Davis et al., 1997; K. Lee et al., 2013; J. W. Miller et al., 2000; Taneja et al., 1995). Consequently, the function of these transcription factors and splicing regulators is impaired, causing global splicing dysfunction across all cell and tissue types (López-Martínez et al., 2020).

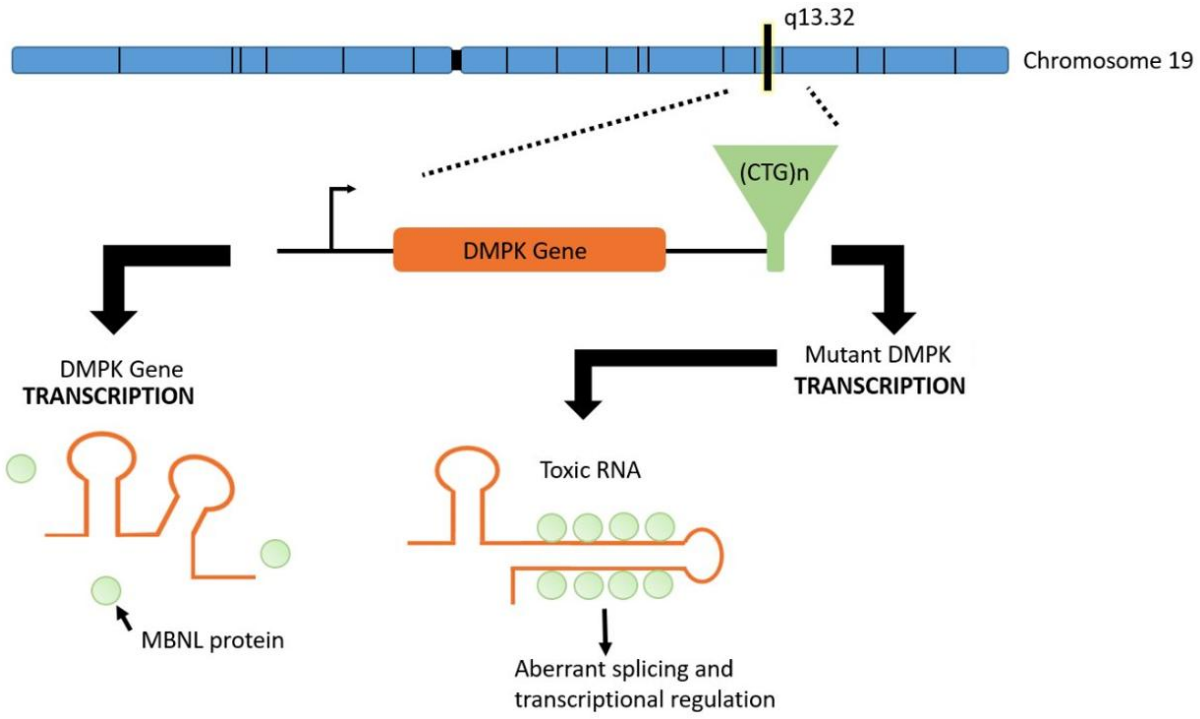

Figure *1*: A schematic showing the genetic cause of DM1 and its generation of pathological RNA transcripts.

The severity and nature of the molecular phenotype and symptoms experienced by patients has been successfully correlated, by several groups, to the number of CTG repeats carried by each patient (Eguchi et al., 1994; Gennarelli et al., 1996; Jaspert et al., 1995). Healthy individuals harbour CTG repeat lengths of 5-37 repeats within the *DMPK* gene, repeat lengths between 38 and 50 are considered to be 'pre-mutation', while repeat lengths of greater than 50 lead to the manifestation of the DM1 phenotype (Turner & Hilton-Jones, 2010). Furthermore, the size of the CTG repeat and the symptom severity are inversely proportional to the age of onset, with the most severely affected patients exhibiting symptoms from an earlier age (Hunter et al., 1992). This has allowed for the sub-categorization of DM1 into five clinical sub-types: congenital DM1 (CDM1), infantile

onset -, juvenile onset -, adult (classical) onset- and late-onset (mild)- DM1 (De Antonio et al., 2016).

CDM1 is the most severe form of DM1, with patients harbouring a median expansion size of 1000 CTG repeats (De Antonio et al., 2016). Affected individuals present symptoms either prenatally or from birth, where severe generalised weakness, hypotonia, respiratory distress and intellectual disability are typically observed (Zapata-Aldana et al., 2018). Life expectancy in CDM1 patients is greatly reduced and the neonatal mortality rate is estimated to be between 30 – 40 % (Echenne & Bassez, 2013; G. Ho, 2015). Infants that survive this critical period experience a biphasic disease course where there may be an improvement or stabilisation in symptoms until adolescence, at which point symptoms of classical adult onset DM1 may begin to emerge (Hageman et al., 1993).

Infantile - and juvenile - onset DM1 patients typically carry more than 800 CTG repeats and first display disease symptoms during childhood (G. Ho, 2015). The initial symptoms to emerge are typically neurological and many patients experience intellectual disability and cognitive and behavioural deficits, before beginning to experience symptoms of adult onset DM1 around adolescence (De Antonio et al., 2016; G. Ho, 2015). In contrast, adult onset DM1 patients display much milder cognitive impairment, harbour 50 –1000 CTG repeats and have a median age of 20 –25 for symptom onset (G. Ho, 2015). These symptoms include severe myotonia, cardiac dysfunction, progressive muscle weakness, insulin resistance, cataracts and excessive daytime sleepiness (Meola & Cardani, 2015; Yum et al., 2017). Respiratory distress, followed by cardiac dysrhythmias are the leading causes of death in this patient population, leading to a reduced overall life expectancy (De Die-Smulders et al., 1998; Groh et al., 2008) . Late-onset DM1 is the only form of DM1 that does not reduce life expectancy and is characterised by mild myotonia and cataracts

(Meola & Cardani, 2015; Yum et al., 2017). These patients carry 50 –150 CTG repeats and often symptoms do not appear until 40 years of age, however, they can manifest as young as 20 years of age (G. Ho, 2015).

In general, DM1 is a highly variable disease and while the above clinical classification subgroups have been defined, there are significant overlaps in CTG repeats and symptom severity between groups (De Antonio et al., 2016; Wenninger et al., 2018). This can partially be attributed to the high somatic instability of the CTG tandem repeats which varies between tissues and individuals and increases with age (Castel et al., 2010). Somatic instability during cell division or DNA replication can lead to the further expansion of CTG repeats, progressing the disease and triggering more severe and earlier onset symptoms (Fortune et al., 2000; Jansen et al., 1994; Martorell et al., 1997). Furthermore, this instability plays a crucial role in the genetic anticipation of DM1, wherein the CTG repeat expansion within germ line cells intensifies disease severity and reduces the age of onset in successive generations (Ashizawa et al., 1992; Monckton et al., 1995). Maternal bias adds an additional layer to this complexity, as the severity of DM1 is often greater when the expanded CTG repeat is maternally inherited. This bias is believed to arise from a combination of somatic instability during oogenesis and differences in the epigenetic regulation between male and female germ cells (Barbé et al., 2017). Such intricate interplay underscores the multifaceted nature of DM1 and contributes to its observed variability.

Animal models of DM1

Animal models have been essential in understanding the molecular mechanisms underlying DM1 pathology, especially the toxic effects of expanded CUG repeats and their

impact on skeletal muscle, heart, and CNS function. These models have helped demonstrate the role of RNA toxicity in disease progression and the potential for therapeutic interventions. The most commonly used models are outlined below.

The HSA-LR mouse model

The HSA-LR (human skeletal actin long repeat) model is one of the most widely used *in vivo* models of DM1. These mice express a human *ACTA1* transgene, on a friend leukemia virus B (FVB/N) background, which contains an expanded CUG repeat tract of 250 repeats within its 3' UTR (Mankodi et al., 2000). The expression of this gene is restricted to the skeletal muscles and recapitulates several key aspects of DM1 pathology. As seen in DM1 patients, these mice display alternative splicing in skeletal muscles and develop myotonia, myopathy, and reduced grip strength (Mankodi et al., 2000). This model is commonly used for preclinical testing of DM1 therapeutics in the skeletal muscles with effective therapies being able to reverse myotonia and correct mis-splicing events (Wheeler et al., 2012; Klein et al., 2019).

The DMSXL mouse model

The DMSXL mouse model (Huguet et al., 2012) was generated by breeding DM300 mice, containing a human *DMPK* transgene harbouring 300 CTG repeats, to produce offspring that express over 1000 CTG repeats in the *DMPK* locus. However, neonatal mortality is high, with approximately 60% of homozygous DMSXL mice dying during the first month of life (Huguet et al., 2012). While this is similar to the high neonatal mortality rate (30-40 %) observed in congenital DM1 (Echenne et al., 2008), it can make the model challenging to

work with. Nevertheless, the DMSXL model exhibits a multisystemic phenotype that closely mirrors the human disease, including *foci* formation, mild splicing defects, and RNA dysregulation in the heart, skeletal muscle, brain, and other tissues (Huguet et al., 2012). DMSXL mice show hallmark DM1 features such as decreased muscle strength, motor impairment, abnormal muscle histology, cardiac conduction defects and respiratory impairment (Huguet et al., 2012; Hernández-Hernández et al., 2013). The DMSXL model has also revealed neurological impairments such as axonopathy, neuronopathy, and reduced motor neuron counts, leading to compromised motor function and cognitive deficits (Panaite et al., 2011; Hernández-Hernández et al., 2013). Furthermore, mice exhibit progressive neurodegeneration, including impaired synaptic function, reduced long-term potentiation (LTP), and abnormal spatial learning and memory (Hernández-Hernández et al., 2013). These phenotypes align with DM1 patient symptoms, making the DMSXL model a valuable tool for studying CNS involvement in DM1.

The LC15 mouse model

The LC15 mouse model was recently developed to study the cardiac and multisystemic effects of DM1. The model contains an uninterrupted expanded 250 – 400 CTG repeat tract harboured within the 3'UTR of a human *DMPK* transgene. The transgene and therefore expanded CUG repeat RNA is particularly expressed in the heart. Consequently, LC15 mice recapitulate many of the cardiac phenotypes observed in DM1 patients, including prolonged QRS and QTc intervals, indicative of cardiac conduction abnormalities (Tylock et al., 2020). Despite these abnormalities, LC15 mice generally do not exhibit spontaneous arrhythmias under normal conditions. However, when challenged with flecainide, a sodium channel blocker, they show increased susceptibility to lethal

ventricular arrhythmias, suggesting a heightened vulnerability to stress-induced cardiac events (Tylock et al., 2020).

At the cellular level, LC15 mice exhibit RNA *foci* in over 80% of ventricular myocytes and mis-splicing events similar to those observed in human DM1 patients (Tylock et al., 2020). Consequently, the LC15 model may serve as an important tool for understanding the molecular mechanisms underlying DM1-associated cardiac defects.

MBNL Knockout Mice

Double knockout (DKO) of MBNL1 and MBNL2 results in embryonic lethality, demonstrating the critical importance of these proteins in early development (K. Lee et al., 2013). However single or conditional knockout models of MBNL proteins have been particularly informative in deciphering the role of splicing regulators in DM1. MBNL1 knockout mice exhibit cataracts, myotonia, and cardiac defects, but they do not display muscle wasting or significant cognitive impairment, suggesting that MBNL2 compensates for some of MBNL1's functions in the CNS (Dixon et al., 2015; Matynia et al., 2010). In contrast, MBNL2 knockout mice develop only mild muscle pathology but show severe CNS phenotypes, including sleep disturbances, defective spatial memory, abnormal synaptic activity, and increased susceptibility to seizures (Charizanis et al., 2012). These findings underscore the differential roles of MBNL1 and MBNL2 in tissue-specific spliceopathy and support the hypothesis that CNS involvement in DM1 is largely mediated by MBNL2 dysfunction. Meanwhile, conditional knockout models targeting specific tissues have revealed that inactivation of both MBNL1 and MBNL2 in skeletal muscle and the CNS

results in enhanced disease phenotypes, including severe neonatal mortality, respiratory distress, and widespread splicing and gene expression defects (Thomas et al., 2017).

Other DM1 mouse models

Other lesser used but still valuable DM1 mouse models include the EPA960 model and DM5 model. The EPA960 model introduces inducible CTG repeats in the 3' UTR of the DMPK gene. This model, like the DMSXL, demonstrates both cardiac and muscular phenotypes, along with neurological abnormalities, including impaired spatial learning and memory (G. S. Wang et al., 2007). The model's electrophysiological profiling revealed impaired hippocampal function, specifically reduced long term potentiation, suggesting postsynaptic abnormalities (P. Y. Wang et al., 2017).

Meanwhile the DM5 model expresses short CTG repeats in the DMPK 3' UTR, resulting in myotonia and cardiac conduction defects, though without detectable RNA *foci* (Mahadevan et al., 2006). The absence of *foci* in this model suggests that soluble CUG RNA is also pathogenic, indicating that the toxicity of repetitive RNA is not solely determined by the repeat length but also by the abundance of the transcripts (Mahadevan, 2012). This model highlights the potential for different mechanisms of RNA toxicity and may serve as a complement to longer-repeat models such as the HSA-LR and DMSXL models.

MBNL proteins

The MBLNL proteins are a family of tissue specific regulators of developmentally programmed gene expression that bind to double-stranded RNA hairpins formed by large

CUG repeat tracts (J. W. Miller et al., 2000). In mammals the family is comprised of 3 proteins, encoded by the genes: *MBNL1*, *MBNL2* and *MBNL3*. *MBNL1* and *MBNL2* are ubiquitously expressed with *MBNL1* being more dominant in the majority of tissues. Contrastingly, in the central nervous system (CNS), *MBNL2* is the more abundantly expressed gene (Charizanis et al., 2012; Fardaei et al., 2002; Kanadia, Johnstone, et al., 2003; Kanadia, Urbinati, et al., 2003). Meanwhile, *MBNL3* is limited to more specific expression in differentiating and regenerating adult muscle tissues and the placenta (Konieczny et al., 2014; Poulos et al., 2013).

All *MBNL* paralogs are structurally similar with exons 1,2 and 4 from of each paralog, encoding for four zinc finger domains (ZnFs) (Begemann et al., 1997; J. W. Miller et al., 2000). The four ZnF domains are arranged into two tandem pairs which bind 5-'YGCY-3' motifs (where Y is pyrimidine), the consensus binding motif of MBNL pre-messenger RNA (mRNA) targets. These motifs are also especially abundant in CUG expanded RNA, as found in DM1 *DMPK* transcripts (Goers et al., 2010). Additionally, the expression of each paralog is regulated by alternative splicing in a tissue- and cell type-specific manner, influenced by the developmental stage (Konieczny et al., 2014; Terenzi & Ladd, 2010).

Functionally, MBNL proteins play a central role in regulating alternative splicing (E. T. Wang et al., 2012), particularly during development. For example, *MBNL1* and *MNBL2* are typically upregulated during differentiation, with a marked elevations particularly in heart, brain and skeletal muscle (Artero et al., 1998; Begemann et al., 1997; J. W. Miller et al., 2000). As a result, MBNL1 and MBNL2 promote embryonic stem cell differentiation and induce a transition from fetal to adult splicing patterns (H. Han et al., 2013). Such regulation is critical for generating protein diversity and ensuring proper gene expression in a tissue- and developmentally specific manner. Beyond splicing regulation, MBNL proteins

are also present in the cytoplasm (Hammond et al., 2017; Thomas et al., 2017) where they also play a role in mRNA nuclear export and cytoplasmic localization (Adereth et al., 2005; E. T. Wang et al., 2012) and mRNA stability (Du et al., 2010; Masuda et al., 2012), consequently impacting protein translation.

MBNL1 dependent splicing regulation

As the most widely expressed *MBNL* gene, *MBNL1* has been the focus of much research, allowing for the elucidation of the functional roles of its exons. Extensive analyses of *MBNL1* deletion constructs, in embryonic and human cell lines, have identified that the inclusion of exon 5 and the presence of the KRAEK motif, conserved within exon 6, together form a bipartite nuclear localization signal (NLS) (Fernandez-Costa & Artero, 2010; Terenzi & Ladd, 2010; Tran et al., 2011). This NLS is vital for directing MBNL1 into the nucleus, where it regulates the alternative splicing of a variety of pre-mRNA targets. The KRAEK motif provides the basic amino acid clusters required for nuclear import, while exon 5 appears to enhance and modulate the localization process, ensuring that MBNL1 can effectively carry out its nuclear functions, such as binding to RNA targets and influencing splicing events (Fernandez-Costa & Artero, 2010; Tran et al., 2011).

Exon 7, on the other hand, plays a pivotal role in the dimerization of MBNL1, promoting the formation of multimeric ring-like structures when bound to toxic RNA hairpins, such as those containing expanded CUG repeats, a hallmark of diseases such as DM1 (Tran et al., 2011; Yuan et al., 2007). This was confirmed by yeast two-hybrid assays, which demonstrate that exon 7 enhances the protein's ability to self-associate, thereby influencing its overall functional activity in RNA binding and regulation (Tran et al., 2011).

Additionally, exon 3, a region that is almost universally included in MBNL1 transcripts, encodes for a linker sequence that is crucial for the protein's RNA binding and splicing regulation activities. Deletion of exon 3 severely impairs the binding affinity of MBNL1 with the current hypothesis being that this linker region increases the protein's flexibility, permitting the binding of MBNL1 to a range of targets (Cass et al., 2011; Tran et al., 2011). Although, in the case of DM1, it has been shown that the deletion of the exon 3 linker region has very little effect on interactions with the toxic CUG repeat expanded RNA *foci* (Rehman et al., 2014).

Overall, the alternative splicing of exons within *MBNL1*, such as exon 5, 7, and 3, generates a diverse array of protein isoforms with distinct functional properties. This splicing regulation allows MBNL1 to adapt its activity according to the needs of specific tissues or developmental stages, ensuring precise control over gene expression programs and enabling MBNL1 to play multiple roles in cellular function. However, in the context of diseases like DM1, the inclusion of exons 5 and 7 can contribute to pathological processes. For example, while the inclusion of exon 5 enhances the nuclear localization of MBNL1, in a DM1 context this facilitates sequestration into RNA *foci*, further exacerbating the loss of functional MBNL1 (Tran et al., 2011). Similarly, exon 7 promotes MBNL1 dimerization, strengthening interactions with CUG repeat RNA and intensifying entrapment in the *foci*. Consequently, exon 5 and 7 inclusion, although essential for MBNL1's normal function, play a significant role in the mis-regulation of splicing and gene expression observed in DM1 due to their involvement in MBNL1 sequestration.

As previously mentioned, MBNL1 is also critically involved in the regulation of the transition from fetal to adult splicing patterns during development. Normally, MBNL1 represses fetal splicing variants and promotes the inclusion of adult-specific exons, which

is vital for proper maturation and function in tissues such as muscle, heart, and the central nervous system (Artero et al., 1998; Begemann et al., 1997; J. W. Miller et al., 2000). In DM1, sequestration of MBNL1 impairs its ability to regulate this splicing transition due to lack of functional protein. This results in the persistence of fetal splicing patterns in adult tissues, causing the expression of fetal-specific isoforms that are inappropriate for mature tissue functions (Du et al., 2010; Kalsotra et al., 2008; Kanadia, Johnstone, et al., 2003; Lin et al., 2006). For instance, in DM1, the retention of fetal splicing patterns in skeletal muscle leads to the inclusion of embryonic exons in proteins like *CLCN1*, which disrupts chloride channel function and contributes to symptoms such as myotonia in patients and DM1 models (Charlet-B. et al., 2002; Lueck et al., 2007; Mankodi et al., 2002). Similarly, the failure to exclude fetal exons in cardiac and CNS proteins contributes to the cardiac and neurological abnormalities observed in DM1(López-Martínez et al., 2020). Overall, therefore, the sequestration of MBNL1 by toxic RNA prevents the critical fetal-to-adult splicing transition, driving many of the clinical symptoms associated with DM1.

MBNL1 and MBNL2 compensatory mechanisms

As MBNL1 and MBNL2 share high structural and functional similarity and play similar roles in regulating alternative splicing, the two proteins exhibit a compensatory mechanism where here one protein can partially offset the loss or dysfunction of the other (K. Lee et al., 2013; E. T. Wang et al., 2012). Indeed, MBNL knockout studies in mice have shown that when MBNL1 function is compromised, such as in DM1 due to sequestration by CUG repeats, MBNL2 is upregulated and can partially take over its role in regulating alternative splicing, helping to mitigate some of the splicing defects. However, the compensatory capacity of MBNL2 is limited and often insufficient to fully prevent splicing defects,

particularly in tissues such as heart and skeletal muscles where MBNL1 is more heavily relied upon (K. Lee et al., 2013).

CUGBP Elav-like family protein 1 (CELF1)

Although the sequestration of MBNL1 alone accounts for a significant portion of the splicing defects seen in DM1, the mis-regulation of CELF1, a member of the CUGBP Elav-like family, also significantly contributes to the induction of fetal splicing patterns in DM1 tissues. CELF1 is a ubiquitously expressed heterogenous nuclear ribonuclear protein (hnRNP) that specifically binds CUG repeats in RNA (L. T. Timchenko et al., 1996). The protein plays a role in mRNA processing, including modulation mRNA stability, with its expression promoting a fetal patterning of splicing (Ho et al., 2004; Kalsotra et al., 2008; Meola 2013; Nikonova 2024).

As such, CELF1 acts as an antagonistic regulator of splicing to MBNL1, therefore in DM1, a functional loss of MBNL1, results in increased CELF1 activity (T. H. Ho et al., 2005; Mahadevan et al., 2006; Savkur et al., 2001; N. A. Timchenko et al., 2004, 2005). It has been shown, using transgeniinc mice overexpressing CELF1, that CELF1 does not directly interact or co-localise with nuclear *foci* but rather binds single-stranded CUG repeats preferentially (L. T. Timchenko et al., 1996). Subsequent research into the DM1 associated increase in CELF1 activity has shown, in both human cells and tissues and DM1 mouse modesl, that this occurs via an activation of protein kinase C (PKC), associated with expanded CUG repeats, hyper-phosphorylating of CELF1 (Kuyumcu-Martinez et al., 2007). Consequently, the stability and steady-state levels of CELF1 are increased, therefore further exacerbating and promoting the inversion to foetal splicing patterning in

DM1 tissues (Kalsotra et al., 2008; Kuyumcu-Martinez et al., 2007). Furthermore, conditional upregulation of CELF1 in murine skeletal muscles led to muscle wastage, myopathy and impaired motor function, accompanied my mis-splicing events (Ward et al., 2010).

Despite its overexpression in DM1, CELF1 levels increase at the protein level rather than through transcriptional changes. In DM1 mouse models, inhibition of CELF1 has been shown to correct abnormal translational regulation in muscle, leading to improved motor function and muscle histopathology, though it does not address myotonia, splicing defects, or cardiac issues (Y. K. Kim et al., 2014). This supports the widely held hypothesis that DM1 pathology is predominantly attributed to MBNL sequestration and its loss of function with regards to splicing regulation.

DM1 as multisystemic disorder

As previously detailed, DM1 is characterised by global splicing mis-regulation, primarily due to a shift from adult to foetal splicing patterning that is caused by MBNL protein sequestration and CELF1 upregulation. It should also be noted that expanded DMPK mRNAs are also spliced, however their sequestration to the nucleus due to *foci* formation prevents translation (Davis et al., 1997). More than 32 alternatively spliced transcripts in patients and over 60 in mouse models have been identified. (Kalsotra et al., 2008; López-Martínez et al., 2020). This spliceopathy results in alternatively spliced transcripts that are insufficient for the functional requirements of adult tissues, consequently contributing to the DM1 pathology and symptoms observed in patients. The ubiquitous expression of *MBNL* and *DMPK* genes dictates that this process can occur in almost all tissues, however the

somatic mosaicism of *DMPK* repeat expansions results in the greatest levels of aberrant splicing and DM1 pathology affecting the skeletal muscles, CNS and heart (Ballester-Lopez et al., 2020; Thornton et al., 1994).

Skeletal muscle

The splicing alteration of at least 24 genes have been reported in DM1 patients muscle biopsies (López-Martínez et al., 2020). Of the three mammalian MBNL paralogs, MBNL1 is the primary regulator of splicing in the skeletal muscles and is itself aberrantly spliced in DM1 pathology, with exon 7 known to be developmentally regulated by MBNL1 homotypic interactions. As such, inclusions of exon 5, 7 and 10 have been reported in DM1 patient skeletal muscle biopsies (Konieczny et al., 2014; Nakamori et al., 2013; Yamashita et al., 2012). Therefore, in addition to MBNL1 sequestration, these alterations in *MBNL1* splicing isoforms also contribute to the disease pathology, as they too lead to the generation of alternative protein isoforms.

One of the best documented splicing alterations in DM1 skeletal muscles, caused by MBNL1 depletion, is the inclusion of exon 7a in the transcript of chloride voltage-gated channel 1 (*CLCN1*) (Lueck et al., 2007; Nakamori et al., 2013). Additionally, exon 2 inclusion in the *CLCN1* transcript has been reported in DM1 patient and animal model tissues, with the inclusion of the two additional introns resulting in a premature stop codon (Charlet-B. et al., 2002; Mankodi et al., 2002). This results in a truncated protein that is unable to localise to the muscle membrane. As the main chloride ion channel in skeletal muscles, CLCN1 is responsible for ion conductance and muscle membrane excitability, therefore the impaired function of CLCN1 in DM1 leads to chloride channelopathy,

hyperexcitability of the muscle membrane and ultimately myotonia (Lueck et al., 2007; Mankodi et al., 2002; Wheeler et al., 2007) .

In addition to myotonia, muscle weakness is another key phenotype of DM1 skeletal muscles, with alternative splicing events being shown to contribute. For example, the exclusion of exon 11 in bridging integrator 1 (*BIN1*) transcripts leads to the translation of an inactive protein, unable to play its role in T tubule generation and therefore impairing excitation-contraction coupling within the sarcomere (Fugier et al., 2011). Similarly, exclusion of exon 29 in the *CACNA1S* transcript, which encodes the calcium channel CAV1.1, leads to causes impaired excitation-contraction coupling as a result of increased channel conductance and voltage sensitivity (Tang et al., 2012). Both of these alternative splicing events are directly related to MBNL1 depletion and result in skeletal muscle weakness (Fugier et al., 2011; Tang et al., 2012).

Another protein involved in calcium homeostasis affected by DM1 is sarcoplasmic/endoplasmic reticulum calcium ATPase (SERCA)1, which is encoded for by *ATP2A1.* This calcium ATPase responsible for the reuptake of calcium into the sarcoplasmic reticulum during muscle relaxation (Brandl et al., 1986). In DM1, the inclusion of *ATPA1* exon 22, alters SERCA1 protein structure and impairs calcium homeostasis in patient muscle cells, thus contributing to the muscle weakness and fatigue, characteristic of the disease, and leading to muscle degeneration (Kimura et al., 2005).

Several other splicing alterations have been linked to DM1 skeletal muscle weakness, including exclusions of exons in transcripts encoded by *DTNA*, *RYR1*, *CAPN3, LDB3* and *DMD* (Kimura et al., 2005; Nakamori et al., 2013; Rau et al., 2015; Yamashita et al., 2012). Alterations in the splicing of *DMD*, a gene which encodes dystrophin are particularly interesting, given that out of frame mutations in *DMD* cause Duchenne muscular dystrophy

(DMD), another severely debilitating muscle wastage disorder (Worton & Thompson, 1988). In DM1, the exclusion of exon 78 is thought to contribute to muscle weakness given the role of dystrophin in the maintenance and integrity of the muscle membrane (Yamashita et al., 2012). This is supported by a report of exon 78 skipping causing a mild case of DMD, characterised by sarcolemma instability (Traverso et al., 2018). Meanwhile research, using human patient biopsies, has shown that alterations in *LDB3* splicing lead to defective interactions between X-disc proteins, causing sarcomere disorganisation and muscle fibre instability which impairs muscle function and contributes to progressive muscle weakness (Nakamori et al., 2013).

The largest alternative splicing effect described in DM1 patient samples to date is the alternative splicing of son of sevenless homolog 1 (*SOS1*), which encodes a guanine nucleotide exchange factor involved in the RAS-MAPK signalling pathway (Cherniack et al., 1994; Corbalan-Garcia et al., 1996). In DM1 patients 16% of *SOS1* transcripts contain exon 25, vs 99% in healthy individuals (Nakamori et al., 2013). Disrupted splicing of SOS1 impairs critical signalling pathways important for muscle cell proliferation and differentiation (Gilbert et al., 2021), likely exacerbating the issues of muscle regeneration and repair in DM1 and contributing to muscle atrophy and weakness over time.

Beyond splicing alterations related to muscle function and weakness, metabolic processes in DM1 skeletal muscles are also impaired. DM1 skeletal muscles are well documented in exhibiting insulin resistance, linked to alternative splicing in *INSR*, which encodes the insulin receptor (Savkur et al., 2001). The *INSR* gene undergoes alternative splicing to generate two protein isoforms: insulin receptor A and B (INSR-A and INSR-B), with the latter being more prevalent in adult tissues. However, in DM1 patients, there is a shift toward the fetal isoform, INSR-A, which has a reduced ability to mediate insulin signaling

(Savkur et al., 2001). This abnormal splicing contributes to the insulin resistance commonly observed in DM1 patients (Matsumura et al., 2009; Moxley et al., 1978; Tevaarwerk & Hudson, 1977), underscoring the metabolic disturbances that accompany the disease.

In summary there are numerous mis-splicing events that comprise the DM1 pathology in skeletal muscles and contribute to symptoms experienced by patients. Many of those described above are used as biomarkers for the testing of DM1 therapeutics, however they represent only a fraction of the genes impacted by the disease's broad splicing dysregulation.

Heart

Cardiac involvement in DM1 is a major contributor to morbidity and mortality in patients and typically presents as arrhythmias, conduction abnormalities, and cardiomyopathy (Matsumura et al., 2009; Petri et al., 2014). The primary mechanism behind cardiac dysfunction in DM1, as in skeletal muscle, is the widespread mis-regulation of RNA splicing due to the sequestration of MBNL1 by toxic RNA repeats, which is further exacerbated by CELF1 upregulation (Kalsotra et al., 2008).This leads to abnormal splicing of multiple cardiac-related genes, resulting in impaired function.

One of the most studied splicing alterations in DM1 cardiac tissue is in the *SCN5A* gene, which encodes the alpha subunit of the cardiac sodium voltage channel NaV1.5. MBNL1 depletion in DM1 patient hearts causes the inclusion of exon 6a in *SCN5A*. This leads to the production of non-functional sodium channels, impairing the cardiac action potential

and contributing to conduction block and arrhythmias (Freyermuth et al., 2016; Nakamori et al., 2013).

Cardiac conduction impairment in DM1 patient cardiac tissues has also been linked to mis-splicing of *ATP2A2* and *RBFOX2* gene. In the case of *ATP2A2* this is as a result of an intronic inclusion which disrupts the function of the SERCA2 calcium channel, leading to a dysregulation of calcium influx (Dixon et al., 2015; Kimura et al., 2005). Meanwhile splicing alterations in RNA-binding protein, RBFOX2, another regulator of splicing, are thought to be related to cardiac conduction delay (Misra et al., 2020).

Three final genes have been reported to be alternatively spliced in DM1 cardiac tissue: *TNNT2*, *TTN* and *LDB3*. Inclusions in the transcripts of these genes have been linked to alterations in contractile properties, impaired myofiber assembly and cardiac tissue morphological abnormalities, respectively (Dixon et al., 2015; Lin et al., 2006; Nakamori et al., 2013; Yamashita et al., 2012).

CNS

DM1 spliceopathy occurs in both neuronal and glial cells in the CNS and is predominantly driven by MBNL2 sequestration, due to it being the primarily expressed MBNL paralog within CNS tissue (Kanadia, Urbinati, et al., 2003). One key target of MBNL2 dysregulation in the CNS is the *GRIN1* gene, which encodes a subunit of the N-methyl-D-aspartate (NMDA) receptor. Mis-splicing of *GRIN1*, in MBNL2 knock-out mice, has been linked to decreased dendritic localization of glutamate receptors, impairing synaptic transmission and plasticity (Charizanis et al., 2012) . Furthermore, in the same study, mis-splicing of *TANC2* was shown to exacerbate glutamate receptor mislocalization, further disrupting

synaptic function (Charizanis et al., 2012). This altered glutamatergic transmission, particularly in the frontal cortex, may contribute to the cognitive impairments observed in DM1 patients, including deficits in memory and learning (S. Han et al., 2010; Jiang et al., 2004).

Additional splicing defects in genes such as *CACN1* and *NDRG4* are thought to impair neuronal activity and learning, as they are associated with disrupted calcium channel function and neuronal differentiation (Charizanis et al., 2012; Yamamoto et al., 2011). Notably, RNA sequencing analyses of DM1 frontal cortex tissues have shown a gradient of splicing alterations in neurotransmitter receptors that correlate with disease severity (Otero et al., 2021).

Mis-splicing of genes involved in synaptic trafficking and scaffolding also plays a crucial role in the CNS pathology of DM1. For instance, *GRIP1*, a gene involved in localizing AMPA receptors (AMPARs) to synapses, is mis-spliced in DM1 patients, which disrupts its association with kinesin (Otero et al., 2021). This impairs synaptic trafficking and may lead to synaptic dysfunction, further contributing to the neurodegenerative aspects of DM1, aligning with human transcriptomic data which presents a downregulation of neuronal genes in the frontal cortex of DM1 patients (Otero et al., 2021).

Another hallmark of DM1 in the CNS is tauopathy, characterized by the abnormal accumulation and hyperphosphorylation of tau protein (Caillet-Boudin et al., 2014; Sergeant et al., 2001; Vermersch et al., 1996). Mis-splicing of the *MAPT* gene, which encodes tau, leads to an abnormal distribution of tau isoforms in patient brains, contributing to the formation of neurofibrillary tangles (NFTs). This accumulation of hyperphosphorylated tau interferes with axonal transport and neurosecretion, likely exacerbating neurodegeneration in DM1 (Dhaenens et al., 2011; Sergeant et al., 2001;

Vermersch et al., 1996). Such tauopathies are typically associated with progressive cognitive decline, and neurodegenerative diseases such as Alzheimer's disease (Hanger et al., 2009; Y. Huang et al., 2011), this correlates with the signs of cognitive decline observed in DM1 patients (Modoni et al., 2004, 2008).

DM1, mis-regulated splicing also affects CNS neurotransmission. It has been shown that DM1 patients exhibit altered glutamatergic transmission in the frontal lobe and heightened sensitivity to gamma-aminobutyric acid (GABA) agonists, which may contribute to hyperexcitability similar to that seen in epilepsy, although epilepsy itself is rare in DM1 (Meola & Sansone, 2007; Takado et al., 2015). This abnormal neurotransmission is likely another contributing factor to the cognitive and behavioural disturbances observed in DM1.

Beyond neurons, splicing dysregulation additionally affects glial cells. *MBNL2* sequestration leads to the formation of nuclear *foci* in neurons, glia, and oligodendrocytes (Jiang et al., 2004), which disrupts their normal function. Transcriptomic data suggest an increase in microglial activation in DM1 brains, consistent with the neuroinflammation observed in these patients (Otero et al., 2021). Additionally, gliosis has been reported in DM1 patient CNS tissues, further indicating an ongoing inflammatory response (Itoh et al., 2010). Furthermore, a relatively recent study using DMSXL mice, revealed, using RNA sequencing, that over 128 transcripts are mispliced in primary DMSXL astrocytes, with cell adhesion, cytoskeleton regulation and morphogenesis pathways being primarily affected (Dincã et al., 2022). Validation of the results revealed that mis-splicing of transcripts involved in these process, including *Sorbs1*, *Fermt2*, *Itga6*, *Itgb4* and *Dmd*, extended to the frontal cortex and hippocampus of not only DMSXL samples but also to human *postmortem* CNS samples (Dincã et al., 2022).

Disease modifying therapeutics for neuromuscular disease

Introduction to antisense oligonucleotides (ASOs)

Neuromuscular diseases, which progressively weaken muscles and impair mobility due to dysfunction in muscle tissue or nerves, have historically been difficult to treat, due to the tissues affected being well-protected by their biological membranes. However, in recent years, there has been significant progress in developing disease-modifying therapeutics aimed at addressing the underlying causes of these disorders. One such therapeutic approach is through the use of ASOs. ASOs are nucleic acid polymers typically comprised of 14 to 30 nucleotides. These short synthetic sequences of nucleic acids are single stranded and able to target and bind to RNA via Watson-Crick base pairing in order to modulate gene expression. ASOs are highly specific, binding to a precise target sequence within the RNA, which allows for rational design tailored to individual genes with a minimal risk of off-target effects. This specificity offers the potential for ASOs to be applied as precision medicine tools, targeting not only disease-related genes but also specific sequences, alleles (Giorgio et al., 2019; V. M. Miller et al., 2003) and transcript isoforms (Crnković-Mertens et al., 2006) i.e. patient-specific sequences (J. Kim et al., 2019), opening the door to personalized medicine approaches.

With respect to ASOs for the treatment of neuromuscular disease, ASOs can be categorized into two classes based on their mode of action: RNase H1 dependent ASOs and steric blocking ASOs (RNase H-1 independent). RNase H1-dependent ASOs operate by forming a hybrid duplex with the target RNA, which is then recognized by the RNase H1 enzyme. The enzyme cleaves the RNA strand within this RNA-DNA duplex, leading to degradation of the target RNA and reduced gene expression (Wu et al., 2004). ASOs

functioning via this mechanism are often referred to as "gapmers" because they typically consist of a central DNA segment, approximately 10 nucleotides long, that is complementary to the target RNA sequence. This central segment is flanked by 2 to 5 chemically modified nucleotides on either side (Monia et al., 1993). These modifications protect the flanking regions from RNase H1 activity, while improving the overall binding affinity to the target RNA. This design allows the gapmer to be highly effective in degrading the RNA without triggering off-target cleavage. RNase H1-dependent ASOs have proven effective for gene silencing in various diseases, with four currently having gained regulatory approval for treatment in patients: fomivirsen for the treatment of cytomegalovirus (CMV) retinitis (Geary et al., 2002), mipomersen for familial hypercholesterolemia (Raal et al., 2010), inotersen for hereditary transthyretin-mediated amyloidosis (HATTR) (Benson et al., 2018) and volanesorsen for familial chylomicronemia syndrome (FCS) (Gaudet et al., 2015). It should, however, be noted that mipomersen was rejected by the European Medicines Agency (EMA) on the grounds of patient safety, while formivirsen is now discontinued due to limited clinical need.

Steric-block ASOs, by contrast, do not induce RNA degradation but instead act by binding with a high affinity to specific RNA sequences, thereby preventing transcript interactions with RNAs or proteins. Their chemical modifications render them incapable of triggering RNase H1 activity. Steric-block ASOs have been most widely applied to modulate alternative splicing, allowing for exon inclusion or exclusion, depending on the therapeutic needs (Dominski & Kole, 1993; Singh & Singh, 2018; Wan & Dreyfuss, 2017). This mechanism is used in splice-switching therapies, where ASOs mask splicing signals to alter the splicing pattern of pre-mRNA. For example, this approach has been used to restore the translational reading frame in genetic diseases, such as DMD (Aartsma-Rus et

al., 2017). There are currently 6 FDA-approved splice-switching ASOs to date: eteplirsen (Aartsma-Rus & Krieg, 2017), golodirsen (Heo, 2020), viltolarsen (Czifrus & Berlau, 2023) and casimersen (Shirley, 2021) all for the treatment of DMD, milasen for Batten disease (J. Kim et al., 2019) and Nusinersen for the treatment of spinal muscular atrophy (SMA) (Corey, 2017; Finkel et al., 2016).

Beyond splicing regulation, steric-block ASOs have other applications, such as preventing ribosome access to mRNA to inhibit translation (Baker et al., 1997), altering polyadenylation signals to stabilize transcripts (Vickers et al., 2001) and blocking sequences of RNA with a toxic gain of function mechanism (Kanadia et al., 2006; Klein et al., 2019; Mulders et al., 2009). These diverse mechanisms make steric-block ASOs highly versatile in treating various RNA-mediated diseases.

Despite this progress in ASO therapeutics, a significant challenge hindering their broader application lies in the difficulty of effectively delivering these molecules to target tissues and organs beyond the liver and kidney and their rapid degradation in serum (Eder et al., 2009; Geary, Norris, et al., 2015; Tsui et al., 2002). Consequently, two strategies are being employed to enhance ASO delivery: chemical modification and bioconjugation.

Chemical modification of ASOs

Chemical modification is one of the most fundamental strategies for improving the efficacy and delivery of ASOs. Modifying various aspects of ASOs—including the nucleic acid backbone, ribose sugar, and nucleobases—can significantly enhance their pharmacokinetics, pharmacodynamics, and biodistribution, thereby improving their overall therapeutic potential (Brad Wan & Seth, 2016; Roberts et al., 2020). These modifications

are particularly important in enabling ASOs to avoid serum and nuclease degradation and penetrate target tissues and organs effectively.

One of the most widely used chemical modifications is the inclusion of phosphorothioate (PS) linkages. Here, replacement of a non-bridging oxygen atom in the phosphate backbone with sulphur increases resistance to nuclease degradation (Sayers et al., 1989). PS linkages also promote interactions with plasma proteins, improving circulation time and overall pharmacokinetics (Gaus et al., 2019; Watanabe et al., 2006).

Meanwhile, ribose sugar modifications at the 2' position are particularly common. Substituting the 2'-hydroxyl group with 2'-O-methyl (2'-OMe), 2'-O-methoxyethyl (2'-MOE), or 2'-fluoro (2'-F) groups enhances nuclease resistance, improves target binding affinity, and stabilizes the ASO in plasma (Manoharan, 1999). These modifications also reduce immunogenicity, making ASOs safer for therapeutic use (Hamm et al., 2010). Specifically, with regards to gapmers, such ribose modifications can be used in the flanking regions to boost binding without disrupting RNase H1 activity (Geary, Baker, et al., 2015). However, the application of these modifications also extends to ASOs that modulate their action by steric blocking or splice switching mechanisms. For example, Nusinersen, the first approved ASO for the treatment of SMA, comprises a 2’MOE backbone that is sufficient for the effective treatment of disease affected motor neurons, increasing levels of full length SMN protein and ameliorating symptoms experienced by patients (Finkel et al., 2016; Mercuri et al., 2017).

Another innovative approach involves the use of bridged nucleic acids, such as locked nucleic acids (LNAs) and constrained ethyl (cEt) nucleotides. These modifications constrain the ribose sugar to a 3'-*endo* conformation by the creation of a bridge between carbons at the 2’ and 4’ positions of the ribose sugar. This significantly increases binding

affinity to target RNA and enhances stability against nucleases (Morita et al., 2002; Obika et al., 1998, 2001). Again, this has proven particularly beneficial in gapmer designs, where the introduction of LNA or cEt modifications into the flanking regions has been shown to improve efficacy (Hung et al., 2013). However, as these modifications are not RNAse H1 competent, they cannot be included in gapmer flanking regions. This is the same for the 2' sugar modifications discussed in the previous paragraph.

Other advanced modifications include phosphorodiamidate morpholino oligomers (PMOs) and peptide nucleic acids (PNAs), which feature neutral backbones that increase serum stability and reduce protein interactions (Hudziak et al., 1996; H. J. Larsen et al., 1999; Summerton & Weller, 1997). In the case of PMOs, the nucleotide backbone is substituted with a 6 membered morpholino rings (Summerton & Weller, 1997), while in the case of PNAs, the backbone is replaced with pseudopeptide analogues (Saarbach et al., 2019). The neutrality of these modifications also easily enables the conjugation of delivery-enhancing moieties, such as cell-penetrating peptides, to improve tissue targeting (Betts et al., 2012; Hammond et al., 2017; Klein et al., 2019). PMOs, in particular, have shown promise in treating neuromuscular diseases. For example, Sarepta Therapeutics has developed several federal drug agency (FDA) approved PMO drugs such as eteplirsen, casimersen and golodirsen, which target specific exons of the dystrophin gene to treat DMD. These therapies work by skipping disease-causing exons and enabling the production of a functional, albeit truncated, dystrophin protein (Aartsma-Rus & Krieg, 2017; Heo, 2020; Shirley, 2021).

However, while many of these chemically modified ASOs demonstrate remarkable stability and specificity, challenges remain in achieving effective tissue distribution, particularly in skeletal muscle. For example, a cEt-modified gapmer, developed by Ionis Therapeutics for

the treatment of DM1 showed promising efficacy in preclinical models (Jauvin et al., 2017) achieving sufficient ASO concentrations in skeletal muscle. However, in a phase 1/2a clinical trial (Thornton et al., 2023; IONIS, NCT02312011), insufficient compound reached the skeletal muscles to elicit a therapeutic benefit and the trial was discontinued. Consequently, a significant amount of research is focusing on enhancing ASO delivery through bioconjugation and alternative delivery methods to improve stability, biodistribution, and ultimately therapeutic outcomes.

ASO conjugation

Various conjugation strategies have been developed to improve the delivery and therapeutic efficacy of ASOs, aiming to enhance their tissue specificity, cellular uptake, and overall bioavailability. These approaches leverage different targeting mechanisms to direct ASOs to specific cells or tissues. For example, N-acetylgalactosamine (GalNAc) conjugation targets the asialoglycoprotein receptor on hepatocytes, making it an effective delivery strategy for ASOs designed to treat hepatic conditions (Prakash et al., 2014; Tanowitz et al., 2017). Meanwhile lipid conjugation, involving the attachment of hydrophobic molecules such as cholesterol or fatty acids, can increase compound potency by enhancing association with plasma lipoproteins to extend circulation time, reducing renal clearance, and enhancing endosomal escape (M. T. Larsen et al., 2016; Østergaard et al., 2019; S. Wang et al., 2019). However, among the various conjugation techniques, peptide and antibody conjugates are two of the most advanced and widely used for targeting neuromuscular diseases.

Peptide ASOs

Peptide conjugation of an ASO using a cell-penetrating peptide moiety (CPP) is a particularly attractive approach for enhancing the cellular uptake and tissue-specific delivery of ASOs, proteins and small molecules. CPPs are short, cationic, or amphipathic peptides, of less than 30 amino acids, that can transport ASOs across cell membranes, enhancing cellular uptake (Lehto et al., 2016). As described in greater detail by McClorey & Banerjee, 2018, many of the early CPPs were derived from naturally occurring proteins that contain peptide sequences capable of facilitating membrane translocation. Examples include Penetratin-1, derived from the *Drosophila* Antennapedia homeodomain (Derossi et al., 1994), the HIV-Tat protein, Transportan (Pooga et al., 1998), and cationic sequences such as polyarginines (Futaki et al., 2001). Subsequent generations of CPPs have been iterative advancements of these original molecules, with each iteration designed to optimize their translocation efficiency, stability and targeting specificity.

CPPs achieve membrane translocation via various mechanisms, dependent on their size, cargo, and charge. These mechanisms of entry into the cell can be broadly categorized into direct translocation and endocytosis. Direct translocation allows CPPs to cross cell membranes in an energy-independent manner, often through mechanisms such as pore formation or lipid reorganization in the membrane (Ehrenstein & Lecar, 1977; Pouny et al., 1992; Rydström et al., 2011). Meanwhile other CPP molecules favour endocytic pathways (Fittipaldi et al., 2003; Nakase et al., 2007).

Another critical aspect of CPP-based delivery systems is ensuring that the cargo avoids endosomal entrapment and subsequent lysosomal degradation. Common approaches used to achieve endosomal escape include designing CPPs that exploit the low pH within the endosome or through direct interactions between the CPP and the endosomal

membrane (McClorey & Banerjee, 2018). For example, some CPPs induce endosomal escape by disrupting the membrane through proton-sponge effects, which increase osmotic pressure and cause the endosome to rupture (Lo & Wang, 2008). While other CPPs are designed to destabilize the endosomal membrane through interactions that lead to the release of the peptide and its cargo into the cytoplasm (Lehto et al., 2014; Wadia et al., 2004).

Conjugating CPPs to neutral backbone ASOs, such as PMOs or PNAs has shown promise in the field of neuromuscular disorders (Godfrey et al., 2015; Ivanova et al., 2008; Yin et al., 2011). In particular, studies have shown that PMO conjugation to an arginine rich peptide, Pip6a, which feature arginine-rich sequences flanked by a hydrophobic core, enhances ASO delivery to skeletal and cardiac muscles (Godfrey et al., 2015). The Wood group (University of Oxford, UK) has used this approach to great advantage to treat disease phenotypes in mouse models of several neuromuscular diseases including DMD, SMA and DM1 (Betts et al., 2012; Hammond et al., 2017; Klein et al., 2019).

While cell CPP-PMOs greatly improve ASO delivery and efficacy, a major concern associated with CPPs is nephrotoxicity. In preclinical studies, CPP-PMOs, particularly those with arginine-rich CPPs, have been linked to renal damage in animal models (Amantana et al., 2007; Klein et al., 2019). Indicators of kidney dysfunction, such as elevated kidney injury marker 1 (KIM-1) and creatinine levels, have been observed in rodent experiments, while in non-human primate studies, arginine-rich CPP-PMOs exhibited signs of tubular degeneration in the kidneys (Moulton & Moulton, 2010).

To address this issue, research is focused on optimizing CPP chemistry to reduce toxicity without compromising efficacy. Within the Wood research group, strategies for this include modifying the length of the peptide, adjusting the arginine content, and introducing

structural alterations. Alternatively, many research groups are exploring less toxic delivery moieties as alternative approaches for ASO delivery.

Antibody-ASOs

Antibody-antisense oligonucleotide (Ab-ASO) conjugates are an emerging approach for improving the targeted delivery of ASOs to specific tissues. By conjugating ASOs to antibodies that recognize cell surface receptors, these conjugates enhance cellular uptake and tissue specificity, increasing therapeutic efficacy while minimizing off-target effects (Dugal-Tessier et al., 2021). This strategy is akin to that used by antibody-drug conjugates (ADCs), which have long been employed to deliver chemotherapeutic agents directly to cancer cells (Sievers & Senter, 2013). The first ADC, Mylotarg, was approved in 2000 and since then, 14 ADCs have gained FDA approval, with over 100 more being investigated in clinical trials (Z. Fu et al., 2022).

Among the most studied targets for Ab-ADCs is the transferrin receptor 1 (TfR1), a glycoprotein responsible for the transport of iron-bound transferrin into cells, that is often overexpressed in cancer cells, due to their high iron requirements (Das Gupta & Shah, 1990; Ding Cheng Yang et al., 2001; Kondo et al., 1990; Seymour et al., 1987). TfR1-targeting antibodies have been conjugated to anti-tumor agents to direct these therapies specifically to cancer cells, with the goal of enhancing the therapeutic index and reducing potential side effects. This approach has shown promise in preclinical studies, with several anti-TfR1 targeting ADCs demonstrating efficient delivery and anti-tumor effects in cancer models (Candelaria et al., 2021; Daniels et al., 2011; Leoh et al., 2018).

Beyond oncology, TfR1 has also been a key target on the blood-brain-barrier (BBB) for achieving drug delivery to the CNS, a major challenge for neurotherapeutics. Early anti-TfR1 constructs, such as OX26, 8D3, and R17-217, demonstrated the ability to bind TfR1, without disrupting transferrin binding or iron transport, and effectively deliver therapeutic agents to the CNS (Friden et al., 1991; Kissel et al., 1998; H. J. Lee et al., 2000; Pardridge, 2002). More recent advances, including lower-affinity and bispecific antibodies, have further improved brain accumulation and distribution (Webster et al., 2016; Yu et al., 2011). For example, bispecific antibodies combining an anti-TfR1 arm with another therapeutic target have shown enhanced CNS penetration for treating conditions like Alzheimer's disease (Yu et al., 2011).

The use of antibody-ASO conjugates has expanded the therapeutic potential of anti-TfR1 strategies to neuromuscular diseases. The Wood group exemplified this approach by using a TfR1-targeting antibody-PMO conjugate to deliver PMOs across the BBB in an SMA mouse model, achieving sufficient delivery to the brain to reverse the disease phenotype, while also reaching peripheral tissues such as skeletal muscle and liver (Hammond et al., 2022). This highlights a potential dual benefit of TfR1-targeted therapies for both CNS and systemic tissue delivery.

Similarly, other research has demonstrated the success of TfR1-targeting strategies for skeletal muscle and heart delivery. For example, Sugo et al. (2016) showed that anti-TfR1 conjugates could effectively deliver small interfering RNAs (siRNAs) to skeletal muscle and cardiac tissue in animal models. More recently, two companies, Dyne Therapeutics and Avidity Biosciences, have advanced anti-TfR1 antibody based oligonucleotide conjugates into clinical trials for neuromuscular diseases such as DMD and DM1, where these

conjugates have shown promise in improving muscle targeting and therapeutic efficacy (ACHIEVE: NCT05481879; MARINA: NCT05027269; HARBOUR: NCT06411288).

TfR1 expression, function and regulation

TfR1 is the primary importer of cellular iron, playing a crucial role in maintaining cellular iron homeostasis which itself is vital for oxygen transport, energy generation, mitochondrial function, DNA synthesis and ultimately cell survival (Cairo et al., 2006).As part of the transferrin receptor family, TfR1 shares a 45-60% structural homology with transferrin receptor 2 (TfR2) (Calzolari et al., 2007; Kawabata et al., 2000), which is selectively expressed in human hepatocytes and erythroid precursors and not present at all in the mouse genome (Deaglio et al., 2002). In contrast, TfR1 protein is ubiquitously expressed across almost all vertebrate tissues, reflecting its essential role in iron uptake (Lambert & Mitchell, 2007) .

TfR1 exists at the cell surface as a 97 kDa type 2 glycoprotein homodimer (Kühn et al., 1984; McClelland et al., 1984) and mediates iron uptake via cell-mediated endocytosis of the iron carrier protein, transferrin (Cheng et al., 2004; Mayle et al., 2012). Under acidic endosomal conditions, iron dissociates from transferrin and is then enzymatically reduced and released into the cytosol via divalent metal transporter 1 (DMT1) (Andrews, 1999; Tabuchi et al., 2000). Meanwhile transferrin bound TfR1 is recycled to the cell membrane, with a cycling time of approximately 17 min (Ciechanover et al., 1983). However, regardless of receptor occupancy, TfR1 constitutively undergoes endocytosis(Ajioka & Kaplan, 1986) and has for a long time been a target of interest for the delivery of therapeutic agents to specific tissues or cells.

The expression of TfR1 protein is tightly regulated to meet cellular iron demands. Under iron-deficient conditions or hypoxia, TfR1 expression increases through both transcriptional and post-transcriptional mechanisms. TfR1 is encoded by the *Tfrc* gene and hypoxia-inducible factors (HIFs) are able to upregulate *Tfrc* transcription by binding to hypoxia response elements (HREs) in its promoter (Tacchini et al., 1999; Xu et al., 2017). Post-transcriptionally, iron response proteins (IRPs) bind to iron-responsive elements (IREs) in the 3' UTR of *Tfrc* mRNA, stabilizing the transcript and enhancing expression when iron levels are low (Cheng et al., 2004; Rouault, 2006). Conversely, in states of iron excess, these regulatory mechanisms promote mRNA degradation to reduce receptor expression (Iwai et al., 1998; Yikilmaz et al., 2005). Additionally, TfR1 recycling can shift towards lysosomal degradation under conditions of iron overload, further modulating cellular iron uptake (Tachiyama et al., 2011).

The general protein expression pattern of TfR1 correlates with tissue iron requirements and cellular proliferation rates. It is highly expressed in rapidly dividing cells, such as activated lymphocytes and erythroblasts, where iron is essential for functions such as heme synthesis (Gatter et al., 1983; Jefferies et al., 1984). Expression levels are lower in non-proliferating cells but remain significant in various tissues, including the basal epidermis, pancreas, and endothelial cells of brain capillaries (Gatter et al., 1983; Oh et al., 1986). In the brain, TfR1 is enriched in capillary endothelium and serves as a key mediator for iron transport across the BBB (Jefferies et al., 1984). This makes it an appealing target for therapeutic delivery to the CNS, with several studies exploring anti-TfR1 antibodies to facilitate drug transport across the BBB.

To date, there are no comprehensive studies denoting a high expression of TfR1 protein on the cell surface of skeletal muscles and heart, relative to other systemic tissues.

However, TfR1's expression is also hypothesised to be prominent in skeletal muscle and heart tissue, reflecting their high iron content and demand, and indeed the Human Protein Atlas shows mRNA expression Tfrc in these tissues is particularly high relative to other tissues and organs (Uhlen et al., 2015). Skeletal muscle comprises approximately 10-15% of the body's total iron, mainly stored in myoglobin, while cardiomyocytes rely on iron for efficient mitochondrial function (Hoes et al., 2018; Wittenberg & Wittenberg, 2003). As a consequence, TfR1 has become a target of interest for ASO delivery into muscles within the context of neuromuscular disorders.

Therapeutic strategies for DM1

ASOs for DM1

ASO therapies have been a major focus of DM1 treatment research for many years. Both steric block and RNase H1-dependent ASO strategies have been applied in the preclinical development of treatments for DM1. Steric block ASOs, bind to CUG repeat expansions with a high affinity. This consequently prevents the binding and sequestration of MBNL1, alleviating abnormal splicing events caused by the loss of MBNL1 function (Klein et al., 2019; Mulders et al., 2009; Wheeler et al., 2009). In contrast, RNase H1-dependent gapmers target and bind the expanded *DMPK* RNA repeats, recruiting RNAse H1 and leading to the cleavage and degradation of the toxic RNA. This again leads to a reduction in DM1 alternative splicing events (Jauvin et al., 2017; J. E. Lee et al., 2012; Wheeler et al., 2012; Yadava et al., 2020).

While early-generation ASOs, such as IONIS-DMPKRx, showed promise in preclinical models, challenges with drug delivery, particularly with regards to achieving sufficient ASO

concentrations in skeletal muscle tissues, have limited their success in clinical trials (Thornton et al., 2023; IONIS, NCT02312011). To overcome these limitations, efforts have focused on conjugating ASOs to enhance delivery to key tissues such as muscle, heart, and, potentially, the central nervous system (CNS). As such there are now peptide and antibody conjugated ASO therapies currently in patient clinical trials.

Regarding peptide conjugated ASOs for DM1, peptides, such as pip6a, have demonstrated enhanced PMO delivery into muscle and heart tissues in the HSA-LR model, using a steric blocking ASO. This resulted in a reversal of both mis-splicing events and functional myotonia (Klein et al., 2019). While progressions to clinical trials were halted, subsequent iterations of the pip6a series resulted in the generation of CPPs now licensed to the company PepGen (Oxford, UK) where the CPP-PMO, PGN-EDODM1, was developed as DM1 treatment. PGN-EDODM1 is currently in Phase 1 clinical trials (FREEDOM-DM1, NCT06204809) with preclinical studies having demonstrated efficacy in alleviating the DM1 skeletal muscle phenotype, enhanced PMO delivery into heart (although not CNS) and a reduced toxicity profile relative to pip6a.

With respect to antibody based ASO conjugates for DM1, there are currently two such compounds being tested in DM1 patient clinical trials. Both compounds utilise antibody-based technologies which targeting TfR1 for the purpose of achieving enhanced ASO delivery into skeletal muscles and heart. Del-desiran, developed by Avidity Biosciences, comprises of a monoclonal anti-TfR1 antibody conjugated to an siRNA which target CUG repeat expansion and induces mutant *DMPK* transcript knockdown. Meanwhile Dyne-101, developed by Dyne Therapeutics, is formed of an anti-TfR1 targeting antibody fragment conjugated to a gapmer ASO targeting the *DMPK* CUG repeat. Both therapies have shown efficacy in reducing toxic RNA levels in animal models of DM1 and are being evaluated in

Phase 3 and Phase 1/2 clinical trials, respectively (HARBOUR: NCT06411288; ACHIEVE: NCT05481879). The data reported from these trials appears positive with regards to efficacy, impact on patient quality of life and safety.

Other DM1 therapies

Beyond ASOs, a number of small molecules are also being investigated for DM1, with several candidates in clinical trials. These drugs can either target the toxic RNA itself or address specific disease symptoms. The advantage of small molecules is their potential for oral administration, which simplifies treatment and enhances patient compliance. Examples of small molecules in DM1 patient clinical trials include: Tideglusib, a glycogen synthase kinase 3 beta (GSK3B) inhibitor, originally developed for Alzheimer's disease, which has shown potential for DM1 by reducing toxic *DMPK* RNA levels and correcting splicing defects and improving muscle function (Horrigan et al., 2020; Wei et al., 2018; AMO Pharma Ltd, NCT02858908); ERX-963: a small molecule in phase 1 clinical trials that is specifically designed to bind and neutralize the toxic RNA hairpin (Expansion therapeutics, NCT03959189); and MYD-0124 (erythromycin), a repurposed antibiotic being evaluated for its ability to reduce RNA *foci* and correct splicing abnormalities (Japan Agency for Medical Research Development, jRCT2051190069).

In addition to small molecules, gene therapies are also being explored a therapeutic option for DM1. These therapies aim to either excise expanded CTG repeats in the *DMPK* gene at the DNA level or degrade the toxic RNA molecules produced upon transcription (Batra et al., 2021; Lo Scrudato et al., 2019). However, these technologies are currently still in a

relatively early stage of development. As such, so far, ASO conjugates offer the most immediate promise of hope to DM1 patients.

Aims of Study

The most advanced ASO therapeutics for DM1 involve utilising both CPP and anti-TfR1 targeting ASO conjugates. Both strategies are displaying good progress in DM1 patient clinical trials, however, there remain limitations associated with each approach. Firstly, in the case of CPP-ASOs, it was noted upon the preclinical development of the CPPs licensed to PepGen by the Wood group, that the reduction in toxicity relative to the CPP predecessor, pip6a, comes with a compromise regarding compound activity (data not disclosed). I therefore hypothesised that there is scope to further optimise future CPP iterations of pip6a in order to enhance compound while maintaining an improved safety profile.

Meanwhile, with regards to the antibody-based ASO conjugates currently in clinical trials, it is unknown whether these therapies can treat DM1 patient CNS symptoms, given that their design and evaluation has been termed specifically for skeletal and cardiac muscle. As CPP-ASOs have generally displayed limited CNS penetration in DM1 (Klein et al., 2019), there remains a significant need to develop treatment strategies that can reach the CNS and address neurological symptoms of DM1. Recent research, within the field of treatment development for SMA, has shown that using an anti-TfR1 antibody with a reduced affinity for TfR1 ($8D3_{130}$) (Webster et al., 2019), increases its ability to deliver compounds into the CNS and allows for the successful treatment of SMA mouse models (Hammond et al., 2022). The antibody-ASO employed was able to correct the disease phenotype in both CNS and peripheral tissues. I therefore hypothesis that by employing the same CNS optimised anti-TfR1 antibody ($8D3_{130}$) as an ASO delivery vehicle, it will be possible, using one compound, to treat the DM1 CNS phenotype in addition to skeletal muscle and heart tissues.

Therefore, in light of the limitations associated with CCP-ASO and antibody based ASO conjugates, mentioned above, the aims of this study were to test two ASO conjugates as therapeutic strategies for DM1 in preclinical models. More specifically:

1. To test the novel CPP-ASO conjugate, DEL01-$(CAG)_7$ as a DM1 treatment with an enhanced balance of efficacy and toxicity relative to previous CPP-ASOs developed within the Wood group.

2. To test a CNS-optimised antibody-ASO conjugate targeting TfR1, BBT-$8D3_{130}$-$(CAG)_7$, with the goal of evaluating its potential as a treatment that could reach the CNS, in addition to skeletal muscle and heart.

Results Chapter 1 – *In vitro* evaluation of cell-penetrating peptide conjugated PMOs (CPP-PMOs) for the treatment of DM1

Results

Previously published work in the Wood group demonstrated that the peptide, pip6a, when conjugated to a PMO, significantly enhanced skeletal muscle delivery in a DM1 mouse model, improving mis-splicing and reducing myotonia (Klein et al., 2019). However, progression to clinical trials were halted due to pip6a-associated nephrotoxicity, a known issue with CPP-PMOs in various animal models (Amantana et al., 2007; Gait et al., 2019.

More recently, P1.9 and P3.8 were developed, by the Wood group, as safer CPPs by reducing peptide length and arginine content and have been licensed to PepGen for further development in DM1 and DMD therapies. However, the improved toxicological profile led to reduced efficacy, leaving room for further CPP enhancement. By further optimizing peptide length and arginine content, the Wood group have developed the novel CPP, DEL01. In this chapter, I evaluate DEL01 *in vitro*, as a CPP candidate for DM1 treatment. I assess its cell toxicity relative to P1.9, P3.8, and Pip6a, in addition to its ability to enhance PMO delivery and reverse DM1 pathology in patient-derived myotubes, relative to the same CPPs.

In vitro toxicity testing of DEL01-$(CAG)_7$ in human renal epithelial cells reveals reduced compound-induced toxicity

Prior to any *in vitro* experiments, DEL01, P1.9, P3.8 and pip6a were each conjugated to a 21-mer PMO with a $(CAG)_7$ sequence which targets CUG repeat-expanded RNA. This PMO has has been shown to correct the DM1 phenotype via an RNase H1 independent steric blocking mechanism (Klein et al., 2019; Pantic et al., 2016).

First, to evaluate the cytotoxicity of the CPP-$(CAG)_7$ conjugates, an MTS assay (3-(4,5-dimethylthiazol-2-yl)-5-(3-carboxymethoxyphenyl)-2-(4-sulfophenyl)-2H-tetrazolium assay) for cell viability was carried out on a human renal proximal tubular epithelial cell line (HRPTEpCs) (Figure 2). This cell line was chosen due to the known association of CPP-PMOs with nephrotoxicity (Amantana et al., 2007; Gait et al., 2019), making it a relevant model for assessing potential renal toxicity (J. X. Huang et al., 2015). Cells were transfected for 48 h with increasing concentrations of CPP-PMOs ranging from 1 µM to 80 µM. After 44 h the MTS reagent for cell viability and proliferation was added with absorbance measured 4 h later at 490 nm. The results were normalized to untreated cells, which served as the control (marked in red for comparison, Figure 2).

Across the different CPP conjugates, P1.9, P3.8, DEL01, and pip6a, the cell viability generally decreased in a dose-dependent manner. At the lowest concentration of 1 µM, all CPP-$(CAG)_7$ conjugates exhibited relatively high cell viability, with no significant changes relative to untreated cells, indicating minimal cytotoxicity. As the concentrations increased, a significant reduction in cell viability was observed across all conjugates, although the extent varied by CPP. DEL01, P1.9 and P3.8 conjugates showed significantly better cell viability ($P < 0.05$) at all concentrations compared to pip6a which was confirmed as the most cytotoxic compound. At concentration of 2 µM the cell viability of DEL01, P1.9 and

P3.8 conjugates vs. pip6a-$(CAG)_7$ was 76.5%, 80.8% and 85.5% respectively, while for pip6a-$(CAG)_7$ treated cells the cell viability was 51.3%. Meanwhile at the highest concentrations tested (40 µM and 80 µM), the cell viability pip6a-$(CAG)_7$ treated cells was less than 10%, with visual inspection of the wells suggesting little or no cells present.

More pronounced differences in cell viability also emerged between DEL01 and P3.8 conjugates relative to P1.9-$(CAG)_7$ at higher concentrations (20 µM to 80 µM). DEL01 and P3.8 conjugates displayed a comparatively better profile, maintaining a cell viability of greater than 70% for all tested concentrations, while the cell viability of P1.9-CAG7 declined to less than 70% at a concentration of 10 µM (67.5% viability). At the highest concentration of 80 µM the viability of P1.9-$(CAG)_7$ cells had decreased to 47.1%, allowing the calculation of a lethal concentration 50 (LC50) of 72.79 µM. The LC50 of Pip6a-$(CAG)_7$ was 2.59 µM.

A naked $(CAG)_7$ PMO was included as a control for PMO induced cell toxicity. PMOs are usually regarded as the safest oligonucleotide chemistry due to their uncharged backbone which lack protein bindings, the main source of oligonucleotide toxicity beside sequence specific effects (Zorko & Langel, 2022). While cell viability maintained relatively high across all tested concentrations, the naked $(CAG)_7$ PMO did affect viability at higher concentrations. Promisingly however, its overall viability was similar to that of P3.8 and DEL01 conjugates, suggesting that these CPPs are exhibiting a limited toxic effect.

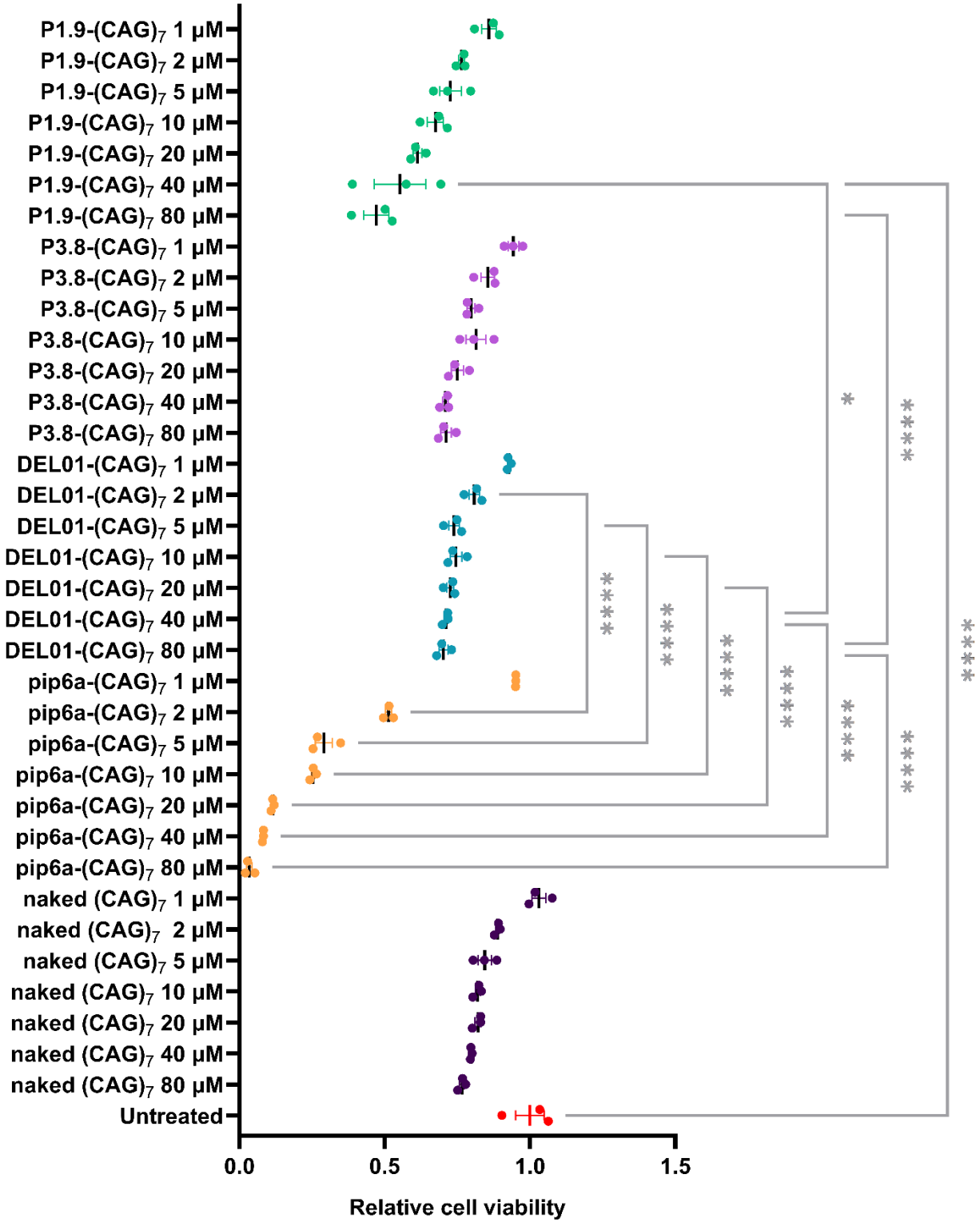

Figure *2*: Effect of CPP-PMO conjugates on human proximal tubule epithelial kidney cell viability.

Viability of HRPTEpCs treated with CPP-$(CAG)_7$ conjugates was assayed via MTS assay, 48 h after gymnotic transfection. Data are normalised to untreated cells and represented as mean ± standard error mean (S.E.M.) (n=3). Naked $(CAG)_7$ PMO and untreated control (shown in red) groups are included for comparison. Statistical analysis via one-way ANOVA corrected for multiple comparisons using Tukey's test showed significant changes ($P < 0.05$) for all treatments greater than 1 μM relative to the untreated control group. Statistically significant differences between DEL01-$(CAG)_7$ treatments and corresponding doses of other CPP-$(CAG)_7$ conjugates are denoted on the graph (*$P < 0.05$, **$P < 0.005$, ***$P < 0.0005$, ****$P < 0.0001$).

Pip6a-$(CAG)_7$ and P1.9-$(CAG)_7$ induce elevations in KIM-1 release from human renal epithelial cells

To more specifically investigate potential nephrotoxic effects of CPPs, the release of KIM-1 in HRPTEpCs was quantified following treatment with the CPP-$(CAG)_7$ conjugates (Figure 3). KIM-1 is released by kidney epithelial tubule cells (J. X. Huang et al., 2015) and is used *in vivo* as a serum and urinary biomarker of drug induced nephrotoxicity (Han et al., 2010; Vaidya et al., 2010). To assess the impact of CCP-$(CAG)_7$ conjugates on KIM-1 release, HRPTEpCs were transfected with CPP-$(CAG)_7$ conjugates via gymnosis at concentrations of 1 μM and 2 μM. The release of KIM-1 into the cell media was then quantified after 48 h via enzyme linked immunosorbent assay (ELISA). This assay is sensitive to low cell viability therefore no higher concentrations were tested, as results in Figure 2 indicated that pip6a-$(CAG)_7$ would induce too great an amount of cell loss for reliable comparison.

At 1 μM concentrations (Figure 3A), only pip6a-$(CAG)_7$ showed a significant increase in KIM-1 levels compared to the untreated control. It was found that the KIM-1 concentration in the media was 30% higher in the pip6a-$(CAG)_7$ treated group compared to untreated cells ($p < 0.0001$), indicating nephrotoxicity. At 2 μM (Figure 3B), both pip6a-$(CAG)_7$ and P1.9-$(CAG)_7$ exhibited a significant increase in KIM-1 levels compared to the untreated control group. The KIM-1 concentration in the media was approximately 32% higher for pip6a-$(CAG)_7$ ($p < 0.0001$) and 26% higher for P1.9-$(CAG)_7$ compared to untreated cells ($p < 0.0001$). Other CPP-PMOs tested at this concentration (DEL01-$(CAG)_7$ and P3.8-$(CAG)_7$) did not result in a significant elevation of KIM-1 levels, and the naked $(CAG)_7$ PMO also showed no significant changes relative to the untreated control.

These results correlate with those observed in the MTS cell viability assay (Figure 2), indicating DEL01 and P3.8 as the safest CPPs with a much-improved toxicity profiles over pip6a and additionally favourable profiles relative to P1.9.

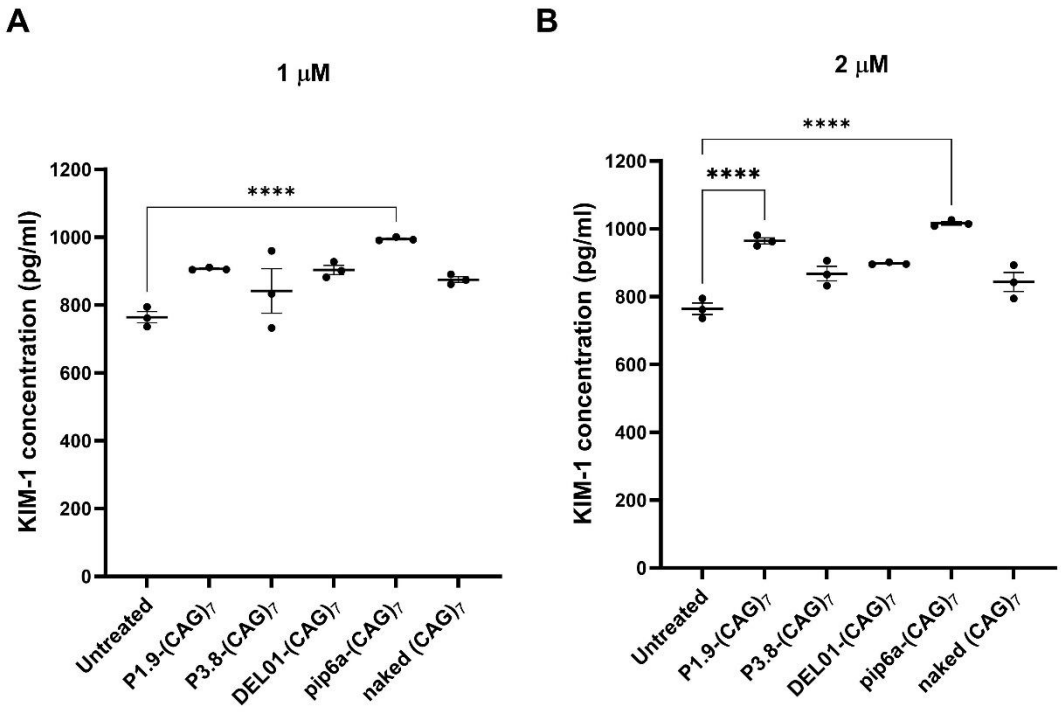

Figure *3*: Levels of KIM-1 released from CPP-PMO treated human proximal tubule epithelial kidney cells.

HRPTEpCs were transfected via gymnosis for 48 h with CPP-$(CAG)_7$ conjugates and the concentration of KIM-1 released to cell media quantified via ELISA. Cells were treated with CPP-PMO concentrations of **(A)** 1 μM and **(B)** 2 μM. A naked $(CAG)_7$ PMO treatment group and untreated group were included for comparison. Data are represented by mean ± S.E.M. (n=3) and statistical significance relative to untreated cells was determined via one-way ANOVA, corrected for multiple comparisons using Dunnett's test (*P < 0.05, **P < 0.005, ***P < 0.0005, ****P < 0.0001).

In vitro screening of CPP-$(CAG)_7$ PMOs in DM1 myoblasts corrects the DM1-specific mis-splicing phenotype

Having demonstrated that DEL01-CAG7 is less toxic than previously developed pip6a-$(CAG)_7$ and additionally P1.9-$(CAG)_7$, the *in vitro* activity of the CPP-$(CAG)_7$ PMO conjugates was next evaluated and compared in immortalised DM1 patient-derived myoblasts containing 2600 CTG repeats (Arandel et al., 2017) (Figure 4). Myoblasts were differentiated to myotubes for 7 d then transfected for 48 h with escalating concentrations of P1.9-$(CAG)_7$, P3.8-$(CAG)_7$, DEL01-$(CAG)_7$, and unconjugated $(CAG)_7$ PMO. Concentrations ranged from 1 µM– 20 µM. A 1 µM pip6a-$(CAG)_7$ treatment group was included as a positive control for activity but no higher concentration was used, given the impact of the conjugate on cell viability (Figure 2). Myoblasts from healthy individuals were also included as a wild-type (WT) control reference.

For each CPP-$(CAG)_7$ conjugate tested at escalating doses, a dose-dependent reversal of DM1 alternatively spliced was observed, with significant correction of MBNL1 dependent splicing defects in *MBNL1*, *DMD* and *SOS1* pre-mRNAs, as analysed via RT-PCR (Figure 4A-D At a dose of 20 µM, P1.9-$(CAG)_7$, P3.8-$(CAG)_7$, and DEL01-$(CAG)_7$ elicited improvements in exon inclusion and overall performed similarly to cells treated with 1 µM pip6a-$(CAG)_7$. All CPP-$(CAG)_7$ conjugates achieved near WT-levels of exon inclusion for *MBNL1* and *SOS1* mRNAs with P1.9-$(CAG)_7$ and DEL01-$(CAG)_7$ conjugates attaining a full correction in *SOS1* exon 25 inclusion. Furthermore, each CPP-$(CAG)_7$ conjugate demonstrated improved activity when compared to 20 µM treatments of naked $(CAG)_7$ PMO, lacking a peptide for cell delivery.

Improvements were also observed in the inclusion of *DMD* exon 78 and *LDB3* exon 11 treated with higher doses of DEL01, P3.8 and1.9 conjugates but to a lesser extent than 1 µM pip6a-$(CAG)_7$. Indeed, a greater level of activity for all compounds, including 1 µM pip6a-$(CAG)_7$ is required to reach WT levels of splicing inclusion for these exons.

In comparison to P1.9-$(CAG)_7$ and P3.8-$(CAG)_7$, DEL01-$(CAG)_7$ displayed less efficacy at the lower concentrations tested (1 µM – 5 µM). However, at the highest concentrations (10 µM – 20 µM), DEL01-$(CAG)_7$ exhibited the greatest correction on all mis-spliced genes.

Lastly, as DEL01-$(CAG)_7$ elicited the greatest correction on splicing of all the novel CPP-$(CAG)_7$ conjugates, a group of cells were also treated at concentration of 20 µM with DEL01 conjugated to a non-template scrambled control PMO sequence (DEL01-NTC). This treatment produced no improvement in splicing relative to untreated cells while being significantly different to DEL01-$(CAG)_7$ at 20 µM (Figure 4A-D). These results are in accordance with the PMO being the active portion of the conjugate and that peptide enhances activity by facilitating improved delivery.

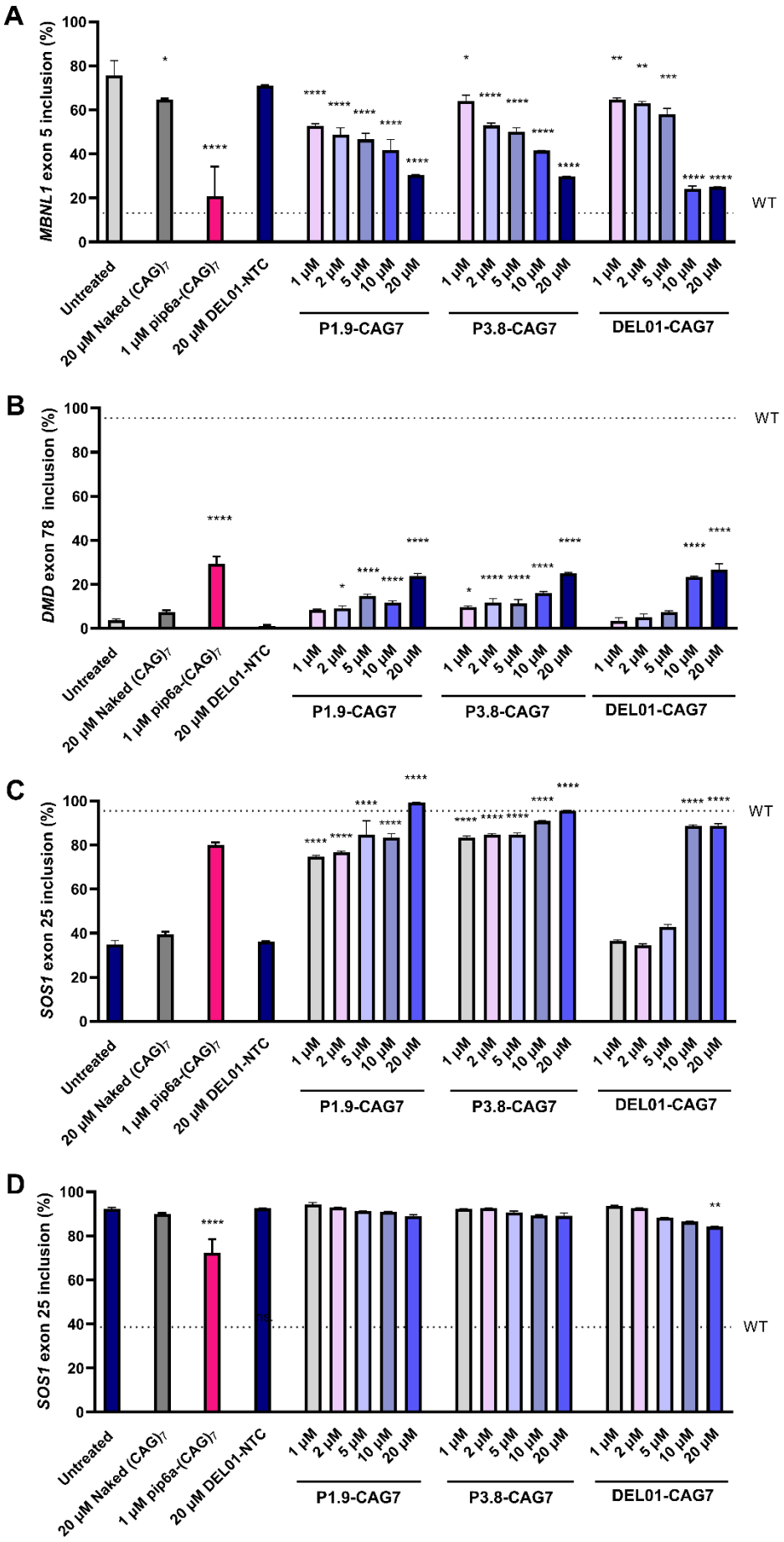
A
MBNL1 exon 5 inclusion (%)
WT
B
DMD exon 78 inclusion (%)
WT
C
SOS1 exon 25 inclusion (%)
WT
D
SOS1 exon 25 inclusion (%)
ns
WT
Untreated
20 μM Naked (CAG)7
1 μM pip6a-(CAG)7
20 μM DEL01-NTC
1 μM
2 μM
5 μM
10 μM
20 μM
P1.9-CAG7
P3.8-CAG7
DEL01-CAG7

Figure *4*: CPP-$(CAG)_7$ PMOs demonstrate partial correction of DM1-specific molecular phenotype in DM1 muscle cells.

7d-differentiated immortalized DM1 myoblasts were transfected with CPP-PMOs and harvested 48 h later. Splicing correction of key DM1-specific mis-spliced biomarkers *MBNL1* **(A),** *DMD* **(B),** *SOS1* **(C)** and *LDB3* **(D)** was quantified by RT-PCR (n = 3), demonstrating increasing splicing correction with escalating doses of candidate CPP-PMOS: P1.9-$(CAG)_7$, P3.8-$(CAG)_7$ and DEL01-$(CAG)_7$. Pip6a-$(CAG)_7$ is included as a benchmark for compound activity**.** Wild-type levels of key exon inclusion are indicated by dotted lines and all data are expressed as mean ± S.E.M. Statistical significance relative to untreated cells determined via one-way ANOVA, corrected for multiple comparisons using Dunnett's test (*P < 0.05, **P < 0.005, ***P < 0.0005, ****P < 0.0001).

DEL01-$(CAG)_7$ reduces the number of RNA *foci* and facilitates MBNL release in DM1 myoblasts

As DEL01-$(CAG)_7$ displayed improvements in efficacy over its P1.9-$(CAG)_7$ and P3.8-$(CAG)_7$ predecessors, its ability to treat RNA *foci*, a hallmark of DM1 pathology, in patient-derived differentiated myoblasts was investigated. This was carried out as part of a collaboration with the Furling group at the Institut national de la santé et de la recherche médicale (INSERM, Paris, France). Differentiated myoblasts were transfected with 10 μM and 20 μM DEL01-$(CAG)_7$ and *foci* analysed after 24 h using a combination of fluorescent in-situ hybridization (FISH) and immunofluorescence for MBNL1 protein (Figure 5). These concentrations were selected as they displayed the greatest splicing correction. The images produced reveal that 10 μM and 20 μM treatment reduces the number of *foci* in DM1 myoblasts (Figure 5B and 5C respectively) relative to untreated control DM1 myoblasts, although interestingly the size of remaining *foci* appears to increase. A reduction in co-localisation of MBNL1 and $(CAG)_7$ FISH staining also suggests the release of sequestered MBNL1 upon DEL01-$(CAG)_7$ treatment.

Overall, these results, complement the correction of splicing observed in Figure 4 and demonstrates the ability of DEL01-$(CAG)_7$ to treat the DM1 phenotype. The combination of improved efficacy over P1.9-$(CAG)_7$ and P3.8-$(CAG)_7$ with a greatly reduced toxicity profile in comparison pip6a-$(CAG)_7$ justifies exploring DEL01-$(CAG)_7$ further, as a treatment for DM1.

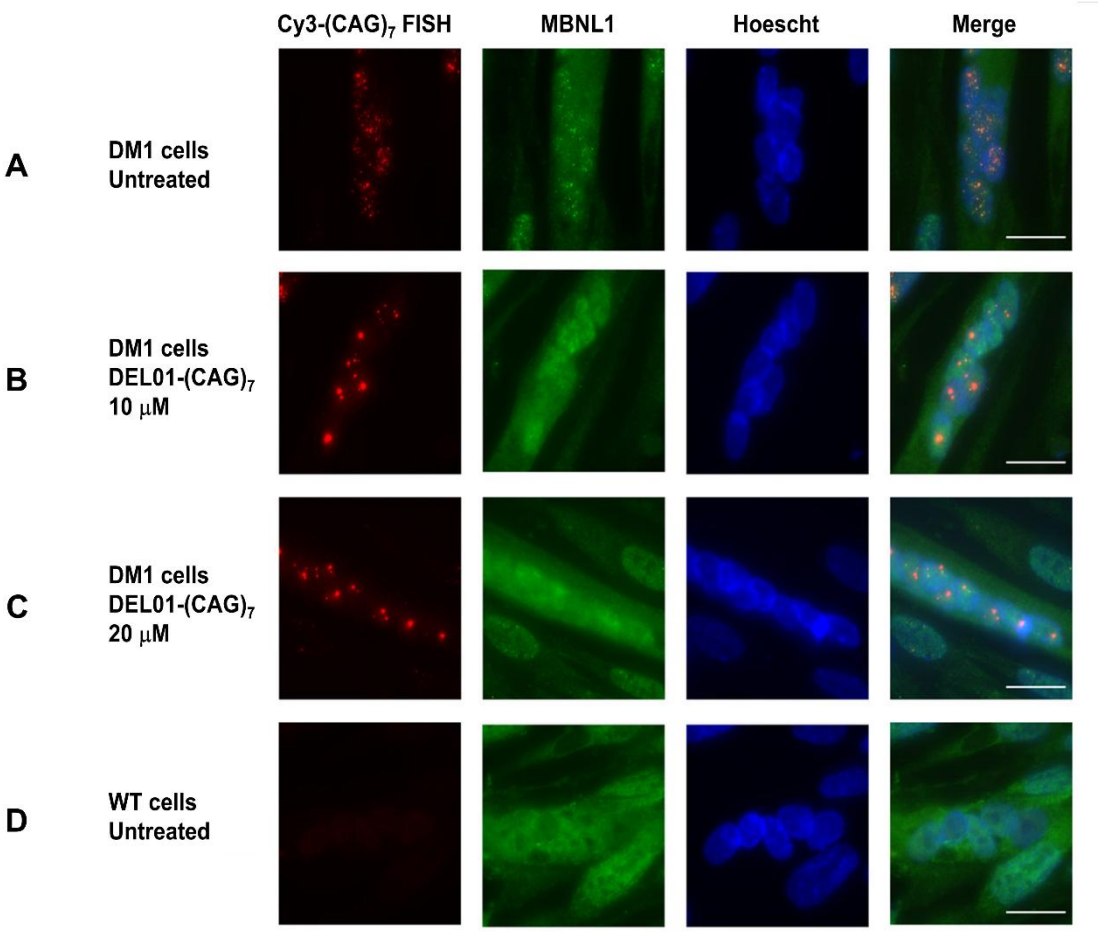

Figure *5*: Treatment with DEL01-$(CAG)_7$ reduces the number of RNA foci and MBNL1 sequestration in DM1 muscle cells.

Combined FISH (Cy3-$(CAG)_7$ (red) and immunofluorescence (MBNL1, green) in day 8 differentiated untreated **(A)** and treated **(B-C)** DM1 myoblasts and untreated WT control myoblasts **(D).** Treated cells were transfected with 10 μM **(B)** and 20 μM **(C)** concentrations of DEL01-$(CAG)_7$ on day 6 of differentiation and elicited both a reduction in the number of RNA *foci* (red) and releases sequestered MBNL1 (green) upon treatment. Scale bars: 20 μm. Data generated by collaborators at INSERM, Paris, France.

Discussion

In vitro screening of DEL01-$(CAG)_7$ demonstrates favourable toxicity relative to pip6a-$(CAG)_7$

One of the primary aims of this work was to evaluate DEL01-$(CAG)_7$ as a potential CPP-PMO for the treatment of DM1 with an improved balance of toxicity and efficacy. To this end, I performed a cell-based evaluation of DEL01-$(CAG)_7$ relative to previously developed CPP-PMO predecessors: pip6a-$(CAG)_7$, P1.9-$(CAG)_7$ and P3.8-$(CAG)_7$. A major concern in the development of PMOs and CPP-PMOs has been the associated toxicity, specifically nephrotoxicity (Amantana et al., 2007; Gait et al., 2019; Sazani et al., 2011). This was a critical issue for the development of pip6a-PMO conjugates in the Wood group, leading to the prevention of their further clinical development. Therefore, the cell toxicity of DEL01-$(CAG)_7$ was initially assessed in a human renal epithelial cell line (HRPTEpCs). Results from the MTS cell viability assay indicated that DEL01-$(CAG)_7$ exhibits a markedly reduced toxicity profile relative to pip6a-$(CAG)_7$ across all tested concentrations, and to a lesser extent, P1.9-$(CAG)_7$.

The results from the MTS assay, in line with previous findings, confirm that the strategy of reducing arginine content and peptide length successfully lowers CPP toxicity. Arginine-rich CPPs are well-documented for their potency and efficiency in cellular uptake, primarily due to the positive charge of the arginine residues, notably the guanidinium side chain, which interacts with negatively charged cell surface molecules such as phospholipids and proteoglycans (Herce et al., 2014; Lättig-Tünnemann et al., 2011; Mitchell et al., 2000; Su et al., 2009). While increased arginine content enhances cellular uptake (Futaki et al., 2001; Mitchell et al., 2000), it also contributes to increased toxicity, as demonstrated by

(Mitchell et al., 2000) where it was shown that CPPs of a shorter peptides and fewer arginine residues exhibit reduced cytotoxicity.

It is likely that a lower arginine content reduces electrostatic interactions with cell membranes, decreasing the risk of membrane destabilization and damage. Additionally, a shorter peptide length would also decrease the number of CPP-cell surface interactions. Consistent with this, DEL01 (6 arginines, 15 amino acids), displayed significantly less cell toxicity than pip6a (10 arginines, 22 amino acids) and, to a slightly less extent, P1.9 (6 arginines, 16 amino acids).

Similarly, results from the KIM-1 ELISA echo those from the MTS assay. Quantification of KIM-1 release in CPP-PMO treated HRPTEpCs revealed that while Pip6a and P1.9 conjugates triggered elevations in KIM-1 release, DEL01-$(CAG)_7$ induced no notable increase. Huang et al. (2015) utilized the same *in vivo* cell line to demonstrate that the release of KIM-1 from proximal tubule epithelial cells can effectively indicate drug-induced nephrotoxicity. Following injury, the conserved ectodomain of KIM-1 is shed from proximal tubular kidney cells, a process observed in patients (W. K. Han et al., 2002; van Timmeren et al., 2007), rodents (Ichimura et al., 1998; Prozialeck et al., 2009; Y. Zhou et al., 2008) and *in vitro* (Bailly et al., 2002). As such, KIM-1 is a well-established and specific biomarker for drug induced nephrotoxicity (W. K. Han et al., 2002; Ozer et al., 2010; Vaidya et al., 2006, 2010) with both the FDA (Federal drug agency) and EMA having qualified KIM-1 as a renal safety biomarker in drug development (Dieterle et al., 2010). Therefore, the results from this study, showing no elevation in KIM-1 following 1 µM and 2 µM DEL01-$(CAG)_7$ treatments, demonstrate a diminished impact on kidney epithelial tubule cells relative to pip6a-$(CAG)_7$.

Unfortunately, due to the high sensitivity of the KIM-1 ELISA assay to reduced cell viability, KIM-1 concentrations in media of cells subjected to higher treatment concentrations (> 2 µM) could not be reliably assessed to give an indication of dose-dependent KIM-1 release. It could be possible to circumvent this issue by quantifying KIM-1 release at an earlier time-point, before the onset of drug-induced cell death. Indeed Huang et al. (2015) show alterations in KIM-1 release following treatment with nephrotoxicants at three discrete time-points (24 h, 48 h and 72 h) showing that even a period of 24 h may be sufficient for detecting alterations in KIM-1 expression. However, determining the optimal assay time-point for the concentrations use was not possible due to patent complications preventing the further synthesis of additional P1.9-$(CAG)_7$ and P3.8-$(CAG)_7$. Consequently, insufficient material was available to conduct this experiment. Nevertheless, combined with findings from the MTS assay, these results implicate DEL01 as a safer CPP alternative to pip6a, with potential to reduce the risk of nephrotoxicity that has previously impeded clinical translation.

Another important aspect of predicting ASO toxicology is the potential off-target effects of the sequence binding to other similar RNA sequences. In the case of the PMO $(CAG)_7$ used in this study, this aspect was already described in Klein et al (2019) where RNAseq showed that despite the repetitive nature of the sequence, the effect on the expression of other genes with CTG tracks longer than seven units was limited. The steric blocking mechanism that the PMO elicits and the accumulation of mutant targets in the nuclei could sponge the effect of the ASO on other targets. Klein et al. also showed that this safety translated to *in vivo* experiments. Following three doses of pip6a-$(CAG)_7$ at 12.5 mg/kg, the number of deregulated genes with greater than seven CAG repeat tracts (fold change >2

when compared with WT mice) was reduced from seventeen to one in gastrocnemius and from 27 to four in quadriceps, two weeks after the treatment.

In vitro screening of DEL01-$(CAG)_7$ demonstrates favourable efficacy on ameliorating DM1 mis-splicing

In addition to its favourable toxicity profile, DEL01-$(CAG)_7$ demonstrated promising therapeutic efficacy in immortalised DM1 patient-derived myotubes relative to P1.9 and P3.8 conjugates. P1.9 and P3.8 are previously developed CPP alternatives to pip6a which exert improved toxicity but at the compromise of reduced efficacy. At lower concentrations (1-5 µM), DEL01-$(CAG)_7$ exhibited slightly less efficacy in correcting DM1 splicing pathology compared to P1.9-$(CAG)_7$ and P3.8-$(CAG)_7$. However, it outperformed both conjugates at the higher concentrations of 10-20 µM, concentrations where maximal improvement in molecular biomarkers was observed. Notably at these concentrations DEL01-$(CAG)_7$ achieved near WT levels of exon inclusion in *MBNL1* and *SOS1*.

The observed differences in concentration-dependent performance between the CPP-conjugates are likely due to variations in their chemical structures, which influence key pharmacodynamic properties such as cellular uptake, target engagement, and intracellular distribution. Structural differences among the CPPs, particularly their peptide lengths, could significantly affect their efficiency in cellular uptake at varying concentrations. Several studies have demonstrated that arginine-rich CPPs typically undergo cellular uptake via endocytosis at lower concentrations (< 2 µM). However, at higher concentrations (> 10 µM), their uptake shifts towards direct penetration (Duchardt et al., 2007; Fonseca et al., 2009; Madani et al., 2011).

A notable structural difference between DEL01 and its predecessors, P1.9 and P3.8, is peptide length, a characteristic known to influence cellular uptake (Futaki et al., 2001; Kamei et al., 2013; Wender et al., 2000). In general, longer peptides exhibit greater efficacy but higher toxicity, as demonstrated by the performance of pip6a-$(CAG)_7$ in these *in vitro* experiments. DEL01, with a peptide length of 14 amino acids, is shorter than P1.9 and P3.8, which have lengths of 16 and 17 amino acids, respectively. Additionally, P3.8 contains one less arginine than P1.9 and DEL01, both of which contain 6 arginines; it has been shown that CPPs containing 5 arginines or less are less efficiently up-taken than those containing 6 arginines or more (Futaki et al., 2001; Mitchell et al., 2000). These structural differences may lead to variations in cellular uptake mechanisms, with the longer P1.9 and P3.8 peptides being more efficiently taken up via endocytosis at lower concentrations (< 5 µM), likely due to their larger size which facilitates increased contact with the cell surface prior to uptake (Kamei et al., 2013). Meanwhile, DEL01 potentially exhibits superior uptake via direct penetration at concentrations of 10 µM and 20 µM, leading to its greater efficacy in correcting splicing defects. Further experiments would be required to confirm this hypothesis, as these structural differences may also affect other pharmacodynamic properties, such as intracellular engagement and endosomal release, which could contribute to the varying efficacies observed at different concentrations. However, what is clear is that at the concentrations eliciting the greatest correction of splicing biomarkers, the chemical structure of the DEL01 CPP—particularly its length and arginine content—demonstrates a refined design that offers enhanced efficacy compared to P1.9 and P3.8.

The panel of biomarkers employed to investigate conjugate efficacy: *MBNL1* exon 7, *SOS1* exon 25, *DMD* exon 78 and *LDB3* exon 11, were selected to match those used in

the previous testing of pip6a-$(CAG)_7$ by Klein et al. (2019). Results pertaining to the efficacy of 1 µM pip6a-$(CAG)_7$ treatment in patient derived myoblasts published as part of that study are consistent with the high levels of splicing correction observed in the present work. As expected, comparison of Pip6a-$(CAG)_7$ to DEL01-$(CAG)_7$ showed pip6a-$(CAG)_7$ to be more potent, achieving similar splicing correction to DEL01-$(CAG)_7$ at 1 µM concentrations versus 20 µM. However, as discussed, the MTS assay revealed DEL01-$(CAG)_7$ treatments to be significantly less toxic than pip6a-$(CAG)_7$. Therefore, the difference in potency becomes less critical, as DEL01-$(CAG)_7$ can still achieve the same therapeutic efficacy as pip6a-$(CAG)_7$, albeit at a higher dose, while maintaining cell viability and low toxicity. Therefore, despite requiring a higher dose, DEL01-$(CAG)_7$ clearly emerges as a viable and safer alternative, offering a balanced approach that combines efficacy with a significantly improved safety profile.

DEL01-$(CAG)_7$ reduces the number of nuclear *foci* in patient derived DM1 myoblasts

The therapeutic potential of DEL01-$(CAG)_7$ is further supported by its ability to reduce RNA *foci*, a hallmark of DM1 pathology. In accordance with previous results obtained in DM1 myoblasts (Arandel et al., 2017; Christou et al., 2019; Kawada et al., 2023; Klein et al., 2019; Mulders et al., 2009; Pantic et al., 2016), treatment with an ASO induced a reduction in the number of nuclear RNA *foci*, coupled with decreased co-localization of MBNL1 within CUG repeats. This indicates that DEL01-$(CAG)_7$ alleviates the sequestration of MBNL1, facilitating its displacement and relocation to the nucleoplasm. Over the years, a number of studies have demonstrated that the release of MBNL1 from nuclear *foci* is aligned with correction in MBNL1 dependent splicing defects, suggesting a restoration of

functional MBNL1 (Arandel et al., 2017; Christou et al., 2019; Klein et al., 2019; Mulders et al., 2009; Wheeler et al., 2009). The dose dependent correction of MBNL1 dependent splicing defects that were observed following treatment with DEL01-$(CAG)_7$ (Figure 4), combined with the reduction the number of RNA *foci* (Figure 5), further support this concept.

Interestingly however, while it is a well-established hypothesis that MBNL1 sequestration by RNA *foci* is a major cause of mis-splicing in DM1, more recent findings suggest that ASO binding to RNA *foci* and the subsequent reduction in *foci* may not entirely account for the observed improvements in splicing correction. Works published by El Boujnouni et al. (2023) suggested a potential disconnect between *foci* reduction and complete splicing correction, with the levels of *foci* reduction following treatment with gapmer or steric blocking ASOs being disproportionate to the levels of splicing correction achieved. These findings indicate that the therapeutic effects of ASOs, including steric blockers, are not fully explained by the current hypothesis and that further investigation is needed to truly understand the contributions of other DM1 mechanisms of pathogenesis and the impact ASO therapies may exert on them. Nevertheless, the clear effectiveness of DEL01-$(CAG)_7$ in reversing key hallmarks of DM1 pathology, including reducing *foci* and correcting aberrant splicing, underscores its potential as a promising therapeutic agent for DM1.

Overall DEL01-$(CAG)_7$ demonstrates a superior balance of efficacy and safety *in vitro*, compared to its predecessor CPP-PMO conjugates and is able to treat multiple hallmarks of DM1 pathology in *in vitro* cell models. These findings emphasize the importance of optimizing CPP sequences to enhance ASO delivery and minimize adverse effects with the long-term goal of being able to offer safer and more effective treatment option for DM1

patients. Overall, these data strongly supported the continued development of DEL01-$(CAG)_7$ and *in vivo* as a promising candidate for DM1 therapy.

Results Chapter 2 – *In vivo* evaluation of DEL01-$(CAG)_7$ as an improved a therapy for DM1

Results

As results from the *in vitro* testing of DEL01-$(CAG)_7$ proved the compound to be a promising candidate for the treatment of DM1, I have endeavoured to further evaluate its potential *in vivo*. In this chapter I evaluate the therapeutic reach, efficacy and toxicity of DEL01-$(CAG)_7$, using two separate animal models of DM1: the HSA-LR model, which harbours a severe skeletal muscle phenotype and the DMSXL model that allows for the added determination of compound efficacy in CNS and heart tissues. Animals were treated in groups comprised of equal numbers of male and females, as previous experiments within the Wood group have shown no difference in disease phenotype between sexes. The CPP-PMOs, P1.9-$(CAG)_7$ and P3.8-$(CAG)_7$ were investigated no further as a result of their licensing to PepGen.

Novel CPP, DEL01, enhances the therapeutic window and reach of $(CAG)_7$ in HSA-LR mice, relative to previously developed CPPs

DEL01-$(CAG)_7$ was first tested *in vivo* using the HSA-LR mouse model. This DM1 mouse model expresses a 250 CTG repeat expansion in the 3'UTR of a human skeletal actin transgene, *ACTA1*, giving rise to ribonuclear *foci* and subsequent MBNL1 sequestration and mis-splicing events in skeletal muscles only (Mankodi et al., 2000). Additionally, HSA-

LR mice display hind-limb myotonia, a disease phenotype also present in the skeletal muscles of DM1 patients (Harper, 2001).

With the goal of assessing the therapeutic window of DEL01-$(CAG)_7$, mice were treated at 8-10 weeks of age, 4 weeks after disease phenotype onset, via single intravenous tail vein injections (Figure 6A) with a range of escalating doses (5 mg/kg, 7.5 mg/kg, 30 mg/kg and 40 mg/kg). Urine, serum and tissues were then collected for assessment (Figure 9A). A group treated with the previously tested 7.5 mg/kg of pip6a-$(CAG)_7$ (Klein et al., 2019) was included as a benchmark for efficacy and a group treated with 30 mg/kg DEL01-NTC were also included as a non-targeting control. The dose of 30 mg/kg was selected for DEL01-NTC as the 30 mg/kg dose of DEL01-$(CAG)_7$ displayed the greatest activity for this conjugate (Figure 6B). An additional group of mice were treated using a multiple dosing strategy (Figure 6B) of four biweekly tail vein administrations of 7.5 mg/kg DEL01-$(CAG)_7$ as several studies have reported that multiple dosing of ASOs can confer greater phenotypic improvements than single dose strategies (Hammond et al., 2016; Hua et al., 2011; Nizzardo et al., 2014; H. Zhou et al., 2015).

Administration of DEL01-$(CAG)_7$ in HSA-LR mice reverses the functional and molecular DM1 phenotype

To gain an initial read out of compound efficacy, the ability of DEL01-$(CAG)_7$ doses to functionally improve the DM1 phenotype in HSA-LR mice was tested. Hind limb myotonia was assessed weekly from the point of initial injection until tissues were harvested using a scoring system (Figure 6C). A score of 4 represents severe myotonia, while a score of 0 corresponds to a mouse displaying no evidence of myotonia. Mice receiving treatments of

7.5 mg/kg pip6a-$(CAG)_7$, 30 mg/kg DEL01-$(CAG)_7$ and 40 mg/kg DEL01-$(CAG)_7$ showed complete and sustained reversal of myotonia 7 d after treatment. Meanwhile animals in the four biweekly 7.5 mg/kg DEL01-$(CAG)_7$ treatment group showed scoring demonstrating complete myotonia reversal from 14 d post initial injection. No improvement in splicing defects or myotonia was observed upon treatment with non-template PMO controls and no improvement or extremely mild and short-lasting effects, were observed following all other treatments.

As previously observed in the DM1 cell model, evaluation of compound efficacy via the splicing analysis of key DM1 skeletal muscle biomarkers *Mbnl1, Clcn1, Ldb3* and *Atp2a1* (Figure 7A-D), demonstrates that DEL01-$(CAG)_7$ is able to reverse the mis-splicing events observed in untreated HSA-LR mice 14 d post-treatment, in a dose dependent manner, in both gastrocnemius and quadriceps. Lower doses of 5 mg/kg and 7.5 mg/kg of DEL01-$(CAG)_7$ produced little or minimal effects on splicing, contrasting with the activity at 7.5 mg/kg of the highly potent and active pip6a-$(CAG)_7$. However, higher doses of 30 mg/kg and 40 mg/kg were significantly effective in fully ameliorating mis-splicing to near wild-type levels. Interestingly, either the 30 mg/kg dose appeared to perform better or there was little difference between these two highest doses. This suggests that at a dose of 40 mg/kg the therapeutic of DEL01-$(CAG)_7$ window has been surpassed and indicates a single administration of 30 mg/kg to be the optimum dosing strategy.

Similarly, to the *in vitro* experiments, administration of 30 mg/kg DEL01-NTC exhibited no significant effect on splicing in any muscle or biomarker, confirming changes in splicing are caused by the PMO moiety of the CPP-PMO conjugate. Meanwhile, comparison to a data set provided by Miguel Varela (Wood Group) for age-matched HSA-LR mice treated with 200 mg/kg naked $(CAG)_7$ (included in Figure 7), showing no significant mis-splicing

correction, demonstrates that while DEL01 is not the active portion of DEL01-$(CAG)_7$, it is key in facilitating PMO cellular delivery and therefore, indirectly, compound activity.

Applying a multiple dosing strategy of four biweekly doses of 7.5 mg/kg DEL01-$(CAG)_7$ showed a marked improvement in activity for each splicing biomarker, relative to a single 7.5 mg/kg dose. Conversely this regime appeared less effective than a single 30 mg/kg dose.

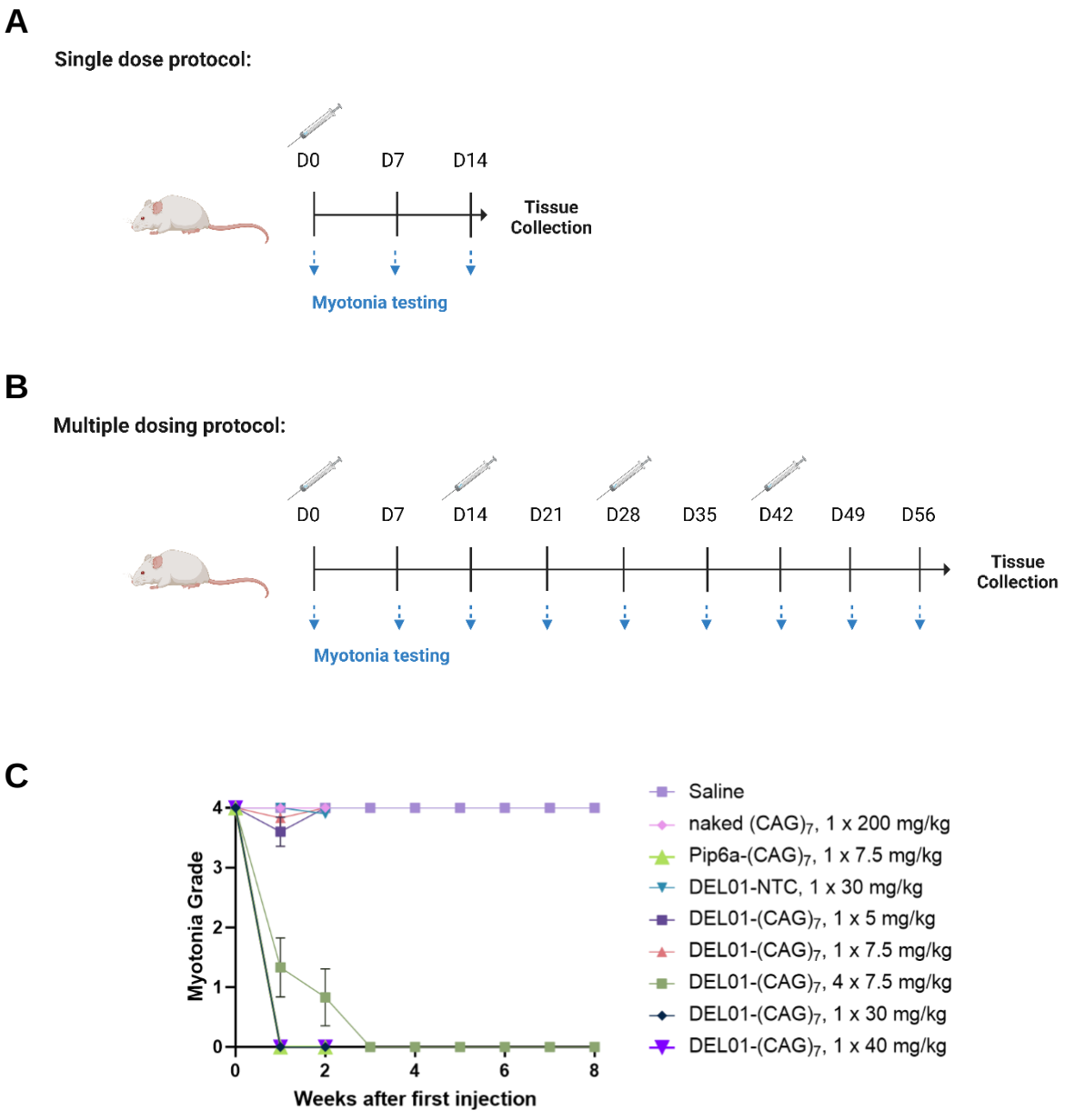

Figure *6*: Functional assessment CPP-PMO treatment activity in DM1, HSA-LR mice.

(A-B) Diagram of study designs. HSA-LR mice were injected with **(A)** a single or **(B)** four bi-weekly treatments of naked $(CAG)_7$, CPP-$(CAG)_7$ conjugates or 0.9% saline via tail vein injection (n=4-5 per treatment group). Myotonia was assessed weekly, and tissues

harvested 14 d post-final administration for analysis. **(C)** Scoring of myotonia in CPP-PMO and naked $(CAG)_7$ treated HSA-LR mice, data are expressed as mean ± S.E.M with 1 x 7.5 pip6a-$(CAG)_7$, 4 x 7.5 mg/kg DEL01-$(CAG)_7$, 1 x 30 mg/kg DEL01-$(CAG)_7$ and 1 x 40 mg/kg DEL01-$(CAG)_7$ treatment regimens being statistically significant from 0.9% saline–treated group, $P < 0.0001$ (log-rank [Mantel-Cox] test). Myotonia scoring was stopped 14 d post final treatment administration.

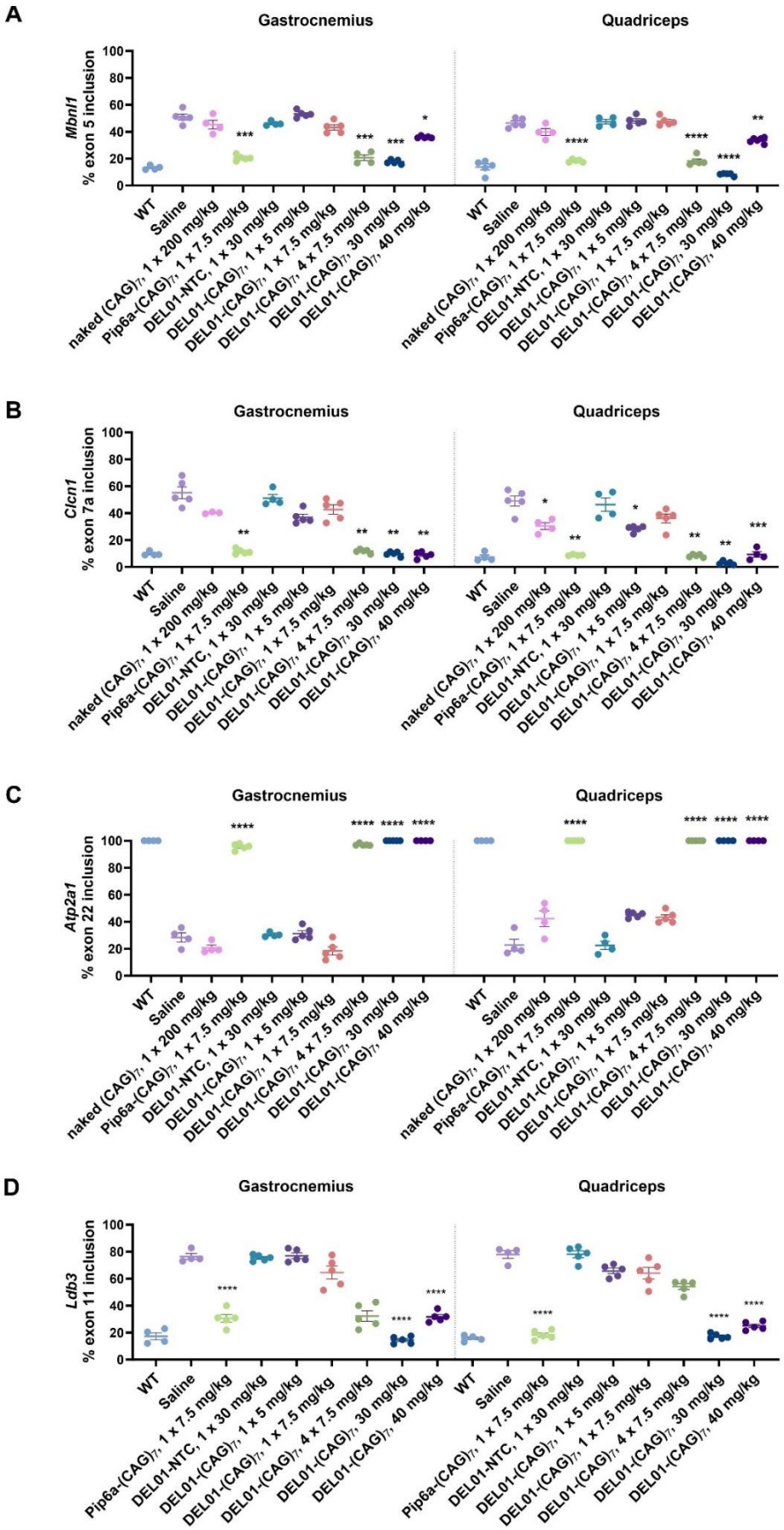
A
Gastrocnemius
Quadriceps
Mbnl1
% exon 5 inclusion
B
Clcn1
% exon 7a inclusion
C
Atp2a1
% exon 22 inclusion
D
Ldb3
% exon 11 inclusion
WT
Saline
naked (CAG)7, 1 x 200 mg/kg
Pip6a-(CAG)7, 1 x 7.5 mg/kg
DEL01-NTC, 1 x 30 mg/kg
DEL01-(CAG)7, 1 x 5 mg/kg
DEL01-(CAG)7, 1 x 7.5 mg/kg
DEL01-(CAG)7, 4 x 7.5 mg/kg
DEL01-(CAG)7, 30 mg/kg
DEL01-(CAG)7, 40 mg/kg

Figure 7: Functional assessment of the activity of CPP-PMO treatment upon skeletal muscle mis-splicing in DM1, HSA-LR mice.

HSA-LR mice were injected with a single or multiple bi-weekly treatments of naked $(CAG)_7$, CPP-$(CAG)_7$ conjugates or 0.9% saline via tail vein injection (n=4-5 per treatment group). Tissues were harvested 14 d post-final administration. Quantification of splicing correction was performed via real-time polymerase chain reaction (RT-PCR) in key DM1 skeletal muscle biomarkers: **(A)** *Mbnl1*, **(B)** *Clcn1*, **(C)** *Atp2a1* and **(D**) *Ldb3* in gastrocnemius and quadriceps. The data set for 1 x 200 mg/kg naked $(CAG)_7$ was provided by Miguel Varela from the Wood group. Data are expressed as mean ± S.E.M. and each dot represents a biological replicate. Statistical significance was determined via one-way ANOVA, corrected for multiple comparisons using Tukey's test. Significance relative to saline treated animals is displayed via representative P-values: *P < 0.05, **P < 0.005, ***P < 0.0005, ****P < 0.0001.

Administration of DEL01-$(CAG)_7$ enhances PMO distribution to critically affected DM1 tissues, beyond the skeletal muscles

While the skeletal muscles are greatly impacted in the pathology of DM1, heart and CNS tissues are also critically affected and display disease pathology in patients and considered major therapeutic targets for many drugs in development (De Serres-Bérard et al., 2022; Stoodley et al., 2023). As HSA-LR mice only carry the repeat expanded *ACTA1* transgene in skeletal muscles, it is not possible to assess compound activity in tissues beyond the skeletal muscles. Therefore, to give an indication of the potential therapeutic reach of DEL01-$(CAG)_7$ relative to other CPP-PMO, PMO concentration were quantified via ELISA, 14 d post treatment, in skeletal muscle, heart and brain cortex (Figure 8A-8C, respectively). PMO concentrations were also quantified in kidney and liver (Figure 8D-8E), tissues known to accumulate PMOs (Amantana & Iversen, 2005). As before, a data set for mice treated with 200 mg/kg $(CAG)_7$ is included for reference as an unconjugated PMO control. Lastly, for this assay an additional data set, kindly provided by Miguel Varela, from mice treated with an 80 mg/kg dose of R6GLY-$(CAG)_7$ is included. R6Gly is a peptide tested in a Phase II Clinical Trial of a CPP-PMO in Duchenne muscular dystrophy patients (Sarepta therapeutics, NCT04004065) and therefore serves as a delivery benchmark to skeletal muscles and heart.

Overall, comparison to the 200 mg/kg naked $(CAG)_7$ data set showed that DEL01 conjugation enhances PMO tissue delivery into skeletal muscle, heart and brain cortex, in a largely dose-dependent manner that correlates with splicing activity (Figure 7). The exception to this was the 40 mg/kg DEL01-$(CAG)_7$ dose which produced lower PMO tissues concentrations than the 30 mg/kg dose, however this again correlates with the patterns observed in splicing activity. Consequently 30 mg/kg was considered the optimum

dose of DEL01-$(CAG)_7$ for delivery into critically affected tissues, achieving the highest PMO tissue concentrations.

In comparison of DEL01-$(CAG)_7$ against other CPP-$(CAG)_7$ conjugates, DEL01-$(CAG)_7$ outperformed R6Gly-$(CAG)_7$, despite a lower administered dose (30 mg/kg vs. 80 mg/kg respectively). DEL01 facilitated PMO concentrations of 3433 ± 376.4 pM in skeletal muscle and 2384 ± 618.7 pM in heart vs. 2488 ±311.0 pM and 652 ± 141.9 pM, respectively for R6Gly-$(CAG)_7$ treated mice. This indicates DEL01 as a superior vehicle for PMO delivery into tissues. With regards to the pip6a CPP, at 7.5 mg/kg, pip6a was able to deliver more PMO into all tissues than the DEL01 conjugate administered at the same dose. This was anticipated given its known potency and the higher splicing activity it also achieves.

Delivery to the brain cortex for all CPP-PMO conjugates was relatively limited. PMO concentrations for 200 mg/kg naked PMO, 80 mg/kg R6Gly-$(CAG)_7$, 30 mg/kg DEL01-NTC, 5 mg/kg DEL01-$(CAG)_7$ and 7.5 mg/kg DEL01-$(CAG)_7$ were undetectable. However, encouragingly higher DEL01-$(CAG)_7$ doses achieved quantifiable delivery into the brain, demonstrating that it is possible to deliver DEL01-$(CAG)_7$ to all key affected DM1 tissues.

As expected, the highest levels of PMO for each dosing regimen were detected in the kidneys followed by liver (Figure 8D-8E). R6Gly-$(CAG)_7$ treated animals had the PMO concentration in these tissues (944.33 ± 78.41 nM for kidney and for liver 27.12 ± 7.90 nM), followed by the 30 mg/kg DEL01-$(CAG)_7$ treatment group (780.91 ± 114.67 nM and 38.48 ± 2.18 nM, respectively). As a result, it was subsequently important to investigate any potential nephrotoxicity or hepatotoxicity associated with higher doses DEL01-$(CAG)_7$.

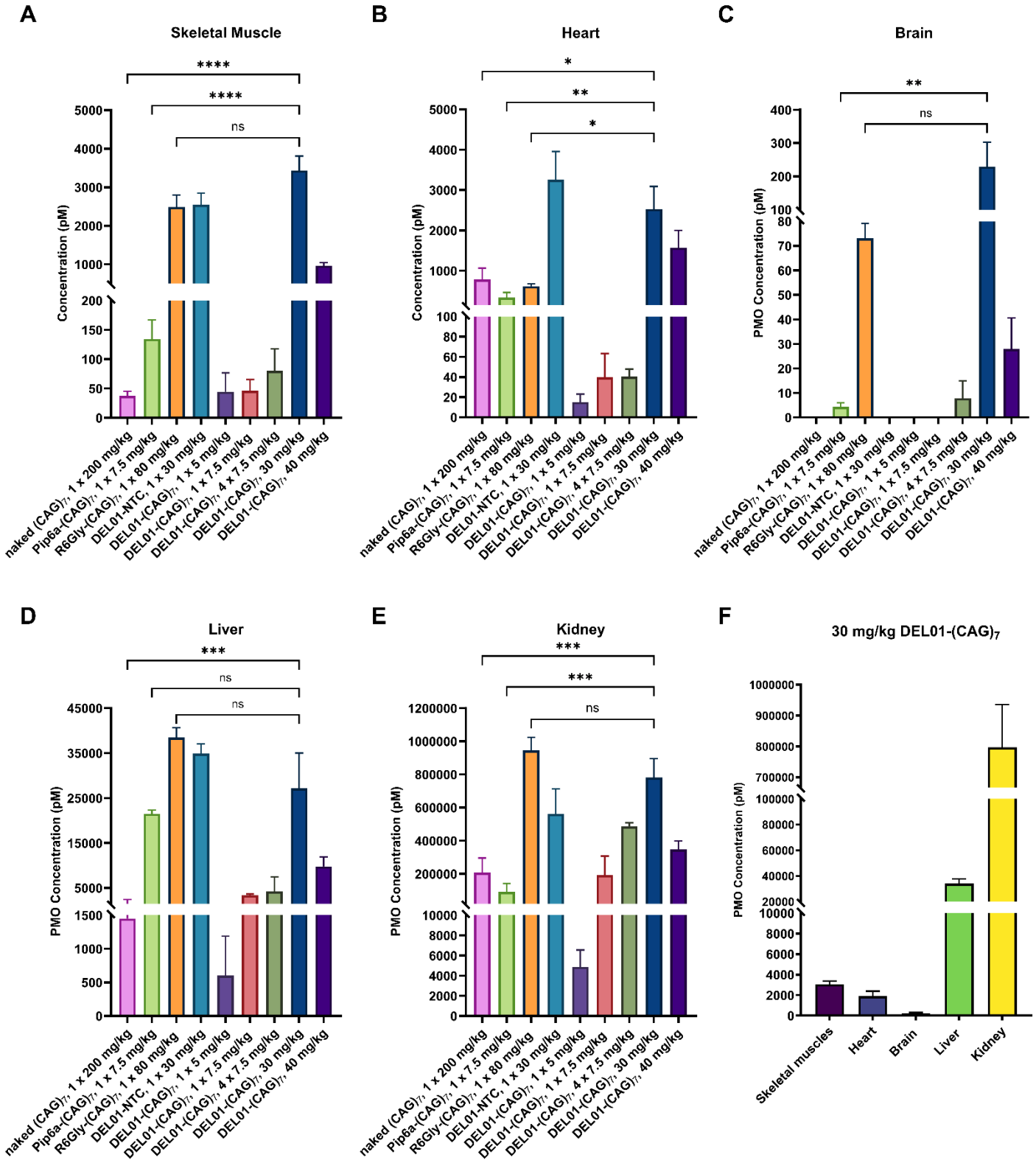

Figure *8*: Tissue biodistribution of CPP-PMO conjugates in DM1, HSA-LR mice.

Animals were injected with a single or multiple bi-weekly treatments of naked $(CAG)_7$ or CPP-$(CAG)_7$ conjugates (n=4-5). Tissues were collected 14 d post-final administration and PMO concentration quantified in **(A)** skeletal muscles, **(B)** heart, **(C)** brain, **(D)** liver and **(E)** kidney via ELISA. **(F)** Overall tissue biodistribution pattern of PMO concentration in mice treated with an optimum treatment regime of single intravenous administration of 30 mg/kg DEL01-$(CAG)_7$. All data are expressed as mean ± S.E.M. and analysed via one way ANOVA, corrected for multiple comparisons using Tukey's test (*P ≤ 0.05; **P ≤ 0.01; ***P ≤ 0.001, ****P ≤ 0.0001). Data sets for naked 200 mg/kg naked $(CAG)_7$ and 80 mg/kg R6Gly-$(CAG)_7$ were kindly provided by Miguel Varela from the Wood Group.

DEL01-$(CAG)_7$ reduces nephrotoxicity in HSA-LR mice

To investigate the toxicological profile of DEL01-$(CAG)_7$, terminal serum and urine 2 d and 7 d post- single or final administration, were collected from treated animals (see Figure 9A for experimental timeline) and analysed for markers of toxicity and changes in key metabolites (Figure 9). To evaluate CPP-PMO conjugate induced kidney toxicity, the urinary concentration of KIM-1 in treated mice was measured via ELISA and normalised to creatinine (Figure 9B). For all dosing regimen of DEL01-$(CAG)_7$ at 30 mg/kg or less, relative levels of KIM-1 at d 2 were no greater than 0.35 ± 0.16 (DEL01-$(CAG)_7$ 30 mg/kg) and significantly reduced when compared to the pip6a-$(CAG)_7$ (28.68 ± 10.05) and R6Gly-$(CAG)_7$.(1.01 ± 0.39) at doses of 7.5 mg/kg and 80 mg/kg respectively. Furthermore, any treatment induced elevation in KIM-1 levels was returned to untreated levels 14 d post-administration, overall showing DEL01 to be a safer CPP conjugation option.

Serum calcium (Figure 9C) was also measured; it has been observed within the Wood group in previous experiments that CPPs can elicit an effect on this metabolite. Changes in serum calcium can be an indicator of kidney disease, with hypocalceamia being associated with poor renal outcomes (Lim et al., 2014; Nakamura et al., 2024). The data here shows that R6Gly-$(CAG)_7$, the clinical benchmark peptide conjugate, does indeed alter urinary calcium levels, demonstrating a 56.9% decrease relative to saline treated control animals. DEL01-$(CAG)_7$, on the other hand, did not cause any deviation in calcium levels. Moreover, analysis of creatinine in the terminal serum (Figure 9D), another biomarker of kidney damage (Perrone et al., 1992), showed no change with DEL01-$(CAG)_7$ treatment, furthering the case for a safe toxicological profile.

To detect potential liver toxicity, levels of biomarkers commonly used for liver function tests (Giannini et al., 2005): aspartate transaminase (AST) alanine transaminase (ALT) and

alkaline phosphatase (ALP) (Figure 9E-9G respectively), were evaluated in terminal serum. With the exception of a 30.0% decrease in ALP levels upon 7.5 mg/kg DEL01-$(CAG)_7$ treatment, relative to the saline control group, no significant changes were detected for any other treatment group. It is also important to note that data was not collected for KIM-1 levels of DEL01-$(CAG)_7$ and serum calcium of DEL01-$(CAG)_7$ at doses of 7.5 mg/kg and 40 mg/kg respectively, due to insufficient sample collection volumes. However, given that the 30 mg/kg DEL01-$(CAG)_7$ treatment group shows the greatest splicing activity and penetration into key tissues, it is the toxicological profile of mice from this treatment group which is of the greatest interest and most value.

Lastly, kidney and liver samples from animals treated at high doses of 30 mg/kg and 40 mg/kg DEL01-$(CAG)_7$ (n=6) were submitted for histopathological analysis. Several mild structural variations were denoted but these were consistent with the usual patterning of spontaneous background findings in saline treated control mice (Table 1). Overall, no structural changes associated with the onset of hepatotoxicity or nephrotoxicity could be reported, confirming the promising safety profile of DEL01-$(CAG)_7$ suggested by the serum and urine analysis.

	Saline								DEL01-$(CAG)_7$ 30 mg/kg					DEL01-$(CAG)_7$ 40 mg/kg				
Liver	Male			Female					Male			Female		Male			Female	
mononuclear cells infiltration	1f	-	-	1m	-	-	1m	1f	1f	-	-	1f	-	-	1f	1f	1f	-	1f
hepatocyte vacuolation	-	-	-	-	-	-	-	-	-	-	-	-	-	-	-	-	-	-	-
hepatocellular cytoplasmic rarefaction	-	-	-	-	-	-	-	-	-	-	-	-	-	-	-	-	-	-	-
hepatocyte hypertrophy	-	-	-	-	-	-	-	-	-	-	-	-	-	-	-	-	-	-	-
hepatocellular inclusion	-	-	-	-	-	-	-	-	-	-	-	-	-	-	-	-	-	-	-
hepatocellular necrosis	-	-	1f	-	-	1m	-	-	-	-	-	-	-	1f	-	-	-	1f	-
Kidney																			
mononuclear cells infiltration	-	-	-	1f	-	-	-	-	1f	-	-	-	1f	-	-	-	-	-	-
tubular basophilia	-	-	-	-	-	-	-	-	-	-	-	-	-	-	-	-	-	-	-
tubular proteinuria	-	-	-	-	-	-	-	-	-	-	-	-	-	-	-	-	-	-	-
tubular hydropic degeneration	-	-	-	-	-	-	-	-	-	-	-	-	-	-	-	-	-	-	-
tubular pigment	-	-	-	-	-	-	-	-	-	-	-	-	-	-	-	-	-	-	-
tubular swelling and dilation	-	-	-	-	-	-	-	-	-	-	-	-	-	-	-	-	-	-	-

Table *1*: Histopathological assessment of HSA-LR mouse liver and kidney tissues 14 d post-administration of 30 mg/kg or 40 mg/kg DEL01-$(CAG)_7$.

Structural abnormalities were graded for severity from 1-4 and distribution noted. Grading is denoted as follows: 1, minimal; 2, mild, 3, moderate, 4, marked, with a distribution of focal, multifocal, or diffuse. Distribution of abnormality in tissues is noted as follows: f, focal; m, multifocal; d, diffuse. "-"denotes that no abnormalities were documented. N=6 per treatment group.

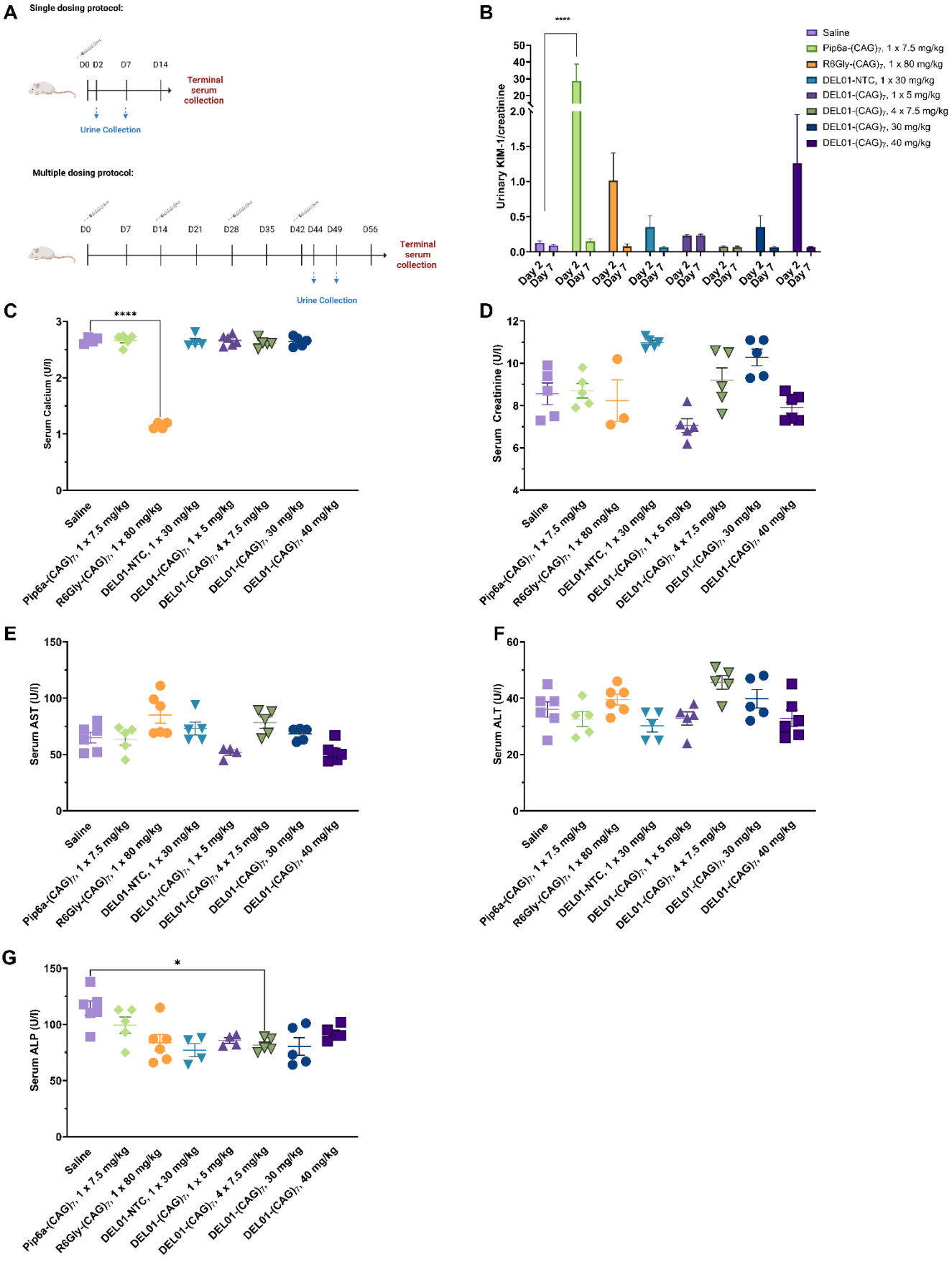
A
Single dosing protocol:
D0 D2 D7 D14
Terminal serum collection
Urine Collection
Multiple dosing protocol:
D0 D7 D14 D21 D28 D35 D42 D44 D49 D56
Terminal serum collection
Urine Collection
B
****
Urinary KIM-1/creatinine
Day 2
Day 7
Saline
Pip6a-(CAG)7, 1 x 7.5 mg/kg
R6Gly-(CAG)7, 1 x 80 mg/kg
DEL01-NTC, 1 x 30 mg/kg
DEL01-(CAG)7, 1 x 5 mg/kg
DEL01-(CAG)7, 4 x 7.5 mg/kg
DEL01-(CAG)7, 30 mg/kg
DEL01-(CAG)7, 40 mg/kg
C
****
Serum Calcium (U/l)
D
Serum Creatinine (U/l)
E
Serum AST (U/l)
F
Serum ALT (U/l)
G
*
Serum ALP (U/l)

Figure *9*: Toxicological Assessment of CPP-PMOs in DM1, HSA-LR mice.

(A) Diagram of study designs. HSA-LR mice were injected with a single or multiple bi-weekly treatments of naked $(CAG)_7$, CPP-$(CAG)_7$ conjugates or 0.9% saline via tail vein injection (n=5). Urine was collected 2 d and 7 d (urine) post-final administration and **(B)** urinary KIM-1 levels quantified via ELISA and normalised to urinary creatinine levels. Terminal serum was collected 14 d post final administration and levels of key serum metabolites **(C)** calcium, **(D)** creatinine, **(E)** AST, **(F)** ALT and **(G)** ALP were analysed via a clinical chemistry analyzer at Harwell MRC, UK. All data are expressed as mean ± S.E.M., with each data point representing a biological replicate. Statistical significance was determined via one-way ANOVA, corrected for multiple comparisons using Dunnett's test (*P < 0.05, **P < 0.005, ***P < 0.0005, ****P < 0.0001) and outliers removed using Grubb's test for outliers.

Treatment of DMSXL mice with DEL01-$(CAG)_7$ shows enhanced delivery to key tissues targets but no phenotypic correction

As the HSA-LR mouse model only allows for the testing of compound activity in skeletal muscles but DM1 also critically affects cardiac and CNS tissues, the potential of DEL01-$(CAG)_7$ as a preclinical candidate for DM1 was further evaluated using the DMSXL, DM1 mouse model, which displays mild mis-splicing phenotype in heart, CNS, and skeletal muscle tissues (Huguet et al., 2012). This was done in collaboration with the Furling / Gourdon group at INSERM, Paris, owners and experts of this mouse model.

Given that DMSXL mice are notoriously difficult to treat, with previous experiments employing pip6a-$(CAG)_7$ showing that doses effective in phenotypic correction in the HSA-LR model were ineffective in DMXSL mice, an increased dosing strategy of 50 mg/kg DEL01-$(CAG)_7$, administered via biweekly tail vein injections (Figure 10A), was selected to maximize the potential therapeutic impact. This approach led to effective tissue penetration, as demonstrated by PMO concentrations in skeletal muscle, heart, brain cortex, liver, and kidney tissues (Figure 11A). These distribution patterns were consistent with those observed in HSA-LR mice treated with 30 mg/kg of DEL01-$(CAG)_7$ (Figure 8F). Notably, DEL01-$(CAG)_7$ achieved strong delivery into critical tissues affected by DM1, including the heart and skeletal muscle (782.6 ± 138.1 pM, and 2382.0 ± 305.1 pM, respectively). This PMO concentration in muscle has been previously associated with the complete recovery of the disease phenotype in HSA-LR (Klein et al., 2019). A PMO concentration of 497.2 ± 63.15 pM was also detectable in the frontal cortex.

Despite successful delivery, phenotypic analysis post-treatment revealed no significant improvement of the DM1 pathology. Weight measurements, taken before and after the treatment period, showed no significant changes in growth for male or female DMSXL

mice compared to saline-treated controls (Figure 10B). Additionally, grip strength tests performed on forelimbs and hindlimbs, similarly indicated no improvement in muscle strength following DEL01-$(CAG)_7$ treatment (Figure 10C-10D).

At the molecular level, relative quantification h*DMPK* and m*Dmpk* transcript levels via real time quantitative polymerase chain reaction (RT-qPCR) in the heart, tibialis anterior (TA) muscle, and brain frontal cortex did not show any significant reduction in CUG repeat-expanded mRNA after treatment with DEL01-$(CAG)_7$ (Figure 11B-C). Furthermore, splicing correction analysis for key DM1 biomarkers, *Fermt2* exon 4a*, Itg6a* exon 27, and *Sorbs1* exons 6 and 27 (as described by Dincã et al., 2022), revealed no significant splicing correction in any of the tested tissues (Figure 11D-G).

Overall, while DEL01-$(CAG)_7$ successfully penetrated target tissues, it failed to produce therapeutic effects in terms of molecular or functional phenotypic improvement in DMSXL mice. The significance of this finding will be explored in more detail in the discussion section.

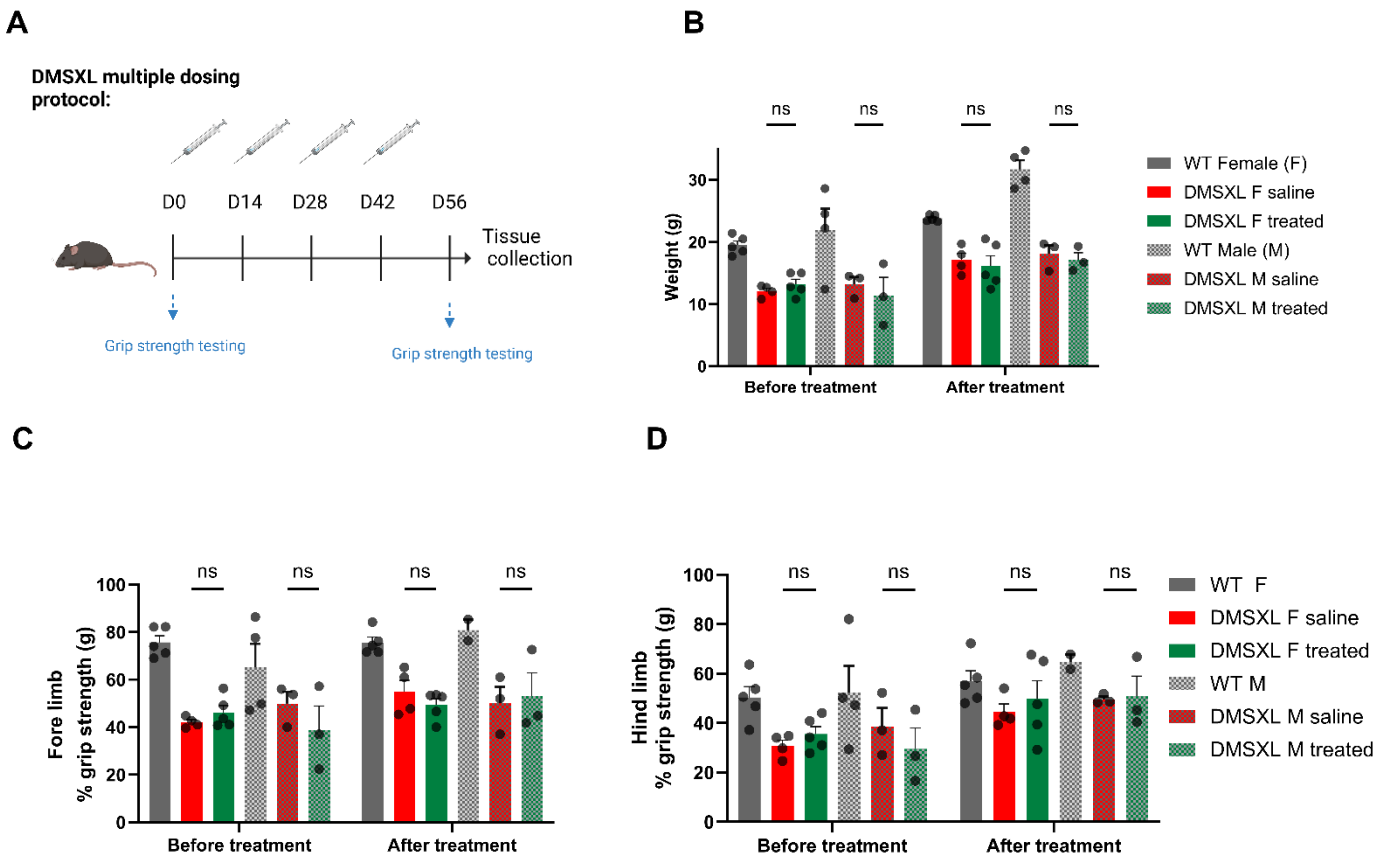

Figure *10*: Functional and observational assessment of DEL01-(CAG)7 treated DMSXL mice.

(A) Experimental timeline: DMSXL mice were administered four 50 mg/kg biweekly tail vein injections of DEL01-$(CAG)_7$ or 0.9% saline, at a dose of 50 mg/kg (n=8). Weights of mice **(B)** were recorded immediately before and 14 d after the final injection. **(C-D)** Grip strength was measured in both **(C)** forelimbs and **(D)** hindlimbs front legs before and after the treatment protocol in male, M, and female, F, animals, showing no improvement post treatment. All data are expressed as mean ± S.E.M. and each dot represents a biological replicate. Statistical comparison between sex-specific saline and DEL01-$(CAG)_7$ treatment groups was determined via students t test, showing no significance (ns) in any data set (ns

>0.05). Data in figure generated by collaborators in the Furling group at INSERM, Paris, France.

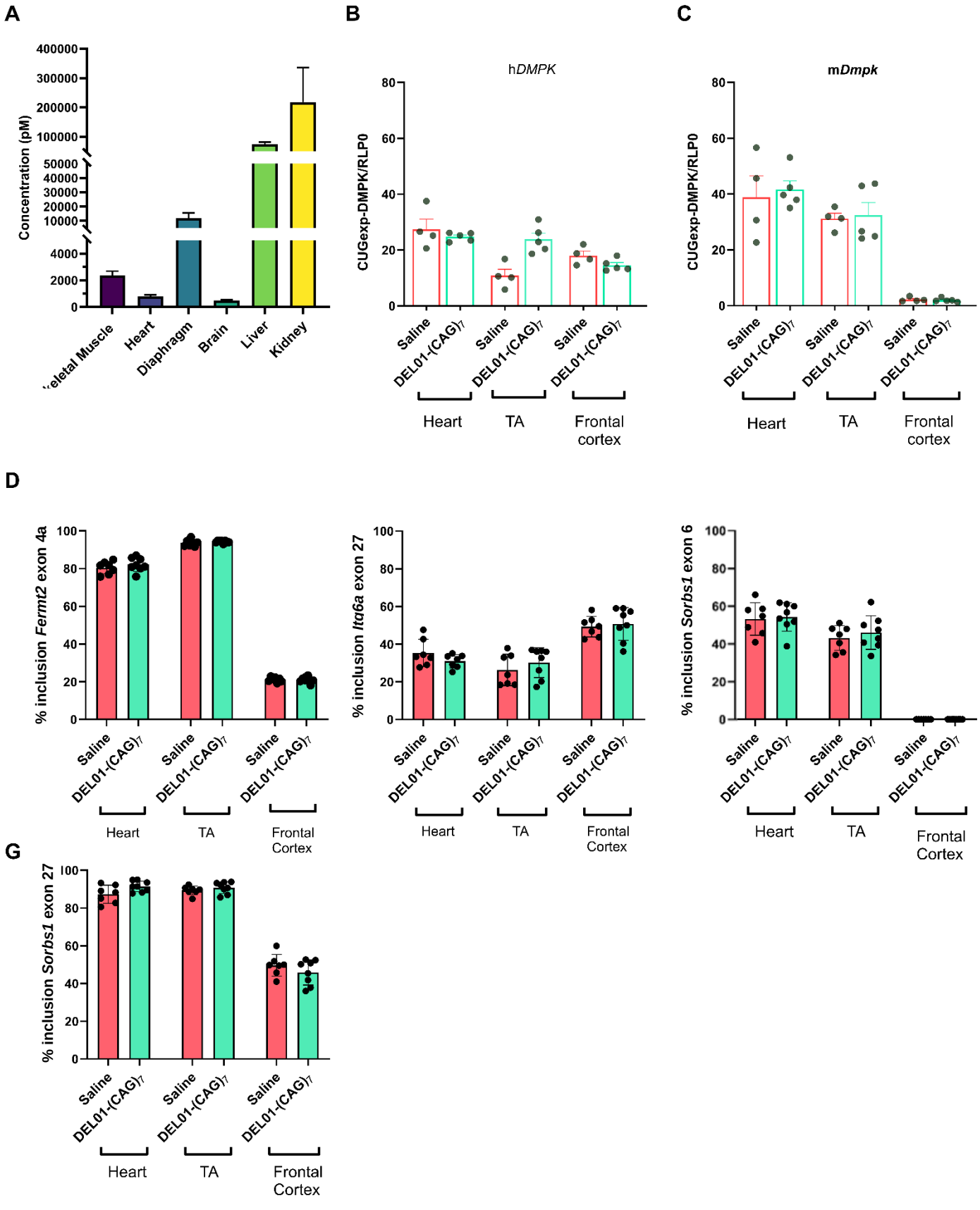
A
B
C
D
G
Concentration (pM)
Heart
Diaphragm
Brain
Liver
Kidney
hDMPK
mDmpk
CUGexp-DMPK/RLP0
Saline
DEL01-(CAG)7
Heart
TA
Frontal cortex
% inclusion Fermt2 exon 4a
% inclusion Ita6a exon 27
% inclusion Sorbs1 exon 6
% inclusion Sorbs1 exon 27
Frontal Cortex

Figure *11*: Treatment of DMSXL mice with DEL01-$(CAG)_7$ achieves skeletal muscle delivery but fails to correct DM1 phenotype.

DMSXL mice were administered four biweekly tail vein injections of DEL01-$(CAG)_7$ at a dose of 50 mg/kg (n=8). 14 d after the final injection animals were sacrificed and tissues analysed. **(A)** ELISA analysis PMO tissue biodistribution in skeletal muscle, heart, diaphragm, brain, liver and kidney. **(B-C)** RT-qPCR quantification of CUG repeat-expanded **(B)** human *DMPK* (h*DMPK*) and **(C)** mouse CUG repeat-expanded *Dmpk* (m*Dmpk*) transcripts after saline or DEL01-$(CAG)_7$ treatment in key target tissues: heart, skeletal muscle (TA) and brain. Data are normalised to *Rlp0*. **(D-G)** Quantification of splicing correction via RT-PCR in key DM1 skeletal muscle biomarkers **(D)** *Fermt2* exon 4a, **(E)** *Itg6a* exon 27, **(F)** *Sorbs1* exon 6 and **(G)** *Sorbs1* exon 27 in key target tissues. All data are expressed as mean ± S.E.M. and each data point represents a biological replicate. Statistical comparison between saline and DEL01-$(CAG)_7$ treatment groups was determined via students t test, showing no significance (ns) in any data set (ns >0.05). Data for **(B-G)** was generated by collaborators in the Furling group at INSERM, Paris, France.

Discussion

Single 30 mg/kg dose of DEL01-$(CAG)_7$ is sufficient for reversal of DM1 phenotype in HSA-LR mice

The aim of the work this chapter was to further evaluate the potential of DEL01-$(CAG)_7$ as an improved CPP-PMO candidate for the treatment of DM1 using *in vivo* models. Firstly, treatment of HSA-LR mice with escalating doses of DEL01-$(CAG)_7$ corrected biomarkers of DM1 aberrant splicing events in a dose dependent manner. The splicing correction observed correlated to a reversal in functional myotonia, which was anticipated given that treatment corrected *Clcn1* exon 7a inclusion, a known cause of myotonia in DM1 animal models and patients (Charlet-B. et al., 2002; Mankodi et al., 2002). This supports the ability of DEL01-$(CAG)_7$ to restore splicing biomarkers to wild-type levels, reinforcing its therapeutic potential in line with previous studies on CPP-PMO efficacy in DM1 (Klein et al., 2019; PepGen, FREEDOM-DM1: NCT06185764; Vertex, NCT06185764).

A dose of 30 mg/kg dose was most effective in correcting the DM1 skeletal muscle phenotype and consequently was established the optimal dose. Interestingly, increasing the DEL01-$(CAG)_7$ dose to 40 mg/kg did not result in additional splicing or functional improvement. A similar phenomenon was observed in a dose escalation study where a mouse model of spinal muscular atrophy was treated with a PMO conjugate (Hammond et al., 2022) and overall suggests that a saturation point or therapeutic ceiling has been reached.

As previous studies have reported that multiple dosing strategies can confer greater compound activity (Hammond et al., 2016; Hua et al., 2011; Klein et al., 2019; Nizzardo et al., 2014; Zhou et al., 2015), a multiple-dose regimen of DEL01-$(CAG)_7$ at 7.5 mg/kg (four

doses totalling 30 mg/kg) was tested. As previously observed, this approach offered some improvement over a single 7.5 mg/kg dose. However, it did not surpass the efficacy of a single 30 mg/kg dose, most likely due to pharmacokinetic factors such as differential drug absorption, distribution and elimination half-life. To more fully investigate the potential benefits of multiple dosing for DEL01-$(CAG)_7$ in the future, it may be beneficial to test repeat administrations of the optimal 30 mg/kg dose. However, given that a single 30 mg/kg dose was sufficient for full correction of DM1 biomarkers of skeletal muscle misplicing and myotonia and that no improvement was observed increasing to a higher single dose, it is uncertain whether additional administrations at such an effective dose would confer any therapeutic benefit. Nevertheless, PepGen have reported enhanced mis-splicing correction and muscle delivery in HSA-LR mice treated with four repeat 30 mg/kg doses of PGN-EDODM1, a CPP-PMO with an extremely similar structure to DEL01-$(CAG)_7$, relative to a single 30 mg/kg administration (Pepgen, 2023) suggesting that investigation could be merited.

The following four biomarkers were selected to evaluated treatment efficacy for this study: *Mbnl1* exon 5, *Clcn1* exon 7a, *Atp2a*1 exon 22 and *Ldb3* exon 11. These biomarkers were selected based on those used in Klein et al.'s 2019 evaluation of pip6a-$(CAG)_7$ in HSA-LR mice. Since the inception of this current work, however, it has become more common to use a broader panel of biomarkers in DM1 research. For instance, Dyne Therapeutics has employed over 35 splicing biomarkers in preclinical testing of an antibody-Fragment ASO in HSA-LR mice (Dyne Therapeutics, 2021), based on mis-splicing events assessed and indexed by Tanner et al., 2021. Similarly, it is now an established practise in DM1 clinical trials (Dyne Therapeutics, ACHIEVE: NCT05481879; Avidity, MARINA: NCT05027269) to assess compound efficacy by analysing splicing correction in 22 genes from which a

composite alternative splicing index (CASI-22) can be calculated (Provenzano M et al., 2024). While the core set used in this chapter appear in the extensive panels now utilised in preclinical and clinical practices and provide valuable insights into the efficacy of DEL01-$(CAG)_7$, expanding the panel in future studies could yield more robust and comprehensive data, ultimately strengthening findings. Furthermore, a wider range of biomarkers would also align with current clinical practices, potentially facilitating a smoother translation towards clinical trials.

DEL01-$(CAG)_7$ administration in HSA-LR mice exhibits an enhanced therapeutic window relative to previous CPP-$(CAG)_7$ conjugates

Similarly to results from the *in vitro* testing of DEL01-$(CAG)_7$, detailed and discussed in results chapter 1, the results in this chapter demonstrate that relative to the pip6a CPP, DEL01 offers an improved therapeutic window with an improved safety profile, relative to pip6a-$(CAG)_7$. These results therefore address a critical limitation in CPP-PMO development.

As previously described, the preclinical development of pip6a-$(CAG)_7$ was halted due to elevated levels nephrotoxicity. It is well documented that CPP-PMOs accumulate in the kidneys which consequently presents a persistent issue in the development of CPP-PMOs across various animal models (Amantana et al., 2007; Gait et al., 2019. Previous unpublished data from the Wood group revealed a > 20-fold elevation of KIM-1 observed 2 days after 7.5 mg/kg compound administration when compared to saline animals. Meanwhile histopathological assessment of the liver and kidney of pip6a-$(CAG)_7$ treated animals revealed dose dependent hypertrophy and intranuclear inclusions of the liver and

tubular proteinuria, dose dependent tubular basophilia and tubular hydropic degeneration in kidneys (Klein et al., 2019). Changes in the liver were reversed after 6 months, however only partial recovery was observed in the kidney abnormalities. It was therefore imperative to develop a safer alternative treatment.

Here, it is again shown that a single 7.5 mg/kg dose, pip6a-$(CAG)_7$ causes a dramatic increase in KIM-1 levels, underscoring the substantial nephrotoxicity associated with pip6a. By contrast, DEL01-$(CAG)_7$ showed little evidence of toxicity in any of the liver or renal function tests conducted at the highest tested doses. Serum liver enzymes, such as ALT, AST and ALP, as well as renal toxicity markers serum calcium and serum creatinine, all remained within normal ranges. This lack of toxicity highlights a key advantage of DEL01-$(CAG)_7$, positioning it as a safer alternative to pip6a. Furthermore, histopathological assessment of kidney and liver tissues from mice treated with higher doses (30 mg/kg and 40 mg/kg) of DEL01-$(CAG)_7$ revealed no changes in no structural changes associated with the onset of hepatotoxicity or nephrotoxicity.

Histopathological assessment is considered the “gold standard” with regards to assessing drug induced renal toxicity, therefore the improved toxicity profile of DEL01-$(CAG)_7$ is extremely significant in the progression of developing non-toxic CPP-PMOs. These results are made more impressive by the fact that a 30 mg/kg dose of DEL01-$(CAG)_7$ delivers significantly more compound to the kidney than pip6a-$(CAG)_7$ (see Figure 8E). This suggests that it is a difference in CPP chemistry and not compound concentration that elicits these toxicological differences. The improvement in DEL01-$(CAG)_7$ safety is likely due to its optimized design of reduced arginine content and peptide length in the composition of DEL01, relative to pip6a. This is discussed in greater detail in results chapter 1.

In addition to outperforming pip6a in terms of safety, DEL01-$(CAG)_7$ also demonstrated superior safety compared to R6Gly-$(CAG)_7$. R6Gly is another CPP, comprised of 6 arginines and one glycine residue, currently under clinical investigation as CPP-PMO conjugate (SRP-5051) for the treatment of Duchenne muscular dystrophy (DMD) (Gan et al., 2022; Sarepta, MOMENTUM: NCT04004065) and was included in this body of work as an industry standard benchmark for tissue penetration and safety, at the time of writing. While R6Gly has made encouraging clinical progress, it has been associated with toxicities, including a temporary hold to the MOMENTUM phase 2 clinical trial of SRP-5051, as a result of the hypomagnesemia experienced by some patients (Sarepta Therapeutics, 2024). This hypomagnesemia was later shown to be transient and manageable with supplementation, allowing the continuation of the trial, however hypomagnesemia can be indicative of kidney dysfunction or metabolic alterations and therefore requires close monitoring (Bosman et al., 2021; Keating et al., 1977; Uslu Gökceoğlu et al., 2014) Intriguingly, the results in this chapter reveal significant hypocalcaemia in mice treated with R6Gly, another phenomenon associated with poor renal outcomes (Lim et al., 2014; Nakamura et al., 2024). In contrast, DE01-$(CAG)_7$ elicited no effect on serum calcium levels, suggesting DEL01 to be safer than a CPP approved for testing in patients, adding to its weight as a CPP with enhanced safety.

With regards to efficacy, while a single 7.5 mg/kg dose of pip6a-$(CAG)_7$ demonstrated enhanced activity over DEL01-$(CAG)_7$ administered at the same dose, exhibiting stronger splicing correction and myotonia reversal, a 30 mg/kg DEL01-$(CAG)_7$ treatment performed similarly, if not slightly better for certain splicing biomarkers readouts in specific muscles (*Mbnl1* exon 5 in quadriceps and *Ldb3* exon 11 in gastrocnemius, Figure 7A and 7D). Although these results re-emphasize the higher potency of pip6a, they also show that

DEL01-$(CAG)_7$ is able to achieve similar therapeutic outcomes using a higher but less toxic dose. Consequently, and consistent with the results from results chapter 2, despite requiring a higher dose, DEL01-$(CAG)_7$ clearly emerges as a viable and safer alternative, offering a balanced approach that combines efficacy with a significantly improved safety profile.

DEL01-$(CAG)_7$ demonstrates an improved therapeutic reach with enhanced penetration into critically affected tissues *in vivo*

DEL01-$(CAG)_7$ not only exhibited improved efficacy in skeletal muscle but also demonstrated, superior biodistribution and penetration into the skeletal muscles and other critically affected tissues including heart and brain. This is particularly significant because achieving therapeutic concentrations in these tissues is crucial for addressing other systemic manifestations of DM1, including cardiac and neurological symptoms, which have previously been neglected by therapeutic strategies focused primarily on targeting skeletal muscle.

The results show that at a dose of 30 mg/kg, DEL01-$(CAG)_7$ delivered a higher concentration of PMO to skeletal muscles in comparison to naked $(CAG)_7$ PMO administered at a higher dose (200 mg/kg) and that this concentration was sufficient for reversing myotonia and normalising splicing. As a reference for the level of tissue delivery achieved, the PMO tissue concentrations achieved by DEL01 were compared to those attained by R6Gly, a CPP designed to enhance PMO delivery and treatment in DMD. Despite a higher administered dose of the R6Gly-$(CAG)_7$ (80 mg/kg), a 30 mg/kg administration of DEL01-$(CAG)_7$ led to superior skeletal muscle penetration. This is

particularly notable as the R6Gly CPP was specifically designed to improve delivery into tissues crucially affected by DMD, a neuromuscular disorder that, similarly to DM1, is characterized by progressive muscle weakness in both skeletal muscles and heart (Flanigan, 2014).

The fact that DEL01 performs better than R6Gly—a CPP considered to have sufficient skeletal muscle efficacy to warrant clinical trials —underscores its potential as a more efficient delivery vehicle. However, it is important to note that the integrity of the skeletal muscle membrane in DMD has been reported as damaged and more porous (Clarke et al., 1993; Pestronk et al., 1982), while the structural integrity of the DM1 muscle membrane appears unaffected (González-Barriga et al., 2015). Therefore, care should be taken when comparing the relationship between tissue penetration and efficacy across these two neuromuscular diseases, as differences in membrane permeability may influence delivery outcomes.

While skeletal muscles are the tissue most heavily targeted by DM1 therapies in development, DM1 patients experience also experience extensive cardiac issues including cardiomyopathies and arrhythmias (Groh et al., 2008; Nguyen et al., 1988), the latter of which is associated with the mis-splicing of S*CN5a*, a gene encoding a cardiac voltage gated sodium channel (Freyermuth et al., 2016). Furthermore, cardiac involvement is a leading cause of mortality in DM1 patients (De Die-Smulders et al., 1998; Groh et al., 2008). Consequently, to be able to treat heart tissues would also be of great benefit to patients. Again, encouragingly, significantly higher PMO concentration was achieved in heart tissues using DEL01 as a PMO delivery vehicle relative to R6Gly and even pip6a, demonstrating its enhanced therapeutic reach to tissues beyond the skeletal muscles. Unfortunately, the HSA-LR model employed does not present with a DM1 phenotype in

heart, therefore determination of whether the levels of PMO delivered was therapeutically meaningful was not possible.

One model that could provide insight into whether DEL01-$(CAG)_7$ elicits activity in heart is the more recently developed LC15 mouse (Tylock et al., 2020). This mouse contains a human *DMPK* transgene harbouring a repeat tract of 250 – 400 repeats and exhibits robust cardiac expression of repeat expanded CUG RNA. Mice present with missplicing and RNA *foci* in cardiac tissues, in addition to electrophysiological cardiac deficits. As such, it could be extremely interesting to test DEL01-$(CAG)_7$ in LC15 in the future, to establish whether the impressive PMO delivery into heart translates into a meaningful improvement to the DM1 cardiac phenotype.

In addition to enhanced skeletal muscle and heart penetrance, DEL01 also improved PMO delivery to the brain with 3-fold more PMO delivered relative to R6Gly and 57-fold more in comparison to pip6a. However, unsurprisingly, the levels of PMO concentration in the brain still remained relatively low and were less than 300 pM. Previous work in the CPP-ASO field, such as studies using the Tat CPP, have also similarly struggled with efficient brain delivery (Al Humaidan et al., 2022), underscoring the challenge of achieving effective CNS delivery. Overall, this is a significant hurdle for treating DM1 patients, as CNS involvement in DM1 contributes to cognitive and behavioural issues that severely impact the quality of life, particularly in earlier onset patient groups, such as congenital and infantile onset patients (Angeard et al., 2011; Douniol et al., 2012; Ekström et al., 2009). However, while CNS symptoms in adult patients are milder, adult or later onset DM1 patients also display increased cognitive decline and fetal CNS splicing patterns (Degener et al., 2022), which may also benefit from therapeutic intervention.

The CNS has long been known as one of the most difficult tissues targets for treatment, due to the impenetrable nature of the BBB. With the exception of small molecules, most approved CNS treatments circumvent this issue by direct brain or intrathecal delivery, as in the case of Nusinersen, the first FDA approved ASO, for SMA (Finkel et al., 2016; Ottesen, 2017). Given that DM1 is a multi-systemic disease, a systemically delivered therapy that can penetrate all critically affected organs would be the optimum outcome for patients. While CPPs seem a promising delivery mechanism for many other tissue targets, it is clear that much work is still needed to make them viable options for brain delivery, and it is possible that other delivery platforms may be more effective.

For example, two compounds developed by Dyne Therapeutics and Avidity and currently in clinical trials for DM1, employ antibody-based technologies targeting TfR1, for the tissue delivery of a gapmer ASO and siRNA respectively. The TfR1 receptor is well documented as highly expressed on the BBB and has consequently been greatly exploited as a CNS drug delivery target for several decades (Paterson & Webster, 2016; Sievers & Senter, 2013). So far, anti-TfR1 targeting DM1 treatments have generated promising preclinical delivery in heart, skeletal muscle, and CNS (Avidity Biosciences, 2021; Dyne Therapeutics, 2023; Dynes Therapeutics, 2022) and both have shown encouraging safety and skeletal muscle activity in patients (Dyne Therapeutics, ACHIEVE: NCT05481879; Avidity, MARINA: NCT05027269), however any neurological benefit remains to be seen. These two DM1 therapies are discussed further in results chapter 3.

DEL01-$(CAG)_7$ fails to display correction of the DM1 phenotype in DMSXL Mice

Despite the promising results in HSA-LR mice, the efficacy of DEL01-$(CAG)_7$ did not translate to the DMSXL mouse model. The DMSXL mode is a more complex model, displaying a broader range of DM1 pathology, including aberrant splicing and functional phenotypes in skeletal muscle, heart and the CNS (Hernández-Hernández et al., 2013; Huguet et al., 2012). The hope was therefore to be able to additionally test DEL01-$(CAG)_7$ activity in the heart and CNS, tissues for which HSA-LR mice have no DM1 phenotype, due to the skeletal muscle specific expression of the *ACTA1* gene (Mankodi et al., 2000).

DEL01-$(CAG)_7$ achieved good tissue penetration in the DMSXL mice, similar to the levels observed in the HSA-LR model at a 40 mg/kg dose. As a result, there was optimism that an improvement in skeletal muscle and heart phenotype may be observed. Disappointingly, no alterations in mis-splicing were observed in either tissue, nor was there any improvement in muscle strength, as determined by the grip strength testing. Similarly, no misplacing correction was observed in the frontal cortex, following treatment. However, this was not wholly unexpected as the levels of PMO delivered to the brain remained relatively low (497.2 ± 63.15 pM).

The failure of DEL01-(CAG)7 in the DMSXL model could be attributed to several factors, including the inherent challenges of treating this more severe model of DM1. DMSXL mice carry a larger CTG repeat expansion and present with widespread mis-splicing events, which may require more potent therapeutic strategies. It is also possible that the differences in efficacy observed between mouse models are due to differences in the stoichiometry of the target for each model as it has been shown that the abundance of repeat expanded CUG transcripts varies greatly between mouse models, with RNA for

ACTA1 transgene being 1000-fold more abundant that that from the *Dmpk* gene (Gudde et al., 2016). Conversely, the *DMPK* transgene in DMSXL mice has 10-fold lower expression than the endogenous *Dmpk* gene.

In general, the DMSXL model is known within the DM1 field as being notoriously challenging to treat, as highlighted again by the failure of DEL01-$(CAG)_7$, despite a rigorous treatment regime of four biweekly administrations of 50 mg/kg. To my current knowledge, no report exists of a PMO able to treat the DMSXL DM1 phenotype. However, in 2017, Jauvin et al. published a report of an ASO gapmer (ISIS 486178) able to effectively treat this model, facilitating knockdown in repeated expanded DMPK transcripts in skeletal muscle and heart (70% and 30%, respectively) alongside reductions in RNA *foci* and improvements in muscle strength and histology. The gapmer acted via an RNAse dependant mechanism that leads to the breakdown of *DMPK* transcripts. This differs greatly from the mechanism of a PMO, which acts by sterically blocking the sequestration of splicing factors to *DMPK* transcripts (Mulders et al., 2009; Wheeler et al., 2009).

Given that our results indicate good delivery into skeletal muscle and heart, and the lack of published data showing PMO efficacy in DMSXL mice, it could be argued that PMOs are perhaps not potent enough to elicit meaningful activity and perhaps other ASO chemistries with alternative mechanisms of action better suited to this disease model.

The lack of efficacy in DMSXL mice potentially raises important concerns about the suitability of this model for evaluating PMO compounds or its applicability as a model for therapies nonspecific towards treating earlier onset DM1 patients. As DMSXL mice exhibit relatively mild mis-splicing and myotonia but present with severe neurological deficits and a high neonatal mortality rate (Hernández-Hernández et al., 2013; Huguet et al., 2012), the model more closely aligns with congenital DM1 patients who similarly experience severe

neurological and cognitive deficits and high neo-natal mortality but typically lack muscle weakness until later in life (Angeard et al., 2007; Douniol et al., 2012; Echenne et al., 2008). In contrast, adult or later-onset DM1 patients, tend to have more pronounced muscle weakness and myotonia with fewer central nervous system symptoms (Harper, 2001), which is better modelled by HSA-LR mice which display severe myotonia and aberrant splicing in skeletal muscles (Mankodi et al., 2000). Given the emphasis that has been placed on treating skeletal muscles cells in the development of DEL01-$(CAG)_7$, the PMO conjugate is more appropriate and more intentionally designed as treatment for adult or later forms. Furthermore, considering that CPPs show limited penetration into the CNS, the DMSXL may not be the most clinically relevant model for testing DEL01-$(CAG)_7$.

The CPP-$(CAG)_7$ conjugate, PGN-EDODM1, currently being tested by PepGen in a P1 clinical trial (FREEDOM-DM1, NCT06204809) in DM1 patients, has not been tested in the DMSXL model. Given the overlap between these compounds, with DEL01 being an iteration of the CPP employed by PepGen, it is unlikely that PGN-EDODM1 would yield significantly different results in the DMSXL model. Should PepGen's compound demonstrate clinical efficacy without being tested in DMSXL mice, this would challenge the relevance of the DMSXL model in predicting clinical outcomes for DM1 therapies, at least in adult-onset patients. Ultimately, the results of PepGen's clinical trials could help clarify whether DMSXL is useful as a predictor of treatment efficacy in skeletal muscle, or if the HSA-LR mouse model remains the more reliable predictor of therapeutic outcomes in human patients.

Overall, despite the failure to achieve phenotypic amelioration in all animal models tested, the work in this chapter reveals DEL01 to be a promising delivery modality for penetrating skeletal muscle and heart, while maintaining a safe toxicological profile. The results

demonstrate great improvement on previous CPP-PMO iterations and make a case for the potential employment of our DEL01 as a PMO delivery vehicle in other neuromuscular diseases amenable to ASO therapies. For example, DMD is a disease shown to be treatable using PMOs, that would benefit from enhanced delivery into skeletal muscle and heart. Future work will therefore focus on the furthering development of DEL01-$(CAG)_7$ towards clinical trials and additionally extending the clinical applications of DEL01 into other disease contexts.

Results Chapter 3 – Preclinical development of Ab-PMOs for the treatment of DM1

Results

Previous work published by the Wood group demonstrated that the systemic intravenous administration of a PMO conjugated to the BBT-8D3$_{130}$ antibody, a human Immunoglobulin G (IgG) antibody produced and optimized by AstraZeneca (Cambridge, UK) for targeting murine TfR1 on the BBB (Webster et al., 2016), was able to facilitate sufficient delivery to the brain parenchyma to reverse the disease phenotype observed in an SMA mouse model (Hammond et al., 2022). Furthermore, the antibody-PMO conjugate (Ab-PMO) was also able to penetrate and treat tissues beyond the CNS, including skeletal muscles and liver. Building on these promising results, this approach was adapted to test, as a proof of concept, anti-TfR1-targeting Ab-PMOs as a treatment strategy for DM1. Thus, the (CAG)$_7$ PMO, employed in previous chapters, was conjugated to the BBT-8D3$_{130}$ antibody, generating the TfR1 targeting PMO conjugate, BBT-8D3$_{130}$-(CAG)$_7$. The rationale behind this strategy was the potential for a systemic DM1 treatment with the added benefit of penetrating the CNS, a tissue that, at the inception of this study, remained largely inaccessible to DM1 therapeutics.

In addition to BBT-8D3$_{130}$-(CAG)$_7$, two control conjugates were synthesized: NIP228-(CAG)$_7$, a non-targeting antibody-PMO control, and BBT-8D3$_{130}$-NTC, which served as a TfR1 targeting non-template PMO control. Given the lack of availability of a murine DM1 cellular model for the *in vitro* screening of the Ab-PMO conjugates, the compounds were tested directly *in vivo*. Here I present the findings from the testing of BBT-8D3$_{130}$-(CAG)$_7$ in

HSA-LR mice, along with subsequent follow-up experiments, after the compound failed to ameliorate the DM1 phenotype.

Evaluation of BBT-8D3$_{130}$-(CAG)$_7$ in HSA-LR mice

It was decided to initially test the Ab-PMO conjugates in the HSA-LR model as it is the DM1 model for which there is an established colony within the Wood group. Although the model only expresses a DM1 phenotype in skeletal muscle, the model can be used to establish compound biodistribution to all critically affected DM1 tissues e.g. skeletal muscles, heart and CNS. Evaluation of efficacy in skeletal muscles could also provide an initial measure of compound activity that could subsequently be used to support further testing of compound activity in CNS and heart tissues via collaboration with groups possessing the relevant animal models, e.g. LC15 and DMSXL models (Huguet et al., 2012; Tylock et al., 2020).

Toxicological evaluation of Ab-PMOs in HSA-LR mice

As a 50 mg/kg dose of a BBT-8D3$_{130}$-conjugated PMO was shown to be sufficient for treating SMA mice in the dose-response study conducted by Hammond et al. (2022), HSA-LR mice were treated with a single intravenous 50 mg/kg administration of either BBT-8D3$_{130}$-(CAG)$_7$, NIP228-(CAG)$_7$, BBT-8D3$_{130}$-NTC or 0.9% saline (n= 6 per group). All tissues were collected 14 d post treatment for evaluation of tissue biodistribution and efficacy in skeletal muscle. Additionally terminal serum and day 2 and day 7 urine was collected for toxicological assessment (Figure 12A). Very limited investigation into compound-induced toxicity had been carried out as part of the SMA study, it was therefore paramount to establish here whether the Ab-PMO conjugates induced any toxicity,

especially given the history of nephrotoxicity associated with alternative PMO conjugates (Amantana et al., 2007; Gait et al., 2019; Sazani et al., 2011).

To evaluate whether Ab-PMO conjugates induced kidney toxicity, the urinary concentration of KIM-1 in treated mice was measured via ELISA and normalised to urinary creatinine concentration (Figure 12B). No significant changes were observed in KIM-1 levels in any of the treatment groups on days 2 or 7, when compared to the 0.9% saline control group. Similarly, assessment of additional serum biomarkers of nephrotoxicity, serum calcium and serum creatinine (Figures 12C-D) (Lim et al., 2014; Perrone et al., 1992; Vaidya et al., 2010), revealed no notable alterations from the 0.9% saline treated animals.

To detect potential liver toxicity, levels of biomarkers commonly used for liver function tests (Giannini et al., 2005): AST, ALT and ALP (Figure 12E-G), were evaluated in terminal serum. Again, no concerning deviations from 0.9 % saline treated controls were observed for any of the Ab-PMO conjugates administered. Taken together, this suggests that Ab-PMOs administered at 50 mg/kg do not induce toxic effects in the liver or kidneys, the classical sites of ASO drug induced toxicity issues. Furthermore, in support of the safety of compound suggested by these data, a recovery time of 0 min after compound administration was noted for each Ab-PMO conjugate. Recovery time is estimated based on clinical observations of lethargy and/or hypoapnea post-administration of treatment.

Lastly, as it was expected that BBT-8D3$_{130}$-(CAG)7 would be able to penetrate the CNS, transcript levels of *Gfap* and *Aif1* were assessed, as previously evaluated by IONIS in their testing of a DM1 gapmer via intracerebral ventricular administration (Ait Benichou et al., 2022), to give an indication of neuroinflammation or CNS toxicity (Figure 12H-I). As with all other toxicological biomarkers assessed, there were no changes observed in *Gfap* or *Aif1*

expression following treatment with BBT-8D3$_{130}$-(CAG)$_7$ and its controls relative to 0.9% saline treated animals.

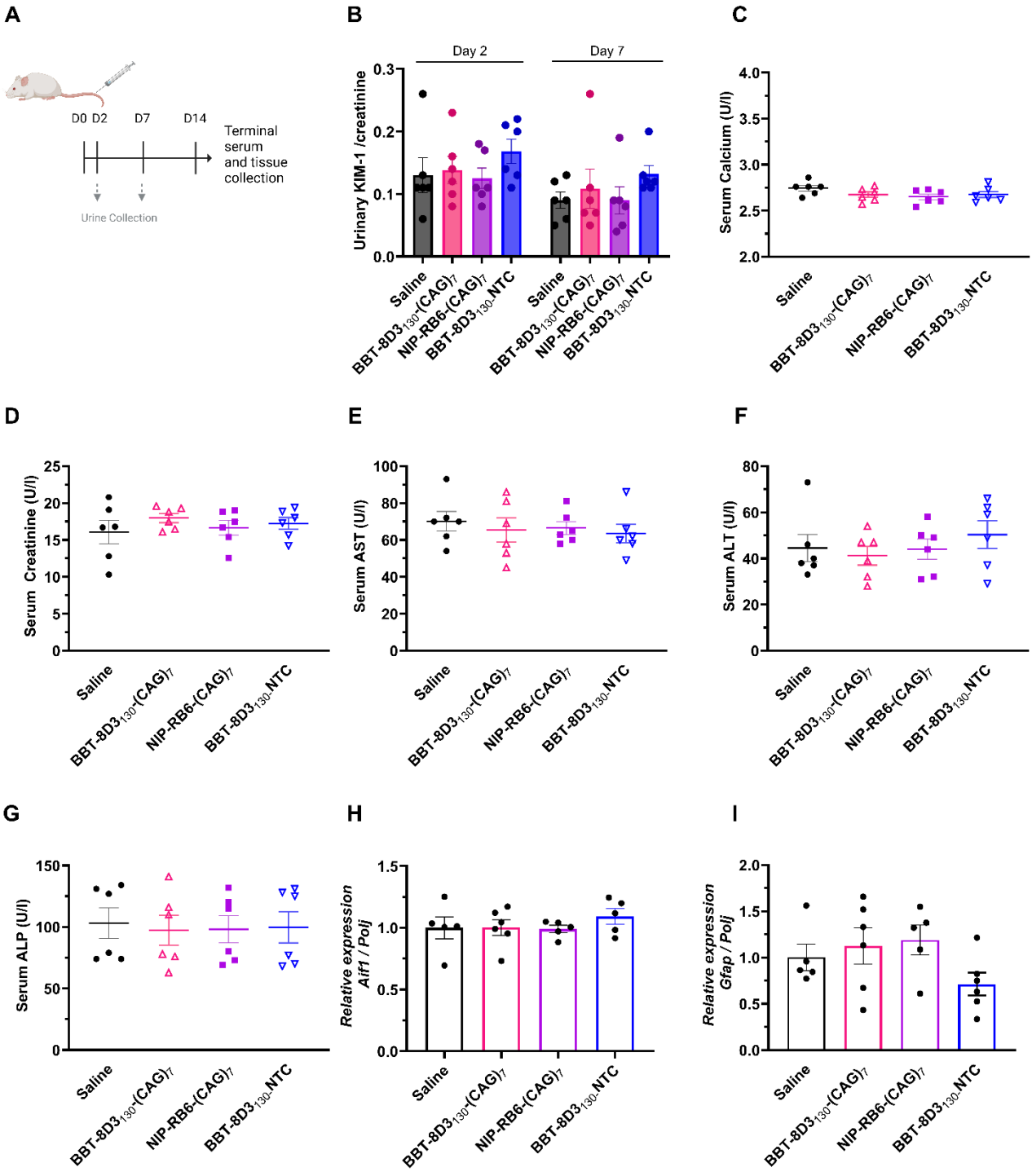

Figure *12*: Toxicological Assessment of Ab-PMOs in DM1, HSA-LR mice.

(A) Diagram of experimental sample collection: HSA-LR mice were injected with a single

50 mg/kg dose of an Ab-PMO or 0.9% saline (n=6). Urine was collected 2 d and 7 d (urine) post-final administration while terminal serum and cortex tissues were collected 14 d post administration. **(B)** urinary KIM-1 levels quantified via ELISA and normalised to urinary creatinine levels. **(C-G)** Analysis of key terminal serum metabolites: **(C)** calcium **(D)** creatinine, **(E)** AST, **(F)** ALT and **(G)** creatinine, via a clinical chemistry analyser at Harwell MRC, UK. Analysis of biomarkers of CNS toxicity **(H)** *Aif1* and **(I)** *Gfap* were quantified via qPCR with data normalised to *Polj*. All data are expressed as mean ± S.E.M. and each dot represents a biological replicate. Statistical significance was determined via one-way ANOVA, corrected for multiple comparisons using Dunnett's test. All comparisons between all treatment groups were non-significant ($P > 0.05$).

Anti-TfR1-PMO penetrates the CNS in HSA-LR mice

To assess BBT-8D3$_{130}$-(CAG)$_7$ penetration into the CNS, the PMO concentration in CNS tissues was quantified via ELISA assay (Figure 13C). Cortex, cerebellum and brain stem were collected, and, for each region, BBT-8D3$_{130}$-(CAG)$_7$ was able to penetrate and deliver PMO at significantly higher concentrations than NIP228-(CAG)$_7$.

Additionally, to further explore penetration specifically into neurons and astrocytes, key CNS cell types affected by DM1, an extra set of mice were treated with 50 mg/kg administrations of BBT-8D3$_{130}$-(CAG)$_7$ and NIP228-(CAG)$_7$. After 24 h the animals were sacrificed and brains perfused and fixed for immunostaining. Neurons were labelled using Nissl staining and astrocytes via immunostaining of glial fibrillary accessory protein (GFAP). Meanwhile, to detect Ab-PMO conjugates, a goat anti-human IgG was employed, to detect the human IgG antibody component of the conjugates. The images generated reveal that BBT-8D3$_{130}$-(CAG)$_7$ colocalises with neurons and partially with astrocytes, no such co-localisation was observed with NIP228-(CAG)$_7$ treatment (Figures 13A-B). This suggests delivery of BBT-8D3$_{130}$-(CAG)$_7$ into these cell types, albeit at varying levels. Combined with the CNS ELISA results, the data strongly suggests successful delivery of BBT-8D3$_{130}$-(CAG)$_7$ into the CNS and its target cell types.

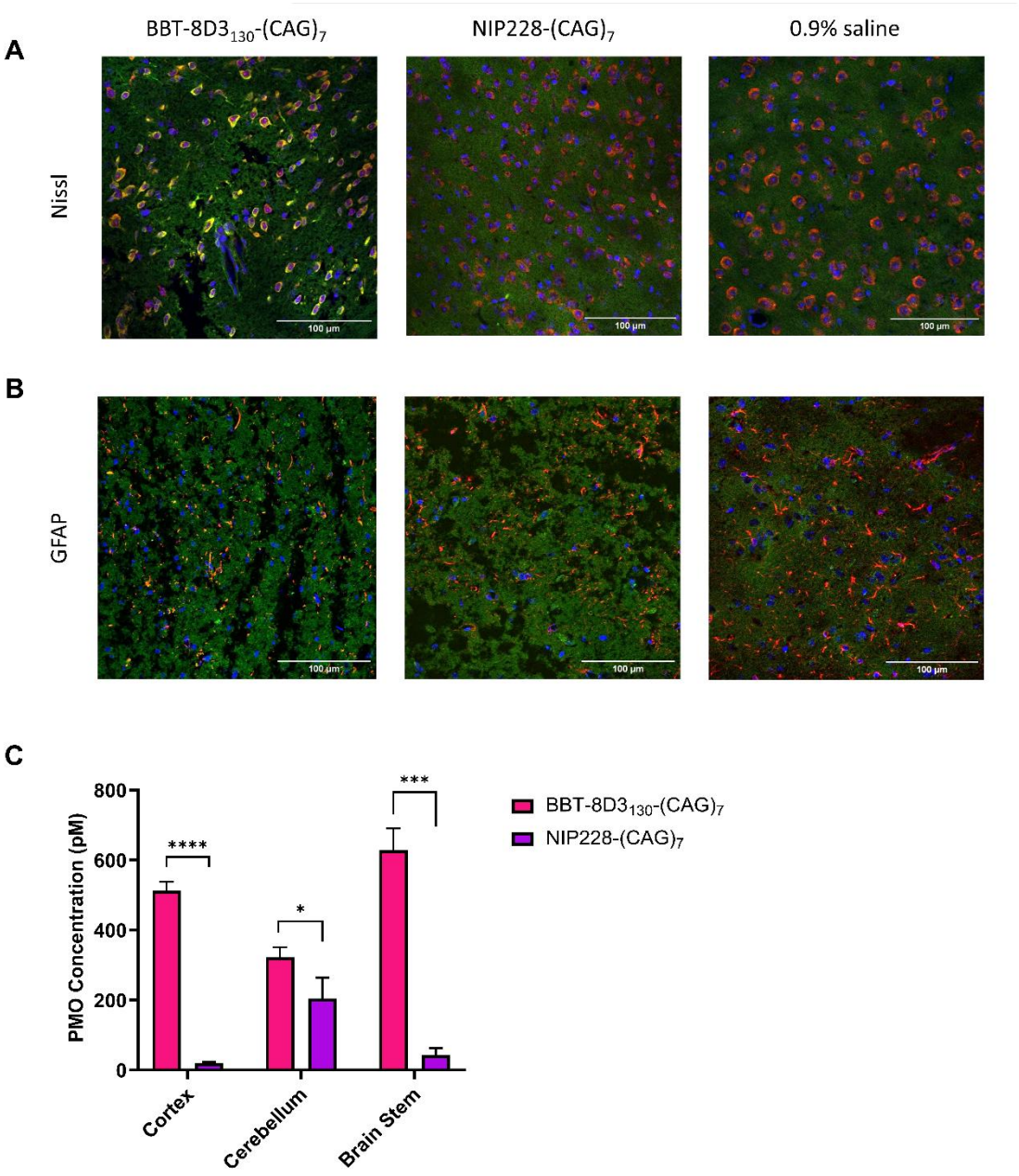

Figure *13*: BBT-8D3$_{130}$-CAG7 penetrates CNS tissues and colocalises with neurons.

8–10-week-old HSA-LR mice were treated with 50 mg/kg intravenous administrations of BBT- BBT-8D3$_{130}$-(CAG)$_7$, NIP228-(CAG)$_7$ or 0.9% saline. For immunohistochemistry **(A-B)**, brains were perfused, fixed and harvested 24 h later. Immunostaining was performed on 20

μm cortex slices and representative images are shown using DAPI (blue) antibodies targeting specific murine CNS cells (red) and human antibody conjugates (green). **(A)** Nissl staining (red) in mice receiving BBT-8D3$_{130}$-(CAG)$_7$, NIP228-(CAG)$_7$ or 0.9% saline. **(B)** GFAP (red) staining for astrocytes in mice receiving BBT-8D3$_{130}$-(CAG)$_7$, NIP228-(CAG)$_7$ or 0.9% saline (n=3 per treatment group). Scale bars: 100 μm. **(C)** PMO concentration quantified via ELISA in regions of CNS, harvested 14 d post-treatment. Data shown as the mean ± S.E.M, n = 5-6 per group. Statistical significance (representative P values) was performed using an unpaired students t-test between treatment groups within each tissue set. (*P ≤ 0.05; **P ≤ 0.01; ***P ≤ 0.001, ****P ≤ 0.0001).

Anti-TfR1-PMOs fail to correct skeletal muscle mis-splicing and myotonia in HSA-LR mice

To gain an initial read out of penetration into the skeletal muscles and the efficacy the of BBT-8D3$_{130}$-(CAG)$_7$, skeletal muscle biomarkers of DM1 mis-splicing: *Mbnl1, Clcn1, Ldb3* and *Atp2a1* (Figure 14A-D), were analysed in gastrocnemius and quadriceps 14 d after 50 mg/kg Ab-PMO administrations. Surprisingly, no correction or change in splicing was observed for BBT-8D3$_{130}$-(CAG)$_7$ or any control treatments when compared to 0.9% saline treated mice. Similarly, no clear amelioration in hind-limb myotonia was observed for any treatment group, prior to the harvesting of tissues (data not shown).

Consistent with the disappointing lack of efficacy in the skeletal muscles, ELISA analysis of PMO concentrations within the skeletal muscles revealed that extremely low levels, of less than 120 pM, are delivered into these tissues (Figure 14E). However, one encouraging result was the relatively good PMO delivery into heart observed following BBT-8D3$_{130}$-(CAG)$_7$ treatment. This was significantly enhanced relative to NIP228-(CAG)$_7$, suggesting at least some specific delivery via TfR1. However, not all delivery can be attributed to TfR1-mediated delivery as NIP228-(CAG)$_7$ still achieved a PMO concentration in heart of 797.9 ± 249.6 pM, ~ 53% of that achieved by BBT-8D3$_{130}$-(CAG)$_7$ (1493.7 ± 131.1 pM).

As the lack of Ab-PMO activity could be attributed to the low concentrations of PMO delivered into the skeletal muscles, it was decided to treat one further group of mice with an increased dose of BBT-8D3$_{130}$-(CAG)$_7$, to see if this would produce sufficient PMO delivery into the skeletal muscles to elicit a therapeutic effect. Given the apparent lack of drug-induced toxicity at a dose of 50 mg/kg and that double the dose had already been trialed in the preceding SMA body of work (Hammond et al., 2022), a 100 mg/kg dose of

BBT-8D3$_{130}$-(CAG)$_7$ was decided upon and administered to HSA-LR mice (n=6). Both surprisingly and disappointingly again, no splicing correction or improvement in functional myotonia (data not shown) was observed (Figure 15A-D). A very slight increase in the PMO concentration delivered into the skeletal muscles was observed (Figure 15E), however this still remained relatively low (< 245 pM). Material constraints meant that it was not possible to synthesis sufficient NIP228-(CAG)$_7$ or BBT-8D3$_{130}$-NTC for testing at a high dose. Nevertheless, it is clear that doubling the dose of BBT-8D3$_{130}$-(CAG)$_7$ administered provides little benefit.

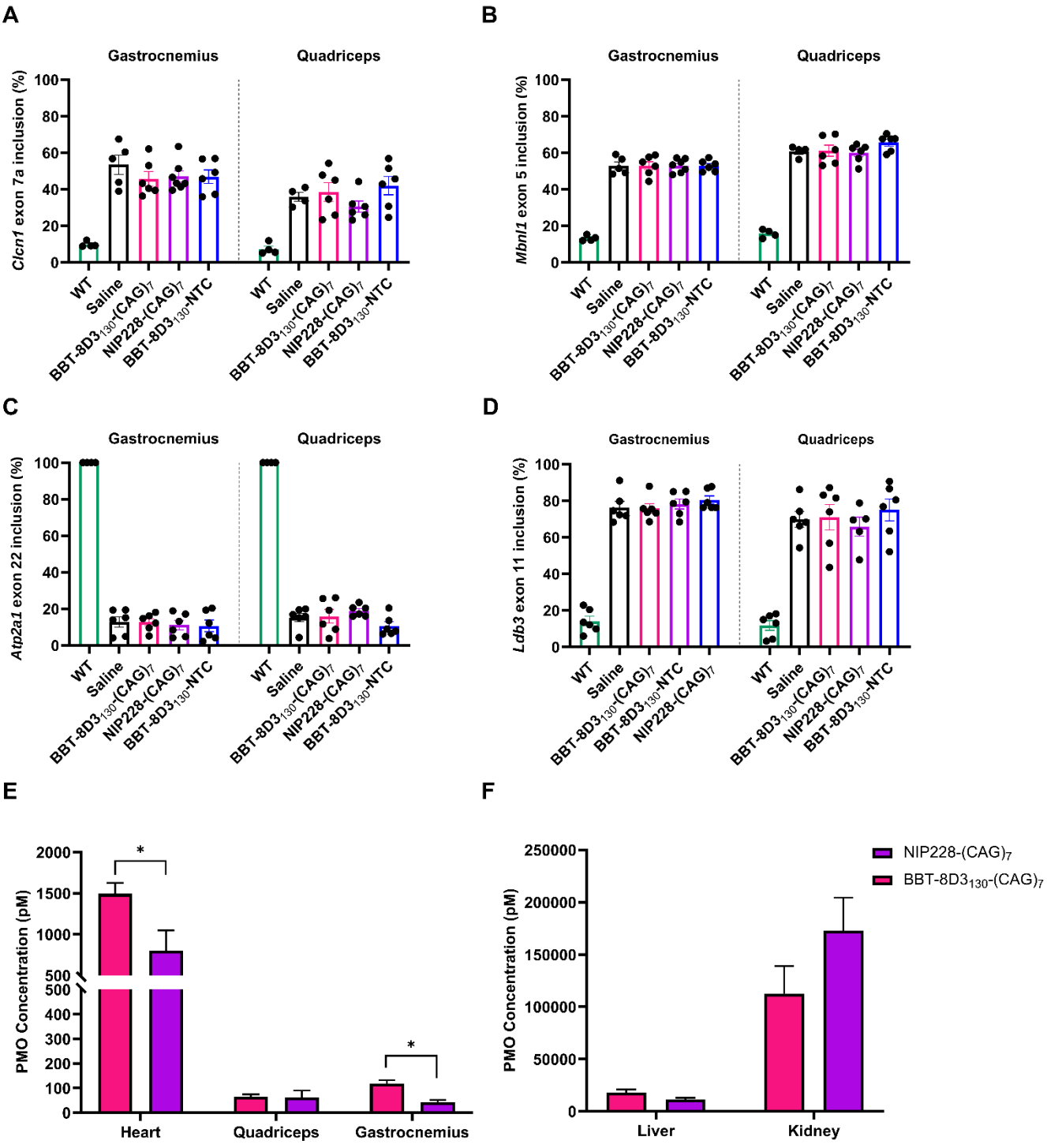

Figure *14*: Peripheral tissue biodistribution and efficacy of anti-TfR1-PMO conjugates in ameliorating DM1 skeletal muscle phenotype in DM1 mice.

HSA-LR mice were injected with single intravenous administrations of BBT-8D3$_{130}$-(CAG)$_7$,

NIP228-$(CAG)_7$, $BBT8D3_{130}$-NTC or 0.9% saline and analysed 2 weeks after treatment. Splicing analysis and inclusion of key exons was measured via RT-PCR in gastrocnemius and quadriceps for **(A)** *Mbnl1* exon 5, **(B)** *Clcn1* exon 7a, **(C)** *Atp2a1* exon 22 and **(D)** *Ldb3* exon 11. One-way ANOVA with Tukey's multiple comparison test was performed on data and showed no significance (ns) differences between any treatment groups (ns > 0.05). WT exon inclusion data is included for reference. Tissue PMO concentration was quantified via ELISA in **(E)** heart and skeletal muscles and **(F)** liver and kidney. Statistical significance (representative P values) was performed using an unpaired students t test between treatment groups within each tissue set. (*P ≤ 0.05; **P ≤ 0.01; ***P ≤ 0.001, ****P ≤ 0.0001). All data are represented as mean ± S.E.M. and each dot represents a biological replicate (n=5-6 per treatment group).

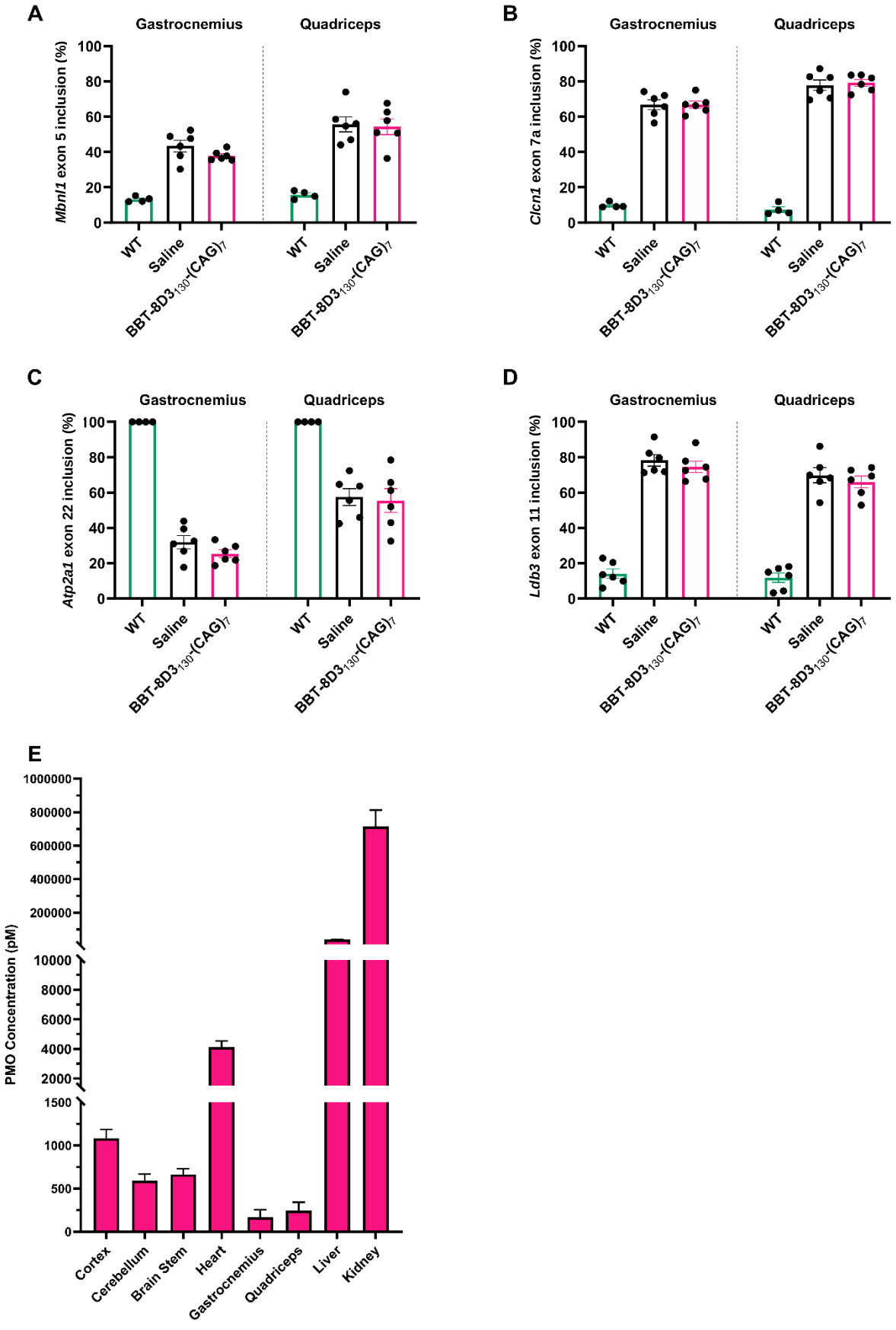
A
Gastrocnemius
Quadriceps
Mbnl1 exon 5 inclusion (%)
100
80
60
40
20
0
WT
Saline
BBT-8D3130-(CAG)7
B
Clcn1 exon 7a inclusion (%)
C
Atp2a1 exon 22 inclusion (%)
D
Ldb3 exon 11 inclusion (%)
E
PMO Concentration (pM)
1000000
800000
600000
400000
200000
10000
8000
6000
4000
2000
1500
1000
500
0
Cortex
Cerebellum
Brain Stem
Heart
Gastrocnemius
Quadriceps
Liver
Kidney

Figure *15*: Treatment of HSA-LR mice with 100 mg/kg BBT-8D3130-(CAG)7 fails to improve DM1 phenotype.

HSA-LR mice were injected with single 100 mg/kg intravenous administrations of BBT-$8D3_{130}$-$(CAG)_7$ or 0.9% saline and analysed 2 weeks after treatment. Splicing analysis and inclusion of key exons was measured via RT-PCR in gastrocnemius and quadriceps for **(A)** *Mbnl1* exon 5, **(B)** *Clcnl1* exon 7a, **(C)** *Atp2a1* exon 22 and **(D)** *Ldb3* exon 11A student's t test was performed on data and showed no significance differences between treatment groups for any biomarker assessed ($P > 0.05$). WT exon inclusion data are included for reference. **(E)** Tissue PMO concentration treated animals quantified via ELISA. All data is represented as mean ± S.E.M. and each dot represents a biological replicate (n=6 per treatment group).

Understanding the failings of BBT-8D3$_{130}$-(CAG)$_7$ to penetrate and treat skeletal muscles in HSA-LR mice

Assessment of expression of Ab-PMO delivery target, TfR1, in DM1 patient-derived DM1 myotubes and HSA-LR mice

It was illogical to pursue testing the compound further in additional DM1 models as collaborations were unlikely to be fostered, given the lack of activity shown by BBT-8D3$_{130}$-(CAG)$_7$. Furthermore, to test even higher doses of BBT-8D3$_{130}$-(CAG)$_7$ was not economically viable, given the amount of BBT-8D3$_{130}$ that would be required. I therefore sought to understand why BBT-8D3$_{130}$-(CAG)$_7$ had failed in the DM1 animal model, when it had shown such promise in the previous work conducted in SMA mice (Hammond et al., 2022). One possible hypothesis that warranted further investigation was the concept that the expression of TfR1, the receptor target of the BBT-8D3$_{130}$ antibody, may be reduced in the HSA-LR DM1 model, relative to WT or even SMA mice. This hypothesis stemmed from data generated in human myoblasts, as part of another study, which shows that TfR1 expression in differentiated patient derived DM1 myoblasts is reduced, relative to a WT control line (Figure 16). This reduction in expression was found to be consistent on an mRNA, protein and cell surface expression level (29%, 61% and 60% TfR1 expression reduction, respectively) and reversible following CPP-PMO treatment with 20 μM DEL01-(CAG)$_7$.

To establish whether TfR1 expression is similarly affected in the DM1 HSA-LR model, TfR1 expression was compared in tissues harvested from 10 week old untreated HSA-LR mice and mice from their WT background strain, FVB/N. Tissues were also harvested from the transgenic *hSMN2* SMA mouse model, used by Hammond et al. (2022), to aid

rationalising any potential differences in TfR1 expression and how that may relate to the differing activity results for BBT-8D3$_{130}$-PMO conjugates observed between their study and this body of work.

TfR1 expression was assessed across a panel of tissues comprised of quadriceps, gastrocnemius, heart, brain cortex, liver and kidney, initially focusing on RNA and protein expression. qPCR analysis of *Tfrc* transcript expression (Figure 17) revealed that *Tfrc* is overexpressed by ~ 1.4 – 1.9-fold in HSA-LR skeletal muscles, relative to both FVB/N and SMA transgenic mice. *Tfrc* transcript expression also appears to be elevated in the brain cortex and kidney of HSA-LR mice, however this elevation does not carry through to an elevation in protein expression. In contrast, western blot analysis of TfR1 protein expression shows that TfR1 protein expression is significantly increased in the quadriceps and gastrocnemius of HSA-LR mice (4.1-fold and 2.7-fold, respectively. Figure 18A-C). Furthermore, assessment of TfR1 expression in HSA-LR treated tissues suggests that this related to the DM1 disease pathology, with 30 mg/kg DEL01-(CAG)$_7$ treatment leading to a reversal in *Tfrc* and TfR1 protein expression towards WT FVB/N levels (Figure 19).

These findings show differential TfR1 expression in HSA-LR mice, although not the reduced expression that was hypothesized. However, the level of expression most crucial to therapeutics exploiting TfR1 as a cellular delivery target, is the cell surface expression (CSE). Therefore, the CSE of TfR1, also known in the context of cell surface experiments as cluster of differentiation marker (CD) 71, was also analysed in single skeletal muscle cell types via fluorescent activated cell sorting (FACs) and flow cytometry. Single cell suspensions from HSA-LR, FVB/N and transgenic hSMN2 SMA mice were sorted into four discrete cell populations: satellite cells (CD45- CD31- SCA1- VCAM+), mesenchymal cells (CD45- CD31-SCA1+), endothelial cells (CD45- CD31+) and macrophages (CD45+

CD163+) (Figure 20A). CD71 CSE was assessed for each cell type (Figure 20B-F) and it was found that its expression is significantly elevated specifically in macrophages and endothelial cell populations. No significant changes were seen in mesenchymal and satellite cell populations.

While certainly intriguing, as these findings did not show the same reduction in TfR1 expression as seen in DM1 myotubes, they do not align with the hypothesis that TfR1 expression is reduced in HSA-LR mice and therefore do not explain why BBT-8D3$_{130}$-(CAG)$_7$ fails to penetrate or treat DM1 skeletal muscles.

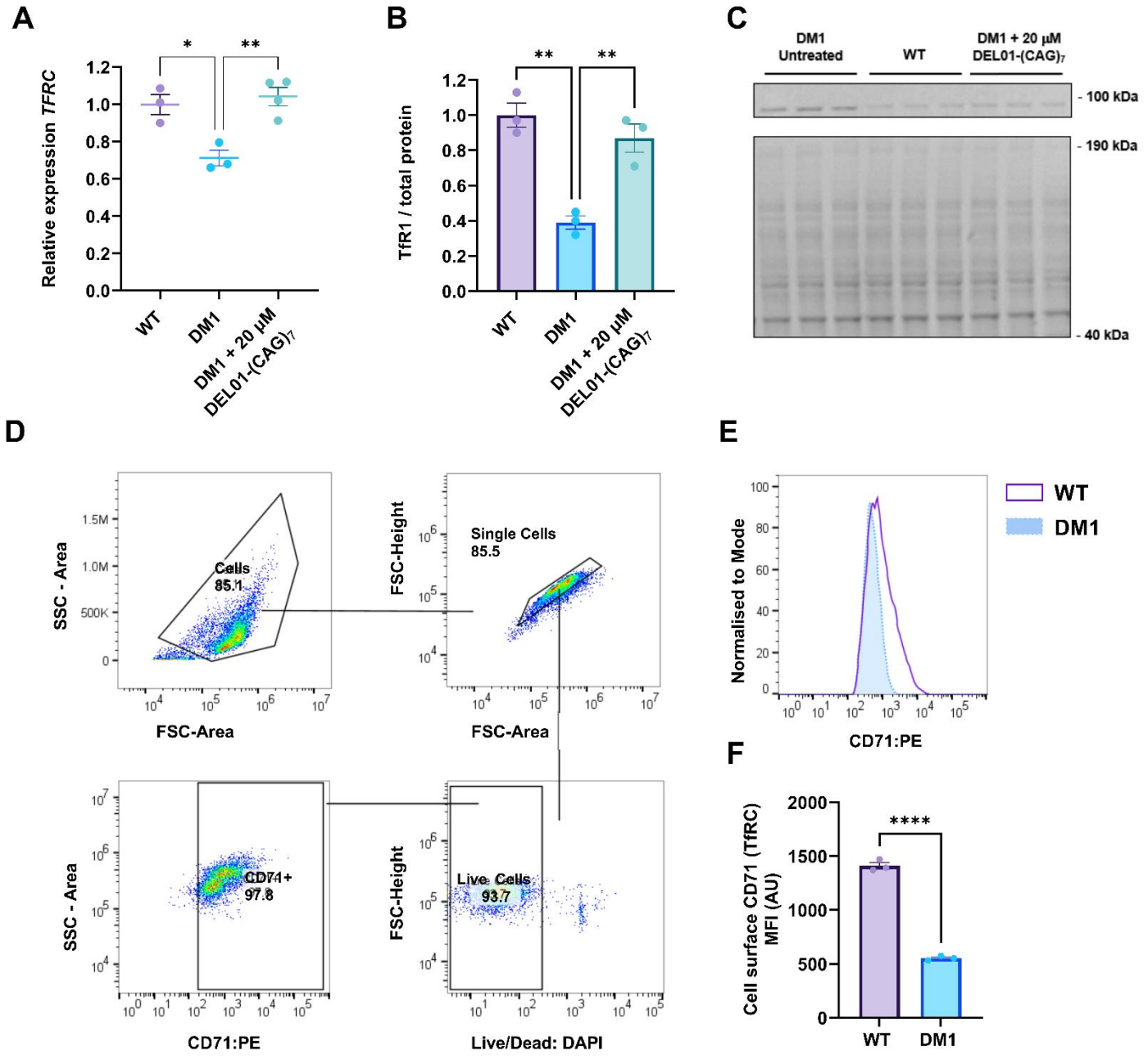

Figure *16*: DM1 patient derived myotubes exhibit reduced TfR1 expression.

TfR1 expression was analysed in 8 day differentiated WT, untreated patient derived DM1 myoblasts and **(A-B)** patient derived DM1 myotubes treated with 20 µM DEL01-$(CAG)_7$. **(A)** *TFRC* transcript expression was analysed via RT-qPCR with data normalised to *GAPDH*

and then to WT myotubes. **(B)** TfR1 total protein expression was analysed via western blot with data normalised to total protein then to WT myotubes. **(C)** Representative blots of TfR1 (top) and total protein (bottom) are also shown. **(D-F)** Cell surface expression of CD71 (TfR1) was analysed via flow cytometry. **(D)** gating strategy for selection of CD71+ myotubes via discrimination of debris, doublets and dead cells and selection of cells expressing CD71. **(E)** Fluorescent intensity of CD71+ populations were assessed showing a significant reduction in CD71 fluorescent intensity in DM1 myotubes (grey) relative to WT (white), corresponding to **(F)** a statistically significant reduction in DM1 myotube mean fluorescent intensity (MFI) analysed via student's t test. With the exception of **(D-E)**, all data are expressed as mean ± S.E.M and each dot represents one biological replicate (n=3 per group). For RT-qPCR and western blot, statistical analysis was performed via one-way-ANOVA corrected for multiple comparisons via Tukey's test. Representative *P* values for all data: *P ≤ 0.05; **P ≤ 0.01; ***P ≤ 0.001, ****P ≤ 0.0001.

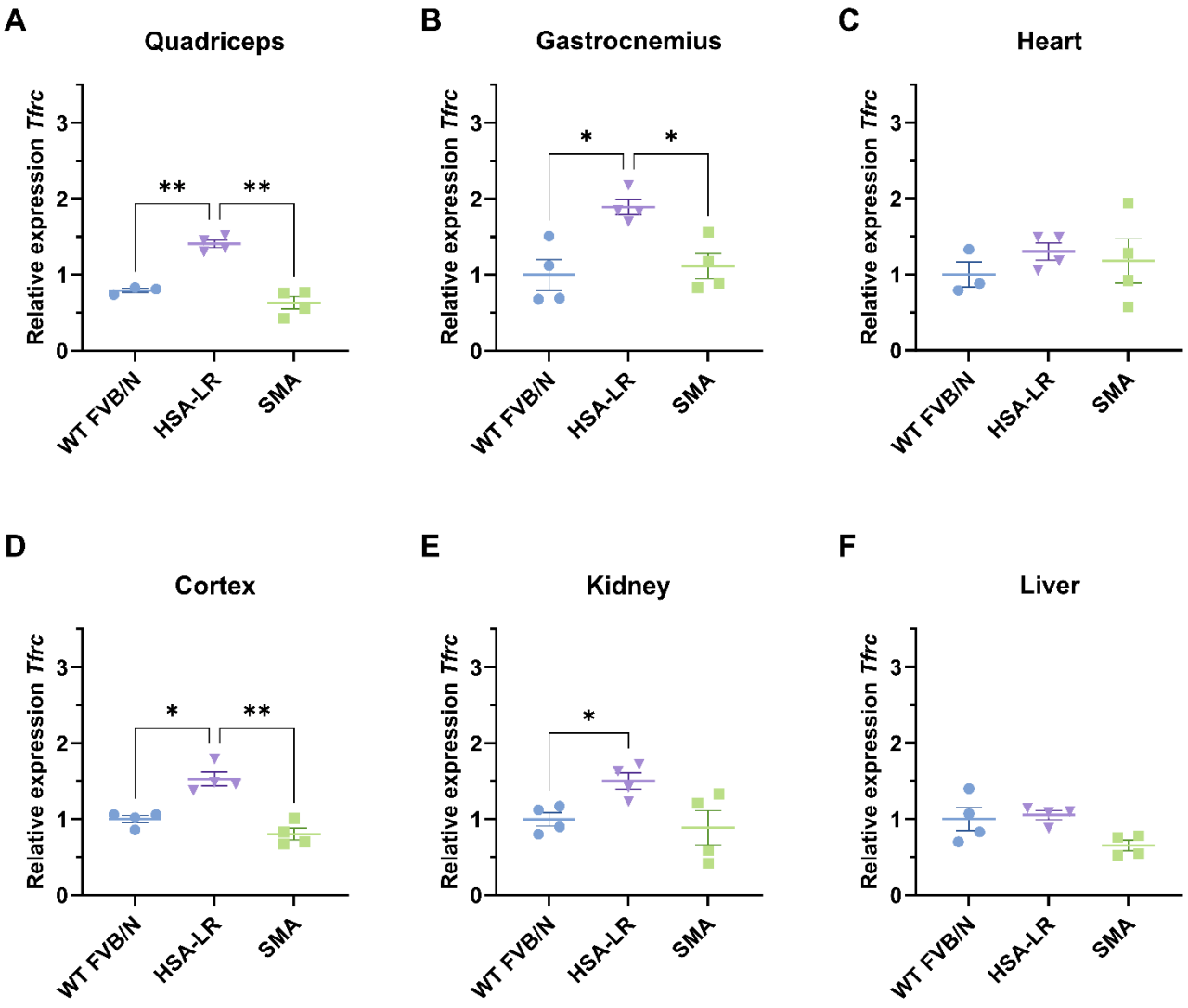

Figure *17*: Analysis of Tfrc transcript expression across tissues in HSA-LR, WT and SMA mice.

(A-F) *Tfrc* transcript levels were quantified via RT-qPCR relative in 10-week-old untreated WT FVB/N, HSA-LR and SMA mice in **(A)** quadriceps, **(B)** gastrocnemius, **(C)** heart, **(D)** brain cortex, **(E)** kidney and **(F)** liver. Data are normalized to *Polj* transcript expression then to WT FVB/N mice. Each dot represents a biological replicate (n = 4). Data are represented

as mean ± S.E.M. and compared with a one-way ANOVA test with Tukey's multiple comparison test (*P ≤ 0.05; **P ≤ 0.01; ***P ≤ 0.001, ****P ≤ 0.0001).

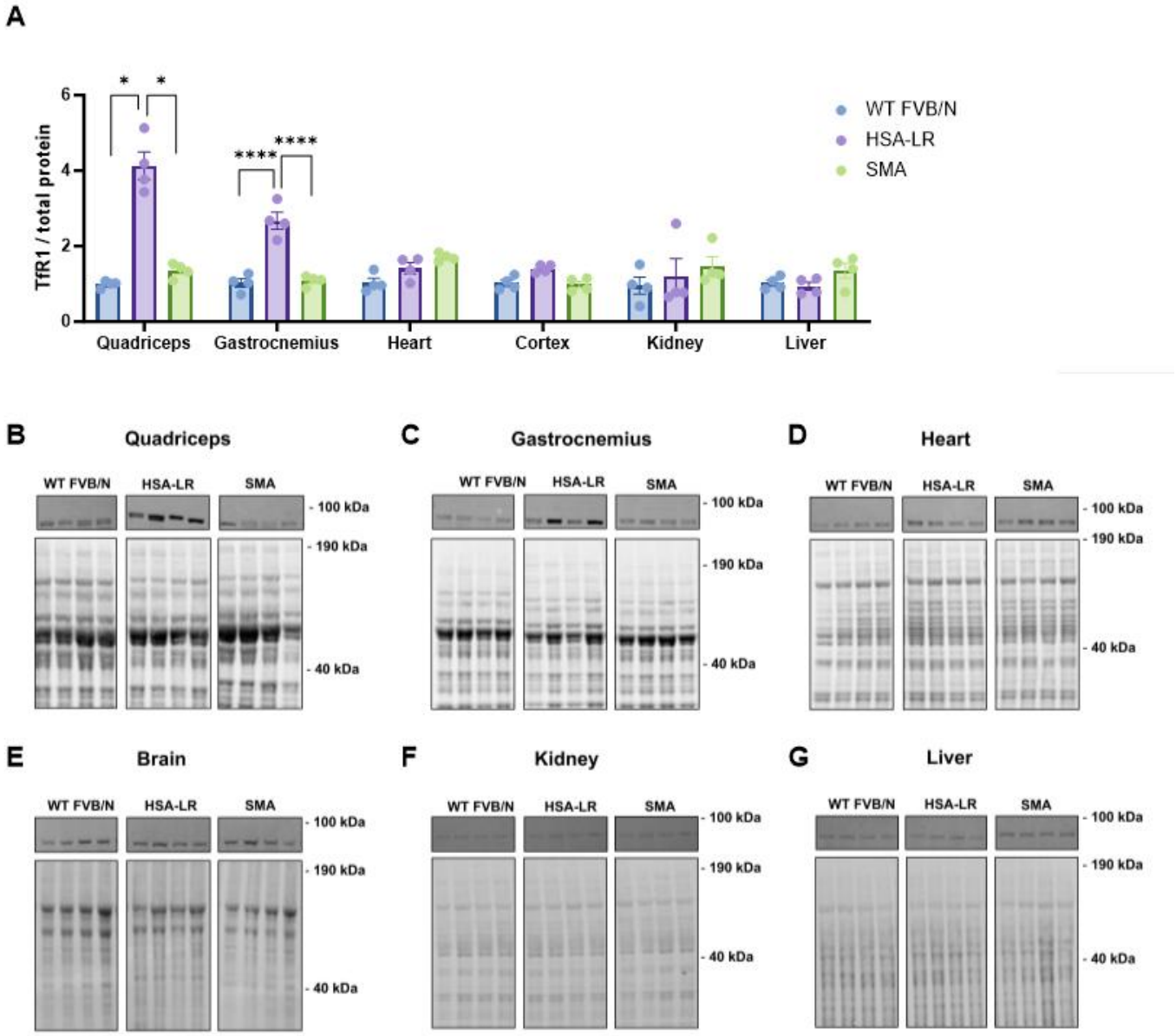

Figure *18*: Analysis of TfR1 protein expression across tissues in HSA-LR, WT and SMA mice.

(A) TfR1 protein levels were quantified via western blot relative to total protein in 10-week-old untreated WT FVB/N, HSA-LR and SMA mice. All data are normalized to WT FVB/N mice and each dot represents a biological replicate (n = 4). **(B-G)** Representative western blots show TfR1 protein in **(B)** quadriceps, **(C)** gastrocnemius, **(D)** heart, **(E)** brain cortex,

(F) kidney and **(G)** liver of WT FVB/N, HSA-LR and SMA mice (top). A representative section of total protein stain, used for protein normalization, is also shown (bottom). Size in kilodalton (kDa) is indicated on the right. Data are represented as mean ± S.E.M. and compared with a one-way ANOVA test with Tukey's multiple comparison test (*P ≤ 0.05; **P ≤ 0.01; ***P ≤ 0.001, ****P ≤ 0.0001).

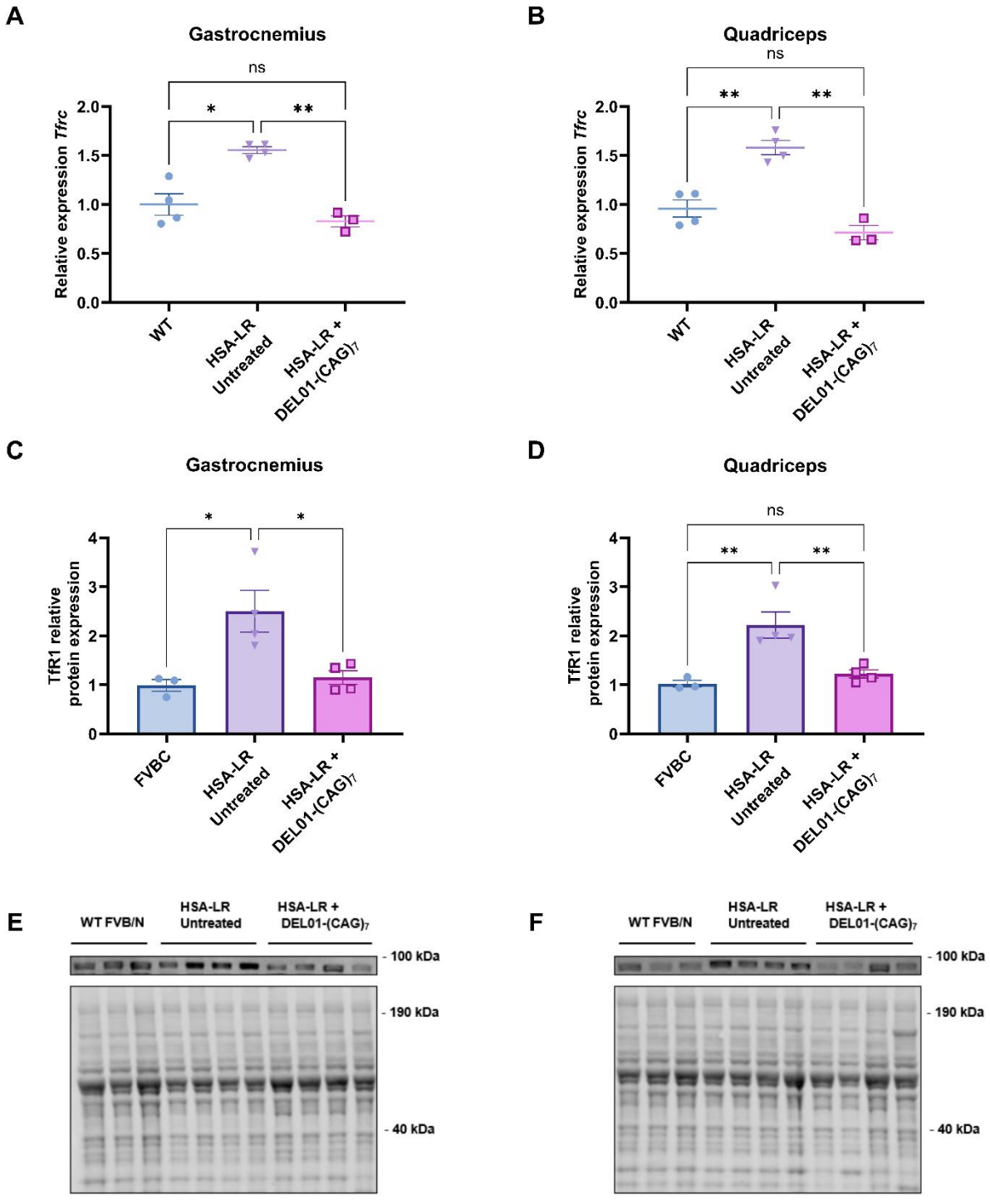

Figure *19*: Elevated TfR1 expression in DM1 HSA-LR skeletal muscles is reversed upon treatment.

10-week-old HSA-LR mice were injected with single intravenous administrations of 30 mg/kg DEL01-$(CAG)_7$ and skeletal muscles were harvested 14 d post treatment, in addition to tissues from untreated HSA-LR and WT FVB/N mice. *Tfr1* transcript expression in **(A)** gastrocnemius and **(B)** quadriceps was analysed via RT-qPCR and normalised to *Polj*. TfR1 total protein expression in **(C)** gastrocnemius and **(D)** quadriceps was analysed via western blot and normalised to total protein. Below, representative blots **(E-F)** of TfR1 (top) and total protein (bottom) are shown for both **(E)** gastrocnemius and **(F)** quadriceps. All data are normalised to untreated WT FVB/N group and expressed as mean ± S.E.M. Each dot represents one biological replicate (n=3 per group). Statistical analysis was performed via one-way-ANOVA corrected for multiple comparisons via Tukey's test. Representative *P* values for all data: *P ≤ 0.05; **P ≤ 0.01; ***P ≤ 0.001, ****P ≤ 0.0001.

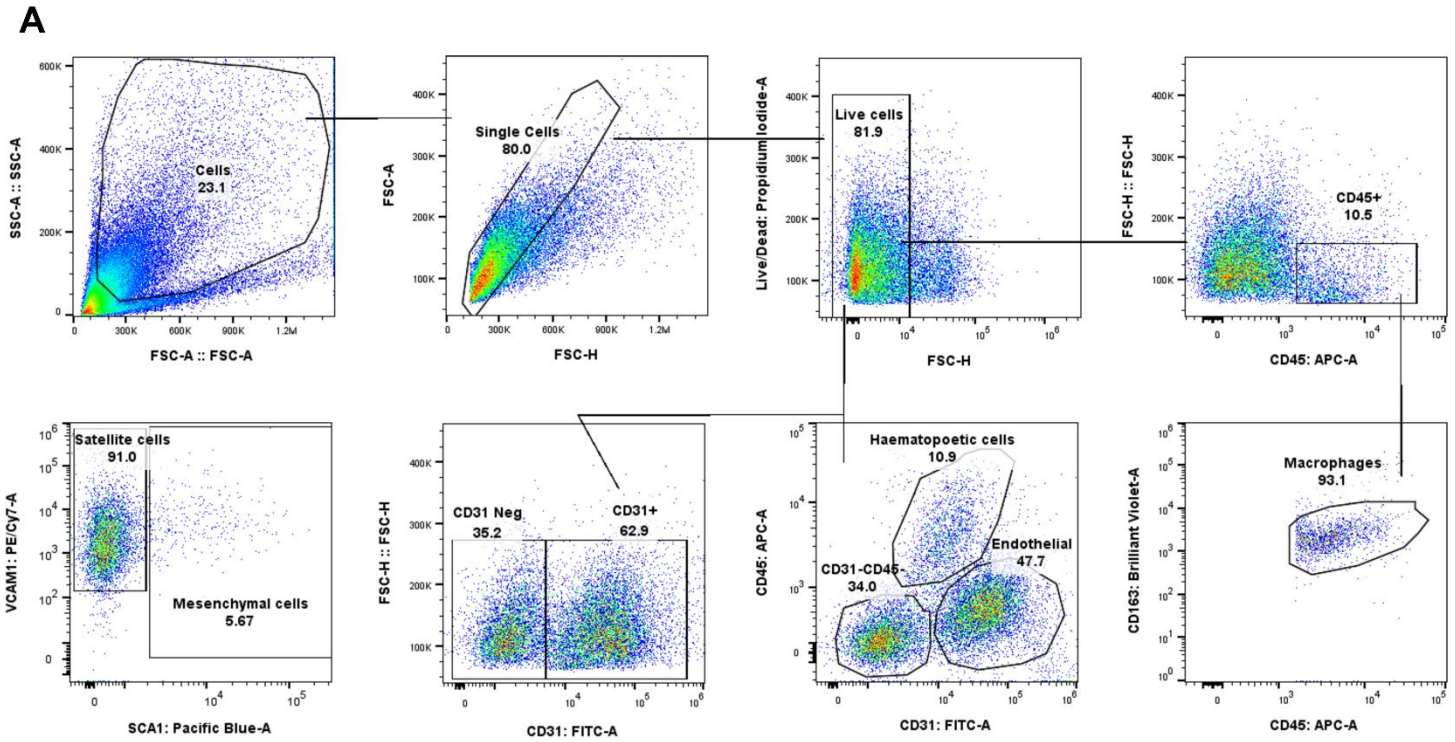
A
SSC-A :: SSC-A
FSC-A :: FSC-A
Cells
23.1
FSC-A
FSC-H
Single Cells
80.0
Live/Dead: Propidium Iodide-A
FSC-H
Live cells
81.9
FSC-H :: FSC-H
CD45: APC-A
CD45+
10.5
VCAM1: PE/Cy7-A
SCA1: Pacific Blue-A
Satellite cells
91.0
Mesenchymal cells
5.67
FSC-H :: FSC-H
CD31: FITC-A
CD31 Neg
35.2
CD31+
62.9
CD45: APC-A
CD31: FITC-A
Haematopoetic cells
10.9
Endothelial
47.7
CD31-CD45-
34.0
CD163: Brilliant Violet-A
CD45: APC-A
Macrophages
93.1

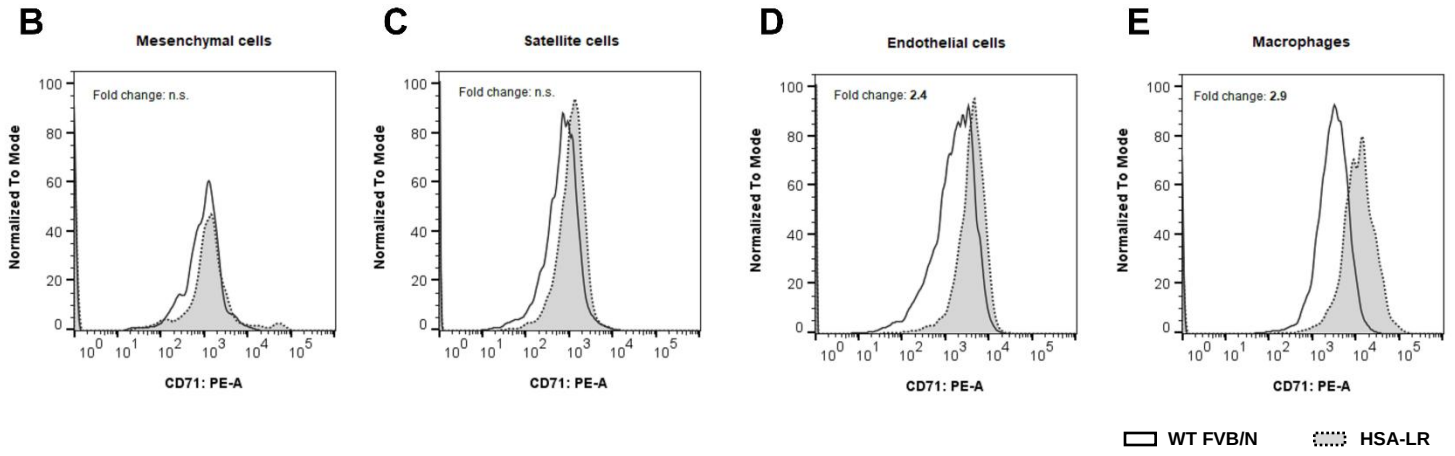
B
Mesenchymal cells
Fold change: n.s.
Normalized To Mode
CD71: PE-A
C
Satellite cells
Fold change: n.s.
Normalized To Mode
CD71: PE-A
D
Endothelial cells
Fold change: 2.4
Normalized To Mode
CD71: PE-A
E
Macrophages
Fold change: 2.9
Normalized To Mode
CD71: PE-A
WT FVB/N
HSA-LR

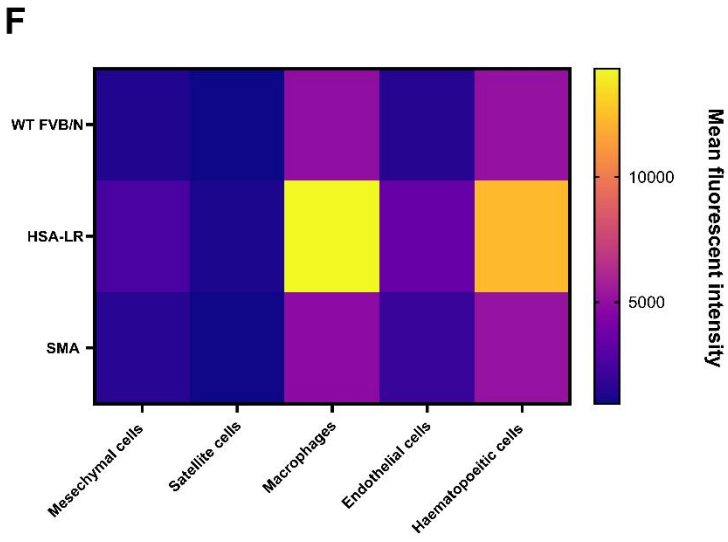
F
WT FVB/N
HSA-LR
SMA
Mesenchymal cells
Satellite cells
Macrophages
Endothelial cells
Haematopoeitic cells
10000
5000
Mean fluorescent intensity

Figure *20*: Analysis of CD71 (TfR1) cell surface expression in single skeletal muscle cells of HSA-LR, WT and SMA mice.

(A) Gating strategy for obtaining primary single cell types from WT FVB/N, SMA transgenic and DM1 HSA-LR skeletal muscle in 10-week-old mice (n=4 per group). Single cells were obtained via discrimination of debris, doublets and dead cells. Cell populations were then selected based on fluorescence intensity to identify skeletal muscle cell populations. Briefly, macrophages were identified from the CD45+ CD163+ cell population, endothelial cells were identified as CD45- CD31+ while from the CD45- CD31- population, mesenchymal stem cells (SCA1+) and satellite cells (SCA1- VCAM+) were identified. **(B-F)** Fluorescent intensity of cell surface CD71 (TfR1) was analysed in WT FVB/N, DM1 HSA-LR and SMA transgenic mice. **(B-E)** Mean fluorescent intensity (MFI) in **(B)** mesenchymal cells **(C)** satellite cells **(D)** endothelial cells and **(E)** macrophages for WT FVB/N mice (solid black line) and DM1 HSA-LR (dotted line, grey fill) with data normalised to the mode. Significant fold-change was calculated using mean fluorescent intensity for each sample followed by one-way ANOVA with Tukey's multiple comparison test (*P ≤ 0.05; **P ≤ 0.01; ***P ≤ 0.001, ****P ≤ 0.0001). **(F)** Heatmap for CD71 mean fluorescent intensity in all cell populations analysed for WT FVB/N, DM1 HSA-LR and SMA transgenic mice.

Comparison of DM1 and SMA BBT-8D3$_{130}$- and NIP228- conjugate PMO tissue concentrations

In an attempt to differentiate whether the lack of BBT-8D3$_{130}$-(CAG)$_7$ mice skeletal muscle activity was related to the animal model used or an issue with the compound itself, HSA-LR mice were treated with 50 mg/kg administrations the PMO conjugates utilized by Hammond et al. (2022) in their treatment of an SMA model. These were conjugates comprised of the BBT-8D3$_{130}$- and NIP228- antibodies conjugated to a PMO sequence targeting the intron splice silencer N1 (ISSN1) site of intron 7 in the *SMN2* gene (Porensky et al., 2012). Tissues were harvested 14 d post-administration and PMO concentrations were again analysed via ELISA. The results generated show a general trend of the SMA Ab-PMOs being able to deliver higher concentrations of PMO into the tissues than the Ab-PMOs designed to target the DM1 phenotype (Figure 21). Consequently, it could be concluded that there is potentially an issue with the synthesis, stability or uptake of BBT-8D3$_{130}$-(CAG)$_7$ and its non-targeting control NIP228-(CAG)$_7$. A Wood group chemist has also since reported that more issues of aggregation were experienced when synthesizing BBT-8D3$_{130}$-(CAG)$_7$ and NIP228-(CAG)$_7$ relative to their SMA BBT-8D3$_{130}$-PMO and NIP228-PMO counterparts. However, it should also be noted that the PMO concentrations delivered to the skeletal muscles by the SMA BBT-8D3$_{130}$- and NIP228- PMO conjugates are still relatively low, when one considers what can be achieved using high doses (> 30 mg/kg) of CPP-PMOs (see Figure 8). If similar skeletal muscle concentrations to the SMA Ab-PMOs were reached using BBT-8D3$_{130}$-(CAG)$_7$ and NIP228-(CAG)$_7$, the compounds would still be unlikely to meaningfully correct the DM1 phenotype in this mode if one compares to the levels of PMO concentration required by CPP-PMOs to exert an effect on splicing.

Overall, while BBT-8D3$_{130}$-(CAG)$_7$ is able to deliver PMO across the BBB into the CNS in HSA-LR mice, it was unable to deliver sufficient PMO concentration into the skeletal muscles to ameliorate the DM1 phenotype. Investigations to understand this failure to penetrate the skeletal muscles were not entirely conclusive but suggest that it may be related to the compound itself or that higher doses, which are not viable within the funding constraints of the project, may be required. Consequently, no further exploration of BBT-8D3$_{130}$-(CAG)$_7$ was conducted.

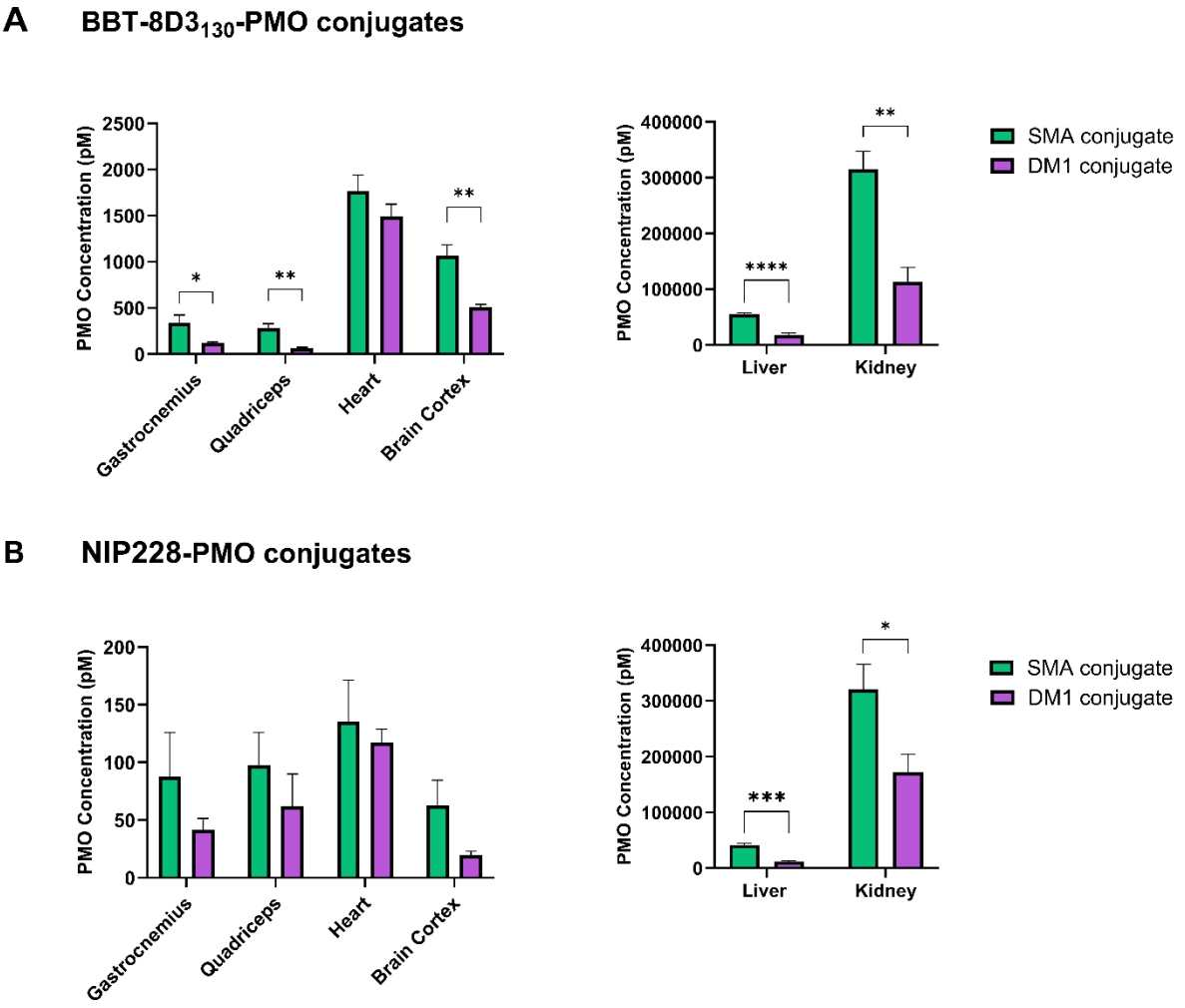

Figure *21*: Comparison of Ab-PMOs for SMA and DM1 in HSA-LR mice.

HSA-LR mice were injected with single 50 mg/kg intravenous administrations of **(A)** BBT-8D3$_{130}$ PMO conjugates or **(B)** NIP228-PMO conjugates or 0.9% saline and analysed 14 d post-administration. The BBT-8D3$_{130}$ PMO conjugates were comprised of the BBT-8D3$_{130}$ antibody conjugated to either a PMO for the treatment of SMA (ISSN-1 targeting) or DM1 (CAG_7). Similarly, NIP228-PMO conjugates were comprised of the NIP228 antibody conjugated to either a PMO for the treatment of SMA or DM1 (CAG_7). Tissue PMO concentration was quantified via ELISA in skeletal muscle, heart, brain cortex, liver and kidney. All data is represented as mean ± S.E.M. and each dot represents a biological

replicate (n=5-6 per treatment group). Statistical significance (representative P values) was determined using a student's t test. (*P ≤ 0.05; **P ≤ 0.01; ***P ≤ 0.001, ****P ≤ 0.0001).

Discussion

Anti-TfR1 targeting Ab-PMO, BBT-8D3$_{130}$-(CAG)$_7$, penetrates the CNS

The aim of this study was to evaluate the potential of an anti-TfR1 targeting Ab-PMO conjugate, BBT-8D3$_{130}$-(CAG)$_7$, as a proof of concept for a systemically delivered therapy for DM1, with the distinct advantage of therapy delivery into the CNS, in addition to other key affected tissues in DM1 pathology. In their naked form, systemically delivered ASOs are unable to cross the BBB, similarly conjugation to moieties such as CPPs only demonstrates limited improvement on CNS penetration (see Figure 8C).The data in this chapter demonstrates that BBT-8D3$_{130}$ is able to deliver (CAG)$_7$ PMO across the BBB in the DM1, HSA-LR mouse model with PMO detected in all areas of the CNS tested and the BBT-8D3$_{130}$ antibody detectable in cells within the brain parenchyma.

The BBT-8D3$_{130}$ anti-TfrR1 antibody is specifically optimized to penetrate the brain parenchyma via binding with low affinity to TfR1 on the luminal side of endothelial cells on the mouse BBB (Webster et al., 2016). The antibody is the daughter of the previously developed 8D3 antibody (Kissel et al., 1998) which binds to TfR1 with a stronger affinity (130 nM vs. 1.2 nM, respectively). It is indicated that 8D3 is capable of some transduction into the brain parenchyma, with fusion to the neuroprotective glycoprotein cytokine erythropoietin (EPO) demonstrating a modest effect in models of Alzheimer's disease (Q. H. Zhou et al., 2010). However, the lower affinity binding BBT-8D3$_{130}$ allows for improved transduction across the BBB and release into the parenchyma, contrasting with antibodies exhibiting high affinity for TfR1 which largely accumulate in brain capillaries rather than to the abluminal side (Cabezón et al., 2015; Manich et al., 2013; Moos & Morgan, 2001; Yu

et al., 2011). Thus, conjugation of BBT-8D3$_{130}$ to a PMO designed to treat SMA disease models, displayed high levels of bioavailability in the CNS and therapeutically relevant levels of SMN2 splicing and full-length SMN protein expression in a systemically treated transgenic h*SMN2* animal model (Hammond et al., 2022). The results presented in the chapter are in accordance with this study, again demonstrating the ability of BBT-8D3$_{130}$ to facilitate uptake of a PMO into the CNS and supports the concept that one can employ anti-TfR1 targeting antibodies as a means of delivering therapeutics into the CNS for the treatment of DM1 affected CNS cells.

In contrast to the previous work by Hammond et al. (2022), immunohistochemical experiments in this chapter showed that BBT-8D3$_{130}$ localises with both neuronal and astrocytes in HSA-LR mice, in contrast to merely the glial cell penetration seen in the h*SMN2* SMA model. The reason for this difference is unclear, beyond possible differences in animal models or unexpected differences arising from differing PMO sequences. However, the potential to treat both cell types would be of great benefit to DM1 patients, who may suffer from cognitive dysfunction and decline, fatigue and hypersomnia (Gallais et al., 2017; Heatwole et al., 2012; Kierkegaard et al., 2009). Loss of signaling in both dopaminergic and serotonergic neurons has been reported in adult DM1 patients, in addition to abnormal glutamatergic transmission (Takado et al., 2015). While downregulation of the glutamate transporter 1 (GLT1) has been reported in DM1 patient and DMSXL astrocytes, with the latter proving to lead to impaired glutamate transportation and ultimately excitotoxicity in neurons (Sicot et al., 2017). Furthermore, nuclear *foci* and spliceopathy have been documented in both cell types (Jiang et al., 2004; Sicot et al., 2017).

A limitation of the immunohistochemistry experiments that should be noted, however is that the PMO component of the conjugate is not detected by the staining, only the antibody moiety. There is therefore an assumption that the Ab-PMO conjugates are not degraded prior to cellular uptake. Nevertheless, combined with the PMO concentrations quantified in HSA-LR tissues via ELISA and the evidence of CNS efficacy in the Hammond et al. study, the data strongly suggests successful delivery of BBT-8D3$_{130}$-(CAG)$_7$ into the CNS and its target cell types. Furthermore, a comparison of PMO concentrations in the brain cortex following treatment with BBT-8D3$_{130}$-(CAG)$_7$ and the CPP-(CAG)$_7$ conjugates tested in results chapter 2 reveals that a 50 mg/kg dose of BBT-8D3$_{130}$-(CAG)$_7$ delivers more than twice the amount of PMO to the cortex compared to the 30 mg/kg DEL01-(CAG)$_7$, which was the most effective CPP-(CAG)$_7$ regimen tested and, with regard to molarity, provides a significantly higher dose of ASO. This highlights the significant advantage of anti-TfR1 conjugation in enhancing CNS penetration for PMO delivery.

This is not the first anti-TfR1 antibody or antibody fragment to have successfully leveraged this pathway for the delivery of drug cargoes into the CNS. For example, the use of TfR1 antibodies in drug delivery has been explored in the development of bispecific antibodies, such as those employed by Yu et al. (2011, 2014). In their work, an anti-TfR1 arm is conjugated to enzyme β-secretase (BASE1) to enhance its CNS penetration for the degradation of amyloid precursor proteins associated with Alzheimer's disease.

More recently, Roche (Germany) has developed a bispecific fusion protein, trontinemab (RG6102), which is currently undergoing clinical trials for Alzheimer’s disease (Roche, NCT04639050). This compound fuses an anti-amyloid-beta antibody with a Brainshuttle™ module targeting human TfR1, allowing for significantly improved BBB penetration compared to traditional antibody therapies (Grimm et al., 2023). Beyond Alzheimer's

disease, Roche's Brainshuttle platform has been designed for broader CNS delivery, with potential applications in delivering nucleic acids and other therapies.

Additionally, TfR1-targeting antibodies have been employed in other therapeutic areas, such as the treatment of mucopolysaccharidosis II (MPSII). The bispecific antibody JR-141, which combines a TfR1-targeting domain with the enzyme iduronate-2-sulfatase, showed promising results in preclinical studies in mice and non-human primates, reaching the cerebellum and hippocampus, in addition to peripheral tissues (Sonoda et al., 2018). JR-141 was later progressed to clinical trials, where it has been shown to reduce cerebrospinal fluid glycosaminoglycan levels, a key biomarker of MPSII (Giugliani et al., 2021). However, as noted by Hammond et al. (2022), the specificity of the TfR1 binding remains unclear as no antibody isotope control was tested in these studies.

Despite the amount of CNS targeting therapies that already exploit TfR1, this successful proof of concept of PMO delivery into the CNS is particularly notable for the field of DM1. DM1 therapies have historically struggled to achieve CNS penetration, with most efforts primarily focused on skeletal muscle delivery. The only published DM1 ASO that has been shown to improve the CNS phenotype remains IONIS 486178, a gapmer that targets mutant *DMPK* transcripts. This compound has demonstrated an ability to ameliorate spliceopathy in induced pluripotent stem cell (iPS)-derived DM1 neural cells and was able to reduce expanded *DMPK* transcripts in the CNS of DMSXL mice while also reversing behavioral abnormalities (Ait Benichou et al., 2022). However, to ensure efficacy, IONIS 486178 was administered directly into the brain via intracerebroventricular injection.

While there are currently two anti-TfR1 targeting ASO therapies in clinical trials for DM1, DYNE-101 (Dyne Therapeutics and AOC-1001 / del-desiran (Avidity Biosciences), their primary treatment targets have been skeletal muscle and heart, with much of the

preclinical and clinical trial data presented focusing on those two tissues. However, Dyne Therapeutics recently presented data indicating that their TfR1 targeting delivery ‘FORCE’ platform enables widespread ASO delivery to the brain in non-human primates following intravenous administration, outperforming an intrathecally delivered naked ASO (Dyne Therapeutics, 2024). While it is important to note that this data is unpublished and has yet to be peer-reviewed, this achievement could be highly promising for DM1 patients, particularly when considered alongside the positive results from the ongoing Phase I/II ACHIEVE clinical trial (Dyne Therapeutics, NCT05481879).

Efficient traversing of the BBB is also a persistent challenge in the broader context of neuromuscular diseases, particularly with regards to ASO therapies. For instance, Tominersen, an ASO developed as a treatmant for Huntington's disease by IONIS Pharmaceuticals and Roche requires direct intrathecal delivery to bypass the BBB (Tabrizi SJ et al., 2019). Similarly, Nusinersen, an ASO for SMA, also developed by IONIS Pharmaceuticals, is again administered to patients intrathecally (Finkel et al., 2016).While these therapies have greatly improved patient outcomes, intrathecal administration is highly invasive and costly. Moreover, a number of neuromuscular diseases including SMA (i.e. DM1 and DMD), present with systematic disease pathology that would benefit from the treatment of peripheral tissues. In the same way that the BBB limits the systemic delivery of unconjugated ASOs to the CNS, it can also impede the delivery of intrathecally administered ASOs to peripheral tissues. In this context, utilizing an intravenous anti-TfR1-PMO delivery method offers a non-invasive strategy to reach the brain, expanding the potential for systemic treatment of both CNS and peripheral organ pathologies.

Anti-TfR1 targeting Ab-PMO, BBT-8D3$_{130}$-(CAG)$_7$, penetrates the heart

In addition to achieving PMO delivery to the CNS, BBT-8D3$_{130}$-(CAG)$_7$, also demonstrated effective delivery into heart tissues of HSA-LR mice. As previously discussed in results chapter 2, DM1 patients experience extensive cardiac issues including cardiomyopathies and arrhythmias (Groh et al., 2008; Nguyen et al., 1988), with cardiac involvement being a leading cause of mortality in DM1 patients (De Die-Smulders et al., 1998; Groh et al., 2008). Therefore, the ability to treat cardiac tissues is of great therapeutic benefit.

While BBT-8D3$_{130}$-(CAG)$_7$ achieved heart delivery, its efficacy was somewhat lower than that of CPP-PMO conjugates when compared at doses expressed in mg/kg. However, direct comparisons in mg/kg are misleading due to the significant difference in molecular weight between the two conjugates. BBT-8D3$_{130}$-(CAG)$_7$ is approximately 18.5 times larger than DEL01-(CAG)$_7$ (168,624 g/mol vs. 9,126 g/mol). Therefore, a 50 mg/kg administration of BBT-8D3$_{130}$-(CAG)$_7$ is equimolar to only a 2.7 mg/kg dose of DEL01-(CAG)$_7$. At these equimolar doses, it becomes apparent that Ab-PMO has enhanced delivery to the heart, particularly when considering that a 7.5 mg/kg dose of DEL01-(CAG)$_7$ results in concentrations of less than 50 nM of PMO in the heart whereas a 50 mg/kg administration of BBT-8D3$_{130}$-(CAG)$_7$ (equimolar to 2.7 mg/kg of DEL01-(CAG)$_7$) led to a PMO concentration in the heart of ~ 1500 pM. This therefore renders BBT-8D3$_{130}$-mediated PMO delivery to the heart particularly impressive, especially given that the upper limit of Ab-PMO tolerance in mice has not yet been reached (or even fully determined), due to the high cost of the antibody. Moreover, when considering clinical applications, the significantly higher manufacturing costs of antibody conjugates compared to CPPs may also be a consideration for in determining the overall cost-benefit ratio with regards to delivery to the heart.

Interestingly, the mechanisms leading to BBT-8D3$_{130}$-(CAG)$_7$ heart delivery appear to be only partially mediated by TfR1. The non-targeting isotope control antibody conjugate NIP228-(CAG)$_7$ also displayed reasonable uptake in the heart, indicating the involvement of an alternative mechanism of cellular uptake. Furthermore, small amounts of non-specific uptake can also be noted in other tissues (see Figures 13-15). One possible route of uptake could be via the neonatal Fc receptor (FcRn). FcRn interacts with, transports and recycles immunoglobulin G (IgG), preventing its lysosomal degradation (Roopenian & Akilesh, 2007). The expression of FcRn is relatively widespread across tissues and species, with its expression being consistently high among endothelial cells and macrophages (Latvala et al., 2017). It is therefore possible that circulating BBT-8D3$_{130}$ and the control antibody NIP228 could interact with endothelial FcRn, facilitating non-TfR1-mediated cellular uptake. In general, FcRn uptake of antibody-drug-conjugates is underexplored but further could be extremely valuable given its potential to influence delivery efficiency of many antibody-based therapies.

Anti-TfR1 targeting Ab-PMO, BBT-8D3$_{130}$-(CAG)$_7$, fails to treat skeletal muscles in HSA-LR mice

Despite the promising results in the CNS and heart, BBT-8D3$_{130}$-(CAG)$_7$ showed disappointing penetration and therapeutic efficacy in HSA-LR skeletal muscles, a critical issue given that muscle weakness and myotonia are hallmark features of DM1. Analysis of key splicing biomarkers in gastrocnemius and quadriceps showed no significant amelioration of splicing, while similarly there was no improvement in functional hind limb myotonia. This was the same for administrative doses of both 50 mg/kg and 100 mg/kg.

The lack of activity observed can be explained by the remarkably low PMO concentrations (< 250 pM) detected within the skeletal muscle, suggesting that insufficient delivery is the primary limitation to treatment efficacy. This low skeletal muscle penetration was, however, initially puzzling, especially given that SMA mice were able to be successfully treated by an BBT-8D3$_{130}$-PMO conjugate (Hammond et al., 2022) and the successful use of other anti-TfR1-ASO conjugates designed for enhancing skeletal muscle activity. For example, as previously mentioned, both Dyne Therapeutics and Avidity Biosciences have compounds in clinical trials for the treatment of several neuromuscular diseases, including DMD, DM1 and fascioscapulohumeral muscular dystrophy (FSHD). Their advanced compounds utilize TfR1 targeting antibody-based platforms that are able to successfully facilitate the skeletal muscle, heart and diaphragm delivery of ASOs and siRNAs (Desjardins et al., 2022; Malecova et al., 2023), which contrasts with the limited muscle delivery observed in the current study. Similarly, Sugo et al. (2016) showed that the conjugation of an siRNA to an anti-TfR1 antibody resulted in improved delivery and silencing activity in skeletal muscles and cardiac tissue in WT BALB/C mice. Meanwhile their isotope IgG control–siRNA was not active in the skeletal muscle.

To understand the lack of skeletal muscle activity, TfR1 expression in tissues of HSA-LR mice were investigated as previous experiments in DM1 differentiated patient derived myotubes had shown that TfR1 is downregulated relative to cells from healthy controls. No such effect was observed in HSA-LR skeletal muscles, rather TfR1 was shown to be overexpressed in HSA-LR muscles and specifically on the cell surface of skeletal muscle endothelial cells and resident macrophages. As such, this renders altered TfR1 expression an unlikely explanation for the lack of $(CAG)_7$ delivery by BBT-8D3$_{130}$ into skeletal muscles.

It should be noted, however, that while expression of TfR1 was assessed the functional activity and its cellular internalisation was not investigated.

A more likely rationale for the failure of BBT-8D3$_{130}$-(CAG)$_7$ delivery to skeletal muscles lies with the compound itself and the dose administered. Treatment of HSA-LR mice with BBT-8D3$_{130}$- and NIP228- PMO conjugates, previously employed in the SMA study by Hammond et al. (2022), showed enhanced delivery over the BBT-8D3$_{130}$- and NIP228-(CAG)$_7$ conjugates tested in this body of work. Coupled with chemist reports that the (CAG)$_7$ antibody conjugates were challenging to synthesize and prone to aggregation, it is possible that physiochemical properties may contribute to the lack of skeletal muscle uptake. Nevertheless, it is important to highlight that the PMO concentrations delivered to skeletal muscles by the SMA BBT-8D3$_{130}$-PMO conjugates are still considered to be relatively low. Historically, it has been found, from studies involving CPP-PMOs in the Wood group, that significant changes in DM1 splicing biomarkers are only observed when skeletal muscle PMO concentrations exceeded a threshold of 400 pM following single intravenous administrations. This is supported by the results presented in results chapter 2 (see figures 7 and 8). Therefore, even if BBT-8D3$_{130}$-(CAG)$_7$ delivered PMO into skeletal muscles to the same level as SMA BBT-8D3$_{130}$-PMO, it is unlikely that the compound would be able to significantly treat the DM1 phenotype in HSA-LR skeletal muscles.

In the case of SMA, the therapeutic mechanism involves a single PMO binding to the ISSN1 site on *SMN2* pre-mRNA, leading to splicing correction and translation of the full-length SMN2 protein, effectively ameliorating the disease phenotype (Hua et al., 2008; Porensky et al., 2012). However, treating DM1 presents a more complex challenge due to differences in stoichiometry. DM1 therapies using steric-blocking, non-RNase H-dependent PMOs, such as (CAG)$_7$, may require multiple PMOs to bind to a single repeat-

expanded transcript. This is because a single transcript in DM1 can sequester multiple MBNL1 proteins, thus potentially requiring more PMOs to effectively neutralize the toxic RNA. Such stoichiometric differences could therefore further explain the differences in efficacy observed in this study and the previous work carried out in SMA mice, as a higher PMO concentration is required to disrupt MBNL1 sequestration in DM1 muscles cells and correct the DM1 phenotype. Ultimately in the case of BBT-8D3$_{130}$-(CAG)$_{7,}$ to achieve greater skeletal muscle penetration to elicit meaningful activity, a greater dose may be required. Unfortunately, this was not viable within the funding constraints of this project.

A final contributor to the poor skeletal muscle penetration of BBT-8D3$_{130}$-(CAG)$_7$ could be the use of BBT-8D3$_{130}$ as the anti-TfR1 moiety. BBT-8D3$_{130}$ was specifically optimized for improved CNS penetration by reducing the binding affinity to TfR1 localised to the BBB (Webster et al., 2016). As already discussed, this resulted in the successful delivery of the (CAG)$_7$ PMO to the CNS in HSA-LR mice, in addition to its proven successful CNS delivery of a PMO for the treatment of SMA (Hammond et al., 2022) and an antagonist against the interleukin-1 receptor (IL-1R) for the treatment of neuropathic pain (Webster et al., 2016). However, the impact of the optimization for CNS delivery has never been investigated with regards to delivery into peripheral tissues. It is possible that binding affinity requirements for optimal internalisation and cytoplasmic release differ between the BBB and the endothelium of other tissues. Consequently, there may not be a ‘one-size-fits-all’ solution with regards to designing anti-TfR1 technologies able to deliver sufficient concentrations of their drug cargo in diseases where there are multiple target tissues, as in the case of DM1.

Despite the disappointing results obtained through the testing of BBT-8D3$_{130}$-(CAG)$_7$ in skeletal muscle, the advancement of two DM1 therapies that take advantage of the TfR1

receptor-mediated uptake to clinical trials mean that this strategy cannot be discounted as a means of treating DM1 skeletal muscle. The 'FORCE platform' developed by Dyne therapeutics comprises of an anti-TfR1 antibody fragment and when conjugated to an ASO which targets DMPK mRNA transcripts (DYNE-101), knockdown is induced, leading to a reversal of the DM1 phenotype in animal models (Dyne Therapeutics, 2021). DYNE-101 is currently in phase 1/2 clinical trials and displaying promising results (Dyne Therapeutic, ACHIEVE: NCT05481879). Meanwhile Avidity Biosciences developed del-desiran or AOC 1001, a compound comprised of a monoclonal TfR1 antibody conjugated to an siRNA targeting *DMPK* mRNA (Malecova et al., 2023). Treatment of patients with del-desiran as part of phase 1/2 clinical trials (Avidity Biosciences, MARINA: NCT05027269) led to functional improvements in muscle strength, mobility and voluntary open hand timing (vHOT), alongside improvements in myotonia and reductions in *DMPK* mRNA. As of this year, del-desiran gained acceleration to a phase 3 clinical trial (Avidity Biosciences, HARBOUR: NCT06411288). Similarly to DYNE-101, del-desiran demonstrated a favourable safety profile.

Ab-PMOs present a safe toxicological profile

One promising result that arose from the testing of the Ab-PMO conjugates, BBT-8D3$_{130}$-(CAG)$_7$ and NIP228-(CAG)$_7$, in HSA-LR was that lack of toxicity detected following treatments. For the duration of the study, all animals appeared healthy and showed no signs of lethargy or compound-induced toxicity. Furthermore, despite high PMO accumulation in the kidneys (Figure 14F), no significant toxicity was observed in any of the antibody conjugate treatment groups for any of the biomarkers assessed (Figure 12).

As suggested by Hammond et al (2022), where similar biodistribution patterns were observed, the absence of kidney toxicity could be explained by the natural renal processing of monoclonal antibodies (mAbs). Most mAbs are reabsorbed in the proximal tubules and recirculated systemically (Lobo et al., 2004). However, as high PMO accumulation in the kidneys occurred and the molecular mass of $8D3_{130}$-PMO is ~ 110 kDa greater than the glomerular filtration cut off (170 kDa vs. 60 KDa), this PMO accumulation is likely due to the conjugate being metabolic cleaved to release free PMO moieties. Subsequent PMO reabsorption by the kidney proximal tubule epithelia would therefore be expected, given previous reports detailing kidneys as a primary site of naked ASO accumulation (Engelhardt, 2016; Sazani et al., 2011). In addition to a lack of nephrotoxicity, no CNS or hepatoxicity was detected in any other toxicity biomarkers analysed.

Overall, the absence of compound-induced toxicity is notable since other PMO conjugates, such as peptide-PMOs, have often been limited by kidney toxicity. The findings suggest a significant advantage of antibody-PMO conjugates over other PMO conjugate types due to the lower toxicity risk. This is further supported by the favourable safety profiles observed in the clinical trials for DYNE-101 and del-desiran (Dyne Therapeutic, ACHIEVE: NCT05481879; Avidity Biosciences, MARINA: NCT05027269).

TfR1 is differentially expressed in DM1 cellular and animal models

Lastly, while proven to be unrelated to the successes and failure of BBT-$8D3_{130}$-$(CAG)_7$ in the HSA-LR mouse, an intriguing observation from the data presented in this chapter is the differential expression of TfR1 between animal models and species models. Specifically, it

was observed that TfR1 expression is reduced in patient-derived DM1 myoblasts differentiated into myotubes. While in contrast, TfR1 was overexpressed in the skeletal muscles of the HSA-LR mouse model.

A possible explanation for this discrepancy, beyond inherent species differences, may lie in the composition of the samples. The human-derived myotube cultures consist of a single cell type, whereas murine skeletal muscles are tissues containing a heterogeneous population of cells where expression patterns may also be influenced by interactions between different cell types and their surrounding environment. Therefore, qPCR and western blot analyses of murine muscles are confounded by this complexity. Single-cell analysis of the TfR1 CSE on HSA-LR skeletal muscles using flow cytometry enabled the separation of different cell types. However, it unfortunately was not possible to isolate single muscle fibres or myotubes via this technique, limiting the ability to directly compare with the data from cultured myotube. Nevertheless, the flow cytometry analysis did interestingly reveal that TfR1 CSE is unchanged in satellite cells and mesenchymal cells but significantly elevated in endothelial cells and macrophages.

Macrophages are particularly sensitive to oxidative stress, a phenomenon well-documented in dystrophic muscles where increased oxidative stress due to mitochondrial dysfunction and chronic inflammation leads to elevated reactive oxygen species (ROS) (Casati S. R et al., 2024; Petrillo et al., 2017; Renjini et al., 2012). Typically, the iron-responsive element/iron regulatory protein (IRE/IRP) system would act to counteract this by reducing TfR1 expression to prevent iron accumulation in stressed cells (Rouault, 2006). Conversely, macrophages, key to detoxifying ROS in stressed tissues, require iron for the production of antioxidant enzymes and so can upregulateTfR1 to facilitate iron import, enabling antioxidant synthesis and overall supporting their metabolic demands

under oxidative stress conditions, as they detoxify tissues and neutralising ROS (Recalcati & Cairo, 2021).

In the context of DM1, although inflammation is present, it is less prominent in comparison to other muscular dystrophies like DMD. However, mitochondrial dysfunction and increased accumulation of ROS have been noted in patients and DM1 cell line (García-Puga et al., 2020; Hasuike et al., 2022; Sahashi K et al., 2005; Toscano et al., 2005), highlighting the potential contribution of oxidative stress to the disease's progression. One could therefore plausibly hypothesize that the observed overexpression of TfR1 in HSA-LR skeletal muscles may be attributed to the oxidative stress and mitochondrial dysfunction characteristic of DM1 pathology, particularly in macrophages.

In contrast, the reduced expression of TfR1 in patient-derived DM1 myotubes may be a result of the differentiation process itself. While conducting these experiments, visual inspection of differentiating cells in the immortalised wild-type (WT) and DM1 patient-derived myoblast cell lines suggested that the lines may be differentiating at different speeds, with the DM1 line appearing to form elongated myotubes more rapidly. This variation was challenging to confirm as typical markers of myoblast differentiation such as myosin heavy chains are affected by the DM1 disease pathology (Rinaldi et al., 2012).There is evidence to suggest that TfR1 expression in skeletal muscle cells decreases with age (Ding et al., 2021), this could explain the downregulation observed in the in vitro models, if the DM1 myotubes are indeed more advanced. However further, more robust, experiments are needed to confirm these hypotheses.

Overall, the distinct cellular environments and cell types involved likely account for the contrasting TfR1 expression patterns observed between human cell cultures and animal models. For future research focused on targeting TfR1, it will be crucial to account for

these differences—not only species and model-specific variations but also discrepancies between healthy and diseased states. These factors have the potential to significantly influence the effectiveness of therapeutic strategies aimed at modulating TfR1 expression. Furthermore, the field may also benefit from more comprehensive studies examining TfR1 biodistribution across tissues, particularly focusing on cell surface expression. Such insights would be invaluable for enhancing and predicting the biodistribution of therapeutic strategies.

General discussion:

The therapeutic landscape of DM1

Antisense therapy

Antisense therapies, utilising ASOs or siRNAs, have been a major focus of DM1 treatment development. Over the years, the chemistry of ASOs and siRNAs has been modified to increase stability, target binding affinity and resistance to nuclease degradation. For example, use of bridged nucleic acids such as locked nucleic acids (LNAs) and cEt modifications improve RNA-binding affinity and protect ASOs from serum and nuclease degradation (Morita et al., 2002; Vester & Wengel, 2004). Meanwhile, PMO modification of an ASO backbone allows for greater nuclease resistance, serum stability and reduced non-specific binding. However, one major drawback of PMOs is that compound neutrality prevents binding to plasma protein, leading to rapid renal clearance (Amantana et al., 2007; Hudziak et al., 1996; Iversen P.L, 2001; Youngblood et al., 2007).

In general, it has been shown across the field of neuromuscular diseases that naked or unconjugated ASOs are not capable on their own of penetrating skeletal muscle at high enough concentrations to enact a therapeutic benefit. For instance, in the case of DM1, despite IONIS-DMPKRx (ISIS 598769), a naked gapmer developed by IONIS Therapeutics, demonstrated good potency and ability to correct the DM1 phenotype in the DMSXL model (Thornton et al., 2023). However, the compound failed in clinical trials, with drug concentrations below the levels predicted to achieve sufficient *DMPK* target reduction in skeletal muscles (Ionis Therapeutics: NCT02312011). While intramuscular administration could overcome such issues for skeletal muscle, the multi-systemic nature of DM1 renders a systemic administration route more desirable and if successful, more

beneficial to patients. Therefore, to circumvent delivery issues many groups and companies in the neuromuscular disease field turned to ASO conjugation as a means of improving ASO delivery into cells and key tissues.

PGN-EDODM1, a CPP-PMO, is currently in phase 1 clinical trials, with initial data expected in the latter phase of 2024 (PepGen: FREEDOM-DM1, NCT06204809). As the first CPP-PMO to be tested in DM1 patients, this is greatly anticipated with safety data of great interest, due to the nephrotoxicity commonly associated with CPPs (Amantana et al., 2007; Gait et al., 2019; Sazani et al., 2011). Promising data from these trials would support the further development of DEL01-$(CAG)_7$, given that the compound utilises the same PMO but employs a more optimised iteration of the PGN-EDODM1 CPP component.

Meanwhile, although BBT-$8D3_{130}$-$(CAG)_7$ was shown to be unsuccessful in treating a DM1 animal model, del-desiran and Dyne-101, developed by Avidity biosciences and Dyne therapeutics respectively, demonstrate the promise of utilising anti-TfR1ASO conjugates as a means to penetrating skeletal muscle and heart. These compounds are more advanced in clinical trials than PGN-EDODM1, with data from patients regarding compound efficacy and impact on quality of life appearing extremely positive (Dyne Therapeutics, ACHIEVE: NCT05481879; Avidity Biosciences, MARINA: NCT05027269). Furthermore, the favourable safety profile that this class of compounds presents, potentially offers a distinct advantage over CPP-ASO conjugates. However, the cost of such compounds will be significantly greater, given the expense of synthesising antibodies relative to peptides. What is yet to be determined is whether their efficacy extends to treating CNS associated DM1 symptoms in patients.

One additional form of ASO conjugation that is being employed as a strategy for improved delivery to DM1 muscle tissues, that was not explored in this thesis, is lipid conjugation. By

conjugating ASOs to hydrophobic lipid moieties, association with lipoproteins such as serum albumin are enhanced and ASO uptake is increased, as a result of albumin interactions with endothelial cell surface receptors, including on skeletal and cardiac muscle cells (Biscans et al., 2019; Khan et al., 2016).

The group of Roberto Artero at the University of Valencia have developed antisense compounds comprised of cholesterol conjugated to antagomiRs which sterically block microRNAs (miRNAs). AntagomiR-23b and antagomiR-218 target miRNA 23b-3p and miRNA 218 respectively, both of which are endogenous repressors of MBNL1 and MBNL2. As a result, MBNL1 protein levels are increased, leading to a correction in skeletal muscle splicing defects (Cerro-Herreros et al., 2018). This has led to the development of ATX-01 (ARTHEx Biotech, Valencia, Spain), an antagomir targeting miR-23b, which has just begun a Phase 1/2 clinical trial (ARTHEx Biotech, NCT06300307) that is expected to conclude late in 2025.

Small molecules

Beyond RNA therapies for DM1, there are number of small molecules being tested in clinical trials, the majority of which are repurposed from the treatment of other diseases. A key advantage of this is that compound safety is already determined, rendering clinical trials and access for patients to effective treatment, a far quicker process. These small molecule therapies can be divided into two main categories: those targeting the underlying cause of DM1 and those addressing specific disease symptoms. The latter category includes Mexiletine, an antiarrhythmic drug which reduces myotonia (Heatwole et al., 2021); cannabinoids, used for chronic pain and myotonia management (Montagnese et al., 2019); pitolisant, which treats excessive daytime sleepiness (Harmony BIosciences, 2024); and metformin, a diabetic drug which has shown potential in correcting splicing

abnormalities via AMPK activation (Bassez et al., 2018). Each of these therapies offer the hope of providing symptomatic relief to patients that may improve their overall quality of life.

Of the small molecule drugs that target the underlying cause, tideglusib is the most advanced. Tideglusib is a GSK3B inhibitor, repurposed from Alzheimer's disease therapy. The compound was shown to be able to reduce elevated GSK3B and CELF1 levels, while decreasingrepeat expanded DMPK RNA in myoblasts derived from DM1 and CDM1 patients (M. Wang et al., 2019). Meanwhile in animal models tideglusib improved muscle weakness and myotonia in HSA-LR mice and enhanced survival and neuromotor activity in the DMSXL model (M. Wang et al., 2019). Given its potential to treat CSN symptoms, tidesglusib is currently in an extended Phase 2/3 clinical trial (AMO Pharma, NCT02858908) for oral administration in CMD and child-onset DM1, groups where the most severe CNS symptoms are observed (Horrigan et al., 2020). Promisingly, patients have reported improvements in both neuromuscular and CNS symptoms, addressing a critical gap in DM1 treatments and offer an advantage over RNA therapeutics, which have yet to demonstrate significant efficacy in the CNS.

Other small molecule therapies aimed at targeting the root causes of DM1, that are in clinical trials, include MYD-0124 (erythromyocin) and ERX-963 (Expansion Therapeutics). Both these compounds selectively bind to the hairpin RNA structure created by CUG repeats, leading to a reduction in RNA *foci* and splicing correction in both DM1 cell and animal models (Nakamori et al., 2024; Rzuczek et al., 2017). MYD-0124 is currently in phase 2 clinical trials (jRCT2051190069) in adult DM1 patients, as a repurposed, orally administered antibiotic. Meanwhile ERX-963 has just completed a phase 1 clinical trial in adult DM1 patients (Expansion therapeutics. NCT03959189), with a benefit of the

molecule being its rational design to bind specifically to pathogenic CUG repeats, thereby reducing off-target effects. It should be noted that ERX-963 is not a repurposed molecule and therefore will likely take longer to progress through patient clinical trials than the other small molecule strategies mentioned. Overall, these small molecule therapies offer significant hope to DM1 patients, particularly with the added convenience of oral administration, which enhances patient compliance and ease of use.

Gene Therapy

A final key, strategy being employed to treat DM1 is the use of gene therapies. These therapies are less advanced relative to other approaches treating DM1, but the success of Zolgensma, an adeno-associated viruses (AAVs) delivered gene replacement therapy approved for use in SMA patients, highlights their substantial potential (Blair, 2022). In the context of DM1, Audentes, a subsidiary of Astellas Gene Therapies, have developed AT466 which utilises an AAV vector to deliver a vectorized ASO-like therapy that targets toxic DMPK RNA via RNA degradation or exon skipping (Gray J. T, 2022). Preclinical studies are ongoing to optimize this approach.

Another emerging approach involves the use of CRISPR/Cas9 genome editing, which can either excise the toxic CTG repeats at the DNA level, thereby preventing transcription of the toxic RNA or can directly target and degrade the RNA itself. Lo Scrudato et al. (2019) have demonstrated a successful AAV-CRISPR/Cas9 application in the DMSXL mouse model, showing excision of long CTG repeats and a reduction in RNA *foci* within muscle tissue, after a single intramuscular injection. Another related approach, targets toxic RNA molecules using PIN-dCas9, a Cas9 variant fused with an RNA endonuclease. When delivered via AAV in HSA-LR models, this method showed sustained expression for up to

three months, leading to the elimination of RNA *foci*, restoration of MBNL1 function, correction of splicing defects, and improvement of myotonia (Batra et al., 2021).

Overall, gene therapies present an exciting future treatment option for DM1. However further studies are needed to determine their long-term safety and potential induced immunoreactivity and use in humans remains a long way off. For now, at least, peptide and antibody conjugated ASOs remain the therapeutic frontrunners.

Impact of this study

In this thesis, I have employed and tested in DM1 models two such methods of ASO conjugation: peptide conjugation, specifically a PMO with a $(CAG)_7$ sequence conjugated to the DEL01 CPP, and antibody conjugation, using the BBT-8D3$_{130}$ anti-TfR1 conjugated again to a $(CAG)_7$ PMO. As discussed in previous chapters (see discussions in results chapters 1-3), both strategies are already proven to have been successful in treating skeletal muscle and achieving heart delivery in animal models and there are now peptide and antibody conjugated ASOs in DM1 clinical trials.

The results obtained in both DM1 myoblasts and HSA-LR mice utilising DEL01-$(CAG)_7$ highlight how adjustments in CPP chemistry, such as peptide length and arginine content can lead to optimising the balance between CPP toxicity and efficacy. DEL01-$(CAG)_7$ was shown to be significantly less toxic than pip6a-$(CAG)_7$ in both human cells and the HSA-LR DM1 mouse model while also outperforming the industry benchmark CPP, R6Gly, conjugated to the $(CAG)_7$ PMO with regards to efficacy and delivery into the heart. Taken without the results generated in the DMSXL model, these findings would make the case for the further development of DEL01-$(CAG)_7$ and at the very least strongly advocate DEL01

as a delivery moiety for other ASO treatable diseases that require ASO delivery into heart and skeletal muscle.

However, the lack of efficacy displayed by DEL01-$(CAG)_7$ in DMSXL mouse heart and skeletal muscles, despite strong delivery into these tissues, raises the question of whether steric blocking ASOs, such as the $(CAG)_7$ PMO, are suitable for treating DM1 patients, especially given that gapmer ASOs have been shown to be successful in treating this model (Jauvin et al., 2017). Furthermore, the DM1 pathology of the DMSXL mouse is caused by the insertion of a human *DMPK* transgene harbouring CTG expansions which, arguably, more truly reflects the genetic cause of DM1 in patients than the HSA-LR mouse model, where the phenotype manifested is caused by the insertion of an expanded *ACTA1* human transgene. It is likely that the difference in the ability of each ASO type is due to stoichiometry, with gapmers needing only to bind once to degrade their target mRNA, whereas steric blocking ASOs are required to bind at multiple points on CUG mRNA expansions to sufficiently release sequestered MBNL proteins. Therefore, in the case of longer repeat expansions, such as the > 1000 CTG expansion harboured in the DMSXL mice and in congenital DM1 patients, the steric blocking ASO strategy appears to be unsuitable.

In light of this, it will be important to see how PepGen's CPP-PMO, PGN-EDODM1, performs in patients (PepGen: FREEDOM-DM1, NCT06204809). Promising results from clinical trials would show that a steric blocking strategy is sufficient to treat adult forms of DM1, where the CTG repeat tract is typically far shorter than 1000 repeats (De Antonio et al., 2016) and as such support the further development of DEL01-$(CAG)_7$ towards clinical trials. However, if PGN-EDODM1 is unsuccessful in improving the DM1 phenotype in patients, coupled with the results of this body of work, the field may need to seriously

consider whether steric blocking ASOs are an appropriate strategy for the treatment of DM1. Nevertheless, the strong delivery achieved by the DEL01 CPP into skeletal muscles and heart, suggests it could be of great benefit in other disease contexts, such as conjugated to exon skipping PMOs for the treatment of DMD.

With regards to using the anti-TfR1 delivery strategy tested in thesis, I have again shown that employing a CNS optimised anti-TfR1 antibody is a viable and successful method for achieving ASO distribution into the CNS. While BBT-8D3$_{130}$ was unable to deliver sufficient levels of PMO into skeletal muscles, making it unsuitable as a treatment approach for systemically treating all tissues critically affected in DM1, my work shows that compound delivery was achieved in both neurons and glial cells within the CNS. As such this approach could be extremely useful as a systemic drug delivery approach for disease more specifically affecting the CNS, particularly those where neuronal drug delivery is paramount. In the context of DM1, no compound has yet been developed that appears to be able treat all three target tissues: skeletal muscle, heart and CNS. Dyne Therapeutics have alluded to some patient reported improvements in CNS symptoms in their clinical trial of DYNE-101 (Dyne Therapeutics, ACHIEVE: NCT05481879), however no data has been shown to support this and they are yet to report any improvements relating to the DM1 cardiac symptoms. Given the challenges of developing a single comprehensive compound, as highlighted by the testing of both DEL01-(CAG)$_7$ and BBT-8D3$_{130}$-(CAG)$_7$ in this thesis, it may be time for the field to consider a more combinatorial approach to treating DM1.

A combinatorial approach could involve tailoring therapies to address specific tissue types using a combination of different modalities e.g. CPPs for skeletal muscle and heart and CNS optimized anti-TfR1 for treating CNS tissues. Alternatively, one could take advantage

of the wide range of diverse therapeutic types in development for DM1 i.e. antisense oligonucleotides, small molecules, and gene-editing strategies, in order to achieve broader therapeutic coverage. Overall, however one incorporates the therapeutic and delivery strategies available, it seems far more likely that a combinatorial approach will address the multifaceted nature of DM1 pathology more effectively than a ‘one-size-fits-all’ solution and give the greatest improvement in patient quality of life.

Conclusion

In this study I have tested CPP-PMO and anti-TfR1-PMO strategies for treatment of critically affected DM1 tissues: skeletal muscle, heart and CNS. *In vitro* studies revealed the CPP-PMO, DEL01-$(CAG)_7$, to be a lead candidate, displaying a more favourable therapeutic window and safer toxicity profile than previous iterations of CPP-PMOs developed within the Wood group. *In vivo* testing of DEL01-$(CAG)_7$ further confirmed this, with the compound demonstrating significantly less nephrotoxicity than its predecessor pip6a-$(CAG)_7$, while maintaining excellent and enhanced delivery into skeletal muscles and heart tissues. Interestingly, DEL01-$(CAG)_7$ was only able to correct the DM1 phenotype in HSA-LR mice and not in the milder DMSXL model. However, PGN-EDODM1 the current CPP-PMO in clinical trials, was untested in the DMSXL model. Should initial results, expected at the end of 2024, show positive outcomes in DM1 patients, it would support the further development of DEL01-$(CAG)_7$ as an effective yet safer alternative CPP-PMO therapy for DM1 patients.

A major limitation of CPP-PMOs, also demonstrated by DEL01-$(CAG)_7$ is the limited drug delivery achieved to CNS tissues. Here I have demonstrated, as a proof of concept, that utilising a CNS optimised, anti-TfR1 targeting antibody as a delivery vehicle enhances PMO biodistribution to the CNS. This offers hope that the two antibody conjugates currently in clinical trials and showing promising results in treating skeletal muscles, may also have the potential to improve CNS symptoms. Disappointing however, in contrast to these compounds, the conjugate tested here, BBT-$8D3_{130}$-$(CAG)_7$, failed to deliver sufficient PMO concentrations for achieving correction of the DM1 phenotype in skeletal muscle. This raises questions about whether specific optimisation for CNS delivery affects

delivery into other tissues or whether a higher dosing strategy for skeletal muscle penetration may be required. However, a conclusive rationale for the lack of skeletal penetration by BBT-8D3$_{130}$-(CAG)$_7$ remains to be, so far, elusive.

A final interesting result to arise from this study is that TfR1 expression is inconsistent between disease models and species and can alter between states of health and disease. Moving forward, this is something that should perhaps be considered more by those exploiting TfR1 as a delivery target and certainly warrants further investigations, even beyond the field of DM1. Nevertheless, the promising advancements of anti-TfR1 targeting, DYNE-101 and del-desiran, in DM1 clinical trials offer great hope for DM1 patients. Combined with the potential of the CPP-PMO, PGN-EDODM1, and the various small molecules progressing through clinical trials, the therapeutic outlook for DM1 patients has never looked so promising.

Materials and Methods

2.1 Materials

All reagents were of an analytical grade and purchased from Sigma-Aldrich (Paisley, UK) unless otherwise stated.

2.1.1 Antisense oligonucleotide (ASO) conjugates

ASO sequences were purchased from Gene Tools (Philomath, USA). The sequence for the DM1, CTG repeat -targeted ASO was CAGCAGCAGCAGCAGCAGCAG for the SMA, ISS-N1–targeted ASO (5′–3′) was GTAAGATTCCTTTCATAATGCTGG and the sequence for scrambled ASO (5′–3′) was CCTCTTACCTCAGTTACAATTTATA. All ASOs had fully modified PMO backbones. Cell-penetrating peptide sequences are listed in Table 2 and were synthesized in-house by the Wood group chemistry team. The low affinity TfR1-targeting antibody, BBT-8D3$_{130}$ and the isotope control antibody, NIP228 (Webster et al., 2016), were kindly provided by AstraZeneca (Cambridge, UK). All CPP- and antibody- ASO conjugates were synthesized for all experiments by the Wood group chemistry team, following methods described by Yin et al. (2011) and Hammond et al. (2022), respectively. In brief, CPPs were directly conjugated to the 3' end of PMO sequences via standard Fmoc chemistry and purified by high-performance liquid chromatography. For Ab-PMO conjugation, PMOs were first conjugated at the 3' end to an amino acid RB6 linker before antibodies were conjugated via amide coupling to the C-terminal carboxylic acid moiety of the linker.

CPP ID	Amino acid sequence
Pip6a	RXRRBRRXRYQFLIRXRBRXRB
P1.9	RBRRBRFQILYBRBRB
P3.8	RBRRBRFQILYRBHBHB
DEL01	RBRRYQFLIRBRXR

Table *2*: CPP amino acid sequences. Amino acid sequences are denoted by IUPAC nomenclature, with B and X representing beta-alanine and artificial amino acid 6-aminohexanoic acid respectively.

2.2 Methods

2.2.1 Cell culture

All cells were grown in a humidified incubator at 37 °C with 5% (v/v) CO_2. Immortalised myoblasts from healthy individuals or a DM1 patient with 2600 CTG repeats (Arandel et al., 2017) were obtained as a kind gift from the Furling group (INSERM, Paris, France). Immortalized myoblasts were maintained in Skeletal Muscle Growth Medium Kit (C-23060, PromoCell, Heidleberg, Germany). To induce myogenic differentiation, confluent cell cultures were switched to a serum-free Skeletal Muscle Differentiation Medium Kit (C-23061, PromoCell) and differentiated for 7 days. Human renal proximal tubule kidney epithelial cells (HRPTEpCs, catalogue no: 930-05A) were obtained from Sigma-Aldrich and maintained in Renal Epithelial Cell Growth Medium 2 Kit (PromoCell, catalogue no: C-26030). All media were supplemented with 1% Gibco Antibiotic-Antimycotic (PSA-

Penicillin, Streptomycin and Amphotericin B) (Gibco™, Thermo Fisher Scientific, Waltham, USA).

MTS assay

To evaluate the toxicity of CPP-PMO conjugates, MTS Cell Proliferation Assay Kit (Abcam, Cambridge, UK) was used. The kit comprises a colourless reagent containing MTS tetrazolium which viable cells convert to coloured formazan, allowing for the colorimetric determination of cell toxicity. Briefly, HRPTEpCs were plated in triplicate into 96-well plates at 3,000 cells per well in 100 μL medium. 6 h later, CPP-PMO conjugates or unconjugated PMO were diluted in 100 μL medium to a 2-x final concentration and added to cells at a range of concentrations from 1 μM to 40 μM. 1 μM staurosporine was included as a treatment to positively control for cell death. Following 44 h of treatment, 20 mL of MTS reagent was added to each well. After 4 h the absorbance at 490 nm was measured using CLARIOstar Microplate Reader (BMG Labtech, Aylesbury, UK). Non-toxic concentrations were determined when absorbance was insignificantly different from untreated control cells and cells appeared viable upon visual inspection.

Assessment of KIM-1 levels in PPMO treated human epithelial kidney cells

To assess potential for PPMO induced nephrotoxicity *in vitro*, KIM-1 was used as a toxicity biomarker. HRPTEpCs were plated in triplicate into 12-well plates at 50,000 cells per well in 900 μL medium. 6 h later, CPP-PMO conjugates or unconjugated PMO were diluted in 100 μL medium to a 10-x final concentration and added to cells. After 72 h of incubation cell supernatants were collected and secreted KIM-1 protein quantified using Human

Serum KIM-1 Quantikine ELISA Kit (R&D Systems Inc, Minneapolis, USA, catalogue no: DSKM-100), following manufacturer's instructions.

Transfection of oligonucleotides for determining *in vitro* efficacy

Immortalised myoblasts were plated in triplicate into 12-well plates at 50,000 cells per well for RT-PCR applications or in Nunc™ Lab-Tek™ II Chamber Slides (Thermo Fisher Scientific) with an initial seeding density of 400,000 to 500,000 cells per well for fluorescent *in situ* hybridization (FISH) of RNA foci. Cells were differentiated for 7 d with media changes every 2-3 days. On day 7, cell media were aspirated and replaced with 900 μL of fresh differentiation medium. CPP-PMO conjugates or unconjugated PMO were then diluted in 100 μL medium to a 10-x final concentration and added to cells. After 48 h of incubation, RNA was extracted for RT-PCR analysis of DM1 splicing biomarkers or cells were fixed for 10 min in 4% paraformaldehyde (PFA), then washed and kept in 1X phosphate buffered saline (PBS) at 4 °C for FISH experiments.

Evaluating *TFRC* transcript expression in immortalised DM1 and control human myoblasts

Immortalized myoblasts were plated in triplicate into 12-well plates at 50,000 cells per well in 1 ml of medium and differentiated for 7 d. On day 7, cell media were aspirated and replaced with 900 μL of fresh differentiation medium. Untreated cells then received an additional 100 μL fresh differentiation medium while treated cells received 100 μL medium containing 100 μM DEL01-$(CAG)_7$ to give a final concentration of 10 μM for each well. After 48 h of incubation RNA was extracted for qPCR analysis.

Evaluating TFR1 protein expression in immortalised DM1 and control human myoblasts

Immortalized myoblasts were plated in triplicate into 6-well plates at 100,000 cells per well in 2 ml of medium and differentiated for 7 d. On day 7, cell media were aspirated and replaced with 900 μL of fresh differentiation medium. Untreated cells then received an additional 100 μL fresh differentiation medium while treated cells received 100 μl medium containing 100 μM DEL01-CAG7 to give a final concentration of 10 μM for each well. After 48 h of incubation protein was extracted for western blot analysis.

2.2.2 Animal work

Conditions and husbandry

With the exception of the collaborative work using the DMSXL mouse model, all animal procedures were carried out at the Biomedical Services Building or Institute of Developmental and Regenerative Medicine at the University of Oxford. All procedures were authorised by the UK Home Office in accordance with the Animals (Scientific Procedures) Act 1986 and by the University of Oxford ethics committee (PPL no: PDFEDC6F0, PIL no: IF26B772A).

Mouse Models

HSA-LR mouse model

The HSA-LR (human skeletal actin-long repeat) transgenic mouse (*mus musculus*) model, FVB/N-Tg(HSA*LR)20bCath/J (Mankodi et al., 2000), was employed for the preclinical

testing of CCP-PMO and antibody-PMO conjugates as treatments for DM1. The colony bred at the University of Oxford, was maintained by homozygous matings on an FVB/N background. HSA-LR mice express a human skeletal actin transgene containing an approximately 220 CTG repeat expansion in the 3'UTR. The transgene is predominantly expressed in skeletal muscles. It is possible that there is minor expression in non-muscles cells, but this has not been systematically examined. The expression of the CTG repeat tract gives rise to RNA foci which sequester MBNL proteins and leads to DM1-like dysregulation of skeletal muscle splicing. HSA-LR mice also display reduced muscle strength, hind limb myotonia from as early as 4 weeks of age and altered muscle histopathology consistent with observations in DM1 patients.

DMSXL mouse model

The DMSXL mouse (*mus musculus*) model (Huguet et al., 2012) was utilized as an additional model for preclinically assessing CPP-PMOs as treatments for DM1. This transgenic model carries > 1,000 expanded CTG repeats in the human DMPK locus, which mimics the genetic mutation observed in DM1 patients. DMSXL mice exhibit toxic RNA foci and mis-splicing, presenting with DM1 phenotypes of muscle weakness, myotonia, cardiac and respiratory abnormalities and behavioural and electrophysiological CNS deficits. Consequently, this model allows for the assessment of the ability of compounds to treat the CNS and heart, in addition to skeletal muscle. The mice used for these studies were bred and maintained by collaborators in the Furling group at INSERM (Paris, France).

hSMN2 mouse model

The *hSMN2*-transgenic mouse [*SMN2*, FVB.Cg-Smn1^{tm1Hung}Tg(SMN2)2Hung/J] was generated and maintained, at the university of Oxford, as previously described (Gogliotti et al., 2010; Hsieh-Li et al., 2000).These mice carry multiple copies of the human SMN2 gene (*hSMN2*) and possess a knockout of the endogenous murine *Smn* gene. The inclusion of the *hSMN2* transgene renders them amenable to the testing of the splice switching ability of ASOs designed for the treatment of SMA. This model was used in experiments comparing TfR1 expression between mouse models to evaluate potential differences in anti-TfR1-ASO conjugates delivery.

FVB/N Mouse Strain

The FVB/N mouse strain (Taketo et al., 1991) is a commonly employed inbred line utilised in genetic and transgenic research and is the background strain from which the HSA-LR and *hSMN2* mouse models were generated. FVB/N mice were utilised as a WT control for the testing of ASO conjugates in HSA-LR mice and as a healthy background control for experiments comparing TfR1 expression between mouse models, to evaluate potential differences in anti-TfR1-ASO conjugates delivery. The colony was bred and maintained at the university of Oxford.

Intravenous administration and preparation of PMOs and PMO conjugates

For *in vivo* testing of DM1 treatments, compounds were administered at volume of 6 μl/g body weight in 8 – 10-week-old mice via intravenous tail-vein administration. All PMO and PMO conjugates were diluted with 9% saline to give a final saline concentration of 0.9%.

For specifically CPP-PMO conjugates, prior to dilution in 9% saline, CPP-PMO stock solutions were incubated at 37 °C for 30 min then sonicated for 5 min. These two additional preparation steps were carried out to ensure CPP-PMOs were fully dissolved in solution and that no precipitate was present. For all administrations the researcher was blinded.

Testing of hind limb myotonia in HSA-LR mice

To assess the ability of treatments to correct the DM1 functional phenotype in HSA-LR mice, myotonia severity was scored prior to treatment and 7 d and 14 d post-treatment. This was conducted via pinching and elongating the hindlimbs (Figure 22) and allocating a score from 1 (no signs myotonia present) to 4 (severe myotonia), based on the speed at which the limbs returned to their natural position. The test was performed in triplicate for each animal at each discrete testing timepoint, with the score denoted being an average of the 3 tests.

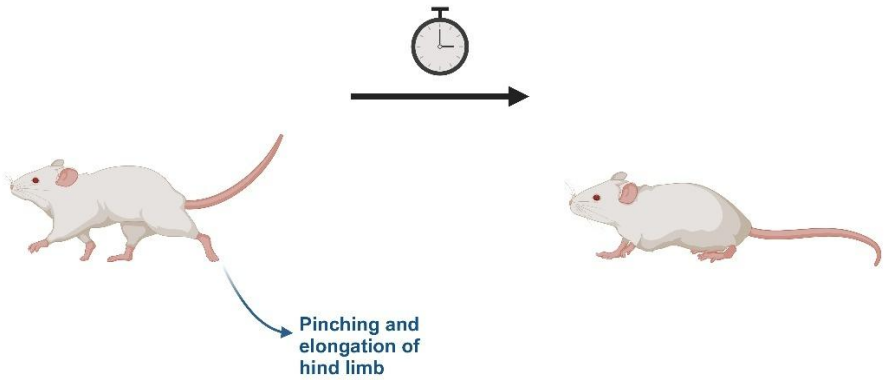

Figure *22*: Schematic of myotonia testing in HSA-LR mice.

Evaluation of weight and grip strength of DMSXL mice

DMSXL mice were weighed and mouse grip strength performance assessed in hind- and fore- limb muscles, immediately prior to initial CPP-PMO treatment and two weeks after final treatment administration. Grip strength in limb muscles was conducted using a commercial grip strength dynamometer (Bioseb, Chaville, France). Briefly, to evaluate hindlimb muscle strength, mice were placed on a grid and gently pulled by their tails in the opposite direction. While to evaluate forelimb muscle strength, mice were lowered over the grid until forepaws were attached before gently pulling the mice backwards by their tails. For each parameter, the maximal strength exerted by the mouse before releasing their grip was recorded five times with the measurement mean taken as an index of grip strength. Mice were allowed a 30 s recovery period between measurements.

Collection and analysis of urinary proteins in HSA-LR mice

To collect urine for toxicity testing, compound or saline treated animals were placed in metabolic cages overnight 1d and 6 d post-treatment and urine collected on days 2 and 7. Urine was stored at –80 °C until analysed. KIM-1 levels in urine were analysed using the Mouse TIM-1/KIM-1/HAVCR Quantikine ELISA Kit (R&D Systems^{TM}, Minneapolis, USA) and normalised to urinary creatinine levels during data analysis. Urinary creatinine levels were analysed using the clinical chemistry analyser at MRC Harwell (Oxford, UK).

Culling and sample collection

With the exception of mice designated for CNS immunohistochemistry experiments (see **section 2.2.4**), mice were sacrificed via rising levels of CO_2. Tissues for ELISAs and RNA

and protein isolation were placed in cryovials and snap-frozen on dry ice before storage at – 80 °C. Liver and kidney tissues for histopathology were fixed in 4% PFA and sent to MRC Harwell (UK), to on the day of harvest, for subsequent sample processing and histopathological assessment. For animals toxicity studies, terminal serum was collected immediately after culling and centrifuged at x 8,000 g at 4 °C for 10 min. Serum supernatant was then collected and sent to MRC Harwell (Oxford, UK) for the analysis of serum metabolites using the clinical chemistry analyser.

Collection of brain for CNS immunohistochemistry. 24 h after treatment administration, mice designated for CNS immunohistochemistry received a terminal intraperitoneal dose of pentobarbital (Bioventa, Ivanovice na Hane, Czech Republic) and were then given a cardiac perfusion of 1X PBS followed by 4% PFA. Brains were collected and stored in 10 ml of 4% PFA overnight before transferral to 10 ml of 12% sucrose solution for 8 h and then subsequent transferral and storage in 10 ml of 30% sucrose solution at 4 °C for up to 1 week. Brains were then halved via the mid-sagittal axis and embedded and frozen in OCT. Samples in OCT were stored at – 20 °C.

2.2.3 Nucleic acid analysis methods

RNA extraction and quantification

Cellular and murine RNA was extracted from 15 – 25 mg of frozen tissue using Maxwell® SimplyTissue (Promega, Madison, USA), in accordance with the manufacturer's instructions. An additional incubation of the samples at 55°C for 10 min prior to the addition of lysis buffer and Proteinase K (Thermo Fisher Scientific, Waltham, USA). The RNA concentration of each sample was measured using Nanodrop (Thermo Fisher

Scientific) and 1 μg of RNA in a 20 μL reaction volume was used to synthesise from the cDNA with the High-Capacity cDNA Reverse Transcription Kit (Thermo Fisher Scientific). The synthesised cDNA was diluted 1:5 with 80 μL of nuclease-free water to give a final concentration of 10 ng/μL.

PCR agarose gel electrophoresis

PCR reactions were carried out on cDNA synthesised from cells and mouse quadricep and gastrocnemius muscles. For each PCR reaction, 8 μL of sample cDNA (80 ng) was added to 17 μL of PCR Dream Taq polymerase master mix (Thermo Fisher Scientific), made according to the manufacturer's instructions and containing a final primer concentration of 0.5 μM. The PCR reactions were run in a thermocycler programmed with an initial heating period of 2 min at 95 °C, followed by 30 cycles of 30 s at 95 °C, 30 s at the annealing temperatures specified in Table 3 and 1 min at 72 °C. The reaction was ended with 5 min at 72 °C. PCR products were diluted with 6X gel loading dye (New England Biolabs, Ipswich, USA) and separated on a 2% (w/v) agarose gel containing 0.5 μg/μl ethidium bromide with 1 x tris-acetate-ethylenediaminetetraacetic acid (EDTA) (TAE) buffer at 120 V for approximately 75 min. HyperLadders™ 50 and 100 bp (Meridian Bioscience, Cincinnati, USA) was used as a reference. The gel was visualised using an ultraviolet (UV) gel imaging system. FIJI (Schindelin et al., 2012) was used to perform a sliding paraboloid background subtraction on each image and to quantify the density of bands obtained on the gel. Band densities were used to calculate the percentage exon inclusion for key exons in target genes.

Transcript	Alternative Exon	Primer Sequence (5'-3')
Human		
MBNL1	5	FW: GCTGCCCAATACCAGGTCAAC RV: GTGGGAGAAATGCTGTATGC
SOS1	11	FW: AGTACCACAGATGTTTGCAGTG RV: TCTGGTCGTCTTCGTGGAGGAA
DMD	78	FW: TTAGAGGAGGTGATGGAGCA RV: GATACTAAGGACTCCATCGC
LDB3	11	FW: GCAAGACCCTGATGAAGAAGCTC RV: GACAGAAGGCCGGATGCTG
Mouse		
Mbnl1	5	FW: GCTGCCCAATACCAGGTCAAC RV: TGGTGGGAGAAATGCTGTATGC
Clcn1	7a	FW: TTCACATCGCCAGCATCTGTGC CACGGAACACAAAGGCACTGAATGT
Atp2a1	22	FW: GCTCATGGTCCTCAAGATCTCAC RV: GGGTCAGTGCCTCAGCTTTG
Ldb3	11	FW: GGAAGATGAGGCTGATGAGTG RV: TGCTGACAGTGGTAGTGCTCTTTC
Sorbs	6	FW: CTGCATCTGGGAAGACTCGCCT RV: GACTTGCTTTCATGCTTCGGAGATTC
Sorbs1	27	FW: CCAGCTGATTACTTGGAGTCCACAGAAG RV: GTTCACCTTCATACCAGTTCTGGTCAATC
Fermt2	4a	FW: GCTTGAGCTGGAAGGACCTCTTATC RV: GCAGAAGTTGGTGACAAAGGGC
Itga6	27	FW: GGGATTCTGATGCTGGCTCTATTAG RV: GGCTTTGGGTAGTGTGAGGTGTTC

Table *3*: Oligonucleotide primer sequences for the splicing analysis of alternative exons. [a]

[a] Alternative exons are numbered according to the FasterDB web interface (http://fasterdb.enslyon.fr/faster/home.pl)

Reverse transcription qPCR (RT-qPCR)

qPCR reactions were performed using Fast SYBR Green Master Mix (Life Technologies, Carlsbad, USA) with target transcripts amplified using gene-specific primers (Table 4), purchased from IDT, and 20 ng cDNA per reaction. Universal cycling conditions were used: 95 °C for 10 minutes, 40 cycles of 95 °C for 15 seconds, 60 °C for 1 minute. Reactions were analysed with Applied Biosystems StepOnePlusTM real-time PCR system (Life Technologies) (Pfaffl, 2001) and reaction efficiencies were corrected for using LinReg software (Untergasser et al., 2021).

Transcript	**Primer Sequence (5'-3')**
Human	
DMPK	FW: GGAGAGGGACGTGTTG RV: CTTGCTCAGCAGTGTCA
KIM-1	FW: CTTCACCTCAGCCAGCAGAAAC RV: GCCATCTGAAGACTCTGTCACG
HPRT1	FW: CTCATGGACTGATTATGGACAGGAC RV: GCAGGTCAGCAAAGAACTTATAGCC
TFRC	FW: GTGCAGATGGGAGCTGTG RV: GGCCACATATGATCCTGACAG
GADPH	FW: ACATCGCTCAGACACCAT RV: TGTAGTTGAGGTCAATGAAGGG
Mouse	
Aif1	FW: CTGGAGGGGATCAACAAGCAATTC RV: CCAGCATTCGCTTCAAGGACATAA
Dmpk	FW: GGAAGAAAGGGATGTATTA RV: CTCAGCAGCGTTAGCA
Gfap	FW: GACCAGCTTACGGCCAACAG RV: TTCATCTTGGAGCTTCTGCCT
Tfrc	FW: TGATGTCATTCCTGCCCA RV: AGGTCAAAGAGGTCACTTAAGC
Polj	FW: ACCACACTCTGGGGAACATC RV: CTCGCTGATGAGGTCTGTGA

Table *4*: Oligonucleotide primer sequences for qRT-PCR analysis.

2.2.4 Immunohistochemistry methods for microscopy

Combined fluorescent *in-situ* hybridisation (FISH) and immunostaining of DM1 myotubes

Combined FISH and immunostaining and visualisation of DM1 myotubes was carried out by collaborators at the Furling group at INSERM (Paris, France). The protocol used is briefly described below.

FISH. Differentiated myoblasts, prepared as described in **section 2.2.1**, were permeabilized with 0.5% Triton X-100 solution for 10 min at room temperature. This was followed by washing and pre-hybridisation in, freshly prepared, 2X SSC (saline sodium citrate UltraPure 20×, Invitrogen, catalogue no: 15557044) containing 40% formamide for 10 min. Subsequently, freshly prepared hybridisation solution (40% formamide, 2× SSC, 0.2% BSA) containing 2′OMe Cy3-(CAG)7 probe (Eurogentec, Seraing, Belgium) at a concentration of 100 nM was added to each well. Samples were incubated at 37 °C for 90 min in a dark humidified chamber. Cells were then washed once with PBS-T (1X PBS (Gibco^{TM}), 0.1% Tween-20) for 5 min at room temperature and subsequently incubated with 2X SSC/40% formamide at 45 °C for 30 min.

Immunostaining. Cells were washed thrice with PBS-T then blocked for 1 h in blocking solution (0.1% Tween-20, 3% bovine serum albumin, 1X PBS (Gibco^{TM}). Next cells were incubated for 1 h at 37 °C with a mouse monoclonal anti-MBNL1 (MB1a clone 4A8 gift, from G.E. Morris, DHSB) at a dilution of 1:100 in blocking solution. Post-incubation, cells were washed three times with PBS-T for 10 min each. Secondary Alexa Fluor 488-conjugated goat anti-rabbit antibody (Life technologies, diluted 1:500 in blocking solution) was added and cells were incubated for 1h at room temperature. Cells were then washed with PBS-T and nuclei counterstained with 2 µg/mL 4′,6-diamidino-2-phenylindole (DAPI) in 1X PBS for 15 min. DAPI was removed and samples were washed a final three times in 1X PBS before being mounted ProLong™ Diamond antifade mounting medium (Molecular Probes, Eugene, USA). Slides were

left to cure for 24 h prior to sealing of the perimeter with clear nail polish. Confocal images were realized at a magnification factor of x100 using a Nikon Ti2 microscope equipped with a motorized stage and a Yokogawa CSU-W1 spinning disk head coupled with a Prime 95 sCMOS camera (Photometrics, Tuscon, USA). Images were processed with Adobe Photoshop software (Adobe Inc, San Jose, USA).

Immunostaining of AbPMO in HSA-LR mouse CNS

OCT embedded tissues were sectioned at a thickness of 20 μm via the mid-sagittal axis onto SuperFrost Plus™ Adhesion slides (Epredia™, Kalamazoo, USA). Slides were stored at –20 °C. Slides were thawed at room temperature for 30 min then the region containing tissue was circled with ImmEdge® Hydrophobic Barrier PAP Pen (Vector Laboraties, Burlingame, USA). Slides were rehydrated for 40 min in 1X PBS, permeabilised in 0.1% Triton X-100 in 1X PBS for 15 min then washed twice in 1X PBS for 5 min. Slide sets designated for Nissl staining or for controls for endogenous tissue background fluorescence and secondary antibody background were incubated at 4 °C overnight in a blocking solution comprised of 3% BSA in 1X PBS blocking solution. For slide sets designated for astrocyte staining, slides were incubated for 4 h at 4 °C with the blocking solution prior to the addition of a rabbit monoclonal primary anti-GFAP antibody (Abcam, catalogue no: ab33922), diluted 1:5000. These slides were then also incubated at 4 °C overnight. The next day, all slides were washed three times in 1X PBS for 5 min then incubated for 2 h at room temperature with secondary antibodies (see Table 5).

For astrocyte staining: slides were staining with Alexa Fluor™ 594 Goat anti-Rabbit IgG (H+L) (Invitrogen) and Alexa Fluor™ 488 Goat anti-Human IgG (H+L) (Invitrogen), both at a dilution of 1:500 in 1 X PBS.

For neuron staining: Slides were incubated with Alexa Fluor™ 488 Goat anti-Rabbit IgG (H+L), at a dilution of 1:500, then washed thrice in 1X PBS for 5 min followed by an additional incubation for 20 min with Nissl NeuroTrace 530/615 (Invitrogen) diluted 1:200 in 1X PBS before proceeding to following steps.

After secondary incubations, all slides were washed thrice in 1X PBS then incubated for 15 min with DAPI, diluted 1:10,000 in 1X PBS. A final set of three 5 min washes in 1X PBS was performed on all slides before drying the slides and mounting them with coverslips using ProLong™ Diamond Antifade Mountant (Invitrogen). Slides were stored at 4 °C until images were taking Olympus FV1000 confocal microscope using Fluoview FV1000 software (Olympus Corporation, Tokyo, Japan). Minimal post-imaging processing was carried out with FIJI (Schindelin et al., 2012).

Application	Primary Antibody	Secondary Antibody	Catalogue No. (Primary)	Catalogue No. (Secondary)	Dilution (Primary)	Dilution (Secondary)
Combined FISH and Immunostaining of DM1 myotubes	Mouse monoclonal anti-MBNL1 (MB1a clone 4A8)	Alexa Fluor 488-conjugated goat anti-rabbit antibody (Life Technologies)	Not specified (gift from G.E. Morris, DHSB)	A-11008	1:100	1:500
Immunostaining of AbPMO in HSA-LR mouse CNS (Astrocytes)	Rabbit monoclonal anti-GFAP antibody (Abcam)	Alexa Fluor™ 594 Goat anti-Rabbit IgG (H+L) (Invitrogen)	ab33922	A-11012	1:5000	1:500
Immunostaining of AbPMO in HSA-LR mouse CNS (Neurons)	Nissl neurotrace 530/615	Alexa Fluor™ 488 Goat anti-Rabbit IgG (H+L) (Invitrogen)	N21482	A-11008	1:5000	1:500
Western Blot	Rabbit polyclonal TfR1 antibody (Abcam)	IRDye® 800CW Goat anti-Mouse IgG (LI-COR Biosciences™)	ab84036	925-32210	1:1000	1:10,000

Table *5*: Antibodies used for Immunostainings, FISH and Western Blot.

2.2.5 Fluorescent activated cell sorting and flow cytometry methods

Preparation and staining of TfR1 in single murine skeletal muscle cells

Single cell dissociation of murine skeletal muscles. Gastrocnemius, quadriceps and TA were collected from 10-week-old HSA-LR mice and minced on ice into 2-4 mm pieces. Minced tissues were immediately subjected to enzymatic digestion using the GentleMACS Dissociator (Miltenyi Biotec, Bergish Gladbach, Germany) and the Skeletal Muscle Dissociation Kit (Miltenyi Biotec, catalogue no: 130-098-305). Briefly, tissue pieces and proprietary enzyme mix were transferred into GentleMACS C Tubes (Miltenyi

Biotec) and processed on the GentleMACS Dissociator using the 'm_ske_mus_02' programme. Following dissociation, cell suspensions were filtered through a 70 µm cell strainer, washed with cold Dulbecco's Modified Eagle Medium (Gibco™), and centrifuged at 300 x g for 20 min at 4 °C. Cell pellets were resuspended in Red Blood Cell Lysis Solution (Miltenyi Biotec, catalogue no.130-094-183) and red blood cells removed, according to manufacturer's instructions. Cell suspensions were then centrifuged again at 300 x g for 20 min and pellets resuspended in 500 uL of a staining buffer comprising of Ham's F-12 Nutrient Mix (Gibco™) with 10% horse serum (Gibco™) and 1% Gibco Antibiotic-Antimycotic (Gibco™), ready for further processing.

Staining of skeletal muscles single cell suspensions

Cell suspensions were incubated for 40 min at 4 °C, protected from light, with a panel of fluorochrome labelled antibodies (CD163, CD31, CD45, Ly-6A/E and CD71) and a CD106 antibody biotinylated for human and mouse samples, respectively. The antibodies were carefully selected to label cell surface TfR1 (CD71, transferrin receptor 1) and other surface antigens expressed on different skeletal muscle cell types (see Table 6 for antibody details and dilutions). After the incubation, cell samples were washed in the staining buffer (Ham's F-12 Nutrient Mix, 10% horse serum and 1% Gibco Antibiotic-Antimycotic) and centrifugated at 500 x g for 5 minutes. Subsequently, cells were resuspended in 500 µL staining buffer containing 5 µL of PE/Cyanine7 Streptavidin (BioLegend) and 15 µL of propidium iodide (PI) (Life Technologies), used as a viability dye, and incubated for 20 min at 4 °C, protected from light. Following incubation, cells were again washed in staining buffer and centrifugated at 500 x g for 5 min. Cells were then filtered through a 40 µm cell strainer and centrifuged at 500 x g for 5 min. Finally, cells were resuspended in 250 µL of staining buffer, ready for sample acquisition.

Target	Species Reactivity	Antibody Label	Antibody Clone	Isotype	Provider	Catalogue No.	Volume /test (uL)
CD163	Mouse	Brilliant Violet 605™	S15049I	IgG2a, κ	BioLegend	155327	5
CD31	Mouse	FITC	MEC13.3	Rat IgG2a, κ	BioLegend	102506	5
CD45	Mouse	APC	30-F11	Rat IgG2b, κ	BioLegend	103112	5
Ly-6A/E	Mouse	Pacific Blue	D7	IgG2a, κ	BioLegend	108120	5
CD106	Mouse	Biotin	429	Rat IgG2a, κ	BioLegend	105704	5
Strept-avidin	N/A	PE/Cy7	N/A	N/A	BioLegend	405206	5
CD71	Mouse	PE	R17217	Rat IgG2a, κ	BioLegend	113807	5
CD71	Human	Alexa Fluor® 700	M-A712	IgG2a, κ	BD Pharmingen	563769	5

Table *6*: List of antibodies used for flow cytometry and cell sorting analysis.

Flow cytometry was performed using a MA900 Multi-Application Cell Sorter (Sony Biotechnology Inc, San Jose, USA) in purity mode using a 100um sorting chip (Sony Biotechnology Inc, San Jose, USA). The instrument was calibrated using Sony Automatic

Setup Beads Kit (Sony Biotechnology Inc, catalogue no: LE-B3001) according to the manufacturer's instructions. To correct for spectral overlap between fluorophores, compensation was set up using BD Biosciences Compensation Beads (BD Biosciences, catalogue no: 55284) and ArC™ Amine Reactive Compensation beads (Thermofisher), with single-stained compensation beads prepared for each fluorophore at the recommended concentrations and run on the flow cytometer. The compensation matrix was created using [compensation wizard] on the instrument software, adjusting the compensation settings until the fluorescence spillover into adjacent channels was minimized.

Cell Sorting and flow cytometry. Cell suspensions were loaded into the flow cytometer, and unstained samples were used to set gates based on forward and side scatter (FSC-A and SSC-A, respectively) to exclude debris and dead cells. Doublets were excluded using forward scatter height (FSC-H) versus forward scatter area plots (FSC-A). Live cells were distinguished from dead cells using propidium iodide negativity. Using a gating strategy established by (Liu et al. (2015), stained cell samples were gated based on fluorescence intensity to identify skeletal muscle cell populations. Haematopoeitic cells were identified as the CD45+ population, from which the majority of cells were CD163+ and therefore identified as macrophages. Endothelial cells were identified as CD45- CD31+, while from the CD45- CD31- population, mesenchymal stem cells (SCA1+) and satellite cells (SCA1- VCAM+) were identified. Once gating and compensation settings were finalized, cells were sorted with targeted drop mode (22 drops/sec) at 20psi, and the acquisition rate was established between 3,000-6,000 events per second for each sample. Each sorted fraction was counted and divided into two different fractions (CD71+ and CD71 Neg) within the target cell populations. Slight adjustments of gates were required to properly visualize the sorted fractions per sample. 10,000 events were recorded for each cell population for analysis of CD71 CSE.

Flow cytometric quantification of TfR1 CSE in control and patient-derived DM1 differentiated myoblasts

Preparation and staining of myoblasts. Immortalized myoblasts were seeded in triplicate into 150 mm petri dishes at 2.5 million cells per dish and differentiated for 7 d as described in **section 2.2.1**. Cells were removed from the dishes using TrypLE™ Express Enzyme (1X) (Gibco™) followed by neutralisation and resuspension with Gibco Dulbecco's Modified Eagle Medium GlutaMAX (DMEM, Gibco™) supplemented with 2% FBS (Gibco™). Cells were spun at 500 x g for 5 min and 1 million cells per sample were resuspended in 3 ml of a wash solution comprised of 1X PBS (Gibco™), supplemented with 2% FBS. Cells were then spun again at 4 °C for 5 min at 1500 x g. Supernatant was removed and cells resuspended with 25 μL of 1 ug/mL DAPI in 1X PBS, then gently vortexed and incubated protected from light 10 min at 4 °C. Following incubation, 50 μL of Alexa Fluor® 700 Mouse Anti-Human CD71 (BD Pharmingen ™), diluted 1:10 in 1X PBS, was added to the cells and cells incubated in the dark at 4 °C for a further 20 min. After incubation, 3 ml of wash solution was added to each sample and samples were spun at 4 °C for 5 min at 1500 x g. Supernatants were removed and cell pellets resuspended in 200 μL of 1X PBS and kept at 4 °C until ready for acquisition of TfR1 cell surface expression (CSE) via flow cytometry.

Flow cytometry. To quantify TfR1 CSE on Flow cytometry was performed using ID7000™ Spectral Cell Analyzer (Sony Biotechnology Inc) was previously calibrated using AllignCheck Particles (Sony Biotechnology Inc, catalogue no: AE700510) and alignment was verified according to the manufacturer's instructions. Instrument settings were adjusted for optimal detection of the fluorochromes used: Alexa Fluor® 700 for CD71 detection, and DAPI for cell viability. Unmixing was not required due to the large spectral gap between the fluorochromes used. Unstained control samples were run first to establish baseline fluorescence and to set gates based on forward and side scatter (FSC-A and SSC-A, respectively) to exclude debris and dead cells. Doublets were excluded using forward scatter height (FSC-H) versus forward scatter area plots (FSC-

A). A single stained DAPI control was used to exclude dead cells with live cells being DAPI negative. A single stained control and isotype control for CD71 were then used to set the appropriate voltage settings and to identify non-specific binding. Finally experimental samples were acquired with 10,000 events recorded per sample for the analysis of CD71 CSE.

*Flow cytometry data analysis*The mean fluorescent intensity (MFI) of CD71 CSE was compared across different cell populations and samples. MFI data were analysed using FlowJo ™ software version 10 (FlowJo-LLC, Ashland, USA) to quantify differences in CD71 expression levels. Statistical analysis and generation of CD71 CSE heat maps were performed using GraphPad Prism (Graph Pad Software, Boston, USA). Statistical significance in human cells was determined via Student's t-test, while for murine skeletal muscle cell types, to compare between multiple mouse lines, one-way analysis of variance (one-way ANOVA) with Dunnett's correction for multiple comparisons was used. Results were considered significant at a confidence of 95% ($p < 0.05$).

2.2.6 Western blot and ELISA methods

Western blot

Extraction and preparation of total protein. For protein extraction, cells or tissues were lysed in Pierce RIPA Buffer (Thermo Scientific, catalogue no. 89900) with complete mini proteinase inhibitors (Roche, Basal, Switzerland). A colorimetric DC Assay Kit (Bio-Rad, Hercules, USA) was used to calculate protein concentration against bovine serum albumin standards. Single-use aliquots of 10 to 15 ug (cells) or 25 to 30 ug (tissues) of total protein per sample were diluted in RIPA buffer containing NuPAGE™ LDS Sample Buffer (4X) (Invitrogen, Catalogue no: NP0007) and NuPAGE™ Sample Reducing Agent (10X) (Invitrogen, Catalogue no: NP0004) and stored at –80 °C, ready for use.

Western blot. Western blot samples were denatured at 95 °C for 5 min then separated on 4 – 12% NuPAGE™ Bis-Tris Midi Protein Gels (Invitrogen, catalogue no. WG1403BOX) at 60 V for 10 min followed by 180 V for 50 min SeeBlue™ Plus2 Pre-stained Protein Standard (Invitrogen). Protein was then transferred to 0.2 μm polyvinylidene fluoride (PVDF) membranes using the Trans-Blot Turbo Transfer System (Bio-Rad) with Trans-Blot Turbo Midi 0.2 μm PVDF Transfer Packs (Bio-Rad, catalogue no: 1704157). To control for transfer efficiency and sample loading, the membrane was incubated in 0.0005% Fast Green FCF (Merck KGaA) stain for 15 min and signal imaged at 690 nm using a ChemiDoc Touch Imaging System (Bio-Rad). Subsequently, the membrane was blocked for 1 h using Odyssey™ Blocking Buffer, PBS (LI-COR Biosciences™, Lincoln, USA) then incubated at 4°C overnight with a primary rabbit polyclonal antibody TfR1 antibody (Abcam, Cambridge, UK, Catalogue no. ab84036), diluted 1:1000. Excess primary antibody was removed by 3 x 5 min washes in 1X PBS and the membrane was incubated for 1 h with IRDye® 800CW goat anti-mouse IgG (LI-COR Biosciences™), diluted 1:10,000. Membranes were imaged again using ChemiDoc Touch Imaging System at 800 nm and analysed with Image Studio™ software (LICOR Biosciences,USA).

ELISA quantification of PMO tissue concentration

Tissue lysate preparation. To detect the concentration of PMO conjugates in the tissues of treated mice, 30 – 80 mg of tissue was homogenised in 10 μl per mg of tissues of RIPA buffer (Thermo Fisher Scientific) using Precellys®24 Tissue Homogenizer and Homogenisation tubes (Precellys). Homogenates were centrifuged at 12,000 x g for 3 min and the supernatant collected and incubated at 55 °C overnight. Samples were centrifuged at 13,000 x g for 15 min to remove debris and supernatants collected and transferred to clean Eppendorf tubes.

*ELISA assay***.** ELISAs were conducted as described in Burki et al. (2015) using phosphorothioate probes (Table 7) double-labelled with digoxigenin and biotin for the detection SMA and DM1 PMO conjugates. In brief, samples were added to a 96-well plate and a standard curve ranging from 25 pM to 2000 pM was included for each PMO conjugate used in the tissues on each ELISA plate. Where necessary, samples were diluted to ensure the concentration measured was within the range of the standard curve. Once plated, the respective PMO probe, diluted in 1X Tris-EDTA (TE) buffer, 1M NaCl, 0.1% v/v Triton X-100, was added to each well to a final concentration of 0.25 nM. The plate was sealed then with Adhesive PCR plate seals (Thermo Fisher Scientific) and incubated at 37 °C for 30 min. 100 µL of the hybridized solution was then transferred to Pierce™ NeutrAvidin™ coated plates (Thermo Fisher Scientific). The plate was resealed and incubated at 37 °C for 30 min to allow the biotinylated probe to bind to the NeutrAvidin coating. The plate was washed thrice then micrococcal nuclease (New England Biolabs) was added to each well, at a final amount of 30 U per well. The plate was sealed and incubated at 37 °C for 1 h to ensure at least 99% enzymatic cleavage of single-stranded (unhybridized) probe. Following three washes, 150 µL of anti-digoxigenin antibody conjugated with alkaline phosphatase (Roche), diluted 1:5,000 in SuperBlock (TBS) Blocking Buffer (Thermo Fisher Scientific) with 0.25% v/v Tween-20, was added to each well. The plate was sealed and incubated at 37 °C for 30 min to allow binding of the antibody to the probe. The plate was washed thrice and 150 µL of AttoPhos substrate (Promega) was added to each well. The plate was sealed, protected from light, and incubated at 37 °C for a final 30 min to facilitate the catalytic removal of a phosphate group from the AttoPhos substrate by alkaline phosphatase, converting it to a highly fluorescent product. The endpoint fluorescent intensity of each ELISA was measured at 444 nm excitation and 555 nm emission using CLARIOstar Microplate Reader (BMG Labtech, Aylesbury, UK). The average fluorescent intensity of saline controls for each tissue was subtracted from samples to normalise for the background fluorescence of each tissue. The PMO standard curve on

the ELISA plate was then used to determine the PMO concentration within each sample.

Probe Target	Sequence
SMA PMO	5'-[DIG]CAGCATTATGAAAGTGAATCTTAC[BIO]-3'
DM1 PMO probe	5'DIG]A*C*G*T*A*C*G*CTGCTGCTGCTGCTGCTGCTG*A*C*G*T*A*C*G[BIO]-3'
NTC PMO	5'-[DIG]T*A*A*A*T*T*G*TAACTGA*G*G*T*A*A*G*A[BIO]-3'

Table *7*: List of ELISA probes for the detection of PMOs in tissues. [DIG] indicates digoxigenin labelling, [BIO] indicates biotin labelling and asterisks (*) indicate phosphorothioate bonds in the sequences.

2.2.7 Data analysis and visualisation

GraphPad Prism software was used to prepare graphs and calculate standard errors of the mean (S.E.M.), where experiments were performed with replicates. For comparison between two groups only, a students t test was performed for statistical analysis. When the mean of multiple groups were compared, a one-way analysis of variance (one-way ANOVA) with Tukey's correction for multiple comparisons was used. When more than two groups were compared to a control group only, a one-way ANOVA with Dunnett's correction for multiple comparison was used. Results were considered significant at a confidence of 95% ($p < 0.05$). Biorender and Power Point were used to prepare cartoons and diagrams.

Bibliography

Aartsma-Rus, A., & Krieg, A. M. (2017). FDA Approves Eteplirsen for Duchenne Muscular Dystrophy: The Next Chapter in the Eteplirsen Saga. In *Nucleic Acid Therapeutics* (Vol. 27, Issue 1, pp. 1–3). Mary Ann Liebert Inc. https://doi.org/10.1089/nat.2016.0657

Aartsma-Rus, A., Straub, V., Hemmings, R., Haas, M., Schlosser-Weber, G., Stoyanova-Beninska, V., Mercuri, E., Muntoni, F., Sepodes, B., Vroom, E., & Balabanov, P. (2017). *Review Development of Exon Skipping Therapies for Duchenne Muscular Dystrophy: A Critical Review and a Perspective on the Outstanding Issues*. https://doi.org/10.1089/nat.2017.0682

Adereth, Y., Dammai, V., Kose, N., Li, R., & Hsu, T. (2005). RNA-dependent integrin α3 protein localization regulated by the Muscleblind-like protein MLP1. *Nature Cell Biology*, *7*(12). https://doi.org/10.1038/ncb1335

Ait Benichou, S., Jauvin, D., De Serres-Bérard, T., Pierre, M., Ling, K. K., Bennett, C. F., Rigo, F., Gourdon, G., Chahine, M., & Puymirat, J. (2022). Antisense oligonucleotides as a potential treatment for brain deficits observed in myotonic dystrophy type 1. *GeneTherapy*, *29*, 698–709. https://doi.org/10.1038/s41434-022-00316-7

Ajioka, R. S., & Kaplan, J. (1986). Intracellular pools of transferrin receptors result from constitutive internalization of unoccupied receptors. *Proceedings of the National Academy of Sciences of the United States of America*, *83*(17). https://doi.org/10.1073/pnas.83.17.6445

Al Humaidan, E. L., Pedersen, S. L., Burkhart, A., Rasmussen, C. L. M., Moos, T., Fuchs, P., Fernandes, E. F. A., Ozgür, B., Strømgaard, K., Bach, A., Brodin, B., & Kristensen, M. (2022). The Cell-Penetrating Peptide Tat Facilitates Effective Internalization of PSD-95 Inhibitors Into Blood–Brain Barrier Endothelial Cells but less Efficient Permeation Across the Blood–Brain Barrier In Vitro and In Vivo. *Frontiers in Drug Delivery*, *2*. https://doi.org/10.3389/fddev.2022.854703

Amantana, A., & Iversen, P. L. (2005). Pharmacokinetics and biodistribution of phosphorodiamidate morpholino antisense oligomers. In *Current Opinion in Pharmacology* (Vol. 5, Issue 5 SPEC.ISS., pp. 550–555). Elsevier BV. https://doi.org/10.1016/j.coph.2005.07.001

Amantana, A., Moulton, H. M., Cate, M. L., Reddy, M. T., Whitehead, T., Hassinger, J. N., Youngblood, D. S., & Iversen, P. L. (2007). Pharmacokinetics, biodistribution, stability and toxicity of a cell-penetrating peptide-morpholino oligomer conjugate. *Bioconjugate Chemistry*, *18*(4), 1325–1331. https://doi.org/10.1021/BC070060V

Andrews, N. C. (1999). The iron transporter DMT1. *International Journal of Biochemistry and Cell Biology*, *31*(10). https://doi.org/10.1016/S1357-2725(99)00065-5

Angeard, N., Gargiulo, M., Jacquette, A., Radvanyi, H., Eymard, B., & Héron, D. (2007). Cognitive profile in childhood myotonic dystrophy type 1: Is there a global

impairment? *Neuromuscular Disorders*, *17*(6). https://doi.org/10.1016/j.nmd.2007.02.012

Angeard, N., Jacquette, A., Gargiulo, M., Radvanyi, H., Moutier, S., Eymard, B., & Héron, D. (2011). A new window on neurocognitive dysfunction in the childhood form of myotonic dystrophy type 1 (DM1). *Neuromuscular Disorders*, *21*(7). https://doi.org/10.1016/j.nmd.2011.04.009

Arandel, L., Espinoza, M. P., Matloka, M., Bazinet, A., De Dea Diniz, D., Naouar, N., Rau, F., Jollet, A., Edom-Vovard, F., Mamchaoui, K., Tarnopolsky, M., Puymirat, J., Battail, C., Boland, A., Deleuze, J. F., Mouly, V., Klein, A. F., & Furling, D. (2017). Immortalized human myotonic dystrophy muscle cell lines to assess therapeutic compounds. *DMM Disease Models and Mechanisms*, *10*(4), 487–497. https://doi.org/10.1242/dmm.027367

Artero, R., Prokop, A., Paricio, N., Begemann, G., Pueyo, I., Mlodzik, M., Perez-Alonso, M., & Baylies, M. K. (1998). The muscleblind gene participates in the organization of Z-bands and epidermal attachments of Drosophila muscles and is regulated by Dmef2. *Developmental Biology*, *195*(2). https://doi.org/10.1006/dbio.1997.8833

Ashizawa, T., Dunne, C. J., Dubel, J. R., Perryman, M. B., Epstein, H. F., Boerwinkle, E., & Hejtmancik, J. F. (1992). Anticipation in myotonic dystrophy: I. statistical verification based on clinical and haplotype findings. *Neurology*, *42*(10). https://doi.org/10.1212/wnl.42.10.1871

Avidity Biosciences. (2021). 2021 AAN Full Data: Avidity Q&A Presentation. In *presentation*. presentation. https://aviditybio.wpengine.com/wp-content/uploads/2021/09/2021-04-18_AAN_full-data_Avidity_FINAL-for-QandA.pdf.

Bailly, V., Zhang, Z., Meier, W., Cate, R., Sanicola, M., & Bonventre, J. V. (2002). Shedding of kidney injury molecule-1, a putative adhesion protein involved in renal regeneration. *Journal of Biological Chemistry*, *277*(42). https://doi.org/10.1074/jbc.M200562200

Baker, B. F., Lot, S. S., Condon, T. P., Cheng-Flournoy, S., Lesnik, E. A., Sasmor, H. M., & Bennett, C. F. (1997). 2'-O-(2-methoxy)ethyl-modified anti-intercellular adhesion molecule 1 (ICAM-1) oligonucleotides selectively increase the ICAM-1 mRNA level and inhibit formation of the ICAM-1 translation initiation complex in human umbilical vein endothelial cells. *Journal of Biological Chemistry*, *272*(18). https://doi.org/10.1074/jbc.272.18.11994

Ballester-Lopez, A., Koehorst, E., Linares-Pardo, I., Núñez-Manchón, J., Almendrote, M., Lucente, G., Arbex, A., Alonso, C. P., Lucia, A., Monckton, D. G., Cumming, S. A., Pintos-Morell, G., Coll-Cantí, J., Ramos-Fransi, A., Martínez-Piñeiro, A., & Nogales-Gadea, G. (2020). Preliminary findings on ctg expansion determination in different tissues from patients with myotonic dystrophy type 1. *Genes*, *11*(11). https://doi.org/10.3390/genes11111321

Barbé, L., Lanni, S., López-Castel, A., Franck, S., Spits, C., Keymolen, K., Seneca, S., Tomé, S., Miron, I., Letourneau, J., Liang, M., Choufani, S., Weksberg, R., Wilson, M. D., Sedlacek, Z., Gagnon, C., Musova, Z., Chitayat, D., Shannon, P., …

Pearson, C. E. (2017). CpG Methylation, a Parent-of-Origin Effect for Maternal-Biased Transmission of Congenital Myotonic Dystrophy. *American Journal of Human Genetics*, *100*(3). https://doi.org/10.1016/j.ajhg.2017.01.033

Bassez, G., Audureau, E., Hogrel, J. Y., Arrouasse, R., Baghdoyan, S., Bhugaloo, H., Gourlay-Chu, M. L., Le Corvoisier, P., & Peschanski, M. (2018). Improved mobility with metformin in patients with myotonic dystrophy type 1: A randomized controlled trial. *Brain*, *141*(10). https://doi.org/10.1093/brain/awy231

Batra, R., Nelles, D. A., Roth, D. M., Krach, F., Nutter, C. A., Tadokoro, T., Thomas, J. D., Sznajder, Ł. J., Blue, S. M., Gutierrez, H. L., Liu, P., Aigner, S., Platoshyn, O., Miyanohara, A., Marsala, M., Swanson, M. S., & Yeo, G. W. (2021). The sustained expression of Cas9 targeting toxic RNAs reverses disease phenotypes in mouse models of myotonic dystrophy type 1. *Nature Biomedical Engineering*, *5*(2). https://doi.org/10.1038/s41551-020-00607-7

Begemann, G., Paricio, N., Artero, R., Kiss, I., Pérez-Alonso, M., & Mlodzik, M. (1997). Muscleblind, a gene required for photoreceptor differentiation in Drosophila, encodes novel nuclear Cys3His-type zinc-finger-containing proteins. *Development*, *124*(21). https://doi.org/10.1242/dev.124.21.4321

Benson, M. D., Waddington-Cruz, M., Berk, J. L., Polydefkis, M., Dyck, P. J., Wang, A. K., Planté-Bordeneuve, V., Barroso, F. A., Merlini, G., Obici, L., Scheinberg, M., Brannagan, T. H., Litchy, W. J., Whelan, C., Drachman, B. M., Adams, D., Heitner, S. B., Conceição, I., Schmidt, H. H., … Coelho, T. (2018). Inotersen Treatment for Patients with Hereditary Transthyretin Amyloidosis. *New England Journal of Medicine*, *379*(1). https://doi.org/10.1056/nejmoa1716793

Betts, C., Saleh, A. F., Arzumanov, A. A., Hammond, S. M., Godfrey, C., Coursindel, T., Gait, M. J., & Wood, M. J. (2012). Pip6-PMO, a new generation of peptide-oligonucleotide conjugates with improved cardiac exon skipping activity for DMD treatment. *Molecular Therapy - Nucleic Acids*, *1*(8), e38. https://doi.org/10.1038/mtna.2012.30

Bhavsar, N. A., Köttgen, A., Coresh, J., & Astor, B. C. (2012). Neutrophil gelatinase-associated lipocalin (NGAL) and kidney injury molecule 1 (KIM-1) as predictors of incident CKD stage 3: The atherosclerosis risk in communities (ARIC) study. *American Journal of Kidney Diseases*, *60*(2). https://doi.org/10.1053/j.ajkd.2012.02.336

Biscans, A., Coles, A., Haraszti, R., Echeverria, Di., Hassler, M., Osborn, M., & Khvorova, A. (2019). Diverse lipid conjugates for functional extra-hepatic siRNA delivery in vivo. *Nucleic Acids Research*, *47*(3). https://doi.org/10.1093/nar/gky1239

Blair, H. A. (2022). Onasemnogene Abeparvovec: A Review in Spinal Muscular Atrophy. *CNS Drugs*, *36*(9). https://doi.org/10.1007/s40263-022-00941-1

Bosman, W., Hoenderop, J. G. J., & De Baaij, J. H. F. (2021). Genetic and drug-induced hypomagnesemia: Different cause, same mechanism. *Proceedings of the Nutrition Society*, *80*(3). https://doi.org/10.1017/S0029665121000926

Brad Wan, W., & Seth, P. P. (2016). The Medicinal Chemistry of Therapeutic Oligonucleotides. In *Journal of Medicinal Chemistry* (Vol. 59, Issue 21). https://doi.org/10.1021/acs.jmedchem.6b00551

Brandl, C. J., Green, N. M., Korczak, B., & MacLennan, D. H. (1986). Two Ca2+ ATPase genes: Homologies and mechanistic implications of deduced amino acid sequences. *Cell*, *44*(4). https://doi.org/10.1016/0092-8674(86)90269-2

Brook, J. D., McCurrach, M. E., Harley, H. G., Buckler, A. J., Church, D., Aburatani, H., Hunter, K., Stanton, V. P., Thirion, J. P., Hudson, T., Sohn, R., Zemelman, B., Snell, R. G., Rundle, S. A., Crow, S., Davies, J., Shelbourne, P., Buxton, J., Jones, C., … Housman, D. E. (1992). Molecular basis of myotonic dystrophy: Expansion of a trinucleotide (CTG) repeat at the 3′ end of a transcript encoding a protein kinase family member. *Cell*, *68*(4), 799–808. https://doi.org/10.1016/0092-8674(92)90154-5

Burki, U., Keane, J., Blain, A., O'Donovan, L., Gait, M. J., Laval, S. H., & Straub, V. (2015). Development and Application of an Ultrasensitive Hybridization-Based ELISA Method for the Determination of Peptide-Conjugated Phosphorodiamidate Morpholino Oligonucleotides. *Nucleic Acid Therapeutics*, *25*(5). https://doi.org/10.1089/nat.2014.0528

Cabezón, I., Manich, G., Martín-Venegas, R., Camins, A., Pelegrí, C., & Vilaplana, J. (2015). Trafficking of Gold Nanoparticles Coated with the 8D3 Anti-Transferrin Receptor Antibody at the Mouse Blood-Brain Barrier. *Molecular Pharmaceutics*, *12*(11). https://doi.org/10.1021/acs.molpharmaceut.5b00597

Caillet-Boudin, M. L., Fernandez-Gomez, F. J., Tran, H., Dhaenens, C. M., Buee, L., & Sergeant, N. (2014). Brain pathology in myotonic dystrophy: When tauopathy meets spliceopathy and RNAopathy. In *Frontiers in Molecular Neuroscience* (Vol. 6, Issue JAN). https://doi.org/10.3389/fnmol.2013.00057

Cairo, G., Bernuzzi, F., & Recalcati, S. (2006). A precious metal: Iron, an essential nutrient for all cells. *Genes & Nutrition*, *1*(1). https://doi.org/10.1007/bf02829934

Calzolari, A., Oliviero, I., Deaglio, S., Mariani, G., Biffoni, M., Sposi, N. M., Malavasi, F., Peschle, C., & Testa, U. (2007). Transferrin receptor 2 is frequently expressed in human cancer cell lines. *Blood Cells, Molecules, and Diseases*, *39*(1). https://doi.org/10.1016/j.bcmd.2007.02.003

Candelaria, P. V., Leoh, L. S., Penichet, M. L., & Daniels-Wells, T. R. (2021). Antibodies Targeting the Transferrin Receptor 1 (TfR1) as Direct Anti-cancer Agents. In *Frontiers in Immunology* (Vol. 12). https://doi.org/10.3389/fimmu.2021.607692

Casati S. R, Cervia D, Roux-Bietat P, Moscheni C, Perotta C, & De Palma C. (2024). Mitochondria and Reactive Oxygen Species: The Therapeutic Balance of Powers for Duchenne Muscular Dystrophy. *Cells*, *13*(7), 574. https://doi.org/10.3390/cells13070574

Cass, D., Hotchko, R., Barber, P., Jones, K., Gates, D. P., & Berglund, J. A. (2011). The four Zn fingers of MBNL1 provide a flexible platform for recognition of its RNA

binding elements. *BMC Molecular Biology*, *12*. https://doi.org/10.1186/1471-2199-12-20

Castel, A. L., Cleary, J. D., & Pearson, C. E. (2010). Repeat instability as the basis for human diseases and as a potential target for therapy. In *Nature Reviews Molecular Cell Biology* (Vol. 11, Issue 3). https://doi.org/10.1038/nrm2854

Cerro-Herreros, E., Sabater-Arcis, M., Fernandez-Costa, J. M., Moreno, N., Perez-Alonso, M., Llamusi, B., & Artero, R. (2018). miR-23b and miR-218 silencing increase Muscleblind-like expression and alleviate myotonic dystrophy phenotypes in mammalian models. *Nature Communications 2018 9:1*, *9*(1), 1–13. https://doi.org/10.1038/s41467-018-04892-4

Charizanis, K., Lee, K. Y., Batra, R., Goodwin, M., Zhang, C., Yuan, Y., Shiue, L., Cline, M., Scotti, M. M., Xia, G., Kumar, A., Ashizawa, T., Clark, H. B., Kimura, T., Takahashi, M. P., Fujimura, H., Jinnai, K., Yoshikawa, H., Gomes-Pereira, M., … Swanson, M. S. (2012). Muscleblind-like 2-Mediated Alternative Splicing in the Developing Brain and Dysregulation in Myotonic Dystrophy. *Neuron*, *75*(3), 437–450. https://doi.org/10.1016/j.neuron.2012.05.029

Charlet-B., N., Savkur, R. S., Singh, G., Philips, A. V., Grice, E. A., & Cooper, T. A. (2002). Loss of the muscle-specific chloride channel in type 1 myotonic dystrophy due to misregulated alternative splicing. *Molecular Cell*, *10*(1), 45–53. https://doi.org/10.1016/S1097-2765(02)00572-5

Cheng, Y., Zak, O., Aisen, P., Harrison, S. C., & Walz, T. (2004). Structure of the Human Transferrin Receptor-Transferrin Complex. *Cell*, *116*(4). https://doi.org/10.1016/S0092-8674(04)00130-8

Cherniack, A. D., Klarlund, J. K., & Czech, M. P. (1994). Phosphorylation of the Ras nucleotide exchange factor son of sevenless by mitogen-activated protein kinase. *Journal of Biological Chemistry*, *269*(7). https://doi.org/10.1016/s0021-9258(17)37603-2

Christou, M., Wengel, J., Sokratous, K., Kyriacou, K., Nikolaou, G., Phylactou, L. A., & Mastroyiannopoulos, N. P. (2019). *Systemic Evaluation of Chimeric LNA/2¢-O-Methyl Steric Blockers for Myotonic Dystrophy Type 1 Therapy*. https://doi.org/10.1089/nat.2019.0811

Ciechanover, A., Schwartz, A. L., Dautry Varsat, A., & Lodish, H. F. (1983). Kinetics of internalization and recycling of transferrin and the transferrin receptor in a human hepatoma cell line. Effect of lysosomotropic agents. *Journal of Biological Chemistry*, *258*(16). https://doi.org/10.1016/s0021-9258(17)44551-0

Clarke, M. S. F., Khakee, R., & McNeil, P. L. (1993). Loss of cytoplasmic basic fibroblast growth factor from physiologically wounded myofibers of normal and dystrophic muscle. *Journal of Cell Science*, *106*(1). https://doi.org/10.1242/jcs.106.1.121

Corbalan-Garcia, S., Yang, S.-S., Degenhardt, K. R., & Bar-Sagi, D. (1996). Identification of the Mitogen-Activated Protein Kinase Phosphorylation Sites on Human Sosl That Regulate Interaction with Grb2. *Molecular and Cellular Biology*, *16*(10). https://doi.org/10.1128/mcb.16.10.5674

Corey, D. R. (2017). Nusinersen, an antisense oligonucleotide drug for spinal muscular atrophy. *Nature Neuroscience*. https://doi.org/10.1038/nn.4508

Crnković-Mertens, I., Semzow, J., Hoppe-Seyler, F., & Butz, K. (2006). Isoform-specific silencing of the Livin gene by RNA interference defines Livin β as key mediator of apoptosis inhibition in HeLa cells. *Journal of Molecular Medicine*, *84*(3). https://doi.org/10.1007/s00109-005-0021-5

Czifrus, E., & Berlau, D. J. (2023). Viltolarsen: a treatment option for Duchenne muscular dystrophy patients who are amenable to exon 53 skipping therapy. In *Expert Review of Neurotherapeutics* (Vol. 23, Issue 10). https://doi.org/10.1080/14737175.2023.2246658

Daniels, T. R., Ortiz-Sánchez, E., Luria-Pérez, R., Quintero, R., Helguera, G., Bonavida, B., Martínez-Maza, O., & Penichet, M. L. (2011). An antibody-based multifaceted approach targeting the human transferrin receptor for the treatment of b-cell malignancies. *Journal of Immunotherapy*, *34*(6). https://doi.org/10.1097/CJI.0b013e318222ffc8

Das Gupta, A., & Shah, V. I. (1990). Correlation of transferrin receptor expression with histologic grade and immunophenotype in chronic lymphocytic leukemia and Non-Hodgkin's lymphoma. *Hematologic Pathology*, *4*(1).

Davis, B. M., Mccurrach, M. E., Taneja, K. L., Singer, R. H., & Housman, D. E. (1997). Expansion of a CUG trinucleotide repeat in the 3′ untranslated region of myotonic dystrophy protein kinase transcripts results in nuclear retention of transcripts. *Proceedings of the National Academy of Sciences of the United States of America*, *94*(14), 7388–7393. https://doi.org/10.1073/pnas.94.14.7388

De Antonio, M., Dogan, C., Hamroun, D., Mati, M., Zerrouki, S., Eymard, B., Katsahian, S., & Bassez, G. (2016). Unravelling the myotonic dystrophy type 1 clinical spectrum: A systematic registry-based study with implications for disease classification. In *Revue Neurologique* (Vol. 172, Issue 10). https://doi.org/10.1016/j.neurol.2016.08.003

De Die-Smulders, C. E. M., Höweler, C. J., Thijs, C., Mirandolle, J. F., Anten, H. B., Smeets, H. J. M., Chandler, K. E., & Geraedts, J. P. M. (1998). Age and causes of death in adult-onset myotonic dystrophy. *Brain*, *121*(8). https://doi.org/10.1093/brain/121.8.1557

De Serres-Bérard, T., Ait Benichou, S., Jauvin, D., Boutjdir, M., Puymirat, J., & Chahine, M. (2022). Recent Progress and Challenges in the Development of Antisense Therapies for Myotonic Dystrophy Type 1. In *International Journal of Molecular Sciences* (Vol. 23, Issue 21). https://doi.org/10.3390/ijms232113359

Deaglio, S., Capobianco, A., Calì, A., Bellora, F., Alberti, F., Righi, L., Sapino, A., Camaschella, C., & Malavasi, F. (2002). Structural, functional, and tissue distribution analysis of human transferrin receptor-2 by murine monoclonal antibodies and a polyclonal antiserum. *Blood*, *100*(10). https://doi.org/10.1182/blood-2002-01-0076

Degener, M. J. F., Van Cruchten, R. T. P., Otero, B. A., Wang, E. T., Wansink, D. G., & Hoen, P. A. C. (2022). A comprehensive atlas of fetal splicing patterns in the brain

of adult myotonic dystrophy type 1 patients. *NAR Genomics and Bioinformatics*, *4*(1). https://doi.org/10.1093/nargab/lqac016

Derossi, D., Joliot, A. H., Chassaing, G., & Prochiantz, A. (1994). The third helix of the Antennapedia homeodomain translocates through biological membranes. *Journal of Biological Chemistry*, *269*(14). https://doi.org/10.1016/s0021-9258(17)34080-2

Desjardins, C. A., Yao, M., Hall, J., O'Donnell, E., Venkatesan, R., Spring, S., Wen, A., Hsia, N., Shen, P., Russo, R., Lan, B., Picariello, T., Tang, K., Weeden, T., Zanotti, S., Subramanian, R., & Ibraghimov-Beskrovnaya, O. (2022). Enhanced exon skipping and prolonged dystrophin restoration achieved by TfR1-targeted delivery of antisense oligonucleotide using FORCE conjugation in mdx mice. *Nucleic Acids Research*, *50*(20). https://doi.org/10.1093/nar/gkac641

Dhaenens, C. M., Tran, H., Frandemiche, M. L., Carpentier, C., Schraen-Maschke, S., Sistiaga, A., Goicoechea, M., Eddarkaoui, S., Van Brussels, E., Obriot, H., Labudeck, A., Gevaert, M. H., Fernandez-Gomez, F., Charlet-Berguerand, N., Deramecourt, V., Maurage, C. A., Buée, L., de Munain, A. L., Sablonnière, B., … Sergeant, N. (2011). Mis-splicing of Tau exon 10 in myotonic dystrophy type 1 is reproduced by overexpression of CELF2 but not by MBNL1 silencing. *Biochimica et Biophysica Acta - Molecular Basis of Disease*, *1812*(7). https://doi.org/10.1016/j.bbadis.2011.03.010

Dieterle, F., Sistare, F., Goodsaid, F., Papaluca, M., Ozer, J. S., Webb, C. P., Baer, W., Senagore, A., Schipper, M. J., Vonderscher, J., Sultana, S., Gerhold, D. L., Phillips, J. A., Maurer, G., Carl, K., Laurie, D., Harpur, E., Sonee, M., Ennulat, D., … Mattes, W. (2010). Renal biomarker qualification submission: A dialog between the FDA-EMEA and Predictive Safety Testing Consortium. In *Nature Biotechnology* (Vol. 28, Issue 5). https://doi.org/10.1038/nbt.1625

Dincã, D. M., Lallemant, L., González-Barriga, A., Cresto, N., Braz, S. O., Sicot, G., Pillet, L. E., Polvèche, H., Magneron, P., Huguet-Lachon, A., Benyamine, H., Azotla-Vilchis, C. N., Agonizantes-Juárez, L. E., Tahraoui-Boris, J., Martinat, C., Hernández-Hernández, O., Auboeuf, D., Rouach, N., Bourgeois, C. F., … Gomes-Pereira, M. (2022). Myotonic dystrophy RNA toxicity alters morphology, adhesion and migration of mouse and human astrocytes. *Nature Communications*, *13*(1). https://doi.org/10.1038/s41467-022-31594-9

Ding Cheng Yang, Wang, F., Elliott, R. L., & Head, J. F. (2001). Expression of transferrin receptor and ferritin H-chain mRNA are associated with clinical and histopathological prognostic indicators in breast cancer. *Anticancer Research*, *21*(1 B).

Ding, H., Chen, S., Pan, X., Dai, X., Pan, G., Li, Z., Mai, X., Tian, Y., Zhang, S., Liu, B., Cao, G., Yao, Z., Yao, X., Gao, L., Yang, L., Chen, X., Sun, J., Chen, H., Han, M., … Xie, L. (2021). Transferrin receptor 1 ablation in satellite cells impedes skeletal muscle regeneration through activation of ferroptosis. *Journal of Cachexia, Sarcopenia and Muscle*, *12*(3). https://doi.org/10.1002/jcsm.12700

Dixon, D. M., Choi, J., El-Ghazali, A., Park, S. Y., Roos, K. P., Jordan, M. C., Fishbein, M. C., Comai, L., & Reddy, S. (2015). Loss of muscleblind-like 1 results in cardiac

pathology and persistence of embryonic splice isoforms. *Scientific Reports*, *5*. https://doi.org/10.1038/srep09042

Dominski, Z., & Kole, R. (1993). Restoration of correct splicing in thalassemic pre-mRNA by antisense oligonucleotides. *Proceedings of the National Academy of Sciences of the United States of America*, *90*(18), 8673. https://doi.org/10.1073/PNAS.90.18.8673

Douniol, M., Jacquette, A., Cohen, D., Bodeau, N., Rachidi, L., Angeard, N., Cuisset, J. M., Vallée, L., Eymard, B., Plaza, M., Héron, D., & Guilé, J. M. (2012). Psychiatric and cognitive phenotype of childhood myotonic dystrophy type 1. *Developmental Medicine and Child Neurology*, *54*(10). https://doi.org/10.1111/j.1469-8749.2012.04379.x

Du, H., Cline, M. S., Osborne, R. J., Tuttle, D. L., Clark, T. A., Donohue, J. P., Hall, M. P., Shiue, L., Swanson, M. S., Thornton, C. A., & Ares, M. (2010). Aberrant alternative splicing and extracellular matrix gene expression in mouse models of myotonic dystrophy. *Nature Structural and Molecular Biology*, *17*(2). https://doi.org/10.1038/nsmb.1720

Duchardt, F., Fotin-Mleczek, M., Schwarz, H., Fischer, R., & Brock, R. (2007). A comprehensive model for the cellular uptake of cationic cell-penetrating peptides. *Traffic*, *8*(7). https://doi.org/10.1111/j.1600-0854.2007.00572.x

Dugal-Tessier, J., Thirumalairajan, S., & Jain, N. (2021). Antibody-Oligonucleotide Conjugates: A Twist to Antibody-Drug Conjugates. *Journal of Clinical Medicine*, *10*(4), 1–17. https://doi.org/10.3390/JCM10040838

Dyne Therapeutics. (2021). Developing therapeutic oligonucleotides to treat myotonic dystrophy type 1. Company poster presentation at the American Society of Gene & Cell Therapy (ASGCT).https://www.dyne-tx.com/wp-content/uploads/2021-ASGCT-Conference-Presentation-Dyne-Therapeutics_Romesh-Subramanian.pdf

Dyne Therapeutics. (2023). 2023 ASGCT DM1 CNS Presentation. https://www.dyne-tx.com/wp-content/uploads/Zanotti_2023_ASGCT_DM1_CNS_FINAL.pdf

Dyne Therapeutics. (2024). The FORCE™ Platform Delivers Oligonucleotides to the Brain in a DM1 Mouse Model and in NHPs. Presented at the American Society of Gene & Cell Therapy (ASGCT) Annual Meeting.https://www.dyne-tx.com/wp-content/uploads/Zanotti_2023_ASGCT_DM1_CNS_FINAL.pdf

Dynes Therapeutics. (2022). 2022 ASGCT Presentation. https://www.dyne-tx.com/wp-content/uploads/2022%20ASGCT%20presentation_FINAL.pdf

Echenne, B., & Bassez, G. (2013). Congenital and infantile myotonic dystrophy. In *Handbook of Clinical Neurology* (Vol. 113). https://doi.org/10.1016/B978-0-444-59565-2.00009-5

Echenne, B., Rideau, A., Roubertie, A., Sébire, G., Rivier, F., & Lemieux, B. (2008). Myotonic dystrophy type I in childhood. Long-term evolution in patients surviving the neonatal period. *European Journal of Paediatric Neurology*. https://doi.org/10.1016/j.ejpn.2007.07.014

Eder, P. S., Devine, R. J., Dagle, J. M., & Walder, J. A. (2009). Substrate Specificity and Kinetics of Degradation of Antisense Oligonucleotides by a 3′ Exonuclease in Plasma. *Https://Home.Liebertpub.Com/Ard*, *1*(2), 141–151. https://doi.org/10.1089/ARD.1991.1.141

Eguchi, I., Koike, R., Onodera, O., Tanaka, K., Kondo, H., & Tsuji, S. (1994). Correlation between degrees of the CTG repeat expansion and clinical features of myotonic dystrophy. *Clinical Neurology*, *34*(2).

Ehrenstein, G., & Lecar, H. (1977). Electrically gated ionic channels in lipid bilayers. *Quarterly Reviews of Biophysics*, *10*(1). https://doi.org/10.1017/S0033583500000123

Ekström, A. B., Hakenäs-Plate, louise, Tulinius, M., & Wentz, E. (2009). Cognition and adaptive skills in myotonic dystrophy type 1: A study of 55 individuals with congenital and childhood forms. *Developmental Medicine and Child Neurology*, *51*(12). https://doi.org/10.1111/j.1469-8749.2009.03300.x

El Boujnouni, N., van der Bent, M. L., Willemse, M., 't Hoen, P. A. C., Brock, R., & Wansink, D. G. (2023). Block or degrade? Balancing on- and off-target effects of antisense strategies against transcripts with expanded triplet repeats in DM1. *Molecular Therapy Nucleic Acids*, *32*. https://doi.org/10.1016/j.omtn.2023.04.010

Engelhardt, J. A. (2016). Comparative Renal Toxicopathology of Antisense Oligonucleotides. In *Nucleic Acid Therapeutics* (Vol. 26, Issue 4). https://doi.org/10.1089/nat.2015.0598

Fardaei, M., Rogers, M. T., Thorpe, H. M., Larkin, K., Hamshere, M. G., Harper, P. S., & Brook, J. D. (2002). Three proteins, MBNL, MBLL and MBXL, co-localize in vivo with nuclear foci of expanded-repeat transcripts in DM1 and DM2 cells. *Human Molecular Genetics*, *11*(7). https://doi.org/10.1093/hmg/11.7.805

Fernandez-Costa, J. M., & Artero, R. (2010). A conserved motif controls nuclear localization of Drosophila Muscleblind. *Molecules and Cells*, *30*(1). https://doi.org/10.1007/s10059-010-0089-9

Finkel, R. S., Chiriboga, C. A., Vajsar, J., Day, J. W., Montes, J., De Vivo, D. C., Yamashita, M., Rigo, F., Hung, G., Schneider, E., Norris, D. A., Xia, S., Bennett, C. F., & Bishop, K. M. (2016). Treatment of infantile-onset spinal muscular atrophy with nusinersen: a phase 2, open-label, dose-escalation study. *The Lancet*. https://doi.org/10.1016/S0140-6736(16)31408-8

Fittipaldi, A., Ferrari, A., Zoppé, M., Arcangeli, C., Pellegrini, V., Beltram, F., & Giacca, M. (2003). Cell Membrane Lipid Rafts Mediate Caveolar Endocytosis of HIV-1 Tat Fusion Proteins. *Journal of Biological Chemistry*, *278*(36). https://doi.org/10.1074/jbc.M303045200

Flanigan, K. M. (2014). Duchenne and becker muscular dystrophies. In *Neurologic Clinics* (Vol. 32, Issue 3). https://doi.org/10.1016/j.ncl.2014.05.002

Fonseca, S. B., Pereira, M. P., & Kelley, S. O. (2009). Recent advances in the use of cell-penetrating peptides for medical and biological applications. In *Advanced Drug Delivery Reviews* (Vol. 61, Issue 11). https://doi.org/10.1016/j.addr.2009.06.001

Fortune, M. T., Vassilopoulos, C., Coolbaugh, M. I., Siciliano, M. J., & Monckton, D. G. (2000). Dramatic, expansion-biased, age-dependent, tissue-specific somatic mosaicism in a transgenic mouse model of triplet repeat instability. *Human Molecular Genetics*, *9*(3). https://doi.org/10.1093/hmg/9.3.439

Freyermuth, F., Rau, F., Kokunai, Y., Linke, T., Sellier, C., Nakamori, M., Kino, Y., Arandel, L., Jollet, A., Thibault, C., Philipps, M., Vicaire, S., Jost, B., Udd, B., Day, J. W., Duboc, D., Wahbi, K., Matsumura, T., Fujimura, H., … Charlet-Berguerand, N. (2016). Splicing misregulation of SCN5A contributes to cardiac-conduction delay and heart arrhythmia in myotonic dystrophy. *Nature Communications*, *7*(1), 25. https://doi.org/10.1038/ncomms11067

Friden, P. M., Walus, L. R., Musso, G. F., Taylor, M. A., Malfroy, B., & Starzyk, R. M. (1991). Anti-transferrin receptor antibody and antibody-drug conjugates cross the blood-brain barrier. *Proceedings of the National Academy of Sciences of the United States of America*, *88*(11). https://doi.org/10.1073/pnas.88.11.4771

Fu, Y. H., Pizzuti, A., Fenwick, R. G., King, J., Rajnarayan, S., Dunne, P. W., Dubel, J., Nasser, G. A., Ashizawa, T., De Jong, P., Wieringa, B., Korneluk, R., Perryman, M. B., Epstein, H. F., & Caskey, C. T. (1992). An Unstable Triplet Repeat in a Gene Related to Myotonic Muscular Dystrophy. *Science*, *255*(5049), 1256–1258. https://doi.org/10.1126/SCIENCE.1546326

Fu, Z., Li, S., Han, S., Shi, C., & Zhang, Y. (2022). Antibody drug conjugate: the “biological missile” for targeted cancer therapy. In *Signal Transduction and Targeted Therapy* (Vol. 7, Issue 1). https://doi.org/10.1038/s41392-022-00947-7

Fugier, C., Klein, A. F., Hammer, C., Vassilopoulos, S., Ivarsson, Y., Toussaint, A., Tosch, V., Vignaud, A., Ferry, A., Messaddeq, N., Kokunai, Y., Tsuburaya, R., De La Grange, P., Dembele, D., Francois, V., Precigout, G., Boulade-Ladame, C., Hummel, M. C., De Munain, A. L., … Charlet-Berguerand, N. (2011). Misregulated alternative splicing of BIN1 is associated with T tubule alterations and muscle weakness in myotonic dystrophy. *Nature Medicine*, *17*(6), 720–725. https://doi.org/10.1038/nm.2374

Futaki, S., Suzuki, T., Ohashi, W., Yagami, T., Tanaka, S., Ueda, K., & Sugiura, Y. (2001). Arginine-rich peptides. An abundant source of membrane-permeable peptides having potential as carriers for intracellular protein delivery. *Journal of Biological Chemistry*, *276*(8). https://doi.org/10.1074/jbc.M007540200

Gait, M. J., Arzumanov, A. A., McClorey, G., Godfrey, C., Betts, C., Hammond, S., & Wood, M. J. A. (2019). Cell-Penetrating Peptide Conjugates of Steric Blocking Oligonucleotides as Therapeutics for Neuromuscular Diseases from a Historical Perspective to Current Prospects of Treatment. *Nucleic Acid Therapeutics*, *29*(1), 1. https://doi.org/10.1089/NAT.2018.0747

Gallais, B., Gagnon, C., Mathieu, J., & Richer, L. (2017). Cognitive decline over time in adults with myotonic dystrophy type 1: A 9-year longitudinal study. *Neuromuscular Disorders*, *27*(1). https://doi.org/10.1016/j.nmd.2016.10.003

Gan L, Wu LCL, Wood JA, Yao M, Treleaven CM, Estrella NL, Wentworth BM, Hanson GJ, Passini MA (2022). A cell-penetrating peptide enhances delivery and efficacy

of phosphorodiamidate morpholino oligomers in mdx mice. *Mol Ther Nucleic Acids.*17(30):17-27. doi: 10.1016/j.omtn.2022.08.019

García-Puga, M., Saenz-Antoñanzas, A., Fernández-Torrón, R., de Munain, A. L., & Matheu, A. (2020). Myotonic Dystrophy type 1 cells display impaired metabolism and mitochondrial dysfunction that are reversed by metformin. *Aging*, *12*(7). https://doi.org/10.18632/aging.103022

Gatter, K. C., Brown, G., Strowbridge, I., Woolston, R. E., & Mason, D. Y. (1983). Transferrin receptors in human tissues: Their distribution and possible clinical relevance. *Journal of Clinical Pathology*, *36*(5), 539–545. https://doi.org/10.1136/jcp.36.5.539

Gaudet, D., Alexander, V. J., Baker, B. F., Brisson, D., Tremblay, K., Singleton, W., Geary, R. S., Hughes, S. G., Viney, N. J., Graham, M. J., Crooke, R. M., Witztum, J. L., Brunzell, J. D., & Kastelein, J. J. P. (2015). Antisense Inhibition of Apolipoprotein C-III in Patients with Hypertriglyceridemia. *New England Journal of Medicine*, *373*(5). https://doi.org/10.1056/nejmoa1400283

Gaus, H. J., Gupta, R., Chappell, A. E., Østergaard, M. E., Swayze, E. E., & Seth, P. P. (2019). Characterization of the interactions of chemically-modified therapeutic nucleic acids with plasma proteins using a fluorescence polarization assay. *Nucleic Acids Research*, *47*(3), 1110–1122. https://doi.org/10.1093/NAR/GKY1260

Geary, R. S., Baker, B. F., & Crooke, S. T. (2015). Clinical and Preclinical Pharmacokinetics and Pharmacodynamics of Mipomersen (Kynamro®): A Second-Generation Antisense Oligonucleotide Inhibitor of Apolipoprotein B. In *Clinical Pharmacokinetics* (Vol. 54, Issue 2). https://doi.org/10.1007/s40262-014-0224-4

Geary, R. S., Henry, S. P., & Grillone, L. R. (2002). Fomivirsen: Clinical pharmacology and potential drug interactions. In *Clinical Pharmacokinetics* (Vol. 41, Issue 4). https://doi.org/10.2165/00003088-200241040-00002

Geary, R. S., Norris, D., Yu, R., & Bennett, C. F. (2015). Pharmacokinetics, biodistribution and cell uptake of antisense oligonucleotides. *Advanced Drug Delivery Reviews*, *87*, 46–51. https://doi.org/10.1016/J.ADDR.2015.01.008

Gennarelli, M., Novelli, G., Andreasi Bassi, F., Martorell, L., Cornet, M., Menegazzo, E., Mostacciuolo, M. L., Martinez, J. M., Angelini, C., Pizzuti, A., Baiget, M., & Dallapiccola, B. (1996). Prediction of Myotonic Dystrophy Clinical Severity Based on the Number of Intragenic [CTG]n Trinucleotide Repeats. *American Journal of Medical Genetics - Seminars in Medical Genetics*, *65*(4). https://doi.org/10.1002/(SICI)1096-8628(19961111)65:4<342::AID-AJMG18>3.0.CO;2-U

Giannini, E. G., Testa, R., & Savarino, V. (2005). Liver enzyme alteration: A guide for clinicians. *Cmaj*, *172*(3), 367–379. https://doi.org/10.1503/cmaj.1040752

Gilbert, C. J., Longenecker, J. Z., & Accornero, F. (2021). Erk1/2: An integrator of signals that alters cardiac homeostasis and growth. In *Biology* (Vol. 10, Issue 4). https://doi.org/10.3390/biology10040346

Giorgio, E., Lorenzati, M., Di Val Cervo, P. R., Brussino, A., Cernigoj, M., Sala, E. Della, Stella, A. B., Ferrero, M., Caiazzo, M., Capellari, S., Cortelli, P., Conti, L., Cattaneo, E., Buffo, A., & Brusco, A. (2019). Allele-specific silencing as treatment for gene duplication disorders: Proof-of-principle in autosomal dominant leukodystrophy. *Brain*, *142*(7). https://doi.org/10.1093/brain/awz139

Giugliani, R., Martins, A. M., So, S., Yamamoto, T., Yamaoka, M., Ikeda, T., Tanizawa, K., Sonoda, H., Schmidt, M., & Sato, Y. (2021). Iduronate-2-sulfatase fused with anti-hTfR antibody, pabinafusp alfa, for MPS-II: A phase 2 trial in Brazil. *Molecular Therapy*, *29*(7). https://doi.org/10.1016/j.ymthe.2021.03.019

Godfrey, C., Muses, S., McClorey, G., Wells, K. E., Coursindel, T., Terry, R. L., Betts, C., Hammond, S., O'Donovan, L., Hildyard, J., Andaloussi, S. El, Gait, M. J., Wood, M. J., & Wells, D. J. (2015). How much dystrophin is enough: The physiological consequences of different levels of dystrophin in the mdx mouse. *Human Molecular Genetics*, *24*(15). https://doi.org/10.1093/hmg/ddv155

Goers, E. S., Purcell, J., Voelker, R. B., Gates, D. P., & Berglund, J. A. (2010). MBNL1 binds GC motifs embedded in pyrimidines to regulate alternative splicing. *Nucleic Acids Research*, *38*(7). https://doi.org/10.1093/nar/gkp1209

Gogliotti, R. G., Hammond, S. M., Lutz, C., & DiDonato, C. J. (2010). Molecular and phenotypic reassessment of an infrequently used mouse model for spinal muscular atrophy. *Biochemical and Biophysical Research Communications*. https://doi.org/10.1016/j.bbrc.2009.11.090

González-Barriga, A., Kranzen, J., Croes, H. J. E., Bijl, S., Van Den Broek, W. J. A. A., Van Kessel, I. D. G., Van Engelen, B. G. M., Van Deutekom, J. C. T., Wieringa, B., Mulders, S. A. M., & Wansink, D. G. (2015). Cell Membrane Integrity in Myotonic Dystrophy Type 1: Implications for Therapy. *PLOS ONE*, *10*(3), e0121556. https://doi.org/10.1371/JOURNAL.PONE.0121556

Gray J. T, A. T. I. (2022). *Nucleic acid molecules containing spacers and methods of use thereof. Patent no: US2018305715A1*. U.S.patentsandtrademarkoffice.

Grimm, H. P., Schumacher, V., Schäfer, M., Imhof-Jung, S., Freskgård, P. O., Brady, K., Hofmann, C., Rüger, P., Schlothauer, T., Göpfert, U., Hartl, M., Rottach, S., Zwick, A., Seger, S., Neff, R., Niewoehner, J., & Janssen, N. (2023). Delivery of the BrainshuttleTM amyloid-beta antibody fusion trontinemab to non-human primate brain and projected efficacious dose regimens in humans. *MAbs*, *15*(1). https://doi.org/10.1080/19420862.2023.2261509

Groh, W. J., Groh, M. R., Saha, C., Kincaid, J. C., Simmons, Z., Ciafaloni, E., Pourmand, R., Otten, R. F., Bhakta, D., Nair, G. V., Marashdeh, M. M., Zipes, D. P., & Pascuzzi, R. M. (2008). Electrocardiographic Abnormalities and Sudden Death in Myotonic Dystrophy Type 1. *New England Journal of Medicine*, *358*(25). https://doi.org/10.1056/nejmoa062800

Gudde, A. E. E. G., González-Barriga, A., van den Broek, W. J. A. A., Wieringa, B., & Wansink, D. G. (2016). A low absolute number of expanded transcripts is involved in myotonic dystrophy type 1 manifestation in muscle. *Human Molecular Genetics*, *25*(8). https://doi.org/10.1093/hmg/ddw042

Hageman, A. T. M., Gabreëls, F. J. M., Liem, K. D., Renkawek, K., & Boon, J. M. (1993). Congenital myotonic dystrophy; a report on thirteen cases and a review of the literature. *Journal of the Neurological Sciences*, *115*(1). https://doi.org/10.1016/0022-510X(93)90072-7

Hamm, S., Latz, E., Hangel, D., Müller, T., Yu, P., Golenbock, D., Sparwasser, T., Wagner, H., & Bauer, S. (2010). Alternating 2′-O-ribose methylation is a universal approach for generating non-stimulatory siRNA by acting as TLR7 antagonist. *Immunobiology*, *215*(7), 559–569. https://doi.org/10.1016/J.IMBIO.2009.09.003

Hammond, S. M., Abendroth, F., Goli, L., Stoodley, J., Burrell, M., Thom, G., Gurrell, I., Ahlskog, N., Gait, M. J., Wood, M. J. A., & Webster, C. I. (2022). Antibody-oligonucleotide conjugate achieves CNS delivery in animal models for spinal muscular atrophy. *JCI Insight*, *7*(24). https://doi.org/10.1172/jci.insight.154142

Hammond, S. M., Hazell, G., Shabanpoor, F., Saleh, A. F., Bowerman, M., Sleigh, J. N., Meijboom, K. E., Zhou, H., Muntoni, F., Talbot, K., Gait, M. J., Wood, M. J. J. A., Paterson, J., Webster, C. I., Silajdzic, E., Bjorkqvist, M., Deguise, M. O., Kothary, R., Kannan, A., … Ekström, A. B. (2017). Systemic peptide-mediated oligonucleotide therapy improves long-term survival in spinal muscular atrophy. *Human Molecular Genetics*, *10*(1), 166–177. https://doi.org/10.1073/pnas.1605731113

Han, H., Irimia, M., Ross, P. J., Sung, H. K., Alipanahi, B., David, L., Golipour, A., Gabut, M., Michael, I. P., Nachman, E. N., Wang, E., Trcka, D., Thompson, T., O'Hanlon, D., Slobodeniuc, V., Barbosa-Morais, N. L., Burge, C. B., Moffat, J., Frey, B. J., … Blencowe, B. J. (2013). MBNL proteins repress ES-cell-specific alternative splicing and reprogramming. *Nature*, *498*(7453). https://doi.org/10.1038/nature12270

Han, S., Nam, J., Li, Y., Kim, S., Cho, S. H., Cho, Y. S., Choi, S. Y., Choi, J., Han, K., Kim, Y., Na, M., Kim, H., Bae, Y. C., Choi, S. Y., & Kim, E. (2010). Regulation of dendritic spines, spatial memory, and embryonic development by the TANC family of PSD-95-interacting proteins. *Journal of Neuroscience*, *30*(45). https://doi.org/10.1523/JNEUROSCI.3128-10.2010

Han, W. K., Bailly, V., Abichandani, R., Thadhani, R., & Bonventre, J. V. (2002). Kidney Injury Molecule-1 (KIM-1): A novel biomarker for human renal proximal tubule injury. *Kidney International*, *62*(1). https://doi.org/10.1046/j.1523-1755.2002.00433.x

Hanger, D. P., Anderton, B. H., & Noble, W. (2009). Tau phosphorylation: the therapeutic challenge for neurodegenerative disease. In *Trends in Molecular Medicine* (Vol. 15, Issue 3). https://doi.org/10.1016/j.molmed.2009.01.003

Harmony BIosciences. (2024). *PRESS RELEASE: Harmony Biosciences presents positive data for pitolisant in the treatment of excessive daytime sleepiness and fatigue in myotonic dystrophy type 1*. https://ir.harmonybiosciences.com/news-releases/news-release-details/harmony-biosciences-presents-positive-data-pitolisant-treatment

Harper P. (2001). Myotonic dystrophy, 3rd edition. *Muscle & Nerve*, *25*(6). https://doi.org/10.1002/mus.1238

Hasuike, Y., Mochizuki, H., & Nakamori, M. (2022). Expanded CUG Repeat RNA Induces Premature Senescence in Myotonic Dystrophy Model Cells. *Frontiers in Genetics*, *13*. https://doi.org/10.3389/fgene.2022.865811

Heatwole, C., Bode, R., Johnson, N., Quinn, C., Martens, W., McDermott, M. P., Rothrock, N., Thornton, C., Vickrey, B., Victorson, D., & Moxley, R. (2012). Patient-reported impact of symptoms in myotonic dystrophy type 1 (PRISM-1). *Neurology*, *79*(4). https://doi.org/10.1212/WNL.0b013e318260cbe6

Heatwole, C., Luebbe, E., Rosero, S., Eichinger, K., Martens, W., Hilbert, J., Dekdebrun, J., Dilek, N., Zizzi, C., Johnson, N., Puwanant, A., Tawil, R., Schifitto, G., Beck, C. A., Richeson, J. F., Zareba, W., Thornton, C., McDermott, M. P., & Moxley, R. (2021). Mexiletine in Myotonic Dystrophy Type 1: A Randomized, Double-Blind, Placebo-Controlled Trial. *Neurology*, *96*(2). https://doi.org/10.1212/WNL.0000000000011002

Heo, Y. A. (2020). Golodirsen: First Approval. In *Drugs* (Vol. 80, Issue 3). https://doi.org/10.1007/s40265-020-01267-2

Herce, H. D., Garcia, A. E., & Cardoso, M. C. (2014). Fundamental molecular mechanism for the cellular uptake of guanidinium-rich molecules. *Journal of the American Chemical Society*, *136*(50). https://doi.org/10.1021/ja507790z

Hernández-Hernández, O., Guiraud-Dogan, C., Sicot, G., Huguet, A., Luilier, S., Steidl, E., Saenger, S., Marciniak, E., Obriot, H., Chevarin, C., Nicole, A., Revillod, L., Charizanis, K., Lee, K. Y., Suzuki, Y., Kimura, T., Matsuura, T., Cisneros, B., Swanson, M. S., … Gomes-Pereira, M. (2013). Myotonic dystrophy CTG expansion affects synaptic vesicle proteins, neurotransmission and mouse behaviour. *Brain*, *136*(3), 957–970. https://doi.org/10.1093/brain/aws367

Ho, G. (2015). Congenital and childhood myotonic dystrophy: Current aspects of disease and future directions. *World Journal of Clinical Pediatrics*, *4*(4). https://doi.org/10.5409/wjcp.v4.i4.66

Ho, T. H., Bundman, D., Armstrong, D. L., & Cooper, T. A. (2005). Transgenic mice expressing CUG-BP1 reproduce splicing mis-regulation observed in myotonic dystrophy. *Human Molecular Genetics*, *14*(11). https://doi.org/10.1093/hmg/ddi162

Ho, T. H., Charlet-B, N., Poulos, M. G., Singh, G., Swanson, M. S., & Cooper, T. A. (2004). Muscleblind proteins regulate alternative splicing. *EMBO Journal*, *23*(15). https://doi.org/10.1038/sj.emboj.7600300

Hoes, M. F., Grote Beverborg, N., Kijlstra, J. D., Kuipers, J., Swinkels, D. W., Giepmans, B. N. G., Rodenburg, R. J., van Veldhuisen, D. J., de Boer, R. A., & van der Meer, P. (2018). Iron deficiency impairs contractility of human cardiomyocytes through decreased mitochondrial function. *European Journal of Heart Failure*, *20*(5). https://doi.org/10.1002/ejhf.1154

Horrigan, J., Gomes, T. B., Snape, M., Nikolenko, N., McMorn, A., Evans, S., Yaroshinsky, A., Della Pasqua, O., Oosterholt, S., & Lochmüller, H. (2020). A

Phase 2 Study of AMO-02 (Tideglusib) in Congenital and Childhood-Onset Myotonic Dystrophy Type 1 (DM1). *Pediatric Neurology*, *112*. https://doi.org/10.1016/j.pediatrneurol.2020.08.001

Hsieh-Li, H. M., Chang, J. G., Jong, Y. J., Wu, M. H., Wang, N. M., Tsai, C. H., & Li, H. (2000). A mouse model for spinal muscular atrophy. *Nature Genetics*. https://doi.org/10.1038/71709

Hua, Y., Sahashi, K., Rigo, F., Hung, G., Horev, G., Bennett, C. F., & Krainer, A. R. (2011). Peripheral SMN restoration is essential for long-term rescue of a severe spinal muscular atrophy mouse model. *Nature*. https://doi.org/10.1038/nature10485

Hua, Y., Vickers, T. A., Okunola, H. L., Bennett, C. F., & Krainer, A. R. (2008). Antisense Masking of an hnRNP A1/A2 Intronic Splicing Silencer Corrects SMN2 Splicing in Transgenic Mice. *American Journal of Human Genetics*, *82*(4). https://doi.org/10.1016/j.ajhg.2008.01.014

Huang, J. X., Kaeslin, G., Ranall, M. V., Blaskovich, M. A., Becker, B., Butler, M. S., Little, M. H., Lash, L. H., & Cooper, M. A. (2015). Evaluation of biomarkers for in vitro prediction of drug-induced nephrotoxicity: comparison of HK-2, immortalized human proximal tubule epithelial, and primary cultures of human proximal tubular cells. *Pharmacology Research and Perspectives*, *3*(3). https://doi.org/10.1002/prp2.148

Huang, Y., Huang, G., Kao, C., Chen, T., Wu, S., & Chen, J. (2011). P4-100: FDG-PET study on dementia of Alzheimer's type of less educated subjects. *Alzheimer's & Dementia*, *7*(4S_Part_21). https://doi.org/10.1016/j.jalz.2011.05.2121

Hudziak, R. M., Barofsky, E., Barofsky, D. F., Weller, D. L., Huang, S. Ben, & Weller, D. D. (1996). Resistance of Morpholino phosphorodiamidate oligomers to enzymatic degradation. *Antisense and Nucleic Acid Drug Development*, *6*(4), 267–272. https://doi.org/10.1089/oli.1.1996.6.267

Huguet, A., Medja, F., Nicole, A., Vignaud, A., Guiraud-Dogan, C., Ferry, A., Decostre, V., Hogrel, J. Y., Metzger, F., Hoeflich, A., Baraibar, M., Gomes-Pereira, M., Puymirat, J., Bassez, G., Furling, D., Munnich, A., & Gourdon, G. (2012). Molecular, Physiological, and Motor Performance Defects in DMSXL Mice Carrying >1,000 CTG Repeats from the Human DM1 Locus. *PLoS Genetics*, *8*(11), 1–19. https://doi.org/10.1371/journal.pgen.1003043

Hung, G., Xiao, X., Peralta, R., Bhattacharjee, G., Murray, S., Norris, D., Guo, S., & Monia, B. P. (2013). Characterization of target mRNA reduction through in situ RNA hybridization in multiple organ systems following systemic antisense treatment in animals. *Nucleic Acid Therapeutics*, *23*(6). https://doi.org/10.1089/nat.2013.0443

Hunter, A., Tsilfidis, C., Mettler, G., Jacob, P., Mahadevan, M., Surh, L., & Korneluk, R. (1992). The correlation of age of onset with CTG trinucleotide repeat amplification in myotonic dystrophy. *Journal of Medical Genetics*, *29*(11). https://doi.org/10.1136/jmg.29.11.774

Ichimura, T., Bonventre, J. V., Bailly, V., Wei, H., Hession, C. A., Cate, R. L., & Sanicola, M. (1998). Kidney injury molecule-1 (KIM-1), a putative epithelial cell adhesion molecule containing a novel immunoglobulin domain, is up-regulated in renal cells after injury. *Journal of Biological Chemistry*, *273*(7). https://doi.org/10.1074/jbc.273.7.4135

Itoh, K., Mitani, M., Kawamoto, K., Futamura, N., Funakawa, I., Jinnai, K., & Fushiki, S. (2010). Neuropathology does not correlate with regional differences in the extent of expansion of CTG repeats in the brain with myotonic dystrophy type 1. *Acta Histochemica et Cytochemica*, *43*(6). https://doi.org/10.1267/ahc.10019

Ivanova, G. D., Arzumanov, A., Abes, R., Yin, H., Wood, M. J. A., Lebleu, B., & Gait, M. J. (2008). Improved cell-penetrating peptide-PNA conjugates for splicing redirection in HeLa cells and exon skipping in mdx mouse muscle. *Nucleic Acids Research*, *36*(20). https://doi.org/10.1093/nar/gkn671

Iversen P.L. (2001). Phosphorodiamidate morpholino oligomers: favorable properties for sequence-specific gene inactivation. *CurrOpinMolThe*, *3*(3), 345–348. https://pubmed.ncbi.nlm.nih.gov/11497346/

Iwai, K., Drake, S. K., Wehr, N. B., Weissman, A. M., LaVaute, T., Minato, N., Klausner, R. D., Levine, R. L., & Rouault, T. A. (1998). Iron-dependent oxidation, ubiquitination, and degradation of iron regulatory protein 2: Implications for degradation of oxidized proteins. *Proceedings of the National Academy of Sciences of the United States of America*, *95*(9). https://doi.org/10.1073/pnas.95.9.4924

Jansen, G., Willems, P., Coerwinkel, M., Nillesen, W., Smeets, H., Vits, L., Höweler, C., Brunner, H., & Wieringa, B. (1994). Gonosomal mosaicism in myotonic dystrophy patients: Involvement of mitotic events in (CTG)n repeat variation and selection against extreme expansion in sperm. *American Journal of Human Genetics*, *54*(4).

Jaspert, A., Fahsold, R., Grehl, H., & Claus, D. (1995). Myotonic dystrophy: Correlation of clinical symptoms with the size of the CTG trinucleotide repeat. *Journal of Neurology*, *242*(2). https://doi.org/10.1007/BF00887824

Jauvin, D., Chrétien, J., Pandey, S. K., Martineau, L., Revillod, L., Bassez, G., Lachon, A., McLeod, A. R., Gourdon, G., Wheeler, T. M., Thornton, C. A., Bennett, C. F., & Puymirat, J. (2017). Targeting DMPK with Antisense Oligonucleotide Improves Muscle Strength in Myotonic Dystrophy Type 1 Mice. *Molecular Therapy - Nucleic Acids*, *7*, 465–474. https://doi.org/10.1016/j.omtn.2017.05.007

Jefferies, W. A., Brandon, M. R., Hunt, S. V., Williams, A. F., Gatter, K. C., & Mason, D. Y. (1984). Transferrin receptor on endothelium of brain capillaries. *Nature*, *312*(5990). https://doi.org/10.1038/312162a0

Jiang, H., Mankodi, A., Swanson, M. S., Moxley, R. T., & Thornton, C. A. (2004). Myotonic dystrophy type 1 is associated with nuclear foci of mutant RNA, sequestration of muscleblind proteins and deregulated alternative splicing in neurons. *Human Molecular Genetics*, *13*(24). https://doi.org/10.1093/hmg/ddh327

Johnson, N. E., Butterfield, R. J., Mayne, K., Newcomb, T., Imburgia, C., Dunn, D., Duval, B., Feldkamp, M. L., & Weiss, R. B. (2021). Population-Based Prevalence

of Myotonic Dystrophy Type 1 Using Genetic Analysis of Statewide Blood Screening Program. *Neurology*, *96*(7), e1045. https://doi.org/10.1212/WNL.0000000000011425

Kalsotra, A., Xiao, X., Ward, A. J., Castle, J. C., Johnson, J. M., Burge, C. B., & Cooper, T. A. (2008). A postnatal switch of CELF and MBNL proteins reprograms alternative splicing in the developing heart. *Proceedings of the National Academy of Sciences of the United States of America*, *105*(51), 20333. https://doi.org/10.1073/PNAS.0809045105

Kamei, N., Kikuchi, S., Takeda-Morishita, M., Terasawa, Y., Yasuda, A., Yamamoto, S., Ida, N., Nishio, R., & Takayama, K. (2013). Determination of the optimal cell-penetrating peptide sequence for intestinal insulin delivery based on molecular orbital analysis with self-organizing maps. *Journal of Pharmaceutical Sciences*, *102*(2). https://doi.org/10.1002/jps.23364

Kanadia, R. N., Johnstone, K. A., Mankodi, A., Lungu, C., Thornton, C. A., Esson, D., Timmers, A. M., Hauswirth, W. W., & Swanson, M. S. (2003). A Muscleblind Knockout Model for Myotonic Dystrophy. *Science*, *302*(5652). https://doi.org/10.1126/science.1088583

Kanadia, R. N., Shin, J., Yuan, Y., Beattie, S. G., Wheeler, T. M., Thornton, C. A., & Swanson, M. S. (2006). Reversal of RNA missplicing and myotonia after muscleblind overexpression in a mouse poly(CUG) model for myotonic dystrophy. *Proceedings of the National Academy of Sciences of the United States of America*, *103*(31). https://doi.org/10.1073/pnas.0604970103

Kanadia, R. N., Urbinati, C. R., Crusselle, V. J., Luo, D., Lee, Y. J., Harrison, J. K., Oh, S. P., & Swanson, M. S. (2003). Developmental expression of mouse muscleblind genes Mbnl1, Mbnl2 and Mbnl3. *Gene Expression Patterns*, *3*(4). https://doi.org/10.1016/S1567-133X(03)00064-4

Kawabata, H., Germain, R. S., Vuong, P. T., Nakamaki, T., Said, J. W., & Koeffler, H. P. (2000). Transferrin receptor 2-α supports cell growth both in iron-chelated cultured cells and in vivo. *Journal of Biological Chemistry*, *275*(22). https://doi.org/10.1074/jbc.M908846199

Kawada, R., Jonouchi, T., Kagita, A., Sato, M., Hotta, A., & Sakurai, H. (2023). Establishment of quantitative and consistent in vitro skeletal muscle pathological models of myotonic dystrophy type 1 using patient-derived iPSCs. *Scientific Reports*, *13*(1). https://doi.org/10.1038/s41598-022-26614-z

Keating, M. J., Sethi, M. R., Bodey, G. P., & Samaan, N. A. (1977). Hypocalcemia with hypoparathyroidism and renal tubular dysfunction associated with aminoglycoside therapy. *Cancer*, *39*(4). https://doi.org/10.1002/1097-0142(197704)39:4<1410::AID-CNCR2820390409>3.0.CO;2-D

Khan, T., Weber, H., Dimuzio, J., Matter, A., Dogdas, B., Shah, T., Thankappan, A., Disa, J., Jadhav, V., Lubbers, L., Sepp-Lorenzino, L., Strapps, W. R., & Tadin-Strapps, M. (2016). Silencing Myostatin Using Cholesterol-conjugated siRNAs Induces Muscle Growth. *Molecular Therapy - Nucleic Acids*, *5*(8), e342. https://doi.org/10.1038/MTNA.2016.55

Kierkegaard, M., Harms-Ringdahl, K., Holmqvist, L. W., & Tollbäck, A. (2009). Perceived functioning and disability in adults with myotonic dystrophy type 1: A survey according to the international classification of functioning, disability and health. *Journal of Rehabilitation Medicine*, *41*(7). https://doi.org/10.2340/16501977-0376

Kim, J., Hu, C., Moufawad El Achkar, C., Black, L. E., Douville, J., Larson, A., Pendergast, M. K., Goldkind, S. F., Lee, E. A., Kuniholm, A., Soucy, A., Vaze, J., Belur, N. R., Fredriksen, K., Stojkovska, I., Tsytsykova, A., Armant, M., DiDonato, R. L., Choi, J., … Yu, T. W. (2019). Patient-Customized Oligonucleotide Therapy for a Rare Genetic Disease. *New England Journal of Medicine*, *381*(17). https://doi.org/10.1056/nejmoa1813279

Kim, Y. K., Mandal, M., Yadava, R. S., Paillard, L., & Mahadevan, M. S. (2014). Evaluating the effects of CELF1 deficiency inamouse model of RNA toxicity. *Human Molecular Genetics*, *23*(2). https://doi.org/10.1093/hmg/ddt419

Kimura, T., Nakamori, M., Lueck, J. D., Pouliquin, P., Aoike, F., Fujimura, H., Dirksen, R. T., Takahashi, M. P., Dulhunty, A. F., & Sakoda, S. (2005). Altered mRNA splicing of the skeletal muscle ryanodine receptor and sarcoplasmic/endoplasmic reticulum Ca2+-ATPase in myotonic dystrophy type 1. *Human Molecular Genetics*, *14*(15). https://doi.org/10.1093/hmg/ddi223

Kissel, K., Hamm, S., Schulz, M., Vecchi, A., Garlanda, C., & Engelhardt, B. (1998). Immunohistochemical localization of the murine transferrin receptor (TfR) on blood-tissue barriers using a novel anti-TfR monoclonal antibody. *Histochemistry and Cell Biology*, *110*(1). https://doi.org/10.1007/s004180050266

Klein, A. F., Varela, M. A., Arandel, L., Holland, A., Naouar, N., Arzumanov, A., Seoane, D., Revillod, L., Bassez, G., Ferry, A., Jauvin, D., Gourdon, G., Puymirat, J., Gait, M. J., Furling, D., & Wood, M. J. A. (2019). Peptide-conjugated oligonucleotides evoke long-lasting myotonic dystrophy correction in patient-derived cells and mice. *Journal of Clinical Investigation*, *129*(11), 4739–4744. https://doi.org/10.1172/JCI128205

Kondo, K., Noguchi, M., Mukai, K., Matsuno, Y., Sato, Y., Shimosato, Y., & Monden, Y. (1990). Transferrin receptor expression in adenocarcinoma of the lung as a histopathologic indicator of prognosis. *Chest*, *97*(6). https://doi.org/10.1378/chest.97.6.1367

Konieczny, P., Stepniak-Konieczna, E., & Sobczak, K. (2014). SURVEY AND SUMMARY MBNL proteins and their target RNAs, interaction and splicing regulation. *Nucleic Acids Research*, *42*, 10873–10887. https://doi.org/10.1093/nar/gku767

Kühn, L. C., McClelland, A., & Ruddle, F. H. (1984). Gene transfer, expression, and molecular cloning of the human transferrin receptor gene. *Cell*, *37*(1). https://doi.org/10.1016/0092-8674(84)90304-0

Kuyumcu-Martinez, N. M., Wang, G. S., & Cooper, T. A. (2007). Increased Steady-State Levels of CUGBP1 in Myotonic Dystrophy 1 Are Due to PKC-Mediated

Hyperphosphorylation. *Molecular Cell*, *28*(1). https://doi.org/10.1016/j.molcel.2007.07.027

Lambert, L. A., & Mitchell, S. L. (2007). Molecular evolution of the transferrin receptor/glutamate carboxypeptidase II family. *Journal of Molecular Evolution*, *64*(1). https://doi.org/10.1007/s00239-006-0137-4

Larsen, H. J., Bentin, T., & Nielsen, P. E. (1999). Antisense properties of peptide nucleic acid. *Biochimica et Biophysica Acta*, *1489*(1), 159–166. https://doi.org/10.1016/S0167-4781(99)00145-1

Larsen, M. T., Kuhlmann, M., Hvam, M. L., & Howard, K. A. (2016). Albumin-based drug delivery: harnessing nature to cure disease. *Molecular and Cellular Therapies*, *4*(1). https://doi.org/10.1186/S40591-016-0048-8

Lättig-Tünnemann, G., Prinz, M., Hoffmann, D., Behlke, J., Palm-Apergi, C., Morano, I., Herce, H. D., & Cardoso, M. C. (2011). Backbone rigidity and static presentation of guanidinium groups increases cellular uptake of arginine-rich cell-penetrating peptides. *Nature Communications*, *2*(1). https://doi.org/10.1038/ncomms1459

Latvala, S., Jacobsen, B., Otteneder, M. B., Herrmann, A., & Kronenberg, S. (2017). Distribution of FcRn Across Species and Tissues. *Journal of Histochemistry and Cytochemistry*, *65*(6). https://doi.org/10.1369/0022155417705095

Lee, H. J., Engelhardt, B., Lesley, J., Bickel, U., & Pardridge, W. M. (2000). Targeting rat anti-mouse transferrin receptor monoclonal antibodies through blood-brain barrier in mouse. *Journal of Pharmacology and Experimental Therapeutics*, *292*(3).

Lee, J. E., Bennett, C. F., & Cooper, T. A. (2012). RNase H-mediated degradation of toxic RNA in myotonic dystrophy type 1. *Proceedings of the National Academy of Sciences of the United States of America*, *109*(11). https://doi.org/10.1073/pnas.1117019109

Lee, K., Li, M., Manchanda, M., Batra, R., Charizanis, K., Mohan, A., Warren, S. A., Chamberlain, C. M., Finn, D., Hong, H., Ashraf, H., Kasahara, H., Ranum, L. P. W., & Swanson, M. S. (2013). Compound loss of muscleblind-like function in myotonic dystrophy. *EMBO Molecular Medicine*, *5*(12), 1887–1900. https://doi.org/10.1002/emmm.201303275

Lehto, T., Ezzat, K., Wood, M. J. A., & EL Andaloussi, S. (2016). Peptides for nucleic acid delivery. In *Advanced Drug Delivery Reviews* (Vol. 106). https://doi.org/10.1016/j.addr.2016.06.008

Leoh, L. S., Kim, Y. K., Candelaria, P. V., Martínez-Maza, O., Daniels-Wells, T. R., & Penichet, M. L. (2018). Efficacy and Mechanism of Antitumor Activity of an Antibody Targeting Transferrin Receptor 1 in Mouse Models of Human Multiple Myeloma. *The Journal of Immunology*, *200*(10). https://doi.org/10.4049/jimmunol.1700787

Lim, L. M., Kuo, H. T., Kuo, M. C., Chiu, Y. W., Lee, J. J., Hwang, S. J., Tsai, J. C., Hung, C. C., & Chen, H. C. (2014). Low serum calcium is associated with poor

renal outcomes in chronic kidney disease stages 3-4 patients. *BMC Nephrology*, *15*(1). https://doi.org/10.1186/1471-2369-15-183

Lin, X., Miller, J. W., Mankodi, A., Kanadia, R. N., Yuan, Y., Moxley, R. T., Swanson, M. S., & Thornton, C. A. (2006). Failure of MBNL1-dependent post-natal splicing transitions in myotonic dystrophy. *Human Molecular Genetics*, *15*(13), 2087–2097. https://doi.org/10.1093/HMG/DDL132

Liu, L., Cheung, T. H., Charville, G. W., & Rando, T. A. (2015). Isolation of skeletal muscle stem cells by fluorescence-activated cell sorting. *Nature Protocols*, *10*(10). https://doi.org/10.1038/nprot.2015.110

Lo, S. L., & Wang, S. (2008). An endosomolytic Tat peptide produced by incorporation of histidine and cysteine residues as a nonviral vector for DNA transfection. *Biomaterials*, *29*(15). https://doi.org/10.1016/j.biomaterials.2008.01.031

Lo Scrudato, M., Poulard, K., Sourd, C., Tomé, S., Klein, A. F., Corre, G., Huguet, A., Furling, D., Gourdon, G., & Buj-Bello, A. (2019). Genome Editing of Expanded CTG Repeats within the Human DMPK Gene Reduces Nuclear RNA Foci in the Muscle of DM1 Mice. *Molecular Therapy*, *27*(8). https://doi.org/10.1016/j.ymthe.2019.05.021

Lobo, E. D., Hansen, R. J., & Balthasar, J. P. (2004). Antibody pharmacokinetics and pharmacodynamics. In *Journal of Pharmaceutical Sciences* (Vol. 93, Issue 11). https://doi.org/10.1002/jps.20178

López-Martínez, A., Soblechero-Martín, P., De-La-puente-ovejero, L., Nogales-Gadea, G., & Arechavala-Gomeza, V. (2020). An Overview of Alternative Splicing Defects Implicated in Myotonic Dystrophy Type I. *Genes*, *11*(9), 1–27. https://doi.org/10.3390/GENES11091109

Lueck, J. D., Lungu, C., Mankodi, A., Osborne, R. J., Welle, S. L., Dirksen, R. T., & Thornton, C. A. (2007). Chloride channelopathy in myotonic dystrophy resulting from loss of posttranscriptional regulation for CLCN1. *American Journal of Physiology - Cell Physiology*, *292*(4). https://doi.org/10.1152/ajpcell.00336.2006

Madani, F., Lindberg, S., Langel, U., Futaki, S., & Graslund, A. (2011). Mechanisms of cellular uptake of cell-penetrating peptides. *Journal of Biophysics*, *2011*.

Mahadevan, M. S. (2012). Myotonic dystrophy: Is a narrow focus obscuring the rest of the field? In *Current Opinion in Neurology* (Vol. 25, Issue 5). https://doi.org/10.1097/WCO.0b013e328357b0d9

Mahadevan, M. S., Yadava, R. S., Yu, Q., Balijepalli, S., Frenzel-Mccardell, C. D., Bourne, T. D., & Phillips, L. H. (2006). Reversible model of RNA toxicity and cardiac conduction defects in myotonic dystrophy. *Nature Genetics*, *38*(9). https://doi.org/10.1038/ng1857

Mahadevan M, Tsilfidis C, Sabourin L, Shutler G, Amemiya C, Jansen G, Neville C, Narong M, Arbarcelo J, O'Hoy K, Nelebond S, Earle-Macdonald J, Dejong P, Wieringa B, & Korneluk R. (1992). *Myotonic Dystrophy Mutation: An Unstable CTG Repeat in the 3' Untranslated Region of the Gene*. https://doi.org/10.1126/science.1546325

Malecova, B., Burke, R. S., Cochran, M., Hood, M. D., Johns, R., Kovach, P. R., Doppalapudi, V. R., Erdogan, G., Arias, J. D., Darimont, B., Miller, C. D., Huang, H., Geall, A., Younis, H. S., & Levin, A. A. (2023). Targeted tissue delivery of RNA therapeutics using antibody-oligonucleotide conjugates (AOCs). *Nucleic Acids Research*, *51*(12). https://doi.org/10.1093/nar/gkad415

Manich, G., Cabezón, I., Del Valle, J., Duran-Vilaregut, J., Camins, A., Pallàs, M., Pelegrí, C., & Vilaplana, J. (2013). Study of the transcytosis of an anti-transferrin receptor antibody with a Fab′ cargo across the blood-brain barrier in mice. *European Journal of Pharmaceutical Sciences*, *49*(4). https://doi.org/10.1016/j.ejps.2013.05.027

Mankodi, A., Logigian, E., Callahan, L., McClain, C., White, R., Henderson, D., Krym, M., & Thornton, C. A. (2000). Myotonic Dystrophy in Transgenic Mice Expressing an Expanded CUG Repeat. *Science*, *289*(5485), 1769–1772. https://doi.org/10.1126/SCIENCE.289.5485.1769

Mankodi, A., Takahashi, M. P., Jiang, H., Beck, C. L., Bowers, W. J., Moxley, R. T., Cannon, S. C., & Thornton, C. A. (2002). Expanded CUG repeats trigger aberrant splicing of ClC-1 chloride channel pre-mRNA and hyperexcitability of skeletal muscle in myotonic dystrophy. *Molecular Cell*, *10*(1), 35–44. https://doi.org/10.1016/S1097-2765(02)00563-4

Manoharan, M. (1999). 2'-Carbohydrate modifications in antisense oligonucleotide therapy: Importance of conformation, configuration and conjugation. In *Biochimica et Biophysica Acta - Gene Structure and Expression*. https://doi.org/10.1016/S0167-4781(99)00138-4

Martorell, L., Johnson, K., Boucher, C. A., & Baiget, M. (1997). Somatic instability of the myotonic dystrophy (CTG)(n) repeat during human fetal development. *Human Molecular Genetics*, *6*(6). https://doi.org/10.1093/hmg/6.6.877

Masuda, A., Andersen, H. S., Doktor, T. K., Okamoto, T., Ito, M., Andresen, B. S., & Ohno, K. (2012). CUGBP1 and MBNL1 preferentially bind to 3' UTRs and facilitate mRNA decay. *Scientific Reports*, *2*. https://doi.org/10.1038/srep00209

Matsumura, T., Iwahashi, H., Funahashi, T., Takahashi, M. P., Saito, T., Yasui, K., Saito, T., Iyama, A., Toyooka, K., Fujimura, H., & Shinno, S. (2009). A cross-sectional study for glucose intolerance of myotonic dystrophy. *Journal of the Neurological Sciences*, *276*(1–2). https://doi.org/10.1016/j.jns.2008.08.037

Matynia, A., Ng, C. H., Dansithong, W., Chiang, A., Silva, A. J., & Reddy, S. (2010). Muscleblind1, but not Dmpk or Six5, contributes to a complex phenotype of muscular and motivational deficits in mouse models of Myotonic Dystrophy. *PLoS ONE*, *5*(3). https://doi.org/10.1371/journal.pone.0009857

Mayle, K. M., Le, A. M., & Kamei, D. T. (2012). The intracellular trafficking pathway of transferrin. In *Biochimica et Biophysica Acta - General Subjects* (Vol. 1820, Issue 3). https://doi.org/10.1016/j.bbagen.2011.09.009

McClelland, A., Kühn, L. C., & Ruddle, F. H. (1984). The human transferrin receptor gene: genomic organization, and the complete primary structure of the receptor

deduced from a cDNA sequence. *Cell*, *39*(2 PART 1). https://doi.org/10.1016/0092-8674(84)90004-7

McClorey, G., & Banerjee, S. (2018). Cell-penetrating peptides to enhance delivery of oligonucleotide-based therapeutics. In *Biomedicines* (Vol. 6, Issue 2). https://doi.org/10.3390/biomedicines6020051

Meola, G., & Cardani, R. (2015). Myotonic dystrophies: An update on clinical aspects, genetic, pathology, and molecular pathomechanisms. In *Biochimica et Biophysica Acta - Molecular Basis of Disease* (Vol. 1852, Issue 4). https://doi.org/10.1016/j.bbadis.2014.05.019

Meola, G., & Sansone, V. (2007). Cerebral involvement in myotonic dystrophies. In *Muscle and Nerve* (Vol. 36, Issue 3). https://doi.org/10.1002/mus.20800

Mercuri, E., Finkel, R., Kirschner, J., Chiriboga, C., Kuntz, N., Sun, P., Gheuens, S., Bennett, C., Schneider, E., & Farwell, W. (2017). Efficacy and safety of nusinersen in children with later-onset spinal muscular atrophy (SMA): end of study results from the phase 3 CHERISH study. *Neuromuscular Disorders*, *27*, S210. https://doi.org/10.1016/j.nmd.2017.06.418

Miller, J. W., Urbinati, C. R., Teng-Umnuay, P., Stenberg, M. G., Byrne, B. J., Thornton, C. A., & Swanson, M. S. (2000). Recruitment of human muscleblind proteins to (CUG)(n) expansions associated with myotonic dystrophy. *EMBO Journal*, *19*(17), 4439–4448. https://doi.org/10.1093/emboj/19.17.4439

Miller, V. M., Xia, H., Marrs, G. L., Gouvion, C. M., Lee, G., Davidson, B. L., & Paulson, H. L. (2003). Allele-specific silencing of dominant disease genes. *Proceedings of the National Academy of Sciences of the United States of America*, *100*(12). https://doi.org/10.1073/pnas.1231012100

Misra, C., Bangru, S., Lin, F., Lam, K., Koenig, S. N., Lubbers, E. R., Hedhli, J., Murphy, N. P., Parker, D. J., Dobrucki, L. W., Cooper, T. A., Tajkhorshid, E., Mohler, P. J., & Kalsotra, A. (2020). Aberrant Expression of a Non-muscle RBFOX2 Isoform Triggers Cardiac Conduction Defects in Myotonic Dystrophy. *Developmental Cell*, *52*(6). https://doi.org/10.1016/j.devcel.2020.01.037

Mitchell, D. J., Steinman, L., Kim, D. T., Fathman, C. G., & Rothbard, J. B. (2000). Polyarginine enters cells more efficiently than other polycationic homopolymers. *Journal of Peptide Research*, *56*(5). https://doi.org/10.1034/j.1399-3011.2000.00723.x

Modoni, A., Silvestri, G., Pomponi, M. G., Mangiola, F., Tonali, P. A., & Marra, C. (2004). Characterization of the pattern of cognitive impairment in myotonic dystrophy type 1. *Archives of Neurology*, *61*(12). https://doi.org/10.1001/archneur.61.12.1943

Modoni, A., Silvestri, G., Vita, M. G., Quaranta, D., Tonali, P. A., & Marra, C. (2008). Cognitive impairment in myotonic dystrophy type 1 (DM1): A longitudinal follow-up study. *Journal of Neurology*, *255*(11). https://doi.org/10.1007/s00415-008-0017-5

Monckton, D. G., Wong, L. J. C., Ashizawa, T., & Caskey, C. T. (1995). Somatic mosaicism, germline expansions, germline reversions and intergenerational

reductions in myotonic dystrophy males: small pool PCR analyses. *Human Molecular Genetics*, *4*(1). https://doi.org/10.1093/hmg/4.1.1

Monia, B. P., Lesnik, E., Gonzalez, C., Lima, W. F., McGee, D., Guinosso, C. J., Kawasaki, A. M., Dan Cook, P., & Freier, S. M. (1993). Evaluation of 2"Modified Oligonucleotides Containing 2'-Deoxy Gaps as Antisense Inhibitors of Gene Expression*. *J. Biol. Chem*, *268*(19), 19954–19962. https://doi.org/10.1016/S0021-9258(19)85268-7

Montagnese, F., White, M., Klein, A., Stahl, K., Wenninger, S., & Schoser, B. (2019). Cannabis use in myotonic dystrophy patients in Germany and USA: a pilot survey. In *Journal of Neurology* (Vol. 266, Issue 2). https://doi.org/10.1007/s00415-018-9159-2

Moos, T., & Morgan, E. H. (2001). Restricted transport of anti-transferrin receptor antibody (OX26) through the blood-brain barrier in the rat. *Journal of Neurochemistry*, *79*(1). https://doi.org/10.1046/j.1471-4159.2001.00541.x

Morita, K., Hasegawa, C., Kaneko, M., Tsutsumi, S., Sone, J., Ishikawa, T., Imanishi, T., & Koizumi, M. (2002). 2'-O,4'-C-ethylene-bridged nucleic acids (ENA): highly nuclease-resistant and thermodynamically stable oligonucleotides for antisense drug. *Bioorganic & Medicinal Chemistry Letters*, *12*(1), 73–76. https://doi.org/10.1016/S0960-894X(01)00683-7

Morriss, G. R., Rajapakshe, K., Huang, S., Coarfa, C., & Cooper, T. A. (2018). Mechanisms of skeletal muscle wasting in a mouse model for myotonic dystrophy type 1. *Human Molecular Genetics*, *27*(16). https://doi.org/10.1093/hmg/ddy192

Moulton, H. M., & Moulton, J. D. (2010). Morpholinos and their peptide conjugates: therapeutic promise and challenge for Duchenne muscular dystrophy. *Biochimica et Biophysica Acta*, *1798*(12), 2296–2303. https://doi.org/10.1016/J.BBAMEM.2010.02.012

Moxley, R. T., Griggs, R. C., & Goldblatt, D. (1978). Decreased insulin sensitivity of forearm muscle in myotonic dystrophy. *Journal of Clinical Investigation*, *62*(4). https://doi.org/10.1172/JCI109198

Mulders, S. A. M., Van Den Broek, W. J. A. A., Wheeler, T. M., Croes, H. J. E., Van Kuik-Romeijn, P., De Kimpe, S. J., Furling, D., Platenburg, G. J., Gourdon, G., Thornton, C. A., Wieringa, B., & Wansink, D. G. (2009). Triplet-repeat oligonucleotide-mediated reversal of RNA toxicity in myotonic dystrophy. *Proceedings of the National Academy of Sciences of the United States of America*, *106*(33). https://doi.org/10.1073/pnas.0905780106

Nakamori, M., Nakatani, D., Sato, T., Hasuike, Y., Kon, S., Saito, T., Nakamura, H., Takahashi, M. P., Hida, E., Komaki, H., Matsumura, T., Takada, H., & Mochizuki, H. (2024). Erythromycin for myotonic dystrophy type 1: a multicentre, randomised, double-blind, placebo-controlled, phase 2 trial. *EClinicalMedicine*, *67*. https://doi.org/10.1016/j.eclinm.2023.102390

Nakamori, M., Sobczak, K., Puwanant, A., Welle, S., Eichinger, K., Pandya, S., Dekdebrun, J., Heatwole, C. R., McDermott, M. P., Chen, T., Cline, M., Tawil, R., Osborne, R. J., Wheeler, T. M., Swanson, M. S., Moxley, R. T., & Thornton, C. A.

(2013). Splicing biomarkers of disease severity in myotonic dystrophy. *Annals of Neurology*, *74*(6), 862–872. https://doi.org/10.1002/ana.23992

Nakamura, K., Kaya, M., Yanagisawa, Y., Yamamoto, K., Takayashiki, N., Ukita, H., Nagura, M., Sugiue, K., Kitajima, M., Hirano, K., Ishida, H., Onoda, C., Kobayashi, Y., Nakatani, E., Odagiri, K., & Suzuki, T. (2024). Denosumab-induced hypocalcemia in patients with solid tumors and renal dysfunction: a multicenter, retrospective, observational study. *BMC Cancer*, *24*(1). https://doi.org/10.1186/s12885-024-11942-2

Nakase, I., Tadokoro, A., Kawabata, N., Takeuchi, T., Katoh, H., Hiramoto, K., Negishi, M., Nomizu, M., Sugiura, Y., & Futaki, S. (2007). Interaction of arginine-rich peptides with membrane-associated proteoglycans is crucial for induction of actin organization and macropinocytosis. *Biochemistry*, *46*(2). https://doi.org/10.1021/bi0612824

Nguyen, H. H., Wolfe, J. T., Holmes, D. R., & Edwards, W. D. (1988). Pathology of the cardiac conduction system in myotonic dystrophy: A study of 12 cases. *Journal of the American College of Cardiology*, *11*(3). https://doi.org/10.1016/0735-1097(88)91547-1

Nizzardo, M., Simone, C., Salani, S., Ruepp, M. D., Rizzo, F., Ruggieri, M., Zanetta, C., Brajkovic, S., Moulton, H. M., Müehlemann, O., Bresolin, N., Comi, G. P., & Corti, S. (2014). Effect of combined systemic and local morpholino treatment on the spinal muscular atrophy δ7 mouse model phenotype. *Clinical Therapeutics*, *36*(3). https://doi.org/10.1016/j.clinthera.2014.02.004

Obika, S., Nanbu, D., Hari, Y., Andoh, J. I., Morio, K. I., Doi, T., & Imanishi, T. (1998). Stability and structural features of the duplexes containing nucleoside analogues with a fixed N-type conformation, 2'-O,4'-C- methyleneribonucleosides. *Tetrahedron Letters*, *39*(30). https://doi.org/10.1016/S0040-4039(98)01084-3

Obika, S., Uneda, T., Sugimoto, T., Nanbu, D., Minami, T., Doi, T., & Imanishi, T. (2001). 2′-O,4′-C-methylene bridged nucleic acid (2′,4′-BNA): Synthesis and triplex-forming properties. *Bioorganic and Medicinal Chemistry*, *9*(4). https://doi.org/10.1016/S0968-0896(00)00325-4

Oh, T. H., Markelonis, G. J., Royal, G. M., & Bregman, B. S. (1986). Immunocytochemical distribution of transferrin and its receptor in the developing chicken nervous system. *Developmental Brain Research*, *30*(2). https://doi.org/10.1016/0165-3806(86)90111-2

Østergaard, M. E., Jackson, M., Low, A., Chappell, A. E., Lee, R. G., Peralta, R. Q., Yu, J., Kinberger, G. A., Dan, A., Carty, R., Tanowitz, M., Anderson, P., Kim, T.-W., Fradkin, L., Mullick, A. E., Murray, S., Rigo, F., Prakash, T. P., Bennett, C. F., … Seth, P. P. (2019). Conjugation of hydrophobic moieties enhances potency of antisense oligonucleotides in the muscle of rodents and non-human primates. *Nucleic Acids Research*, *47*(12), 6045–6058. https://doi.org/10.1093/nar/gkz360

Otero, B. A., Poukalov, K., Hildebrandt, R. P., Thornton, C. A., Jinnai, K., Fujimura, H., Kimura, T., Hagerman, K. A., Sampson, J. B., Day, J. W., & Wang, E. T. (2021).

Transcriptome alterations in myotonic dystrophy frontal cortex. *Cell Reports*, *34*(3). https://doi.org/10.1016/j.celrep.2020.108634

Ottesen, E. W. (2017). ISS-N1 makes the first FDA-approved drug for spinal muscular atrophy. In *Translational Neuroscience*. https://doi.org/10.1515/tnsci-2017-0001

Ozer, J. S., Dieterle, F., Troth, S., Perentes, E., Cordier, A., Verdes, P., Staedtler, F., Mahl, A., Grenet, O., Roth, D. R., Wahl, D., Legay, F., Holder, D., Erdos, Z., Vlasakova, K., Jin, H., Yu, Y., Muniappa, N., Forest, T., … Gerhold, D. L. (2010). A panel of urinary biomarkers to monitor reversibility of renal injury and a serum marker with improved potential to assess renal function. *Nature Biotechnology*, *28*(5). https://doi.org/10.1038/nbt.1627

Pantic, B., Borgia, D., Giunco, S., Malena, A., Kiyono, T., Salvatori, S., De Rossi, A., Giardina, E., Sangiuolo, F., Pegoraro, E., Vergani, L., & Botta, A. (2016). Reliable and versatile immortal muscle cell models from healthy and myotonic dystrophy type 1 primary human myoblasts. *Experimental Cell Research*, *342*(1). https://doi.org/10.1016/j.yexcr.2016.02.013

Pardridge, W. M. (2002). Drug and gene targeting to the brain with molecular Trojan horses. In *Nature Reviews Drug Discovery* (Vol. 1, Issue 2). https://doi.org/10.1038/nrd725

Paterson, J., & Webster, C. I. (2016). Exploiting transferrin receptor for delivering drugs across the blood-brain barrier. *Drug Discovery Today: Technologies*, *20*, 49–52. https://doi.org/10.1016/J.DDTEC.2016.07.009

PepGen. (2023). PGN-EDODM1, an investigational antisense oligonucleotide for the treatment of myotonic dystrophy type 1. Unpublished company presentation. https://investors.PepGen.com/static-files/09a64952-eb56-447f-b90a-c7c7d2f5cef2

Perrone, R. D., Madias, N. E., & Levey, A. S. (1992). Serum Creatinine as an Index of Renal Function: New Insights into Old Concepts. In *Clinical Chemistry* (Vol. 38, Issue 10). https://doi.org/10.1093/clinchem/38.10.1933

Pestronk, A., Parhad, I. M., Drachman, D. B., & Price, D. L. (1982). Membrane myopathy: Morphological similarities to duchenne muscular dystrophy. *Muscle & Nerve*, *5*(3). https://doi.org/10.1002/mus.880050306

Petri, H., Witting, N., Ersbøll, M. K., Sajadieh, A., Dunø, M., Helweg-Larsen, S., Vissing, J., Køber, L., & Bundgaard, H. (2014). High prevalence of cardiac involvement in patients with myotonic dystrophy type 1: A cross-sectional study. *International Journal of Cardiology*, *174*(1). https://doi.org/10.1016/j.ijcard.2014.03.088

Petrillo, S., Pelosi, L., Piemonte, F., Travaglini, L., Forcina, L., Catteruccia, M., Petrini, S., Verardo, M., D'Amico, A., Musaró, A., & Bertini, E. (2017). Oxidative stress in Duchenne muscular dystrophy: Focus on the NRF2 redox pathway. *Human Molecular Genetics*, *26*(14). https://doi.org/10.1093/hmg/ddx173

Pfaffl, M. W. (2001). A new mathematical model for relative quantification in real-time RT–PCR. *Nucleic Acids Research*, *29*(9). https://doi.org/10.1093/nar/29.9.e45

Pooga, M., Hällbrink, M., Zorko, M., & Langel, Ü. (1998). Cell penetration by transportan. *The FASEB Journal*, *12*(1). https://doi.org/10.1096/fsb2fasebj.12.1.67

Porensky, P. N., Mitrpant, C., McGovern, V. L., Bevan, A. K., Foust, K. D., Kaspar, B. K., Wilton, S. D., & Burghes, A. H. M. (2012). A single administration of morpholino antisense oligomer rescues spinal muscular atrophy in mouse. *Human Molecular Genetics*. https://doi.org/10.1093/hmg/ddr600

Poulos, M. G., Batra, R., Li, M., Yuan, Y., Zhang, C., Darnell, R. B., & Swanson, M. S. (2013). Progressive impairment of muscle regeneration in muscleblind-like 3 isoform knockout mice. *Human Molecular Genetics*, *22*(17). https://doi.org/10.1093/hmg/ddt209

Pouny, Y., Rapaport, D., Shai, Y., Mor, A., & Nicolas, P. (1992). Interaction of Antimicrobial Dermaseptin and its Fluorescently Labeled Analogs with Phospholipid Membranes. *Biochemistry*, *31*(49). https://doi.org/10.1021/bi00164a017

Prakash, T. P., Graham, M. J., Yu, J., Carty, R., Low, A., Chappell, A., Schmidt, K., Zhao, C., Aghajan, M., Murray, H. F., Riney, S., Booten, S. L., Murray, S. F., Gaus, H., Crosby, J., Lima, W. F., Guo, S., Monia, B. P., Swayze, E. E., & Seth, P. P. (2014). Targeted delivery of antisense oligonucleotides to hepatocytes using triantennary N-acetyl galactosamine improves potency 10-fold in mice. *Nucleic Acids Research*, *42*(13), 8796–8807. https://doi.org/10.1093/nar/gku531

Provenzano M, Ikegami K, Bates K, Gaynor A, Hartman J. M, Jones A. S, Butler A, Bergenn K. N, Dekdebrun J, Hung M, Lapato D. M, Kiefer M, Thornton C, Johnson N. E, & Hale M. A. (2024). The Splice Index as a prognostic biomarker of strength and function in myotonic dystrophy type 1 . *BioRxiv*.

Prozialeck, W. C., Edwards, J. R., Lamar, P. C., Liu, J., Vaidya, V. S., & Bonventre, J. V. (2009). Expression of kidney injury molecule-1 (Kim-1) in relation to necrosis and apoptosis during the early stages of Cd-induced proximal tubule injury. *Toxicology and Applied Pharmacology*, *238*(3). https://doi.org/10.1016/j.taap.2009.01.016

Raal, F. J., Santos, R. D., Blom, D. J., Marais, A. D., Charng, M. J., Cromwell, W. C., Lachmann, R. H., Gaudet, D., Tan, J. L., Chasan-Taber, S., Tribble, D. L., Flaim, J. A. D., & Crooke, S. T. (2010). Mipomersen, an apolipoprotein B synthesis inhibitor, for lowering of LDL cholesterol concentrations in patients with homozygous familial hypercholesterolaemia: a randomised, double-blind, placebo-controlled trial. *The Lancet*, *375*(9719). https://doi.org/10.1016/S0140-6736(10)60284-X

Rau, F., Lainé, J., Ramanoudjame, L., Ferry, A., Arandel, L., Delalande, O., Jollet, A., Dingli, F., Lee, K. Y., Peccate, C., Lorain, S., Kabashi, E., Athanasopoulos, T., Koo, T., Loew, D., Swanson, M. S., Le Rumeur, E., Dickson, G., Allamand, V., … Furling, D. (2015). Abnormal splicing switch of DMD's penultimate exon compromises muscle fibre maintenance in myotonic dystrophy. *Nature Communications 2015 6:1*, *6*(1), 1–10. https://doi.org/10.1038/ncomms8205

Recalcati, S., & Cairo, G. (2021). Macrophages and iron: A special relationship. In *Biomedicines* (Vol. 9, Issue 11). https://doi.org/10.3390/biomedicines9111585

Rehman, S., Gladman, J. T., Periasamy, A., Sun, Y., & Mahadevan, M. S. (2014). Development of an AP-FRET based analysis for characterizing RNA-protein interactions in myotonic dystrophy (DM1). *PLoS ONE*, *9*(4). https://doi.org/10.1371/journal.pone.0095957

Renjini, R., Gayathri, N., Nalini, A., & Bharath, M. M. S. (2012). Oxidative damage in muscular dystrophy correlates with the severity of the pathology: Role of glutathione metabolism. *Neurochemical Research*, *37*(4). https://doi.org/10.1007/s11064-011-0683-z

Rinaldi, F., Terracciano, C., Pisani, V., Massa, R., Loro, E., Vergani, L., Di Girolamo, S., Angelini, C., Gourdon, G., Novelli, G., & Botta, A. (2012). Aberrant splicing and expression of the non muscle myosin heavy-chain gene MYH14 in DM1 muscle tissues. *Neurobiology of Disease*, *45*(1). https://doi.org/10.1016/j.nbd.2011.08.010

Roberts, T. C., Langer, R., & Wood, M. J. A. (2020). Advances in oligonucleotide drug delivery. In *Nature Reviews Drug Discovery* (Vol. 19, Issue 10, pp. 673–694). Nature Research. https://doi.org/10.1038/s41573-020-0075-7

Roopenian, D. C., & Akilesh, S. (2007). FcRn: The neonatal Fc receptor comes of age. In *Nature Reviews Immunology* (Vol. 7, Issue 9). https://doi.org/10.1038/nri2155

Rouault, T. A. (2006). The role of iron regulatory proteins in mammalian iron homeostasis and disease. In *Nature Chemical Biology* (Vol. 2, Issue 8). https://doi.org/10.1038/nchembio807

Rydström, A., Deshayes, S., Konate, K., Crombez, L., Padari, K., Boukhaddaoui, H., Aldrian, G., Pooga, M., & Divita, G. (2011). Direct translocation as major cellular uptake for CADY self-assembling peptide-based nanoparticles. *PLoS ONE*, *6*(10). https://doi.org/10.1371/journal.pone.0025924

Rzuczek, S. G., Colgan, L. A., Nakai, Y., Cameron, M. D., Furling, D., Yasuda, R., & Disney, M. D. (2017). Precise small-molecule recognition of a toxic CUG RNA repeat expansion. *Nature Chemical Biology*, *13*(2). https://doi.org/10.1038/nchembio.2251

Saarbach, J., Sabale, P. M., & Winssinger, N. (2019). Peptide nucleic acid (PNA) and its applications in chemical biology, diagnostics, and therapeutics. *Current Opinion in Chemical Biology*, *52*, 112–124. https://doi.org/10.1016/J.CBPA.2019.06.006

Sahashi K, Tanaka M, Tashiro M, Ohno K, Ibi T, Takahasi A, & Ozawa T. (2005). Increased mitochondrial DNA deletions in the skeletal muscle of myotonic dystrophy. *FreeRadicRes*, *39*(7), 771–776.

Sarepta Therapeutics. (2024). Sarepta Therapeutics provides update on SRP-5051 for the treatment of Duchenne muscular dystrophy. . In *presentation*. https://investorrelations.sarepta.com/news-releases/news-release-details/sarepta-therapeutics-provides-update-srp-5051-treatment-duchenne

Savkur, R. S., Philips, A. V., & Cooper, T. A. (2001). Aberrant regulation of insulin receptor alternative splicing is associated with insulin resistance in myotonic dystrophy. *Nature Genetics*, *29*(1). https://doi.org/10.1038/ng704

Sayers, J. R., Olsen, D. B., & Eckstein, F. (1989). Inhibition of restriction endonuclease hydrolysis by phosphorothioate-containing DNA. In *Nucleic Acids Research* (Vol. 17, Issue 22). https://doi.org/10.1093/nar/17.22.9495

Sazani, P., Ness, K. P. V., Weller, D. L., Poage, D., Nelson, K., & Shrewsbury, A. S. B. (2011)a. Chemical and mechanistic toxicology evaluation of exon skipping phosphorodiamidate morpholino oligomers in mdx mice. *International Journal of Toxicology*, *30*(3). https://doi.org/10.1177/1091581811403504

Sazani, P., Ness, K. P. V., Weller, D. L., Poage, D. W., Palyada, K., & Shrewsbury, S. B. (2011)b. Repeat-dose toxicology evaluation in cynomolgus monkeys of AVI-4658, a phosphorodiamidate morpholino oligomer (PMO) drug for the treatment of duchenne muscular dystrophy. *International Journal of Toxicology*, *30*(3). https://doi.org/10.1177/1091581811403505

Schindelin, J., Arganda-Carreras, I., Frise, E., Kaynig, V., Longair, M., Pietzsch, T., Preibisch, S., Rueden, C., Saalfeld, S., Schmid, B., Tinevez, J. Y., White, D. J., Hartenstein, V., Eliceiri, K., Tomancak, P., & Cardona, A. (2012). Fiji: An open-source platform for biological-image analysis. In *Nature Methods* (Vol. 9, Issue 7, pp. 676–682). https://doi.org/10.1038/nmeth.2019

Sergeant, N., Sablonnière, B., Schraen-Maschke, S., Ghestem, A., Maurage, C. A., Wattez, A., Vermersch, P., & Delacourte, A. (2001). Dysregulation of human brain microtubule-associated tau mRNA maturation in myotonic dystrophy type 1. *Human Molecular Genetics*, *10*(19). https://doi.org/10.1093/hmg/10.19.2143

Seymour, G. J., Walsh, M. D., Lavin, M. F., Strutton, G., & Gardiner, R. A. (1987). Transferrin receptor expression by human bladder transitional cell carcinomas. *Urological Research*, *15*(6). https://doi.org/10.1007/BF00265663

Shirley, M. (2021). Casimersen: First Approval. *Drugs*, *81*(7). https://doi.org/10.1007/s40265-021-01512-2

Sicot, G., Servais, L., Dinca, D. M., Leroy, A., Prigogine, C., Medja, F., Braz, S. O., Huguet-Lachon, A., Chhuon, C., Nicole, A., Gueriba, N., Oliveira, R., Dan, B., Furling, D., Swanson, M. S., Guerrera, I. C., Cheron, G., Gourdon, G., & Gomes-Pereira, M. (2017). Downregulation of the Glial GLT1 Glutamate Transporter and Purkinje Cell Dysfunction in a Mouse Model of Myotonic Dystrophy. In *Cell Reports* (Vol. 19, Issue 13, pp. 2718–2729). https://doi.org/10.1016/j.celrep.2017.06.006

Sievers, E. L., & Senter, P. D. (2013). Antibody-drug conjugates in cancer therapy. *Annual Review of Medicine*, *64*, 15–29. https://doi.org/10.1146/ANNUREV-MED-050311-201823

Singh, R. N., & Singh, N. N. (2018). Mechanism of Splicing Regulation of Spinal Muscular Atrophy Genes. *Advances in Neurobiology*, *20*, 31–61. https://doi.org/10.1007/978-3-319-89689-2_2

Sonoda, H., Morimoto, H., Yoden, E., Koshimura, Y., Kinoshita, M., Golovina, G., Takagi, H., Yamamoto, R., Minami, K., Mizoguchi, A., Tachibana, K., Hirato, T., & Takahashi, K. (2018). A Blood-Brain-Barrier-Penetrating Anti-human Transferrin Receptor Antibody Fusion Protein for Neuronopathic Mucopolysaccharidosis II. *Molecular Therapy : The Journal of the American Society of Gene Therapy*, *26*(5), 1366–1374. https://doi.org/10.1016/J.YMTHE.2018.02.032

Stoodley, J., Vallejo-Bedia, F., Seone-Miraz, D., Debasa-Mouce, M., Wood, M. J. A., & Varela, M. A. (2023). Application of Antisense Conjugates for the Treatment of Myotonic Dystrophy Type 1. In *International Journal of Molecular Sciences* (Vol. 24, Issue 3). https://doi.org/10.3390/ijms24032697

Su, Y., Doherty, T., Waring, A. J., Ruchala, P., & Hong, M. (2009). Roles of Arginine and Lysine Residues in the Translocation of a Cell-Penetrating Peptide from 13 C, 31 P, and 19 F Solid-State NMR. *Biochemistry*, *48*(21), 4587–4595. https://doi.org/10.1021/bi900080d

Sugo, T., Terada, M., Oikawa, T., Miyata, K., Nishimura, S., Kenjo, E., Ogasawara-Shimizu, M., Makita, Y., Imaichi, S., Murata, S., Otake, K., Kikuchi, K., Teratani, M., Masuda, Y., Kamei, T., Takagahara, S., Ikeda, S., Ohtaki, T., & Matsumoto, H. (2016). Development of antibody-siRNA conjugate targeted to cardiac and skeletal muscles. *Journal of Controlled Release*, *237*, 1–13. https://doi.org/10.1016/J.JCONREL.2016.06.036

Summerton, J., & Weller, D. (1997). Morpholino Antisense Oligomers: Design, Preparation, and Properties. In *ANTISENSE & NUCLEIC ACID DRUG DEVELOPMENT* (Vol. 7). www.liebertpub.com

Tabrizi SJ, Leavitt BR, Landwehrmeyer GB, & et al. (2019). *Tabrizi SJ, Leavitt BR, Landwehrmeyer GB, et al. Targeting Huntingtin Expression in Patients with Huntington's Disease. New England Journal of Medicine. 2019;380(24):2307-2316. doi:10.1056/nejmoa1900907*. https://doi.org/10.1056/NEJMoa1900907

Tabuchi, M., Yoshimori, T., Yamaguchi, K., Yoshida, T., & Kishi, F. (2000). Human NRAMP2/DMT1, which mediates iron transport across endosomal membranes, is localized to late endosomes and lysosomes in HEp-2 cells. *Journal of Biological Chemistry*, *275*(29). https://doi.org/10.1074/jbc.M001478200

Tacchini, L., Bianchi, L., Bernelli-Zazzera, A., & Cairo, G. (1999). Transferrin receptor induction by hypoxia. HIF-1-mediated transcriptional activation and cell-specific post-transcriptional regulation. *Journal of Biological Chemistry*, *274*(34). https://doi.org/10.1074/jbc.274.34.24142

Tachiyama, R., Ishikawa, D., Matsumoto, M., Nakayama, K. I., Yoshimori, T., Yokota, S., Himeno, M., Tanaka, Y., & Fujita, H. (2011). Proteome of ubiquitin/MVB pathway: Possible involvement of iron-induced ubiquitylation of transferrin receptor in lysosomal degradation. *Genes to Cells*, *16*(4). https://doi.org/10.1111/j.1365-2443.2011.01499.x

Takado, Y., Terajima, K., Ohkubo, M., Okamoto, K., Shimohata, T., Nishizawa, M., Igarashi, H., & Nakada, T. (2015). Diffuse brain abnormalities in myotonic

dystrophy type 1 detected by 3.0 t proton magnetic resonance spectroscopy. *European Neurology*, *73*(3–4). https://doi.org/10.1159/000371575

Taketo, M., Schroeder, A. C., Mobraaten, L. E., Gunning, K. B., Hanten, G., Fox, R. R., Roderick, T. H., Stewart, C. L., Lilly, F., Hansen, C. T., & Overbeek, P. A. (1991). FVB/N: An inbred mouse strain preferable for transgenic analyses. *Proceedings of the National Academy of Sciences of the United States of America*, *88*(6). https://doi.org/10.1073/pnas.88.6.2065

Taneja, K. L., McCurrach, M., Schalling, M., Housman, D., & Singer, R. H. (1995). Foci of trinucleotide repeat transcripts in nuclei of myotonic dystrophy cells and tissues. *Journal of Cell Biology*, *128*(6), 995–1002. https://doi.org/10.1083/jcb.128.6.995

Tang, Z. Z., Yarotskyy, V., Wei, L., Sobczak, K., Nakamori, M., Eichinger, K., Moxley, R. T., Dirksen, R. T., & Thornton, C. A. (2012). Muscle weakness in myotonic dystrophy associated with misregulated splicing and altered gating of Ca v1.1 calcium channel. *Human Molecular Genetics*, *21*(6). https://doi.org/10.1093/hmg/ddr568

Tanner, M. K., Tang, Z., & Thornton, C. A. (2021). Targeted splice sequencing reveals RNA toxicity and therapeutic response in myotonic dystrophy. *Nucleic Acids Research*, *49*(4). https://doi.org/10.1093/nar/gkab022

Tanowitz, M., Hettrick, L., Revenko, A., Kinberger, G. A., Prakash, T. P., & Seth, P. P. (2017). Asialoglycoprotein receptor 1 mediates productive uptake of N-Acetylgalactosamine-conjugated and unconjugated phosphorothioate antisense oligonucleotides into liver hepatocytes. *Nucleic Acids Research*, *45*(21), 12388–12400. https://doi.org/10.1093/nar/gkx960

Terenzi, F., & Ladd, A. N. (2010). Conserved developmental alternative splicing of muscleblind-like (MBNL) transcripts regulates MBNL localization and activity. *RNA Biology*, *7*(1). https://doi.org/10.4161/rna.7.1.10401

Tevaarwerk, G. J. M., & Hudson, A. J. (1977). Carbohydrate metabolism and insulin resistance in myotonia dystrophica. *Journal of Clinical Endocrinology and Metabolism*, *44*(3). https://doi.org/10.1210/jcem-44-3-491

Theadom, A., Rodrigues, M., Roxburgh, R., Balalla, S., Higgins, C., Bhattacharjee, R., Jones, K., Krishnamurthi, R., & Feigin, V. (2014). Prevalence of Muscular Dystrophies: A Systematic Literature Review. *Neuroepidemiology*, *43*(3–4), 259–268. https://doi.org/10.1159/000369343

Thomas, J. D., Sznajder, Ł. J., Bardhi, O., Aslam, F. N., Anastasiadis, Z. P., Scotti, M. M., Nishino, I., Nakamori, M., Wang, E. T., & Swanson, M. S. (2017). Disrupted prenatal RNA processing and myogenesis in congenital myotonic dystrophy. *Genes and Development*, *31*(11), 1122–1133. https://doi.org/10.1101/gad.300590.117

Thornton, C. A., Johnson, K., & Moxley, R. T. (1994). Myotonic dystrophy patients have larger CTG expansions in skeletal muscle than in leukocytes. *Annals of Neurology*, *35*(1). https://doi.org/10.1002/ana.410350116

Thornton, C. A., Moxley, R. T., Eichinger, K., Heatwole, C., Mignon, L., Arnold, W. D., Ashizawa, T., Day, J. W., Dent, G., Tanner, M. K., Duong, T., Greene, E. P., Herbelin, L., Johnson, N. E., King, W., Kissel, J. T., Leung, D. G., Lott, D. J., Norris, D. A., … Bennett, C. F. (2023). Antisense oligonucleotide targeting DMPK in patients with myotonic dystrophy type 1: a multicentre, randomised, dose-escalation, placebo-controlled, phase 1/2a trial. *The Lancet Neurology*, *22*(3). https://doi.org/10.1016/S1474-4422(23)00001-7

Timchenko, L. T., Miller, J. W., Timchenko, N. A., Devore, D. R., Datar, K. V., Lin, L., Roberts, R., Thomas Caskey, C., & Swanson, M. S. (1996). Identification of a (CUG)(n) triplet repeat RNA-binding protein and its expression in myotonic dystrophy. *Nucleic Acids Research*, *24*(22). https://doi.org/10.1093/nar/24.22.4407

Timchenko, N. A., Patel, R., Iakova, P., Cai, Z. J., Quan, L., & Timchenko, L. T. (2004). Overexpression of CUG Triplet Repeat-binding Protein, CUGBP1, in Mice Inhibits Myogenesis. *Journal of Biological Chemistry*, *279*(13). https://doi.org/10.1074/jbc.M312923200

Timchenko, N. A., Wang, G. L., & Timchenko, L. T. (2005). RNA CUG-binding protein 1 increases translation of 20-kDa isoform of CCAAT/enhancer-binding protein β by interacting with the α and β subunits of eukaryotic initiation translation factor 2. *Journal of Biological Chemistry*, *280*(21). https://doi.org/10.1074/jbc.M409563200

Toscano, A., Messina, S., Campo, G. M., Di Leo, R., Musumeci, O., Rodolico, C., Aguennouz, M., Annesi, G., Messina, C., & Vita, G. (2005). Oxidative stress in myotonic dystrophy type 1. *Free Radical Research*, *39*(7). https://doi.org/10.1080/10715760500138932

Tran, H., Gourrier, N., Lemercier-Neuillet, C., Dhaenens, C. M., Vautrin, A., Fernandez-Gomez, F. J., Arandel, L., Carpentier, C., Obriot, H., Eddarkaoui, S., Delattre, L., Van Brussels, E., Holt, I., Morris, G. E., Sablonnie, B., Buée, L., Charlet-Berguerand, N., Schraen-Maschke, S., Furling, D., … Sergeant, N. (2011). Analysis of exonic regions involved in nuclear localization, splicing activity, and dimerization of muscleblind-like-1 isoforms. *Journal of Biological Chemistry*, *286*(18). https://doi.org/10.1074/jbc.M110.194928

Traverso, M., Assereto, S., Baratto, S., Iacomino, M., Pedemonte, M., Diana, M. C., Ferretti, M., Broda, P., Minetti, C., Gazzerro, E., Madia, F., Bruno, C., Zara, F., & Fiorillo, C. (2018). Clinical and molecular consequences of exon 78 deletion in DMD gene. *Journal of Human Genetics*, *63*(6). https://doi.org/10.1038/s10038-018-0439-6

Tsui, N. B. Y., Ng, E. K. O., & Lo, Y. M. D. (2002). Stability of endogenous and added RNA in blood specimens, serum, and plasma. *Clinical Chemistry*, *48*(10). https://doi.org/10.1093/clinchem/48.10.1647

Turner, C., & Hilton-Jones, D. (2010). The myotonic dystrophies: Diagnosis and management. In *Journal of Neurology, Neurosurgery and Psychiatry* (Vol. 81, Issue 4). https://doi.org/10.1136/jnnp.2008.158261

Tylock, K. M., Auerbach, D. S., Tang, Z. Z., Thornton, C. A., & Dirksen, R. T. (2020). Biophysical mechanisms for QRS- And QTc-interval prolongation in mice with

cardiac expression of expanded CUG-repeat RNA. *Journal of General Physiology*, *152*(2). https://doi.org/10.1085/JGP.201912450

Uhlén M, Fagerberg L, Hallström BM, Lindskog C, Oksvold P, Mardinoglu A, Sivertsson Å, Kampf C, Sjöstedt E, Asplund A, Olsson I, Edlund K, Lundberg E, Navani S, Szigyarto CA, Odeberg J, Djureinovic D, Takanen JO, Hober S, Alm T, Edqvist PH, Berling H, Tegel H, Mulder J, Rockberg J, Nilsson P, Schwenk JM, Hamsten M, von Feilitzen K, Forsberg M, Persson L, Johansson F, Zwahlen M, von Heijne G, Nielsen J, Pontén F.Tissue-based map of the human proteome. *Science* 2015 347(6220):1260419. DOI: 10.1126/science.1260419

Untergasser, A., Ruijter, J. M., Benes, V., & van den Hoff, M. J. B. (2021). Web-based LinRegPCR: application for the visualization and analysis of (RT)-qPCR amplification and melting data. *BMC Bioinformatics*, *22*(1). https://doi.org/10.1186/s12859-021-04306-1

Uslu Gökceoğlu, A., Comak, E., Dogan, C. S., Koyun, M., Akbas, H., & Akman, S. (2014). Magnesium excretion and hypomagnesemia in pediatric renal transplant recipients. *Renal Failure*, *36*(7). https://doi.org/10.3109/0886022X.2014.917561

Vaidya, V. S., Ozer, J. S., Dieterle, F., Collings, F. B., Ramirez, V., Troth, S., Muniappa, N., Thudium, D., Gerhold, D., Holder, D. J., Bobadilla, N. A., Marrer, E., Perentes, E., Cordier, A., Vonderscher, J., Maurer, G., Goering, P. L., Sistare, F. D., & Bonventre, J. V. (2010). Kidney injury molecule-1 outperforms traditional biomarkers of kidney injury in preclinical biomarker qualification studies. *Nature Biotechnology*, *28*(5), 478–485. https://doi.org/10.1038/nbt.1623

Vaidya, V. S., Ramirez, V., Ichimura, T., Bobadilla, N. A., & Bonventre, J. V. (2006). Urinary kidney injury molecule-1: A sensitive quantitative biomarker for early detection of kidney tubular injury. *American Journal of Physiology - Renal Physiology*, *290*(2). https://doi.org/10.1152/ajprenal.00291.2005

van Timmeren, M. M., van den Heuvel, M. C., Bailly, V., Bakker, S. J. L., van Goor, H., & Stegeman, C. A. (2007). Tubular kidney injury molecule-1 (KIM-1) in human renal disease. *Journal of Pathology*, *212*(2). https://doi.org/10.1002/path.2175

Vermersch, P., Sergeant, N., Ruchoux, M. M., Hofmann-Radvanyi, H., Wattez, A., Petit, H., Dewailly, P., & Delacourte, A. (1996). Specific tau variants in the brains of patients with myotonic dystrophy. *Neurology*, *47*(3). https://doi.org/10.1212/WNL.47.3.711

Vester, B., & Wengel, J. (2004). LNA (locked nucleic acid): high-affinity targeting of complementary RNA and DNA. *Biochemistry*, *43*(42), 13233–13241. https://doi.org/10.1021/BI0485732

Vickers, T. A., Wyatt, J. R., Burckin, T., Bennett, C. F., & Freier, S. M. (2001). Fully modified 2′ MOE oligonucleotides redirect polyadenylation. *Nucleic Acids Research*, *29*(6). https://doi.org/10.1093/nar/29.6.1293

Wadia, J. S., Stan, R. V., & Dowdy, S. F. (2004). Transducible TAT-HA fusogenic peptide enhances escape of TAT-fusion proteins after lipid raft macropinocytosis. *Nature Medicine*, *10*(3). https://doi.org/10.1038/nm996

Wan, L., & Dreyfuss, G. (2017). Splicing-Correcting Therapy for SMA. In *Cell* (Vol. 170, Issue 1). https://doi.org/10.1016/j.cell.2017.06.028

Wang, E. T., Cody, N. A. L., Jog, S., Biancolella, M., Wang, T. T., Treacy, D. J., Luo, S., Schroth, G. P., Housman, D. E., Reddy, S., Lécuyer, E., & Burge, C. B. (2012). Transcriptome-wide Regulation of Pre-mRNA Splicing and mRNA Localization by Muscleblind Proteins. *Cell*, *150*(4), 710. https://doi.org/10.1016/J.CELL.2012.06.041

Wang, G. S., Kearney, D. L., De Biasi, M., Taffet, G., & Cooper, T. A. (2007). Elevation of RNA-binding protein CUGBP1 is an early event in an inducible heart-specific mouse model of myotonic dystrophy. *Journal of Clinical Investigation*, *117*(10). https://doi.org/10.1172/JCI32308

Wang, M., Weng, W.-C., Stock, L., Lindquist, D., Martinez, A., Gourdon, G., Timchenko, N., Snape, M., & Timchenko, L. (2019). Correction of Glycogen Synthase Kinase 3 β in Myotonic Dystrophy 1 Reduces the Mutant RNA and Improves Postnatal Survival of DMSXL Mice . *Molecular and Cellular Biology*, *39*(21). https://doi.org/10.1128/mcb.00155-19

Wang, P. Y., Lin, Y. M., Wang, L. H., Kuo, T. Y., Cheng, S. J., & Wang, G. S. (2017). Reduced cytoplasmic MBNL1 is an early event in a brain-specific mouse model of myotonic dystrophy. *Human Molecular Genetics*, *26*(12). https://doi.org/10.1093/hmg/ddx115

Wang, S., Allen, N., Prakash, T. P., Liang, X. H., & Crooke, S. T. (2019). Lipid Conjugates Enhance Endosomal Release of Antisense Oligonucleotides Into Cells. *Https://Home.Liebertpub.Com/Nat*, *29*(5), 245–255. https://doi.org/10.1089/NAT.2019.0794

Ward, A. J., Rimer, M., Killian, J. M., Dowling, J. J., & Cooper, T. A. (2010). CUGBP1 overexpression in mouse skeletal muscle reproduces features of myotonic dystrophy type 1. *Human Molecular Genetics*, *19*(18). https://doi.org/10.1093/hmg/ddq277

Watanabe, T. A., Geary, R. S., & Levin, A. A. (2006). Plasma protein binding of an antisense oligonucleotide targeting human ICAM-1 (ISIS 2302). *Oligonucleotides*, *16*(2), 169–180. https://doi.org/10.1089/OLI.2006.16.169

Webster, C. I., Hatcher, J., Burrell, M., Thom, G., Thornton, P., Gurrell, I., & Chessell, I. (2016). *Enhanced delivery of IL-1 receptor antagonist to the central nervous system as a novel anti-transferrin receptor-IL-1RA fusion reverses neuropathic mechanical hypersensitivity*. https://doi.org/10.1097/j.pain.0000000000000810

Wei, C., Stock, L., Valanejad, L., Zalewski, Z. A., Karns, R., Puymirat, J., Nelson, D., Witte, D., Woodgett, J., Timchenko, N. A., & Timchenko, L. (2018). Correction of GSK3β at young age prevents muscle pathology in mice with myotonic dystrophy type 1. *FASEB Journal*, *32*(4). https://doi.org/10.1096/fj.201700700R

Wender, P. A., Mitchell, D. J., Pattabiraman, K., Pelkey, E. T., Steinman, L., & Rothbard, J. B. (2000). The design, synthesis, and evaluation of molecules that enable or enhance cellular uptake: Peptoid molecular transporters. *Proceedings of*

the National Academy of Sciences of the United States of America, *97*(24). https://doi.org/10.1073/pnas.97.24.13003

Wenninger, S., Montagnese, F., & Schoser, B. (2018). Core clinical phenotypes in Myotonic Dystrophies. In *Frontiers in Neurology* (Vol. 9, Issue MAY). https://doi.org/10.3389/fneur.2018.00303

Wheeler, T. M., Leger, A. J., Pandey, S. K., Mac Leod, A. R., Wheeler, T. M., Cheng, S. H., Wentworth, B. M., Bennett, C. F., & Thornton, C. A. (2012). Targeting nuclear RNA for in vivo correction of myotonic dystrophy. *Nature*, *488*(7409), 111–117. https://doi.org/10.1038/nature11362

Wheeler, T. M., Lueck, J. D., Swanson, M. S., Dirksen, R. T., & Thornton, C. A. (2007). Correction of ClC-1 splicing eliminates chloride channelopathy and myotonia in mouse models of myotonic dystrophy. *Journal of Clinical Investigation*, *117*(12). https://doi.org/10.1172/JCI33355

Wheeler, T. M., Sobczak, K., Lueck, J. D., Osborne, R. J., Lin, X., Dirksen, R. T., & Thornton, C. A. (2009). Reversal of RNA dominance by displacement of protein sequestered on triplet repeat RNA. *Science*, *325*(5938), 336–339. https://doi.org/10.1126/science.1173110

Wittenberg, J. B., & Wittenberg, B. A. (2003). Myoglobin function reassessed. In *Journal of Experimental Biology* (Vol. 206, Issue 12). https://doi.org/10.1242/jeb.00243

Worton, R. G., & Thompson, M. W. (1988). Genetics of Duchenne muscular dystrophy. In *Annual Review of Genetics* (Vol. 22). https://doi.org/10.1146/annurev.ge.22.120188.003125

Wu, H., Lima, W. F., Zhang, H., Fan, A., Sun, H., & Crooke, S. T. (2004). Determination of the Role of the Human RNase H1 in the Pharmacology of DNA-like Antisense Drugs. *Journal of Biological Chemistry*, *279*(17). https://doi.org/10.1074/jbc.M311683200

Xu, M. M., Wang, J., & Xie, J. X. (2017). Regulation of iron metabolism by hypoxia-inducible factors. In *Sheng li xue bao : [Acta physiologica Sinica]* (Vol. 69, Issue 5).

Yadava, R. S., Yu, Q., Mandal, M., Rigo, F., Bennett, C. F., & Mahadevan, M. S. (2020). Systemic therapy in an RNA toxicity mouse model with an antisense oligonucleotide therapy targeting a non-CUG sequence within the DMPK 3′UTR RNA. *Human Molecular Genetics*, *29*(9), 1440–1453. https://doi.org/10.1093/hmg/ddaa060

Yamamoto, H., Kokame, K., Okuda, T., Nakajo, Y., Yanamoto, H., & Toshiyuki, M. (2011). NDRG4 protein-deficient mice exhibit spatial learning deficits and vulnerabilities to cerebral ischemia. *Journal of Biological Chemistry*, *286*(29). https://doi.org/10.1074/jbc.M111.256446

Yamashita, Y., Matsuura, T., Shinmi, J., Amakusa, Y., Masuda, A., Ito, M., Kinoshita, M., Furuya, H., Abe, K., Ibi, T., Sahashi, K., & Ohno, K. (2012). Four parameters increase the sensitivity and specificity of the exon array analysis and disclose 25

novel aberrantly spliced exons in myotonic dystrophy. In *Journal of Human Genetics* (Vol. 57, Issue 6). https://doi.org/10.1038/jhg.2012.37

Yikilmaz, E., Rouault, T. A., & Schuck, P. (2005). Self-association and ligand-induced conformational changes of iron regulatory proteins 1 and 2. *Biochemistry*, *44*(23). https://doi.org/10.1021/bi0500325

Yin, H., Saleh, A. F., Betts, C., Camelliti, P., Seow, Y., Ashraf, S., Arzumanov, A., Hammond, S., Merritt, T., Gait, M. J., & Wood, M. J. A. (2011). Pip5 transduction peptides direct high efficiency oligonucleotide-mediated dystrophin exon skipping in heart and phenotypic correction in mdx mice. *Molecular Therapy*, *19*(7). https://doi.org/10.1038/mt.2011.79

Youngblood, D. S., Hatlevig, S. A., Hassinger, J. N., Iversen, P. L., & Moulton, H. M. (2007). Stability of cell-penetrating peptide-morpholino oligomer conjugates in human serum and in cells. *Bioconjugate Chemistry*, *18*(1). https://doi.org/10.1021/bc060138s

Yu, Y. J., Atwal, J. K., Zhang, Y., Tong, R. K., Wildsmith, K. R., Tan, C., Bien-Ly, N., Hersom, M., Maloney, J. A., Meilandt, W. J., Bumbaca, D., Gadkar, K., Hoyte, K., Luk, W., Lu, Y., Ernst, J. A., Scearce-Levie, K., Couch, J. A., Dennis, M. S., & Watts, R. J. (2014). Therapeutic bispecific antibodies cross the blood-brain barrier in nonhuman primates. *Science Translational Medicine*, *6*(261). https://doi.org/10.1126/scitranslmed.3009835

Yu, Y. J., Zhang, Y., Kenrick, M., Hoyte, K., Luk, W., Lu, Y., Atwal, J., Elliott, J. M., Prabhu, S., Watts, R. J., & Dennis, M. S. (2011). Boosting brain uptake of a therapeutic antibody by reducing its affinity for a transcytosis target. *Science Translational Medicine*, *3*(84). https://doi.org/10.1126/scitranslmed.3002230

Yuan, Y., Compton, S. A., Sobczak, K., Stenberg, M. G., Thornton, C. A., Griffith, J. D., & Swanson, M. S. (2007). Muscleblind-like 1 interacts with RNA hairpins in splicing target and pathogenic RNAs. *Nucleic Acids Research*, *35*(16). https://doi.org/10.1093/nar/gkm601

Yum, K., Wang, E. T., & Kalsotra, A. (2017). Myotonic dystrophy: disease repeat range, penetrance, age of onset, and relationship between repeat size and phenotypes. In *Current Opinion in Genetics and Development* (Vol. 44). https://doi.org/10.1016/j.gde.2017.01.007

Zapata-Aldana, E., Ceballos-Sáenz, D., Hicks, R., & Campbell, C. (2018). Prenatal, Neonatal, and Early Childhood Features in Congenital Myotonic Dystrophy. *Journal of Neuromuscular Diseases*, *5*(3). https://doi.org/10.3233/JND-170277

Zhou, H., Meng, J., Marrosu, E., Janghra, N., Morgan, J., & Muntoni, F. (2015). Repeated low doses of morpholino antisense oligomer: An intermediate mouse model of spinal muscular atrophy to explore the window of therapeutic response. *Human Molecular Genetics*, *24*(22). https://doi.org/10.1093/hmg/ddv329

Zhou, Q. H., Boado, R. J., Lu, J. Z., Hui, E. K. W., & Pardridge, W. M. (2010). Re-engineering erythropoietin as an IgG fusion protein that penetrates the blood-brain barrier in the mouse. *Molecular Pharmaceutics*, *7*(6). https://doi.org/10.1021/mp1001763

Zhou, Y., Vaidya, V. S., Brown, R. P., Zhang, J., Rosenzweig, B. A., Thompson, K. L., Miller, T. J., Bonventre, J. V., & Goering, P. I. (2008). Comparison of kidney injury molecule-1 and other nephrotoxicity biomarkers in urine and kidney following acute exposure to gentamicin, mercury, and chromium. *Toxicological Sciences*, *101*(1). https://doi.org/10.1093/toxsci/kfm260

Zorko, M., & Langel, Ü. (2022). Cell-Penetrating Peptides. In *Methods in Molecular Biology* (Vol. 2383, pp. 3–32). https://doi.org/10.1007/978-1-0716-1752-6_1